Time-Dependent Deformations of Concrete for Precast/Prestressed Bridge Components

by

Morgan Alise Ellis

A thesis submitted to the Graduate Faculty of
Auburn University
in partial fulfillment of the
requirements for the Degree of
Master of Science

Auburn, Alabama
December 8, 2012

Keywords: Creep, Self-Consolidating Concrete, Maturity, Shrinkage, Strain

Approved by

Robert W. Barnes, Chair, James J. Mallett Associate Professor of Civil Engineering
Anton K. Schindler, Professor of Civil Engineering
James S. Davidson, Professor of Civil Engineering

ABSTRACT

Self-consolidating concrete (SCC) is a material that has properties capable of improving the quality and durability of structures. However, much is still unknown about the hardened properties of this material, including the creep and shrinkage behavior. This thesis presents research aimed at improving knowledge in this area by investigating the creep performance of SCC mixtures and corresponding conventionally-vibrated concrete (CVC) mixtures used for the construction of precast/prestressed concrete bridge girders in Alabama.

All mixtures contained Type III portland cement and included several chemical admixtures as well as slag cement. While the girder concrete was placed, representative cylindrical test specimens were also cast. Each of these mixtures was cured using two forms of accelerated curing, which are representative of typical curing conditions used in prestressed concrete, and two loading ages. Match-cured specimens were loaded at prestress release and tarp-cured specimens were loaded at 26 hours. Time-dependent deformations of the concretes were measured using standard creep testing procedures.

The accuracy of the following nine creep and shrinkage models was also investigated as part of this research.

- ACI 209
- AASHTO 2004
- AASHTO 2010
- NCHRP 628

- MC 90
- MC 90-99
- MC 90-KAV
- MC 2010, and
- Eurocode

The test results were compared against the prediction models investigated and overall, the CVC performed no better than the SCC used in this project. For the prediction of load-induced strain, AASHTO 2010, MC 2010, and ACI 209 all provided acceptable predictions for both SCC and CVC produced in accordance with ALDOT specifications for precast/prestressed concrete girders. For the prediction of shrinkage strain, none of the methods investigated provided accurate predictions for SCC or CVC. Of the most current methods, AASHTO 2010 was the most accurate method for estimating shrinkage strains for the concretes tested in this project. When older methods were considered, the original MC 90 method was more accurate than AASHTO 2010.

ACKNOWLEDGEMENTS

First, I would like to thank God for allowing me the opportunity to come to graduate school and obtain my Master's Degree. Without His blessings and help, none of this would have been possible and I would not have made it to the end. "Now all glory to God, who is able, through his mighty power at work within us, to accomplish infinitely more than we might ask or think or imagine." Ephesians 3:20

I would like to thank my advisor, Dr. Robert W. Barnes, for all of the help and direction he has given throughout this entire process. His time, input, and assistance were invaluable to me over the years and I appreciate the opportunity he gave me to come to Auburn and work for him.

In addition, the efforts of other graduate students who assisted me in the laboratory have not gone unnoticed. To Will Minton, Leslie Warnock, Brian Rhett, Sam Keske, and the structural laboratory technician Billy Wilson: I say thank you for your time and help conducting research for this project.

Finally, the support of my family and friends has been tremendous and is greatly appreciated. To my parents: I thank you for the countless hours spent driving to Auburn and helping me when my work-load seemed unbearable. To Justin: Thank you for the numerous late nights you devoted to assisting me in the lab. I can never repay what you, and many others, have done for me or begin to express how much your encouragement has meant to me, but I thank you for everything and I love you.

TABLE OF CONTENTS

LIST OF TABLES

LIST OF FIGURES

LIST OF ABBREVIATIONS AND SYMBOLS

AASHTO	American Association of State Highway Transportation Officials
ACI	American Concrete Institute
ALDOT	Alabama Department of Transportation
ASTM	American Society for Testing and Materials
AUHRC	Auburn University Highway Research Center
BT-54	Bulb-tee girder 54 in. in height
BT-72	Bulb-tee girder 72 in. in height
CEB	Euro-International Concrete Committee (Comité Euro-International du Béton)
CEN	European Committee for Standardization (Comité Européen de Normalisation)
CVC	Conventionally-vibrated concrete
DEMEC	Demountable, Mechanical (strain gauges)
fib	International Federation for Structural Concrete (fédération internationale du béton)
FIP	International Federation of Prestressing (Fédération Internationale de la Précontrainte)
GGBF	Ground-Granulated Blast-Furnace Slag
HPC	High-Performance Concrete
HRWR	High-Range Water-Reducing (admixture)
LRFD	Load and Resistance Factor Design
MC	Model Code

MC-KAV	CEB Model Code method as modified by Brian Kavanaugh
NCHRP	National Cooperative Highway Research Program
P(SCC)	Self-consolidating concrete for use in precast, prestressed applications
PCI	Precast/Prestressed Concrete Institute
SCC	Self-consolidating concrete
SCM	Supplementary cementing material
ε_{cr}	Creep strain
ε_{sh}	Shrinkage strain
ε_{li}	Load-induced strain
ε_{t}	Total strain

CHAPTER 1
INTRODUCTION

1.1 BACKGROUND

In the past several decades, the precast/prestressed concrete industry has grown rapidly. Key to this industry is that any number of shapes and sizes can be cast and cured in large quantities off-site then transported and used immediately during construction. Figure 1-1 shows a typical bulb-tee bridge girder being moved from a prestressing bed to a storage yard to await use. Offering durability, reduced construction time, cost efficiency, and high flowability, prestressed members often rely on a new advancement in the concrete industry, self-consolidating concrete (SCC).

Figure 1-1: Precast/Prestressed Concrete Bulb-Tee Bridge Girder

In the early 1980's, Japanese researchers at Kochi University saw a need to help alleviate concerns associated with conventional concrete, and to consistently produce a more uniform, well-consolidated product. The team, led by Hajime Okamura, began to develop a concrete mixture that deformed under its own weight so that it would fill forms and encapsulate the reinforcing steel without the need of a skilled laborer to operate vibratory equipment (Okamura and Ouchi 1999).

Okamura's creation was dubbed self-consolidating concrete (SCC) and exhibited a high flow without experiencing segregation issues that are found in conventional concrete mixtures (Khayat 1999). To achieve these properties, SCC consists of a higher fine aggregate content and smaller coarse aggregate than conventional-slump concrete. Large doses of high-range water-reducing (HRWR) admixtures must also be applied in combination with increased volumes of powdered materials in order for SCC to maintain cohesiveness while achieving high flowability (Khayat, Hu, and Monty 1999).

Khayat (1999) defines self-consolidating concrete (SCC) as a "highly flowable concrete that can spread into place under its own weight and achieve good consolidation in the absence of vibration". The use of this concrete, as compared to conventionally-vibrated concrete (CVC), may result in the production of high-quality concrete elements at reduced labor costs. This cost reduction can be especially realized in the precast, prestressed industry where elements are generally narrow and highly congested, and require the expertise of skilled laborers (Khayat 1999).

As the use of self-consolidating concrete becomes more practical for design application, the accuracy of current methods used for prediction of time-dependent deformations is in question. Predicting the amount of creep or shrinkage that may occur is especially

complicated in concrete mixtures that contain chemical admixtures, supplementary materials, or lightweight aggregates. Many of the models currently in use are based on outdated research and were formulated using assumptions that are no longer valid in current practice. Creep and shrinkage in concrete can affect several aspects of the design and construction phases and are therefore important parameters to consider in design, particularly for prestressed concrete.

Creep and shrinkage both directly affect the extent to which the concrete experiences cracking, deflections, and changes in length over time. In prestressed members, these length changes can also result in a change in length of the prestressing tendons which can then cause a loss of prestress. Creep-induced curvature changes can also result in changes in girder camber over time (Cramer and Oliva 2008).

The creep and shrinkage characteristics of concrete are determined and affected by concrete composition, volume to surface ratio, environmental conditions, type of curing, age at loading, and duration of load. With supplementary cementing materials being used in increasing volume and chemical admixtures being developed to modify the behavior of fresh and hardened concrete, the accurate prediction of creep and shrinkage could ultimately result in more efficient prestressed designs or the minimization of construction problems due to inaccurate predictions.

1.2 RESEARCH OBJECTIVES

This research is part of a larger project sponsored by the Alabama Department of Transportation (ALDOT) and is aimed at gaining a further understanding of the behavior of self-consolidating concrete designed for use in prestressed bridge girder applications. The primary objective of this work was to determine the time-dependent deformations of concrete

used in three SCC and two CVC bridge girders (like those seen in Figure 1-1**Error! Reference source not found.**) and compare those deformations to the estimated values predicted in accordance with nine creep and shrinkage prediction methods that were chosen for evaluation.

This thesis outlines the testing and analysis of the creep and shrinkage behavior of the ten girders studied. Specific tasks required to complete the research objectives are stated below:

1. Create a user-friendly interface to calculate the prediction of creep and shrinkage for the chosen nine methods using both SCC and CVC with two different forms of accelerated curing methods.
2. Perform creep and shrinkage testing on SCC and CVC sampled from actual bridge girders and cured along with the girders using tarp-curing and match-curing methods.
3. Compare the creep and shrinkage exhibited by SCC to that of the companion CVC.
4. Compare the creep and shrinkage exhibited by match-cured specimens to that of tarp-cured specimens.
5. Evaluate the accuracy of the prediction methods by comparing predicted results to measured data.
6. Identify any limitations of the methods and recommend future modifications that can be implemented to better predict creep and shrinkage of concrete in girders for ALDOT bridges.

1.3 RESEARCH SCOPE

The work presented in this thesis was conducted to determine the creep and shrinkage behavior of both SCC and CVC mixtures. Each of the five girders studied consisted of Type III portland cement, slag cement, and several property-modifying admixtures. Slag cement may also be referred to as the supplementary cementing material (SCM) ground, granulated blast-furnace slag (GGBS).

Each of the samples were investigated to address the behavior of creep and shrinkage of SCC compared to that of CVC as well as the relative behavior of specimens that underwent match curing versus those that underwent tarp curing. To accomplish this, each concrete batch was studied using a match-cured case with a loading age of 24 hours to match the actual age at prestress release, and a tarp-cured case with a loading age of 26 hours. Creep testing of these specimens was performed for one year after loading where strain readings were taken at specific intervals and the data were analyzed to determine the creep and shrinkage of each test case. Next, a comparison was made to contrast the creep and shrinkage behavior of SCC versus CVC and match- versus tarp-curing methods. In addition, design material behavior models were incorporated for evaluation including those of the ACI Committee Report 209, AASHTO Bridge Design Specifications from 2004 and 2010, NCHRP Report 628, CEB-FIP Model Code 1990 and 1999, Kavanaugh (2008) modifications to Model Code 1990, *fib* Model Code 2010, and Eurocode. These codes provide models for predicting time-dependent material properties including creep and shrinkage.

1.4 ORGANIZATION OF THESIS

Chapter 2 of this report presents a review of relevant literature and includes sections on SCC, creep and the prediction of creep deformations, shrinkage and the prediction of

shrinkage deformations, concrete properties affecting creep and shrinkage, and previous studies related to time-dependent deformations of SCC.

The experimental plan employed during the research of this project is delineated in Chapter 3. This encompasses the casting, preparation, and curing of specimens, a description of the materials used, and the creep and shrinkage test setup. This chapter also contains detailed information of the equipment used in gathering data, including the dimensions of the creep-testing frames, the materials used in construction of the frames, and a description of the climate-controlled room that contains them.

The assumptions and decisions that were made in order to most appropriately apply the nine prediction methods are presented in Chapter 4. Here, any general assumptions that were applied to several methods and any specific applications relevant to just one method are outlined.

The data gathered for the duration of this project, and the subsequent analysis of that data, are presented in Chapter 5. Here, the creep and shrinkage responses that were yielded, along with the conclusions that were formed from the data collection, are presented. Also given is an evaluation of the data with regards to the nine creep and shrinkage prediction methods that were chosen. Additionally, the performance and accuracy of each method is reported with regards to estimating the creep and shrinkage values of both SCC and CVC samples.

A summary of the laboratory work executed during the course of this study, as well as general conclusions and recommendations, are laid out in Chapter 6.

CHAPTER 2
LITERATURE REVIEW

2.1 INTRODUCTION

The *AASHTO LRFD Bridge Design Specifications* (2010) is the governing standard for highway bridge design in the United States. In addition to incorporating its own prediction models for computing creep and shrinkage deformations, this specification allows the use of other models when mix-specific properties are not available: the CEB-FIP model code (MC 90) or ACI 209. The same year AASHTO 2010 was released, a new European model code was also being prepared. Thus, when evaluating the prediction of creep and shrinkage for this research, other methods were also taken into consideration in order to account for these recommendations and updated or modified models.

One of the main objectives of this study was to evaluate nine prediction methods to determine their efficiency in estimating creep and shrinkage of both SCC and CVC mixtures using both tarp and match curing regimes. This was accomplished by measuring the creep and shrinkage strains, ε_{cr} and ε_{sh} respectively, from laboratory testing and comparing this experimental data against the following nine prediction methods:

- ACI 209 (1992)
- AASHTO 2004
- AASHTO 2010
- NCHRP 628 (2009)

- MC 90
- MC 90-99
- MC 90-KAV (2008)
- MC 2010, and
- Eurocode (2004).

2.2 CREEP

The *Prediction of Creep, Shrinkage, and Temperature Effects in Concrete Structures* reported by ACI Committee 209 (1992), henceforth referred to as ACI 209, defines creep as "the time-dependent increase of strain in hardened concrete subjected to sustained stress". The initial deformation that occurs when a load is applied is known as the elastic strain, while the additional strain that occurs over time due to the same sustained load is the creep strain. Creep cannot be measured directly but may be determined by deducting the elastic strain and shrinkage strains from the total strains, as these are not independent phenomena (Nawy 2001).

The creep models presented by ACI 209 show that the creep characteristics of concrete are determined and affected by concrete composition, volume to surface ratio, environmental conditions, curing regime, age at loading, and magnitude and duration of load. Collins and Mitchell (1991) state that it is "hard to estimate the amount of creep concrete will exhibit without tests determining the creep characteristics of the concrete." Studies have shown that a lower creep response is exhibited by concretes that have higher strengths, include harder coarse aggregates, or have been subjected to accelerated curing techniques.

2.3 CREEP PREDICTION METHODS

The following sections outline the procedures for nine creep prediction methods including common U.S. and international models. A concise explanation of each procedure is also provided.

2.3.1 ACI 209 CREEP PREDICTION METHOD

ACI Committee 209 (1992) set forth a prediction method which uses an ultimate creep coefficient that may be adjusted to account for various mixture-specific properties, loading age, specimen geometry, and environmental conditions. In addition to this ultimate creep coefficient, ACI 209 accounts for the growth in creep over time using a time-rate function.

Defined as the ratio of creep strain to initial strain resulting from the application of load, the ultimate creep coefficient, v_u , is computed by the following equation:

$$v_u = 2.35(\gamma_{la} \cdot \gamma_\lambda \cdot \gamma_{vs} \cdot \gamma_\psi \cdot \gamma_s \cdot \gamma_a) \qquad \textbf{Equation 2-1}$$

where,

γ_{la} is the loading age correction factor

γ_λ is the relative humidity correction factor

γ_{vs} is the volume-to-surface-area ratio correction factor

γ_ψ is the fine aggregate percentage correction factor

γ_s is the slump correction factor, and

γ_a is the air content correction factor.

The correction factors seen in Equation 2-1, which are applied to the ultimate value, are used to account for conditions other than standard concrete composition and conditions.

These factors may be used in conjunction with the specific creep or shrinkage data of a specimen tested in accordance with the *Standard Test Method for Creep of Concrete in Compression*, ASTM C512. The correction factors are outlined in Equation 2-2 to Equation 2-8.

The loading age correction factor, γ_{la} , is applied from Equation 2-2 for loading ages later than 7 days for non-accelerated-cured concrete, and from Equation 2-3 for 1 to 3 days for accelerated-cured concrete.

$$\gamma_{la} = 1.25(t_{la})^{-0.118} \quad \text{for non-accelerated cured concrete} \qquad \textbf{Equation 2-2}$$

$$\gamma_{la} = 1.13(t_{la})^{-0.094} \quad \text{for accelerated cured concrete} \qquad \textbf{Equation 2-3}$$

where,

t_{la} is the concrete age at which the load is applied (days).

For ambient relative humidity greater than 40 percent, the correction factor γ_{λ} is to be used.

$$\gamma_{\lambda} = 1.27 - 0.0067\lambda \qquad \textbf{Equation 2-4}$$

where,

λ is the relative humidity (%).

The volume-to-surface area ratio correction factor, γ_{vs} , is calculated using the following equation:

$$\gamma_{vs} = {}^{2}/_{3}\left[1 + 1.13\left(\mathrm{e}^{-0.54({}^{v}/_{s})}\right)\right] \qquad \textbf{Equation 2-5}$$

where,

v is the specimen volume (in^3)

s is the specimen surface area (in^2), and

$^v/_s$ is the volume-to-surface area ratio (in.).

The fine aggregate percentage correction factor, γ_ψ , is determined using Equation 2-6. For fine aggregate percents within this range, this factor is approximately equal to 1.0.

$$\gamma_\psi = 0.88 + 0.0024\psi \quad \textbf{Equation 2-6}$$

where,

ψ is the ratio of fine aggregate to total aggregate by weight (%).

The slump correction factor, γ_s , is to be calculated in accordance with Equation 2-7 for slump values greater than 5 inches. For slump less than 5 inches, this factor is approximately equal to 1.0.

$$\gamma_s = 0.82 + 0.067s \quad \textbf{Equation 2-7}$$

where,

s is the slump (in.).

The air content correction factor, γ_a , is calculated using Equation 2-8. For air content less than 8 percent, this factor is approximately equal to 1.0.

$$\gamma_\alpha = 0.46 + 0.09\alpha \geq 1.0 \quad \textbf{Equation 2-8}$$

where,

α is the air content (%).

To ascertain the predicted creep coefficient for each time step of interest, the ultimate creep coefficient is multiplied by the time parameter that accounts for the age of the concrete:

$$\nu_u(t) = \nu_u \times \nu_t \qquad \textbf{Equation 2-9}$$

The creep coefficient, ν_t, is the ratio of creep strain to initial strain. Equation 2-10 is applicable to normal weight and lightweight concretes, using accelerated and non-accelerated curing, and Types I and III cements, under standard conditions.

$$\nu_t = \frac{t^{0.6}}{10 + t^{0.6}} \qquad \textbf{Equation 2-10}$$

where,

t is the length of time after loading (days).

It is essential to note that the above equation is only applicable to loading ages later than 7 days for non-accelerated-cured concrete samples and later than 1 to 3 days for accelerated-cured samples.

After determining the creep coefficient for each time step, the creep strain can be predicted by multiplying the creep coefficient, $\nu_u(t)$, by the elastic strain that resulted from applying a load.

$$Predicted\ Creep, \varepsilon_{cr}(t) = \nu_u(t) \times elastic\ strain\ from\ loading \qquad \textbf{Equation 2-11}$$

2.3.2 AASHTO 2004 CREEP PREDICTION METHOD

The *AASHTO LRFD Bridge Design Specifications* are the leading standard for bridge design in the U.S. The creep and shrinkage models suggested in this specification changed significantly in 2005. The original AASHTO LRFD model, which was most recently published in the 2004 version of the specification (AASHTO 2004), is referred to herein as

AASHTO 2004. The newer model introduced in the 2005 version of the specification is referred to in this thesis as AASHTO 2010. The AASHTO 2004 creep prediction method should be used to determine the effects of creep on the loss of prestressing force in bridges other than segmentally constructed ones (AASHTO 2004). The methods for obtaining creep and shrinkage in this specification are taken from Collins and Mitchell (1991), and are based on recommendations of ACI 209 and other published data (AASHTO 2004).

The creep shortening of concrete under permanent loads is influenced primarily by the maturity of the concrete at the time of initial loading. Creep is also dependent on the magnitude and duration of the load applied and the relative humidity of the concrete.

The creep coefficient, $\psi(t,t_i)$, is computed by the following equation:

$$\psi(t,t_i) = 3.5k_c \cdot k_f \left(1.58 - \frac{\mathrm{H}}{120}\right) t_i^{-0.118} \left(\frac{(t-t_i)^{0.6}}{10+(t-t_i)^{0.6}}\right) \quad \textbf{Equation 2-12}$$

where,

k_c is the volume-to-surface ratio correction factor

k_f is the concrete strength correction factor

H is the relative humidity (%)

t is the maturity of concrete (days), and

t_i is the concrete age at time of load application (days).

In this model, the concrete maturity, t , at the initial loading time, t_i , is taken as the actual number of day for non-accelerated curing. One day of accelerated curing by steam or radiant heat may be taken as the equivalent of seven days of non-accelerated curing.

The volume-to-surface-area ratio ($^V/_S$) correction factor may be obtained from Equation 2-13. However, it should be noted that the maximum $^V/_S$ ratio considered in the development

of this factor was 6.0 inches and the surface used in determining k_s should only include the area that is exposed to the atmosphere for drying.

$$k_c = \left[\frac{\frac{t}{26e^{0.36(V/S)}+t}}{\frac{t}{45+t}}\right]\left[\frac{1.8-1.77e^{-0.54(V/S)}}{2.587}\right] \qquad \textbf{Equation 2-13}$$

where,

$^{V}/_{S}$ is the volume-to-surface-area ratio (in.).

The factor for the effect of concrete strength is calculated by:

$$k_f = \frac{1}{0.67+\left(\frac{f'_c}{9}\right)} \qquad \textbf{Equation 2-14}$$

where,

f'_c is the specified compressive strength of concrete at 28 days (ksi).

After determining the creep coefficient, the predicted strain due to creep can be obtained by multiplying $\psi(t,t_i)$ by the compressive strain caused by the sustained load as in Equation 2-11.

2.3.3 AASHTO 2010 CREEP PREDICTION METHOD

The current AASHTO LRFD creep prediction method (AASHTO 2010) was first implemented in the 2005 version of the *AASHTO LRFD Bridge Design Specifications*. The AASHTO 2010 should be used to determine the effects of creep on the loss of prestressing force in bridges that are not segmentally constructed. This method was created based on the findings of Huo et al. (2001), Al-Omaishi (2001), Tadros (2003), Collins and Mitchell

(1991), recommendations by ACI Committee 209 and other recently published data (AASHTO 2010).

The provisions of AASHTO 2010 are applicable to specified concrete strengths up to 15.0 ksi, and the predicted creep is influenced by the magnitude and duration of the load applied, the maturity of the concrete at loading, and the relative humidity of the concrete.

The creep coefficient, $\psi(t,t_i)$, is computed using the following equation:

$$\psi(t,t_i) = 1.9\left(k_{hc} \cdot k_s \cdot k_f \cdot k_{td}\right) t_i^{-0.118} \qquad \textbf{Equation 2-15}$$

where,

k_{hc} is the relative humidity correction factor

k_s is the volume-to-surface area ratio correction factor

k_f is the concrete strength correction factor

k_{td} is the time development correction factor, and

t_i is the concrete age at time of load application (days).

Unlike AASHTO 2004, it should be noted that AASHTO 2010 is based on accelerated curing as the standard method of curing. This means that all ages in days are days of accelerated curing.

The relative humidity correction factor may be taken as:

$$k_{hc} = 1.56 - 0.008H \qquad \textbf{Equation 2-16}$$

where,

H is the relative humidity (%). If accurate humidity information is unknown, *H* may be taken from Figure 2-1.

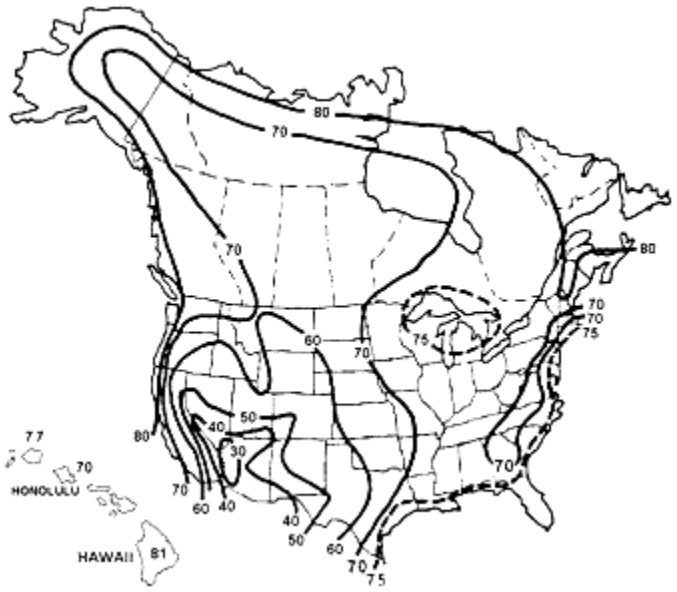

Figure 2-1: Annual Average Ambient Relative Humidity in Percent
(AASHTO 2010, Fig. 5.4.2.3.3-1)

The factor for the effect of the volume-surface ratio of the specimen is given by Equation 2-17, and it should be noted that the surface area used in determining k_s should only include the area that is exposed to the atmosphere for drying.

$$k_s = 1.45 - .13(^{V}/_{S}) \geq 1.0 \qquad \textbf{Equation 2-17}$$

where,

$^{V}/_{S}$ is the volume-to-surface-area ratio (in.).

The concrete strength correction factor is calculated by:

$$k_f = \frac{5}{1 + f'_{ci}} \qquad \textbf{Equation 2-18}$$

where,

f'_{ci} is the specified compressive strength at prestressing for pretensioned members and at time of initial loading for non-prestressed members (ksi). If the age of concrete at initial loading is unknown, f'_{ci} may be taken as $0.8 f'_c$.

The time development correction factor can be used for both precast and cast-in-place concrete components and for accelerated and non-accelerated curing conditions. This parameter is given by:

$$k_{td} = \frac{t}{61 - 4f'_{ci} + t} \qquad \textbf{Equation 2-19}$$

where,

t is the concrete maturity (days); *after* application of the sustained load.

After determining the creep coefficient, the predicted strain due to creep can be obtained by multiplying $\psi(t,t_i)$ by the compressive strain caused by permanent loads as in Equation 2-11.

2.3.4 NCHRP 628 CREEP PREDICTION METHOD

The NCHRP Report 628 (2009) for *Self-Consolidating Concrete for Precast, Prestressed Concrete Bridge Elements* (henceforth called NCHRP 628) proposes changes to the *AASHTO LRFD Bridge Design Specification* for the prediction of creep and shrinkage when using self-

consolidating concrete. Other than the changes listed below, or if CVC mixtures are used, the AASHTO 2010 method should be followed for the predicted creep strain.

The creep coefficient may be taken as:

$$\psi(t, t_i) = 1.9\left(k_{hc} \cdot k_{vs} \cdot k_f \cdot k_{td}\right) t_i^{-0.118} A \qquad \textbf{Equation 2-20}$$

where,

k_{hc} is the relative humidity correction factor, as calculated in Equation 2-16

k_{vs} is the volume-to-surface area ratio correction factor

k_f is the concrete strength correction factor

k_{td} is the time development correction factor

t_i is the concrete age at loading (days), and

A is the cement type factor:

A = 1.19 for Type I/II cement

= 1.35 for Type III + 20% FA binder, which may be used for SCC in precast, prestressed applications, or P(SCC).

The factor for the effect of the volume-surface ratio of the specimen is given by Equation 2-17 but is represented in the NCHRP 628 report in SI units as follows:

$$k_{vs} = 1.45 - 0.0051\left(V/S\right) \geq 0.0 \qquad \textbf{Equation 2-21}$$

where,

V/S is the volume-to-surface area ratio (mm).

It should be noted that the limit in Equation 2-21 contradicts the lower limit of 1.0 in Equation 2-17 from the AASHTO method which the NCHRP 628 was modeled after. The lower limit expressed here should most likely be taken as 1.0.

The concrete strength correction factor is given by Equation 2-18 but is calculated in SI units by:

$$k_f = \frac{35}{7 + f'_{ci}} \qquad \textbf{Equation 2-22}$$

where,

f'_{ci} is the specified compressive strength at prestressing for pretensioned members and at time of initial loading for non-prestressed members (MPa). If the age of concrete at initial loading is unknown, f'_{ci} may be taken as $0.8 f'_c$.

The time development correction factor is given in SI units by:

$$k_{td} = \frac{t}{61 - 0.58 f'_{ci} + t} \qquad \textbf{Equation 2-23}$$

where,

t is the concrete maturity (days); time considered – loading time.

After determining the creep coefficient, the predicted strain due to creep can be obtained by multiplying $\psi(t,t_i)$ by the compressive strain caused by permanent loads as in Equation 2-11.

2.3.5 MC 90 CREEP PREDICTION METHOD

The CEB-FIP Model Code 1990 is a European design code that is applicable for use with concrete mixtures which are subjected to normal conditions. Concrete mixtures that are subjected to extreme high or low temperatures, low relative humidities, or mixtures using structural lightweight aggregate are not valid for this method (Al-Manaseer and Lam 2005). However, the MC 90 creep prediction method does contain provisions that allow for the cement type, curing temperature, high stress levels, and other parameters to be taken into account (CEB 1990).

The procedure for estimating creep with this model is similar in nature to the ACI 209 method in which a creep coefficient, $\Phi(t,t_o)$, is established based on the environmental conditions to which the concrete is subjected along with each mixture's hardened properties.

$$\Phi(t,t_o) = \Phi_o \cdot \beta_c(t - t_o) \qquad \textbf{Equation 2-24}$$

where,

$\Phi(t,t_o)$ is the creep coefficient

Φ_o is the notional creep coefficient

β_c is the coefficient describing development of creep with time after loading

t is the age of concrete at the moment considered (days), and

t_o is the age of concrete at loading.

The notional creep coefficient may be estimated from

$$\Phi_o = \Phi_{RH} \cdot \beta(f_{cm}) \cdot \beta(t_o) \qquad \textbf{Equation 2-25}$$

with,

$$\Phi_{RH} = 1 + \frac{1 - \left(\frac{RH}{RH_o}\right)}{0.46\left(\frac{h}{h_o}\right)^{1/3}}$$ **Equation 2-26**

$$\beta(f_{cm}) = \frac{5.3}{\left(\frac{f_{cm}}{f_{cmo}}\right)^{0.5}}$$ **Equation 2-27**

$$\beta(t_o) = \frac{1}{0.1 + \left(\frac{t_o}{t_1}\right)^{0.2}}$$ **Equation 2-28**

where,

RH is the relative humidity of the environment (%), and

RH_o = 100%

$$h = \frac{2A_c}{u}$$ **Equation 2-29**

A_c is the cross-sectional area (mm^2)

u is the perimeter (mm) exposed to drying

h_o = 100 mm

f_{cm} is the mean compressive strength at 28 days (MPa)

f_{cmo} = 10 MPa, and

t_1 = 1 day.

The development of creep with time is given by

$$\beta_c(t - t_o) = \left[\frac{\frac{(t - t_o)}{t_1}}{\beta_H + \frac{(t - t_o)}{t_1}}\right]^{0.3}$$ **Equation 2-30**

where,

$$\beta_H = 150\left[1 + \left(1.2\frac{RH}{RH_o}\right)^{18}\right]\frac{h}{h_o} + 250 \leq 1500 \qquad \textbf{Equation 2-31}$$

and all other factors are previously defined.

After determining the creep coefficient, the predicted creep strain can be obtained by multiplying $\Phi(t,t_o)$ by the elastic strain that resulted from loading as seen in Equation 2-11.

2.3.5.1 Effect of Temperature During Curing

An elevated-temperature curing cycle was used for each specimen in this research. According to Model Code 1990, the effect of temperature deviations from a concrete temperature of 20°C can change the maturity of concrete, and this change can be accounted for by adjusting the concrete's chronological age, as per Equation 2-32, to more accurately account for the effect of temperature on creep:

$$t_{o,T} = \sum_{i=1}^{n} \Delta t_i \cdot exp\left[13.65 - \frac{4000}{273 + \left(\frac{T(\Delta t_i)}{T_o}\right)}\right] \qquad \textbf{Equation 2-32}$$

where,

t_{oT} is the temperature-adjusted concrete age

Δt_i is the number of days where temperature T prevails

$T(\Delta t_i)$ is the temperature (°C) during the time period Δt_i, and

T_o = 1°C.

According to Model Code 1990, the activation energy required for concrete hydration is influenced by the cement type and additions. Different cement types each have different degrees of hydration. The degree of hydration of concrete reached at a given age controls creep more so than the age of the concrete itself (CEB 1990). In order to account for the effects of the type of cement, the age at loading, t_o, can be modified according to the following equation:

$$t_o = \mathrm{t}_{o,T}\left[\frac{9}{2+\left(\frac{t_{o,T}}{t_{1,T}}\right)^{1.2}}+1\right]^{\alpha} \geq 0.5\ days \qquad \textbf{Equation 2-33}$$

where,

$t_{o,T}$ is the temperature-adjusted age according to Equation 2-32 (days)

$t_{1,T}$ = 1 day, and

α is the cement type factor;

α = -1 for slowly hardening cements (SL), 0 for normal or rapid hardening cements (N and R), and 1 for rapid hardening high strength cements (RS).

It should be noted that this equation should only be used to replace t_o in the computation of the age at loading term $\beta(t_o)$. It should not be used to replace $(t-t_o)$, which actually represents the duration of the load itself or the actual time under load. For example, this substitution should be used in Equation 2-28, but not in Equation 2-30.

2.3.6 MC 90-KAV CREEP PREDICTION METHOD

In an effort to provide more accurate creep predictions for the research conducted by Bryan Kavanaugh (2008), a process was undertaken to modify Model Code 1990. This calibration process modified the parameters in Table 2-1. Here, modifications affecting the creep coefficient, as well as changes to the maturity function, are shown. Although modifications were made for both accelerated and non-accelerated curing conditions, only the accelerated formulations are relevant to this research and thus shown below.

Table 2-1: Kavanaugh Parameters Modified from Model Code 1990

Parameter	Original Formulation	KAV Modification
$\beta(f_{cm})$	$\frac{5.3}{(f_{cm}/f_{cmo})^{0.5}}$	$\frac{4.65}{(f_{cm}/f_{cmo})^{0.5}}$
$\beta(t_o)$	$\frac{1}{0.1+(t_o/t_1)^{0.2}}$	$\frac{1}{0.26+(t_o/t_1)^{0.18}}$
$\beta_c(t-t_o)$	$\left[\frac{(t-t_o)/t_1}{\beta_H+(t-t_o)/t_1}\right]^{0.3}$	$\left[\frac{(t-t_o)/t_1}{\beta_H+(t-t_o)/t_1}\right]^{0.35}$
t_T	$\sum_{i=1}^{n}\Delta t_i\, exp\left[13.65-\frac{4000}{273+\left(\frac{T(\Delta t_i)}{T_o}\right)}\right]$	$\sum_{i=1}^{n}\Delta t_i\, exp\left[18.47-\frac{5410}{273+\left(\frac{T(\Delta t_i)}{T_o}\right)}\right]$

The variables used in Table 2-1 are defined as follows:

f_{cm} is the mean compressive strength at 28 days (MPa)

f_{cmo} = 10 MPa

t_o is the age of concrete at loading

t_1 = 1 day

t is the age of concrete at the moment considered (days)

t_T is the temperature-adjusted concrete age

Δt_i is the number of days where temperature T prevails

$T(\Delta t_i)$ is the temperature (°C) during the time period Δt_i , and

T_o = 1°C.

It should be noted that the Kavanaugh modification to the temperature-adjusted age, t_T, is a single-step process to achieving the modified age and replaces the *combined* application of Equation 2-32 and Equation 2-33. In this method, Equation 2-33 does not apply. All other steps in MC 90, other than the changes listed, were followed as laid out in Section 2.3.5.

2.3.7 MC 90-99 CREEP PREDICTION METHOD

In 1990, CEB-FIP presented a creep and shrinkage model that was developed by Muller and Hilsdorf (1990) (Hassoun and Al-Manaseer 2012). In an effort to include provisions for both normal- and high-strength concretes, and to separate total shrinkage into its autogenous and drying shrinkage parts, CEB merged with FIP to become *fib* and released an update to MC 90 that is herein referred to as MC 90-99. This revised method remains consistent with ACI 209 in that it uses an ultimate creep coefficient that is corrected according to environmental conditions and mixture proportions.

The majority of the creep prediction procedure is executed in the same manner as in MC 90 with the exception of new coefficients that depend on the mean compressive strength of concrete. These are added to modify Equation 2-26 and Equation 2-31 such that:

$$\varphi_{\mathrm{RH}}(h) = \left[1 + \frac{1 - \left(\frac{h}{h_o}\right)}{\sqrt[3]{0.1\left(\frac{(V/S)}{(V/S)_o}\right)}}\alpha_1\right]\alpha_2 \qquad \textbf{Equation 2-34}$$

$$\beta_H = 150\left[1 + \left(1.2\frac{h}{h_o}\right)^{18}\right]\frac{(V/S)}{(V/S)_o} + 250\alpha_3 \leq 1500\alpha_3 \qquad \textbf{Equation 2-35}$$

and,

$$\alpha_1 = \left[\frac{3.5 f_{cmo}}{f_{cm28}}\right]^{0.7} \qquad \textbf{Equation 2-36}$$

$$\alpha_2 = \left[\frac{3.5 f_{cmo}}{f_{cm28}}\right]^{0.2} \qquad \textbf{Equation 2-37}$$

$$\alpha_3 = \left[\frac{3.5 f_{cmo}}{f_{cm28}}\right]^{0.5} \qquad \textbf{Equation 2-38}$$

where,

h is the relative humidity in decimals

$h_o = 1$

V/S is the volume-surface ratio (mm)

$V/S_o = 50$ mm

$f_{cmo} = 10$ MPa

f_{cm28} is the mean compressive strength at 28 days (MPa), and

h_o is the notional creep coefficient.

It should be noted that h is used to represent the humidity in MC 90-99, and not the nominal size as in MC 90.

All other steps in the calculation of the predicted creep strain, besides the changes noted, are to be followed as laid out in Section 2.3.5. This also includes the calculation of the temperature-adjusted age at loading which is detailed in Section 2.3.5.1.

2.3.8 MC 2010 CREEP PREDICTION METHOD

The CEB and FIP were two large international bodies aimed at combining research findings and creating a code that could gain international acceptance. By 2010, the Euro-International Concrete Committee (CEB) and the International Federation of Prestressing (FIP) had become the International Federation for Structural Concrete (*fib*) and released a new model code, MC 2010.

The creep prediction model in this code is much like its predecessor MC 90 with the adaptations of MC 90-99 to incorporate the use of high-strength concretes. Several variables have also been taken out or simplified by substituting 1.0 or 100% in their place. For simplicity, this method will be explained in its entirety to incorporate all of the changes.

The ultimate creep coefficient, $\varphi(t,t_o)$, may be computed from:

$$\varphi(t,t_o) = \varphi_o \cdot \beta_c(t,t_o) \qquad \textbf{Equation 2-39}$$

where,

φ_o is the notional creep coefficient

β_c is the coefficient describing development of creep with time after loading

t is the age of concrete at the moment considered (days), and

t_o is the age of concrete at loading.

The notional creep coefficient may be estimated from:

$$\varphi_o = \varphi_{RH} \cdot \beta(f_{cm}) \cdot \beta(t_o) \quad \textbf{Equation 2-40}$$

with,

$$\varphi_{RH} = \left[1 + \frac{1 - \left(\frac{RH}{100}\right)}{0.1 \cdot \sqrt[3]{h}} \cdot \alpha_1\right] \alpha_2 \quad \textbf{Equation 2-41}$$

$$\beta(f_{cm}) = \frac{16.8}{\sqrt{f_{cm}}} \quad \textbf{Equation 2-42}$$

$$\beta(t_o) = \frac{1}{0.1 + (t_o)^{0.2}} \quad \textbf{Equation 2-43}$$

where,

RH is the relative humidity of the environment (%)

h is the notional size of a member (mm), as defined in Equation 2-29

α is a strength factor defined in Equation 2-46 through Equation 2-48, and

f_{cm} is the mean compressive strength at 28 days (MPa).

The development of creep with time is given by

$$\beta_c(t, t_o) = \left[\frac{(t - t_o)}{\beta_H + (t - t_o)}\right]^{0.3} \quad \textbf{Equation 2-44}$$

where,

$$\beta_H = 1.5h\left[1 + \left(1.2\frac{RH}{100}\right)^{18}\right] + 250\alpha_3 \leq 1500\alpha_3 \quad \textbf{Equation 2-45}$$

α is a strength factor defined in Equation 2-46 through Equation 2-48

and all other factors are previously defined.

The strength factors used in Equation 2-41 and Equation 2-45 are calculated as follows:

$$\alpha_1 = \left(\frac{35}{f_{cm}}\right)^{0.7} \quad \textbf{Equation 2-46}$$

$$\alpha_2 = \left(\frac{35}{f_{cm}}\right)^{0.2} \quad \textbf{Equation 2-47}$$

$$\alpha_3 = \left(\frac{35}{f_{cm}}\right)^{0.5} \quad \textbf{Equation 2-48}$$

After determining the creep coefficient, the predicted creep strain can be obtained by multiplying $\varphi(t,t_o)$ by the elastic strain that resulted from loading as seen in Equation 2-11. The temperature-adjusted age at loading may also be calculated using Section 2.3.5.1 if specimens are exposed to temperatures other than 20ºC. However, in this method, the cement type factor, α, is given as

α = -1 for strength class 32.5N, 0 for strength classes 32.5R, 45.5N, and 1 for strength classes 42.5 R, 52.5N, 54.5R.

2.3.9 EUROCODE CREEP PREDICTION METHOD

In 1990, the introduction of the CEB-FIP MC 90 was a major step towards the coordination of an international code and became the basis for the *Eurocode Design of Concrete Structures* (2004), which is widely accepted in most European countries today (*fib* 2010). The 2004 release of Eurocode 2 uses the updated method for high-strength concrete that was adapted in MC 90-99, and thus Eurocode effectively uses the same procedures for the prediction of creep as are followed in MC 2010. Likewise, the effect of elevated or reduced temperatures on the maturity of concrete and the effect of cement type on the creep

coefficient may be accounted for by adjusting the concrete age as in Equation 2-32 and by using the modified age at loading as in Equation 2-33, respectively.

2.4 SHRINKAGE

Shrinkage is the time-dependent strain measured from an unloaded and unrestrained specimen. The two major components of shrinkage that are commonly presented in codes are drying shrinkage and autogenous shrinkage. Drying shrinkage can be defined as the volumetric change of concrete that occurs primarily due to the evaporation of water during the drying or curing process. This type of shrinkage is often the major contributor to the total shrinkage and occurs over time (Aly and Sanjayan 2008). Autogenous shrinkage is the shrinkage that occurs in the absence of moisture exchange and results from the chemical processes occurring within the concrete (ACI 209 2008). The shrinkage strain is usually presented as the sum of the drying and autogenous shrinkage.

As with creep, shrinkage increases the deformations of members and can cause a loss of prestress in prestressed elements. Shrinkage also plays a major role in serviceability issues such as cracking. Shrinkage can cause a gradual widening of existing cracks and, especially in flexural members, a substantial increase in deflections over time (Gilbert 2001). Shrinkage strain is affected by the cement, aggregate, water content, size of the concrete element, and ambient conditions (Nawy 2001).

2.5 SHRINKAGE PREDICTION METHODS

As mentioned previously, AASHTO 2010 is the reigning U.S. standard in highway bridge design. This specification makes allowances for its own shrinkage-prediction method as well as the use of other methods such as MC 90 and ACI 209. Since a new model code

was released in 2010 and NCHRP 628 recommended that AASHTO 2004 be modified for shrinkage of SCC, several other methods were investigated in this research as well. The following sections outline the procedures for nine shrinkage prediction methods, including commonly used U.S. and international methods. A concise explanation of how each of the methods work is also provided.

2.5.1 ACI 209 SHRINKAGE PREDICTION METHOD

Like the ACI 209 creep prediction method, the shrinkage prediction also relies on the concept of an ultimate value that is modified by a time-dependent development factor in order to yield the desired results (1992).

For circumstances other than standard conditions, the notional ultimate shrinkage strain, $(\varepsilon_{sh})_u$, is computed and modified with correction factors by the following equation:

$$(\varepsilon_{sh})_u = 780 \times 10^{-6}(\gamma_\lambda \cdot \gamma_{vs} \cdot \gamma_\psi \cdot \gamma_s \cdot \gamma_\alpha \cdot \gamma_c) \qquad \textbf{Equation 2-49}$$

where,

γ_λ is the relative humidity correction factor

γ_{vs} is the volume-to-surface-area ratio correction factor

γ_ψ is the fine aggregate percentage correction factor

γ_s is the slump correction factor

γ_α is the air content correction factor, and

γ_c is the cement content correction factor.

The ultimate shrinkage strain in Equation 2-49 is dependent on several correction factors including environmental conditions, specimen size, slump, and mixture proportioning. The correction factors are outlined in Equation 2-50 through Equation 2-57.

For ambient relative humidity greater than 40 percent, the correction factor γ_λ must be used. When the relative humidity falls in the range from 40 to 80 percent, Equation 2-50 should be used. When the relative humidity is greater than 80 percent but less than or equal to 100 percent, Equation 2-51 is required.

$$\gamma_\lambda = 1.4 - 0.0102\lambda \quad \text{for } 40\% \leq \lambda \leq 80\% \qquad \textbf{Equation 2-50}$$

$$\gamma_\lambda = 3 - 0.03\lambda \quad \text{for } 40\% < \lambda \leq 100\% \qquad \textbf{Equation 2-51}$$

where,

λ is the relative humidity (%)

The volume-to-surface-area ratio correction factor, γ_{vs} , is calculated for specimen with a volume-surface area ratio other than 1.5 inches or an average thickness other than 6 inches by the following equation:

$$\gamma_{vs} = 1.2(e^{-0.12(v/s)}) \qquad \textbf{Equation 2-52}$$

where,

v/s is the volume-to-surface area ratio (in.)

The fine aggregate percentage correction factor, γ_ψ , is determined by the following equations. For fine aggregate percentages between 40 and 60 percent, this factor is approximately equal to 1.0.

$$\gamma_\psi = 0.3 + 0.014\psi \quad \text{for } \psi \leq 50\% \qquad \textbf{Equation 2-53}$$

$$\gamma_\psi = 0.9 + 0.002\psi \quad \text{for } \psi > 50\% \qquad \textbf{Equation 2-54}$$

where,

ψ is the ratio of fine aggregate to total aggregate by weight (%)

The slump correction factor, γ_s , is calculated in accordance with Equation 2-55. For slump values less than 5 inches, this factor is within 10 percent of unity.

$$\gamma_s = 0.89 + 0.041s \qquad \textbf{Equation 2-55}$$

where,

s is the slump (in.).

Although it is not stated by ACI 209, application of this factor should be modified for concretes that contain water-reducing admixtures. A more complete discussion of this topic can be found in Section 4.3.1.

The air content correction factor, γ_α , is calculated using Equation 2-56. For air content less than 8 percent, this factor is approximately equal to 1.0.

$$\gamma_\alpha = 0.95 + 0.008\alpha \qquad \textbf{Equation 2-56}$$

where,

α is the air content (%).

The cement content correction factor, γ_α , is calculated using Equation 2-57:

$$\gamma_c = 0.75 + 0.00036c \qquad \textbf{Equation 2-57}$$

where,

c is the cement content (lb/yd^3).

Creep is not very sensitive to this factor. It remains within 10 percent of unity for cement contents ranging from 417 to 972 pcy. No guidance is given regarding the effects of cement replacement using supplementary cementing materials (SCMs).

To calculate the shrinkage time factor, which is the time parameter that accounts for the growth of shrinkage with the age of the concrete, Equation 2-58 is recommended for 7 days of non-accelerated curing and Equation 2-59 for 1 to 3 days of accelerated curing.

$$(\varepsilon_{sh})_t = \frac{t}{35 + t} \qquad \textbf{Equation 2-58}$$

$$(\varepsilon_{sh})_t = \frac{t}{55 + t} \qquad \textbf{Equation 2-59}$$

where,

t is the time from the end of the initial curing (days).

Note that the above equations are only applicable to loading ages later than 7 days for non-accelerated-cured concrete samples and later than 1 to 3 days for accelerated-cured samples.

After determining the shrinkage time factor, the total shrinkage strain at a specific age can be predicted by multiplying the time factor by ultimate shrinkage strain.

$$Predicted\ Shrinkage, \varepsilon_{sh}(t) = (\varepsilon_{sh})_t \times (\varepsilon_{sh})_u \qquad \textbf{Equation 2-60}$$

2.5.2 AASHTO 2004 SHRINKAGE PREDICTION METHOD

The shrinkage prediction method in AASHTO 2004 (and earlier) is affected by parameters such as aggregate characteristics, humidity and curing type. This method is recommended for the prediction of shrinkage strain in bridges other than segmentally

constructed ones, but AASHTO suggests that large concrete members may experience considerably less shrinkage than that measured by laboratory tests of small specimens of the same concrete.

For non-accelerated cured concretes that are void of shrinkage-prone aggregates, the strain due to shrinkage is computed by the following equation:

$$\varepsilon_{sh} = -k_s \cdot k_h \left(\frac{t}{35+t}\right) 0.51 \times 10^{-3} \qquad \textbf{Equation 2-61}$$

If non-accelerated cured concretes are exposed to drying before five days of curing have past, the shrinkage in Equation 2-61 should be increased by 20 percent.

For accelerated-cured concretes:

$$\varepsilon_{sh} = -k_s \cdot k_h \left(\frac{t}{55+t}\right) 0.56 \times 10^{-3} \qquad \textbf{Equation 2-62}$$

where,

k_s is the volume-to-surface area ratio correction factor

k_h is the relative humidity correction factor, and

t is the time since drying began (days).

The volume-surface ratio correction factor is obtained from Equation 2-63, which was replicated in AASHTO 2004 from the PCI manual for Structural Design of Architectural Precast Concrete (1977). However, it should be noted that the maximum $^{V}/_{S}$ ratio considered in the development of this factor was 6.0 inches and the surface area used in determining k_s should only include the area that is exposed to the atmosphere for drying.

$$k_s = \left[\frac{\frac{t}{26e^{0.36(V/S)}+t}}{\frac{t}{45+t}}\right]\left[\frac{1064-94(V/S)}{923}\right] \qquad \textbf{Equation 2-63}$$

where,

$^{V}/_{S}$ is the volume-to-surface area ratio (in.).

The relative humidity correction factor may be approximated by:

$$k_h = \frac{140 - H}{70} \quad \text{for H < 80 \%} \qquad \textbf{Equation 2-64}$$

$$k_h = \frac{3(100 - H)}{70} \quad \text{for H ≥ 80 \%} \qquad \textbf{Equation 2-65}$$

where,

H is the relative humidity (%).

As mentioned previously, AASHTO recommends that when mixture-specific properties are not available, the shrinkage may be estimated using the CEB-FIP model code or ACI 209.

2.5.3 AASHTO 2010 SHRINKAGE PREDICTION METHOD

The shrinkage prediction method currently specified in the AASHTO LRFD (AASHTO 2010) specification should be used to determine the effects of creep on the loss of prestressing force in bridges other than segmentally constructed ones. This method was created based on the findings of Huo et al. (2001), Al-Omaishi (2001), Tadros (2003), Collins and Mitchell (1991), recommendations by ACI Committee 209, and other recently published data (AASHTO 2010).

The provisions of AASHTO 2010 are applicable to specified concrete strengths up to 15.0 ksi, and shrinkage is influenced by aggregate characteristics and proportions, curing method, average humidity, volume-surface ratio of a member, and drying duration.

For concretes that are void of shrinkage-prone aggregates, the strain due to shrinkage at time *t* after exposure to drying is computed according to the following equation:

$$\varepsilon_{sh} = k_{hs} \cdot k_s \cdot k_f \cdot k_{td} \cdot 0.48 \times 10^{-3} \qquad \textbf{Equation 2-66}$$

where,

k_{hs} is the relative humidity correction factor

k_s is the volume-to-surface-area ratio correction factor

k_f is the concrete strength correction factor, and

k_{td} is the time development correction factor.

The relative humidity correction factor for shrinkage may be taken as:

$$k_{hs} = 2.0 - 0.014H \qquad \textbf{Equation 2-67}$$

where,

H is the relative humidity (%).

The factor for the effect of the volume-surface ratio of the specimen, k_s, the concrete strength correction factor, k_f, and time development correction factor, k_{td}, are all calculated exactly as in the creep prediction method and are given by Equation 2-17, Equation 2-18, and Equation 2-19, respectively.

If the concrete is exposed to drying before 5 days of curing have elapsed, AASHTO 2010 recommends that the shrinkage strain be increased by 20 percent. Because this wording was carried over directly from the earlier AASHTO (2004) provisions, it is believed that this refers to 5 days of *non-accelerated* curing, which was the standard measurement of days in the earlier provisions.

The AASHTO 2010 model also recommends that when mixture-specific properties are not available, the shrinkage may be estimated using the CEB-FIP model code or ACI 209.

2.5.4 NCHRP 628 SHRINKAGE PREDICTION METHOD

The NCHRP Report 628 proposes changes to the *AASHTO LRFD Bridge Design Specifications* for the prediction of creep and shrinkage when self-consolidating concrete mixtures are used. Other than the changes listed below, or when CVC mixtures are used, the AASHTO 2004 method should be followed when predicting shrinkage strain.

The strain due to shrinkage for accelerated-cured concrete may be taken as:

$$\varepsilon_{sh} = -k_s \cdot k_h \left(\frac{t}{55+t}\right) 0.56 \times 10^{-3} \times A \qquad \textbf{Equation 2-68}$$

where,

k_s is the size factor

k_h is the relative humidity factor, as calculated in Equation 2-67

t is the drying time (days); time considered – end of curing, and

A is the cement factor for SCC only:

A = 0.918 for Type I/II cement

= 1.065 for Type III + 20% FA binder, which may be used for P(SCC).

The size factor, which is an adaptation from the older AASHTO model (AASHTO 2004), should be calculated as:

$$k_s = \left[\frac{t}{\frac{26e^{0.0142(V/S)}+t}{45+t}}\right]\left[\frac{1064 - 3.70\left(V/S\right)}{923}\right] \qquad \textbf{Equation 2-69}$$

where,

$^{V}/_{S}$ is the volume-to-surface area ratio (mm).

2.5.5 MC 90 Shrinkage Prediction Method

The MC 90 model for shrinkage predicts the mean behavior of a concrete cross section. In this method, shrinkage does not depend on concrete compressive strength, rather it is more affected by cement content and water-cement ratio. MC 90 is valid for ordinary concrete that is subjected to standard conditions, unless special provisions are given.

The total shrinkage or swelling strain, $\varepsilon_{cs}(t,t_s)$, is computed by the following equation:

$$\varepsilon_{cs}(t, t_s) = \varepsilon_{cso} \cdot \beta_s(t - t_s) \qquad \textbf{Equation 2-70}$$

where,

ε_{cso} is the notional shrinkage coefficient

β_s is the coefficient that describes shrinkage with time

t is the age of the concrete at the moment considered (days), and

t_s is the age at the start of shrinkage (days); normally at the end of curing.

The notional shrinkage coefficient is given by:

$$\varepsilon_{cso} = \varepsilon_s(f_{cm})\beta_{RH} \qquad \textbf{Equation 2-71}$$

with,

$$\varepsilon_s(f_{cm}) = \left[160 + 10 \cdot \beta_{sc}\left(9 - \frac{f_{cm}}{f_{cmo}}\right)\right] 10^6 \qquad \textbf{Equation 2-72}$$

where,

f_{cm} is the mean compressive strength at 28 days (MPa)

f_{cmo} = 10 MPa

β_{sc} is the cement type coefficient:

β_{sc} = 4 for slow hardening concrete (SL)

= 5 for normal or rapid hardening concrete (N or R)

= 8 for rapid hardening high-strength concrete (RS)

and,

$$\beta_{RH} = -1.55\beta_{SRH} \quad \text{for } 40\ \% \leq \text{RH} \leq 99\ \% \qquad \textbf{Equation 2-73}$$

$$\beta_{RH} = 0.25 \quad \text{for RH} \geq 99\ \% \qquad \textbf{Equation 2-74}$$

with,

$$\beta_{SRH} = 1 - \left(\frac{RH}{RH_o}\right)^3 \qquad \textbf{Equation 2-75}$$

where,

RH is the ambient relative humidity (%), and

RH_o = 100 %.

The development of shrinkage with time is obtained from:

$$\beta_s(t - t_s) = \left[\frac{(t - t_s)/t_1}{350\left(h/h_o\right)^2 + (t - t_s)/t_1}\right]^{0.5} \qquad \textbf{Equation 2-76}$$

where,

h is the notional size of the member (mm), defined in Equation 2-30

t_1 = 1 day, and

h_o = 100 mm.

Unlike the MC 90 method for predicting creep, the shrinkage predictions do not depend on the maturity of the concrete.

2.5.6 MC 90-99 SHRINKAGE PREDICTION METHOD

In 1998, the CEB and the FIP committees both dissolved in favor of becoming one committee known as the *fib*. In 1999, the *fib* revised the MC 90 shrinkage prediction method in order to more accurately reflect the effects of high-strength concrete and to separate the total shrinkage into autogenous and drying shrinkage components. In this updated model, MC 90-99, the drying shrinkage component is closely related to the original MC 90 method. However, for autogenous shrinkage, new relations were included for normal- and high-performance concretes (ACI 1992).

The total shrinkage of concrete is given by:

$$\varepsilon_{sh}(t, t_c) = \varepsilon_{cas}(t) + \varepsilon_{cds}(t, t_c) \qquad \textbf{Equation 2-77}$$

where,

ε_{cas} is the autogenous shrinkage strain

ε_{cds} is the drying shrinkage strain

t is the age of concrete at the moment considered (days), and

t_c is the age of concrete at the beginning of drying (days).

The autogenous shrinkage component is developed from:

$$\varepsilon_{cas}(t) = \varepsilon_{caso}(f_{cm28}) \cdot \beta_{as}(t) \qquad \textbf{Equation 2-78}$$

where,

$\varepsilon_{cas}(f_{cm28})$ is the notional autogenous coefficient, and

$\beta_{as}(t)$ is the function describing autogenous shrinkage over time.

The notional autogenous shrinkage coefficient is defined by:

$$\varepsilon_{caso}(f_{cm28}) = -\alpha_{as}\left(\frac{f_{cm28}/f_{cmo}}{6 + f_{cm28}/f_{cmo}}\right)^{2.5} \times 10^{-6} \qquad \textbf{Equation 2-79}$$

where,

f_{cm28} is the concrete mean compressive strength at 28 days (MPa)

f_{cmo} = 10 MPa, and

α_{as} is the cement type coefficient, defined in Table 2-2.

The function describing the time development of autogenous shrinkage is given by:

$$\beta_{as}(t) = 1 - exp\left[-0.2\left(\frac{t}{t_1}\right)^{0.5}\right] \qquad \textbf{Equation 2-80}$$

where,

t_1 = 1 day.

The drying portion of the total shrinkage strain is defined by:

$$\varepsilon_{cds}(t, t_c) = \varepsilon_{cdso}(f_{cm28}) \cdot \beta_{RH}(h) \cdot \beta_{ds}(t - t_c) \qquad \textbf{Equation 2-81}$$

where,

$\varepsilon_{cdso}(f_{cm28})$ is the notional drying coefficient

$\beta_{RH}(h)$ is the function influenced by the relative humidity, and

$\beta_{ds}(t\text{-}t_c)$ is the function describing the development of shrinkage with time.

The notional drying coefficient is defined as:

$$\varepsilon_{cdso}(f_{cm28}) = \left[(220 + 110\alpha_{ds1})exp\left(-\alpha_{ds2} \cdot \frac{f_{cm28}}{f_{cmo}}\right)\right] 10^{-6} \quad \textbf{Equation 2-82}$$

where,

α_{ds1} and α_{ds2} are the cement type coefficients, defined in Table 2-2.

Table 2-2: Coefficients for Equation 2-79 and Equation 2-82 (ACI 1992)

Type of cement according to EC2	α_{as}	α_{ds1}	α_{ds2}
SL (slowly-hardening cements)	800	3	0.13
N or R (normal or rapid hardening cements)	700	4	0.12
RS (rapid hardening high-strength cements)	600	6	0.12

The effects of relative humidity on shrinkage are given by:

$$\beta_{RH}(h) = -1.55\left[1 - \left(\frac{h}{h_o}\right)^3\right] \quad \text{for } 0.4 \leq h \leq 0.99\beta_{s1} \quad \textbf{Equation 2-83}$$

$$\beta_{RH}(h) = 0.25 \quad \text{for } h \geq 0.99\beta_{s1} \quad \textbf{Equation 2-84}$$

with,

$$\beta_{s1} = \left(\frac{3.5 f_{cmo}}{f_{cm28}}\right)^{0.1} \leq 1.0 \quad \textbf{Equation 2-85}$$

where,

h is the ambient relative humidity as a decimal

h_o = 1, and

β_{s1} is a coefficient describing the self-desiccation in high-performance concrete.

The function describing the time development of drying shrinkage is defined as:

$$\beta_{ds}(t-t_c) = \left[\frac{(t-t_c)/t_1}{350\left[\frac{V/S}{V/S_o}\right]^2 + (t-t_c)/t_1}\right]^{0.5} \qquad \textbf{Equation 2-86}$$

where,

V/S is the volume-to-surface area ratio (mm), and

V/S_o = 50 mm.

The drying shrinkage predictions do not depend on the maturity (or strength) of the concrete.

2.5.7 MC 2010 Shrinkage Prediction Method

In 2010, the International Federation for Structural Concrete (*fib*) released a new model code, MC 2010, which was much like MC 90-99. The shrinkage prediction model of MC 90-99 had previously been modified to incorporate the use of high-strength concretes and to separate the total shrinkage into autogenous and drying shrinkage. The new model code, MC 2010, also includes these changes and is approximately equal to MC 90-99 in the prediction of shrinkage strain.

2.5.8 EUROCODE SHRINKAGE PREDICTION METHOD

The portion of the Structural Eurocode program which deals in the design of concrete structures is Eurocode 2. Similar to the *fib* model, the Eurocode separates the total shrinkage strain into two components: the drying shrinkage, which develops slowly, and the autogenous shrinkage, which develops in the early stages of hardening.

The total shrinkage strain follows from:

$$\varepsilon_{cs} = \varepsilon_{cd} + \varepsilon_{ca} \qquad \textbf{Equation 2-87}$$

where,

ε_{cs} is the total shrinkage strain

ε_{cd} is the drying shrinkage strain, and

ε_{ca} is the autogenous shrinkage strain.

The drying shrinkage develops over time from:

$$\varepsilon_{cd}(t) = \beta_{ds}(t, t_s) \cdot k_h \cdot \varepsilon_{cd,0} \qquad \textbf{Equation 2-88}$$

where,

β_{ds} is the function describing the shrinkage development with time

k_h is a coefficient depending on the notional size h_0 according to Table 2-3, and Table 2-3$\varepsilon_{cd,0}$ is the basic drying shrinkage strain.

The component describing the development of shrinkage with time is given by:

$$\beta_{ds}(t, t_s) = \frac{(t - t_s)}{(t - t_s) + 0.04\sqrt{{h_0}^3}} \qquad \textbf{Equation 2-89}$$

where,

t is the age of the concrete at the moment considered (days)

t_s is the age of the concrete at the beginning of drying (days), and

h_0 is the notional size of the cross-section (mm); defined in Equation 2-29.

Table 2-3: Values for k_h (CEN 2004)

h_o (mm)	k_h
100	1.0
200	0.85
300	0.75
≥ 500	0.70

The basic drying shrinkage strain is given by:

$$\varepsilon_{cd,0} = 0.85\left[(220 + 110\alpha_{ds1})exp\left(-\alpha_{ds2}\cdot\frac{f_{cm}}{f_{cmo}}\right)\right]10^{-6}\cdot\beta_{RH} \quad \textbf{Equation 2-90}$$

where,

α_{ds1} and α_{ds2} are the cement type coefficients, defined in Table 2-4

f_{cm} is the mean compressive strength (MPa), and

f_{cmo} = 10 MPa.

Table 2-4: Coefficients for Equation 2-90

Cement Class	α_{ds1}	α_{ds2}
S (CEN 32.5N)	3	0.13
N (CEN 32.5R and 42.5N)	4	0.12
R (CEN 42.5R, 52.5N, and 52.5R)	6	0.11

The effects of relative humidity on shrinkage are given by:

$$\beta_{RH} = 1.55\left[1 - \left(\frac{RH}{RH_o}\right)^3\right] \quad \textbf{Equation 2-91}$$

where,

RH is the ambient relative humidity (%), and

RH_o = 100 %.

The autogenous shrinkage follows from:

$$\varepsilon_{ca}(t) = \beta_{as}(t) \cdot \varepsilon_{ca}(\infty) \quad \textbf{Equation 2-92}$$

where,

$$\beta_{as}(t) = 1 - exp(-0.2t^{0.5}) \quad \textbf{Equation 2-93}$$

$\varepsilon_{ca}(\infty) = 2.5(f_{ck} - 10) \times 10^{-6}$, and **Equation 2-94**

f_{ck} is the specified compressive strength at time *t*.

Again, the shrinkage predictions do not depend on the maturity (or strength) of the concrete.

2.6 FACTORS AFFECTING CREEP AND SHRINKAGE

There are several factors that affect the time-dependent strain due to creep and shrinkage of concrete. These factors include, but are not limited to, the aggregate type and content, cement content, environmental conditions, curing age, age at loading, drying age, and compressive strength of concrete. These factors may also be affected by whether the concrete is self-consolidating or conventional concrete. Each of these is discussed in the following sections.

2.6.1 AGGREGATE CONTENT AND TYPE

In concrete mixtures, the aggregate acts to restrain the creep and shrinkage of the cement paste (Nawy 1996). The degree of restraint of a concrete is determined by the aggregate properties; aggregates with rough surfaces or high elastic moduli are more resistant to shrinkage (Nawy 2001). Concrete mixtures with hard coarse aggregates may also experience a reduced amount of creep as compared to mixtures with soft coarse aggregates (Mokhtarzadeh and French 2000). Collins and Mitchell (1991) also indicate that hard, dense aggregates of low absorption result in less shrinkage. However, in self-consolidating concrete where large aggregates could compromise flow and compaction, which are both essential to SCC, one study suggests that SCC may experience higher creep due to the higher paste volume and lower coarse aggregate content (Long and Khayat 2011). Furthermore, other research indicates that a high coarse to total aggregate ratio does not always lead to less drying shrinkage in SCC; rather, a balance must be found between the aggregate size and degree of compaction of the mixture (Bui and Montgomery 1999). While most research indicates that aggregate type, size, and content have a major influence on the creep and shrinkage properties of concrete, ACI 209 is the only prediction model that includes a parameter for aggregate content; specifically the ratio of fine to total aggregate by weight.

2.6.2 CEMENT CONTENT AND COMPOSITION

Ground granulated blast-furnace slag (GGBS) is a pozzolanic material that can be used as a supplementary cementing material (SCM) in order to improve the performance characteristics of concrete such as workability, strength, and volume change properties (Babu

and Kumar 2000). This material has enough cementitious properties that GGBS has been designated “slag cement”.

Slag cement can especially have an effect on shrinkage when added to a cement mixture. Some research suggests that rapid-hardening cements, which generally contain more SCMs, usually tend to shrink more than other types of cement. However, Aly and Sanjayan (2008) showed that concrete mixtures containing slag cement exhibit an expansion within the curing period, which leads to lessened total shrinkage than mixtures that do not contain slag cement. Research efforts, such as those conducted by Saric-Coric and Aïtcin (2003) and Jianyong and Yan (2001), also concluded that drying shrinkage is reduced greatly when a portion of the cement is replaced by GGBS. In addition to affecting the shrinkage, Jianyong and Pei (1997) also suggest that GGBS (or slag cement) can improve a concrete’s long-term compressive strength, which can also lead to a reduction in creep.

In addition to the slag cement used in this research, there are many other supplementary materials that can increase or decrease the shrinkage of concrete. Class C fly ash is one of the most common SCMs used in self-consolidating concrete in the Alabama prestressed industry (Schindler et al. 2007). The NCHRP 628, which suggests modifications to the AASHTO LRFD method, tested three binder types for SCC including two mixtures with 30% slag replacement and one with 20% fly ash. This study showed that the mixture with fly ash developed high filling capacity and higher compressive strength, and was therefore selected for the preferred mixture for that research (NCHRP 628 2009). Figure 2-2 shows that Jianyong and Yan (2001) concluded that when using high-performance concrete, creep is reduced by replacing 30% of the cement with GGBS (“Concrete B”), and is further reduced

by replacing another 10% of the cement with fly ash ("Concrete C"). Similarly, Figure 2-3 also shows a reduction in shrinkage when these SCMs are added.

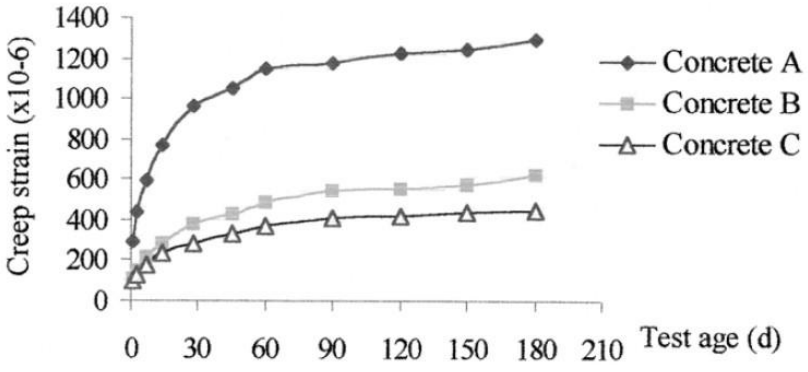

Figure 2-2: Development of Creep of Concrete (Jianyong and Yan 2001)

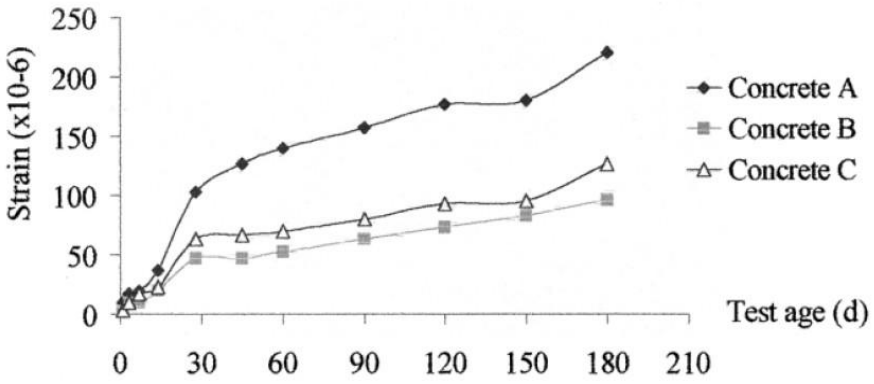

Figure 2-3: Results of Drying Shrinkage Test of Concrete (Jianyong and Yan 2001)

A study by Levy, Barnes, and Schindler (2010) compared SCC mixtures with fly ash (SCC-MA and SCC-HA) and SCC mixtures with slag cement (SCC-MS and SCC-HS) to a control CVC mixture. This research found that both the mixtures using fly ash and the mixtures using slag cement experienced less creep and shrinkage than the control mixture.

However, as seen in Figure 2-4 and Figure 2-5, the GGBS specimens experienced less creep and shrinkage than the specimens utilizing fly ash.

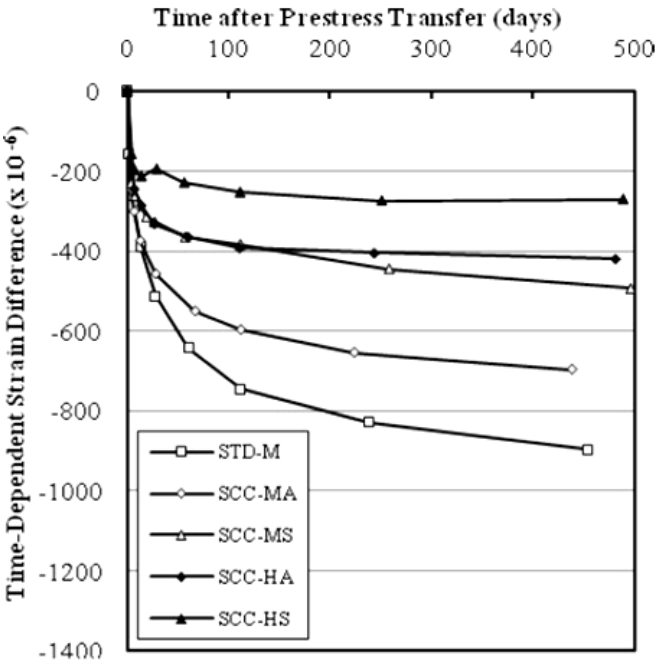

Figure 2-4: Creep Strain versus Time (Levy, Barnes, and Schindler 2010)

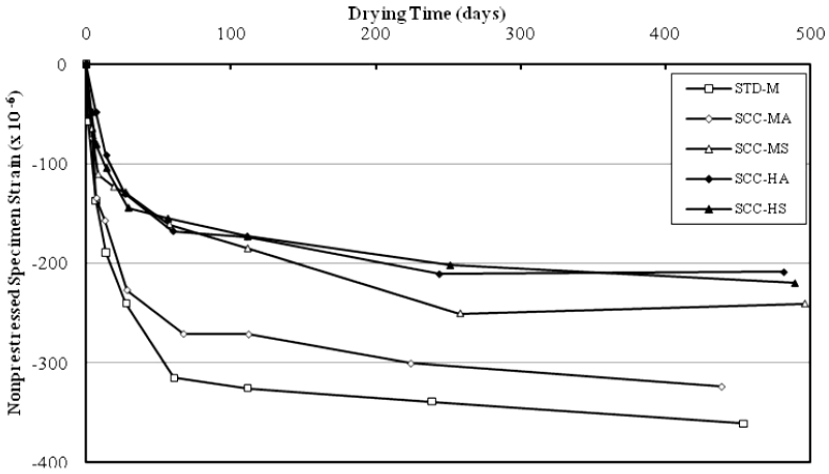

Figure 2-5: Shrinkage Strain versus Time (Levy, Barnes, and Schindler 2010)

With this alteration in the volume-changing properties of concrete, it is surprising that the ACI 209 is the only method that utilizes a parameter for cement content in predicting the shrinkage of concrete and that no prediction model accounts specifically for the type or quantity of SCMs.

2.6.3 Environmental Conditions

The two main environmental conditions that affect the creep and shrinkage of concrete are temperature and humidity. Bažant (2004) proposed that the effect of temperature on creep is generated by two mechanisms. An increase in temperature accelerates cement hydration and thus the aging of concrete, which can reduce the creep rate. However, this same research suggests that an increase in temperature can also speed up the bond breakage and restoration which increases the creep rate and normally prevails over the former effect causing an overall increase in creep. Mokhtarzadeh and French (2000) also agree, reporting that specimens cured at higher temperatures experienced higher creep. In regards to humidity, Nawy (2001) suggests that lowering the relative humidity before applying the load could result in lower creep strain.

The shrinkage of a specimen is due primarily to the loss of moisture within the concrete mixture and thus, is greatly affected by temperature and humidity. While shrinkage tends to stabilize at relatively low temperatures, the relative humidity has an inverse effect on the magnitude of shrinkage of a specimen (Nawy 2006). At high relative humidity, the rate of shrinkage is much lower due to the decrease in the tendency of moisture to escape the concrete. Research by Shams and Kahn (2000) also supports that shrinkage decreases as relative humidity increases.

Each prediction method presented in this study accounts for the humidity of the environment by utilizing a correction factor for relative humidity. This correction factor directly impacts the ultimate creep coefficient and the ultimate shrinkage strain for the predictions. In addition to this, each of the European codes also uses the humidity for the calculation of a combined humidity and size coefficient for creep. This could suggest that the European codes are more heavily influenced by relative humidity when it comes to the prediction of creep than other models. In contrast, although the codes specify a standard temperature range for test specimens, the long-term temperature is not directly called upon in any calculation for the prediction of creep and shrinkage in any of the methods. Temperature during curing is used to compute equivalent age at loading in the European creep prediction methods.

2.6.4 Curing Duration and Age at Loading

The amount of time that specimens are allowed to cure and the age at which a load is applied are events that are extremely significant to the effects of creep and shrinkage on concrete. It should also be noted that the age *at* loading is a different parameter than the age *of* the load. The age *of* the load is the duration the load has been applied to the concrete.

The age at loading is critical to the creep strain (which is dependent on the load) because older concrete, or concrete that is more mature at the time of loading, experiences less creep strain (Nawy 2001). This could be due to the fact that compressive strength develops as the concrete matures, and higher compressive strengths at loading can result in lower creep (Mokhtarzadeh and French 2000). The curing duration also plays a role in the maturity because the longer the concrete cures, the older or more mature the concrete becomes before loading, thus developing a higher strength and resistance to creep.

The loading age is typically utilized in the prediction models one of two ways. The first is the chronological age of the concrete when loading occurs and the second is by calculating the maturity or equivalent age at loading. The methods that utilize the chronological age at loading in the prediction of creep are ACI 209, both AASHTO models, and NCHRP. All of the European methods, including MC 90-KAV, account for the age at loading indirectly by utilizing the maturity of the concrete at loading for the prediction of creep. By computing the maturity, these methods also indirectly account for the type of curing. This is because the maturity is computed by utilizing the temperature history of a specimen, as seen in Section 2.3.5.1 and applied in Section 4.2.4, which is comprised of temperature readings throughout the entire curing cycle. Each type of curing creates a different temperature history and will have a different maturity.

Again, the longer the curing duration, the more mature the concrete becomes, which can also have a significant impact on shrinkage. Autogenous or chemical shrinkage is a volumetric change that occurs without an exchange of water to the surrounding environment and is heavily influenced by the degree of hydration (Aly and Sanjayan 2008). The longer concrete is allowed to cure, the more water is utilized for hydration during the curing process. Aly and Sanjayan (2008) state that when curing is extended, "less water is available at later ages for drying and lower shrinkage occurs" long term. If the drying shrinkage (which is often the largest contributor to total shrinkage) is the volumetric change of concrete that occurs due to the evaporation of water during the drying or curing process, it stands to reason that the longer the curing duration, the more water is utilized during hydration and less water is available to lose when drying shrinkage occurs. Also, extended curing times are especially

recommended for concretes containing SCMs because these supplementary materials have slower hydration reactions (Aly and Sanjayan 2008).

ACI 209 incorporates a table of values for the correction for curing durations other than 7 days of non-accelerated curing for shrinkage prediction. This factor is not addressed for accelerated curing. This is one of the only methods that does not provide information on how to handle accelerated curing outside of the "standard" duration of 1 to 3 days.

Both AASHTO LRFD methods also include a shrinkage correction for "short" curing periods. This increase of 20% is employed for non-accelerated curing periods less than 5 days. This 20-percent increase could be interpreted as also applying to accelerated curing periods of less than 5/7 of a day because the AASHTO codes equate 1 day of accelerated curing to 7 days of non-accelerated curing.

In the European models, neither the drying shrinkage nor the autogenous shrinkage depends on the duration or type of curing. In these models, the predicted shrinkage (autogenous and drying) will be the same whether the concrete equivalent age at the end of curing is 1 day, 1 month, or 1 year.

2.6.5 COMPRESSIVE STRENGTH

Studies have shown that concrete mixtures with higher compressive strength can experience less creep than lower strength concrete mixtures (Hinkle 2006). Research by Hans-Eric and Pentti (1999) showed that for concrete suitable for bridge construction, the compressive strength of SCC increases up to 35% at 1 day, and up to 40% at 28 days, compared to CVC. This research indicates that SCC may have a lesser tendency for creep than CVC. On the other hand, in practice, concrete mixtures are proportioned based on

strength. In order to obtain a more equitable comparison, the creep should be measured for SCC and CVC at the same compressive strength level.

AASHTO 2010 and NCHRP 628 use the compressive strength at transfer for the prediction of creep and shrinkage while all other considered methods, except ACI 209, use the 28-day compressive strength. ACI 209 does not directly consider the effects of compressive strength on creep or shrinkage; rather, it considers the characteristics of the concrete mixture itself. In effect, for the prediction of creep and shrinkage, all methods (excluding the shrinkage predicted by AASHTO 2004) consider the strength of the concrete either explicitly, by utilizing the compressive strength, or indirectly, by utilizing the concrete composition. AASHTO 2004 is the only method that does not consider the strength or the mixture properties at all for the prediction of shrinkage.

2.7 PREVIOUS STUDIES ON CREEP AND SHRINKAGE OF SCC

Because self-consolidating concrete is relatively new and has yet to gain widespread acceptance, there is limited information available for the creep and shrinkage behavior of SCC, especially its long-term behavior. However, because this type of concrete is attractive in many applications, there has been a push to move towards SCC in recent years. As a result, more studies have been undertaken to examine the properties of SCC.

As mentioned in previous sections, one concern is formed based on the concrete aggregate size and fine aggregate content. In contrast to conventional concrete, SCC is created by decreasing the amount of coarse aggregate and increasing the amount of fine material in order to achieve the flowability and passability that is desired for the use in congested prestressed members. However, according to ACI Committee 209 (1992), drying shrinkage increases as the sand-to-total aggregate ratio (S/Agg) increases. This implies that

the total drying shrinkage of SCC is higher than that of similar CVC. Another consequence to the reduction in total aggregate content is that it necessitates the use of a higher volume of cement which can increase the cost and temperature; however, this is not true if the amount of coarse aggregate is simply replaced by fine aggregate. SCC often contains high-volume replacements of SCM such as fly ash, slag cement, limestone filler, or stone dust to enhance fluidity and cohesiveness and limit heat generation (Khayat et al. 1999).

Typically, it is believed that SCC has a higher creep rate than that of conventional concrete. Still, there is some debate in literature regarding the creep behavior of SCC versus CVC. Long and Khayat (2011) indicate that with similar water-to-cement ratios, SCC developed up to 20% higher creep strains after 11 months than those of the evaluated HPC mixtures. This was thought to be due to the coarse aggregate content and degree of restraint known to high-performance mixtures (Long and Khayat 2011). Other researchers found that the creep results of SCC did not differ significantly from those of CVC (Persson 1999) if the compressive strength was held constant. Levy, Barnes, and Schindler (2010) also found that the deformations (both creep and shrinkage) of SCC were no larger than those of CVC at similar compressive strength levels. Still other research claims that at 135 days, for the same binder and aggregate content, SCC mixtures, which were proportioned with a 0.54 water binder ratio with fly ash, presented a 35% lower creep than CVC (Hauke 2001).

MC 90-KAV, which is one of the prediction models investigated in this research, developed from a study on creep behavior of SCC. This research, conducted by Kavanaugh (2008), tested four SCC mixtures with varying water-to-cement ratios and two types of SCMs: Class C fly ash and GGBS (now designated as slag cement). When accelerated curing was used, Kavanaugh found that the creep of all the SCC mixtures was less than creep of the

conventional-slump mixture. This research also indicated that at a fixed water-to-cementitious materials ratio, SCC mixtures made with GGBS exhibited less creep than those made with fly ash. Another goal of this study was to test five creep prediction models for accuracy. Those tested were ACI 209, AASHTO 2007 (AASHTO 2010 in this thesis), CEB 90 (or MC 90 in this thesis), GL 2000, and B3. Kavanaugh found that, overall, the CEB 90 was the most accurate of the models investigated and thus, this method was modified to make it even more precise for the concrete used in that research. However, Kavanaugh did not apply the full, two-step age-modification process described in Section 2.3.5.1 of this thesis that is prescribed in MC 90. Rather, only Equation 2-32 was used. Because the experimental results were not compared to predications computed according to the prescribed MC 90 process, the findings of the Kavanaugh research, where comparison to the MC 90 prediction model is concerned, may not be valid.

Just as there are discrepancies over creep, some authors point out that shrinkage is higher in SCC than in CVC while others, such as Schindler et al. (2007), report finding no significant difference between the two. Some even found lower shrinkage in SCC. On the other hand, each of these studies used different mixtures with various degrees of additives which alter concrete's fresh and hardened properties. Some concrete mixtures containing SCMs such as silica fume or slag (Horta 2005) were found to have increased shrinkage. However, the addition of fly ash or limestone filler has shown to reduce the autogenous and drying shrinkage (Valcuende et al. 2012; Khayat 1999). Another consideration is the length of the study. Persson (2001) reported that after one and a half years of testing, there were similar results for drying shrinkage of SCC and CVC when the strength was held constant.

This was believed to be because the strength of the concrete is a reflection of the concrete's porosity, which affects drying shrinkage.

2.8 SUMMARY

Limited information is available on the creep and shrinkage behavior of self-consolidating concrete, which is becoming increasingly popular in prestressed concrete applications. Nonetheless, creep and shrinkage have a significant impact on the performance of concrete structures by affecting deflections, serviceability, and loss of prestress. Because of this, it is imperative to be able to predict the creep and shrinkage behavior of concrete with some degree of accuracy. Proper understanding of SCC and its properties should be of interest for the design of safe, cost-effective concrete members, including those which are prestressed. Even though there are a variety of methods available for the prediction of creep and shrinkage, the present study is focused on determining which is most accurate for ALDOT bridge girder concrete and if the methods are as accurate for SCC as they are for CVC.

CHAPTER 3
EXPERIMENTAL PROGRAM

3.1 INTRODUCTION

While casting the girders for the four-span bridge in Tallapoosa County, Alabama, concrete test cylinders were cast from batches of concrete that were placed in the girders. Concrete was sampled from five girders, and two curing types were used for each set of sampled concrete to create ten groups of specimens for creep testing. When the casting and curing of a set of specimens for a particular girder was complete, the second phase for those cylinders began. This next phase consisted of the testing of each mixture for the effects of creep and shrinkage. This chapter explains in detail the procedures that were used in the production and testing of specimens during this study. Included is the production of specimens, the preparation of specimens for testing, determination of the required load, the application of this load, and the collection of data.

3.2 GIRDER PRODUCTION

In the fall of 2010, the production of twenty-eight PCI Bulb-Tee girders began for the demonstration bridge over Hillabee Creek in Tallapoosa County, Alabama. This section details the production of the concrete members and test specimens, the fitting of the girders and test cylinders with instrumentation, and the curing regimes that were used during the course of this study.

3.2.1 FABRICATION OF GIRDERS AND TEST SPECIMENS

During the production of the precast, prestressed bulb-tee girders, two girder sizes were cast: a 54 in. girder (BT-54) and a 72 in. girder (BT-72). Both girder sizes were fabricated with a 15 degree skew in order to fit the orientation of the bridge once constructed. The BT-54 girders were 97 ft 10 in. in length and the BT-72 girders were 134 ft 2 in. Each girder was constructed as described in detail by Dunham (2011).

Once, the production of the bridge girders began, representative concrete test cylinders were also constructed using batches of concrete placed in the girders. This was done in order to test the creep and shrinkage of the concrete mixtures under controlled laboratory conditions. Each of the girders and test specimens were cast with either a self-consolidating concrete (SCC) or with a conventionally-vibrated concrete (CVC). Table 3-1 illustrates the target design properties for SCC set forth by the Alabama Department of Transportation. The project-specific required concrete compressive strengths (f'_{ci} and f'_{c}) are given in Table 3-2.

Table 3-1: Required Properties for ALDOT SCC (Dunham 2011)

REQUIRED PROPERTIES OF THE SCC MIX DURING GIRDER PRODUCTION		
Property	**Requirement**	**Test**
Compressive Strength at 28 days	The compressive strength shown on the plans or 5000 psi if it is not shown.	AASHTO T 22
Temperature	Freshly mixed concrete at the time of placing in the forms shall not be less than 50 °F or more than 95 °F.	AASHTO T 309
Total Air Content	Maximum 6.0 % by volume.	AASHTO T 152
Slump Flow[1]	Minimum 25 inches, maximum 29 inches.	ASTM C 1611
Visual Stability Index[2] (VSI)	Less than 2.0.	ASTM C 1611
1. The Slump Flow test shall be performed using the "Filling Procedure B" in ASTM C 1611. 2. A VSI of 1.5 is acceptable. A VSI of 1.5 corresponds to a stable SCC with a minimal mortar halo (< 0.25 inch), good aggregate distribution, and slight noticeable bleeding at the surface of the slump patty.		

Table 3-2: Required Concrete Strengths for Hillabee Creek Bridge Project

Girder Size	**f'_{ci} (psi)**	**f'_c (psi)**
BT-54	5200	6000
BT-72	5800	8000

Each girder was fabricated on one of two casting lines at the prestressing plant that were utilized for this project. The casting lines were long enough to produce three BT-54 girders on a single line cast in one day; however, it was only possible to cast two of the BT-72

girders on a single line. The configuration of the BT-54 girders and the BT-72 girders on a single line can be seen in Figure 3-1 and Figure 3-2, respectively. Because of this arrangement, three days of casting were required for the seven BT-54 girders using SCC mixtures and three days for the seven using CVC mixtures in order to obtain the required number of girders. The "third" day for both mixtures was actually the same: the remaining seventh SCC 54 and seventh CVC BT-54 were cast on the same line on the same day. For the BT-72 girders, four days of casting were required for the seven SCC mixtures and four days for the seven girders cast with CVC mixtures. Likewise, the "fourth" day for both mixtures was the same: the single remaining SCC BT-72 and single remaining CVC BT-72 were cast on the same line on the same day.

Figure 3-1: Casting Configuration of BT-54 Girders

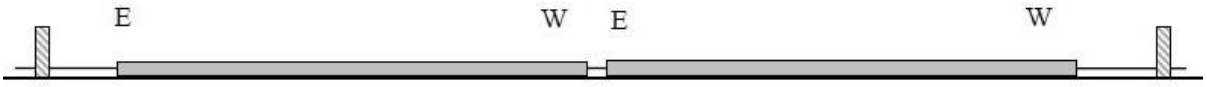

Figure 3-2: Casting Configuration of BT-72 Girders

Because the girders were cast for use in an actual bridge, standard procedures and protocol used by the plant for the production of ALDOT girders were followed in fabrication of the girders. First, the prestressing bed was cleaned and all components required to cast the

girders were gathered. Next, the prestressing strands were pulled in the correct configuration through the headers and hold-down points. Once the strands were in their proper location, they were tensioned and checked according to ALDOT procedures. The hold-up points were raised to their proper elevations to ensure the correct draping pattern once. At this point, the mild steel reinforcing cage was built around the strands. Then, the bed was oiled very carefully ensuring that the oil did not come in contact with the strands or reinforcement, which would compromise the integrity of the bond. Finally, all research-based gauges and devices were installed into the steel cage at their proper locations.

The girders were fitted with thermocouple wiring at one end of the girder. This wiring was installed to measure and regulate the match-curing process that is detailed in Section 3.2.2.1. In Figure 3-3 and Figure 3-4, the blue thermocouple wiring can be seen threading among the steel reinforcement down into the bottom flange in transfer bond region near the end of the unfinished girder.

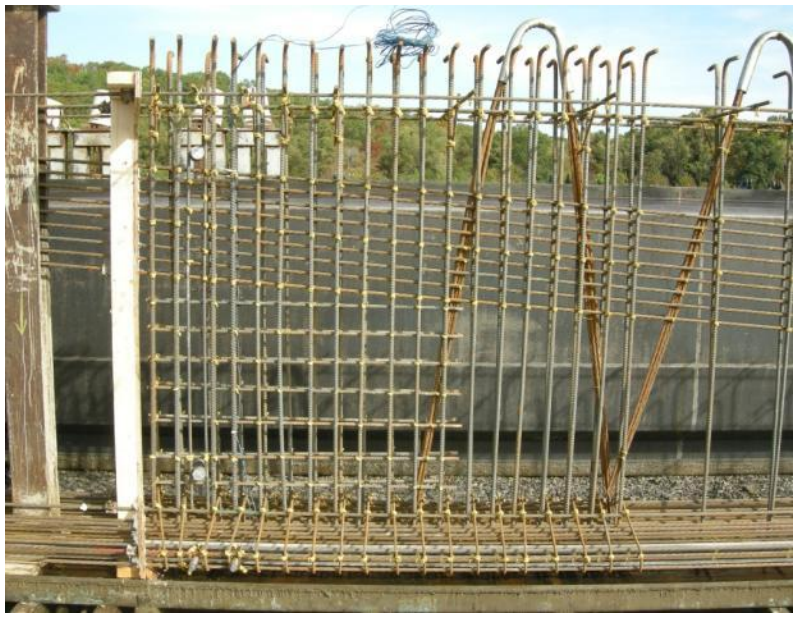

Figure 3-3: Thermocouple Wiring Installed in Unfinished Girder

Figure 3-4: Close-up of Thermocouple Ends in Bottom Flange of Girder

After the inner components of the girders were put into place, the side forms were sprayed with a release agent and secured along the beds as depicted in Figure 3-5. Next, concrete delivery vehicles were used to carry the fresh concrete to the prestressing beds and to fill the girder forms. Each concrete mixture was batched on-site at the precast plant and then transported across the yard to the bridge girder molds. Because the trucks could only hold 4 cubic yards of concrete each, numerous trips were required from the on-site batching area to the beds. Figure 3-6 shows the delivery trucks filling the girder formwork. Trucks were regularly pulled aside to sample and test the concrete and ensure its properties satisfied the specified requirements (Dunham 2011).

Figure 3-5: Girder Formwork Being Put in Place

Figure 3-6: Concrete Delivery Vehicle Filling Girder Forms

At the same time the girder forms were being filled, the cylindrical test specimens were also cast. When the girders were cast to approximately the middle of their span length, the delivery vehicles would unload concrete into a wheelbarrow that was used to transfer the concrete to nearby test cylinder molds which are shown in Figure 3-7.

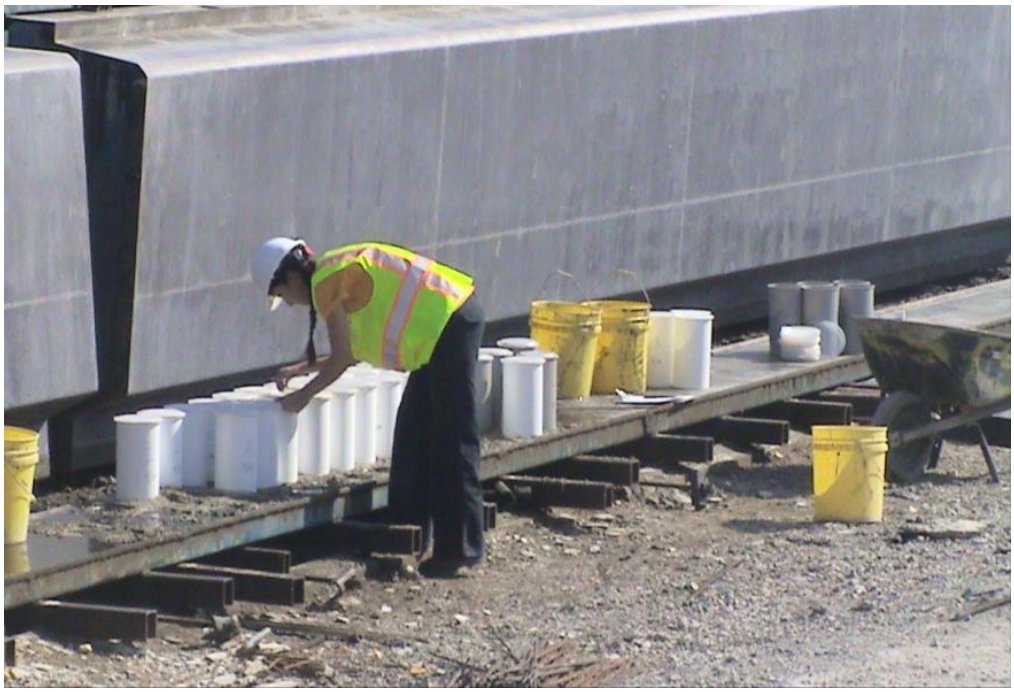

Figure 3-7: Concrete Cylinder Molds Used in Casting Test Specimens

This study required seventy 6 in. x 12 in. concrete cylinders for creep and shrinkage testing purposes. Many more cylinders were cast that were used for testing for other research. All specimens were prepared in cylinder molds in accordance with AASHTO T 126 (2003), and subsequently meet the requirements of ASTM C512 (2002), except where SCC mixtures were used. When dealing with self-consolidating concrete, the following modifications were used:

- All cylinders were cast using three lifts without rodding.

- Between each lift, every cylinder was lightly tamped 10 to 12 times around the perimeter of the mold to remove entrapped air pockets.

Because two different concrete types were utilized, different methods were employed in the casting of both the girders and the test specimens. Where CVC mixtures were used, it was necessary to use vibration to properly consolidate the concrete. This was done in the girders by using both external vibrators that were mounted on tracks that ran along the formwork, and internal vibrators. Figure 3-8 illustrates the filling and rodding of test cylinders for CVC mixtures.

Figure 3-8: Casting and Rodding Test Specimens for CVC Mixtures

Because the SCC mixture flowed into the forms under its own weight, no vibration was needed to ensure the concrete would pass through and encapsulate the reinforcement within the girders. When casting the test cylinders, SCC also eliminated the need for rodding. However, as mentioned earlier, light tamping was done around the perimeter of the cylinder to remove trapped air pockets. This mixture made the casting process faster for both the girders and the test specimens. Figure 3-9 illustrates the filling and tamping of the cylinders when SCC specimens were made.

Figure 3-9: Casting and Tamping Test Specimens for SCC Mixtures

On one occasion for both the BT 54 girders and the BT 72 girders, an SCC and a CVC girder were cast on the same day on the same line. In these cases, the conventional girder was always cast first. Because the formwork was continuous along the entire length of the bed, regardless of the length of the girder, any vibrations applied to one girder would have an

effect on the entire bed. Casting the CVC girder and vibrating it before casting the SCC girder guaranteed that the SCC girder would not be affected by the vibrations.

Once the casting was complete, the girders were roughened by using a metal raking tool to create ¼ inch ridges on the finished surface of the concrete (as seen in Figure 3-10), and the test cylinders were covered with a plastic lid that fit the top of molds (as seen in Figure 3-11). The test cylinders were then split into two curing groups: the majority was placed in the outer shelving of the girder formwork and eight were placed in the match-curing system. Finally, a curing blanket and weatherproof tarp were unrolled to cover the bed, forms, and test specimens for overnight steam curing. The "tarp-cured" test specimens inside the girder form and the whole arrangement being covered by the blanket and tarp can be seen in Figure 3-12.

Figure 3-10: Roughing Girder's Concrete Surface

Figure 3-11: Tarp-Cured Test Specimens in Molds with Plastic Caps

Figure 3-12: Placement of Curing Blankets and Weatherproof Tarp

3.2.1.1 Test Specimen Number and Types

In total, over one hundred 6 in. x 12 in. test cylinders were cast during fabrication of the bridge girders at Hanson Pipe and Precast. Of these, several were tested on-site, seventy were used for the purpose of creep and shrinkage testing in the laboratory, and dozens more remain for future research. The following section is designated to give a further explanation of the number and types of cylinders cast.

Each one of the creep specimens underwent some form of accelerated curing along with the companion girders. Match-cured and tarp-cured cylinders were tested at different chronological ages. Match-cured cylinders were loaded "at release", which corresponded as closely as possible to the chronological girder age at the time of prestress transfer in the plant (approximately 24 hours after mixing). In order to allow adequate time for a second round of specimen loading operations, the tarp-cured cylinders were loaded at a chronological age of 26 hours after mixing.

As explained in Chapter 2, there are multiple factors that contribute to volumetric changes in concrete specimens. Nonetheless, for this research, three components were considered to be the main factors: drying shrinkage, autogenous shrinkage, and creep. In order to accurately measure the creep and shrinkage, specimens were needed for creep testing, shrinkage testing, and strength testing. Also, the cylinders had to be divided into groups by each mixture, curing method, and loading age. In concordance with ASTM C512 Standard Test Method for Creep of Concrete in Compression (2002), no fewer than six specimens had to be made from each batch of concrete for each creep test condition. For this research seven specimens were made for each batch. Table 3-3 illustrates the number and type of test specimens that were cast for each parameter. In this table, the creep specimens

are those that were placed into the creep frames and loaded at a constant stress for the observation of total deformation. The shrinkage specimens, however, had no external load and were used to indicate deformation due to causes other than load. The strength specimens refer to those cylinders which were used to determine the concrete compressive strength immediately prior to loading. Each type of specimen in a single group underwent the same casting, curing, and storage treatment.

Table 3-3: Specimen Type and Number

			Number of Specimens by Type		
Mix Type	**Curing Method**	**Loading Age**	**Creep**	**Shrinkage**	**Strength**
SCC	**Match**	**Release**	4	6	4
	Tarp	**26 Hours**	4	6	4
CVC	**Match**	**Release**	6	9	6
	Tarp	**26 Hours**	6	9	6

In addition to these test specimens, ASTM C512 (2002) requires that plugs be used above and below the creep testing specimens while they are loaded in the creep frames. This ensures that the distribution of stress across the actual creep testing specimen is fairly even. In previous research, 6 in. x 12 in. concrete cylinders, made from high-strength slag cement mixture and allowed to cure for 28 days, were cut in half and sulfur capped according to standards to create these plugs. It was important to use the high-strength slag cement mixture because when properly cured, these plugs would have an ultimate strength that could exceed

any test specimen. Twenty of these plugs were used; one for the top and one for the bottom of each creep frame.

3.2.1.2 Test Specimen Identification

In order to distinguish each of the ten concrete specimen groups, a labeling system was developed to identify several properties of each group. Figure 3-13 illustrates the implemented system where girder height and number, concrete type, curing method, and any other special factors are each denoted.

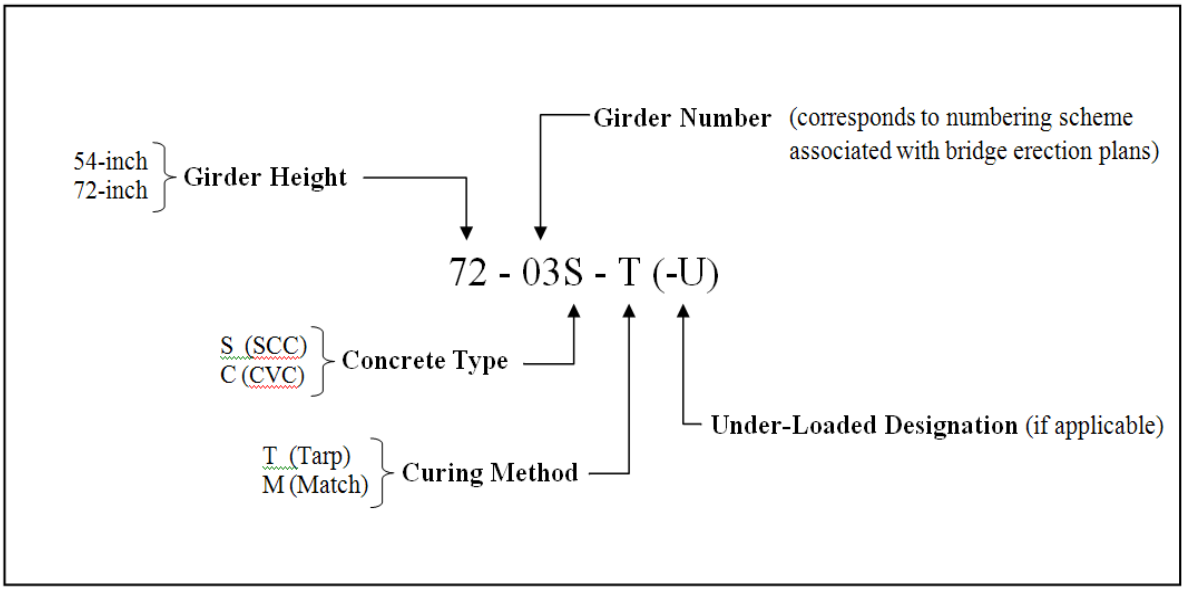

Figure 3-13: Specimen Identification

Together, the girder height and number indicate the specific girder from which the concrete was sampled. Of the specimens tested, six specimen groups were made from the girders 54 inches in height, and four groups from the 72 in. girders. Each of the girders also had to be numbered to aid in the erection process. The precast concrete producer numbered

both the 54 inch girders and the 72 inch girders from 1 to 14. Girders 1 through 7 of each girder size were cast using SCC, denoted with an ‘S’, and girders 8 through 14 were cast using CVC, denoted ‘C’. Only five girders were sampled to create the test cylinders which make up the ten specimen groups tested for creep and shrinkage. Three pairs of SCC test cylinder groups and two pairs of CVC cylinder groups were cast. In each of the pairs of test groups, one set was cured using tarp-curing methods, ‘T’, and one set was cured under match-curing conditions, ‘M’. In summary, out of the ten tested concrete groups, there were five different concrete batches sampled (three SCC and two CVC), and each was subjected to two different curing methods.

Finally, special circumstances also needed to be noted in the designation of certain specimens. In one instance the match-curing apparatus did not function properly; therefore, an asterisk is applied to the curing designation to indicate that the actual cylinder curing conditions are in doubt. In addition, some of the specimens were not loaded to the correct target load and are thus denoted with ‘U’ to clearly indicate that the specimens were under-loaded.

In addition to the system used to label each of the ten testing groups, another system was developed to aid in the data collection for each set of cylinders. The groups were divided by the age at which the load was applied: at release, or 26 hours. Each loading age is associated with five cylinders: two creep frame cylinders and three drying shrinkage cylinders. The two creep cylinders were labeled according to their position within the creep frame and were designated ‘TOP’ or ‘BOTTOM’. The shrinkage cylinders were labeled ‘X’, ‘Y’, and ‘Z’. For every cylinder, strains were measured at three locations around the perimeter of the cylinder and these were labeled ‘A’, ‘B’, and ‘C’.

3.2.2 CURING REGIMES

In this study, two methods of accelerated curing were employed. The first method was a traditional tarp-curing process which is generally practiced in the precast/prestressed concrete industry. The second method was a match-curing process, which was used to match the temperature of the sample concrete to the actual girder concrete. Each of these methods is detailed in this section.

3.2.2.1 Match-Cured Specimens

After casting, the specimens designated for match curing were sealed and placed in the match-curing system as illustrated in Figure 3-14. This system was designed to force the specimens through elevated-temperature cycles in attempt to match the parent temperature profile of the actual steam-cured girders. The schematic of the match-curing system that was utilized in this research is illustrated in Figure 3-15.

Figure 3-14: Inserting Test Cylinders into Match Curing System

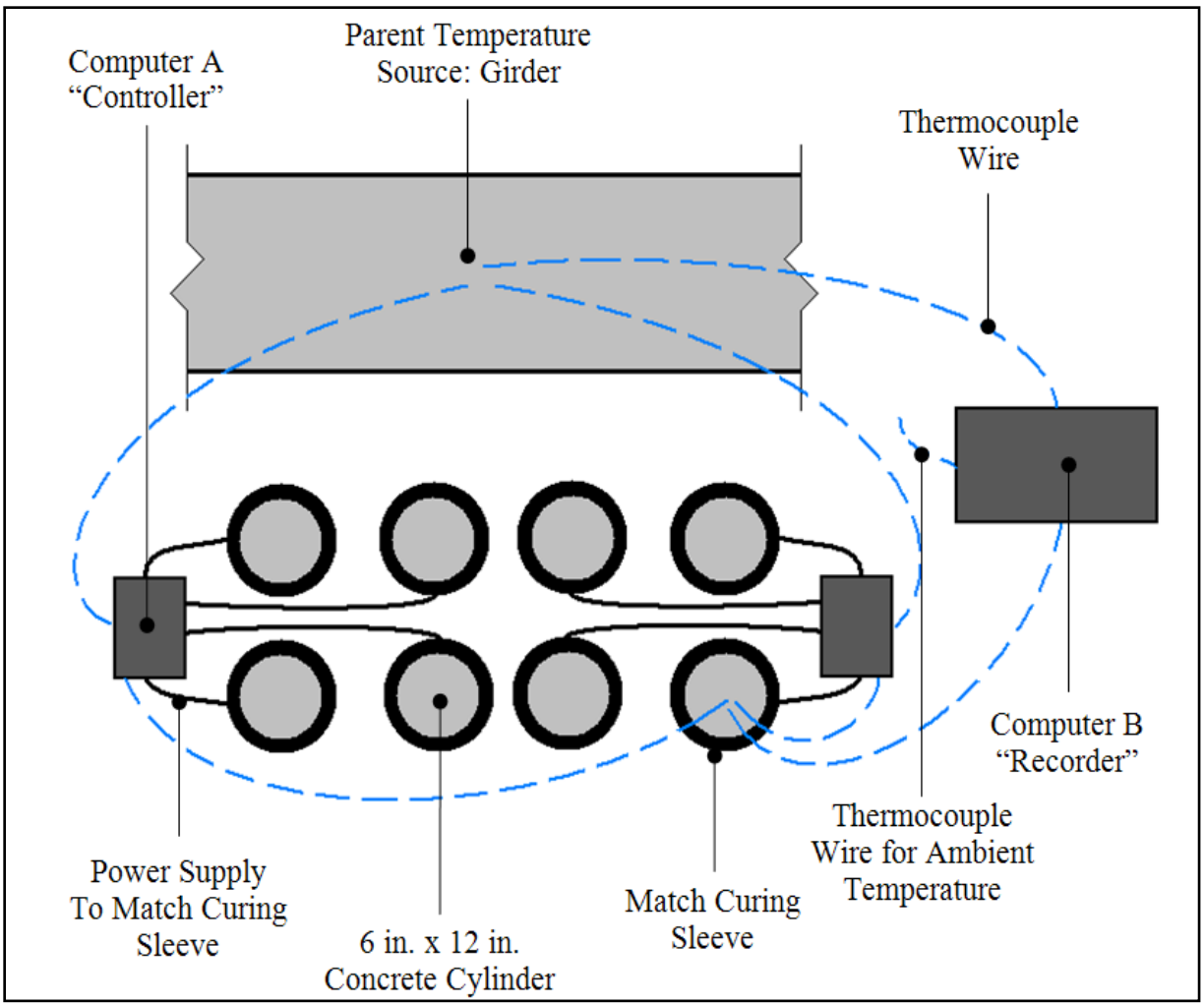

Figure 3-15: Schematic of Match-Curing System

The parent temperature source, or girder, was monitored with thermocouples that were imbedded within the girders, as seen in Figure 3-16, and were linked to the computer of the match-curing system. The computer controller (labeled 'Computer A' in the schematic) then heated the match-curing sleeves and monitored the temperature profile of one of the slave cylinders using another thermocouple. This ensured that the cylinders were only heated as necessary to maintain the temperature of the girder. Testing was not conducted on cylinders with embedded thermocouple wiring to ensure that the integrity of the concrete was not

compromised. Thus, only one cylinder was used to relay temperature data to both temperature-control computers and the temperature-recording computer.

Figure 3-16: Thermocouple Wires in Concrete Girder

Because the match-curing system did not record the temperatures, more thermocouple wires were added to the system so that the temperatures could be recorded by a Campbell Scientific CR1000 system, seen in Figure 3-17. This device ('Computer B' in the schematic) was connected to three thermocouple wires: one exposed to the atmosphere to record the ambient temperature, one inserted in the parent girder to record its temperature, and one inserted into a match-cured cylinder to record a representative curing temperature. This set-up enabled the users to monitor the temperature profiles of both the parent girder and the slave cylinders in order to ensure continuity.

Figure 3-17: Equipment Used to Record Temperature Profiles

Furthermore, each match-curing computer was only capable of monitoring four cylinder sleeves so the system was doubled in order to create an adequate amount of match-cured specimens. This was accomplished by adding another thermocouple to the girder and creating a new, parallel match-cured set rather than using the first set as a parent and chaining the second set to the first set. This option was chosen in order to avoid compounding errors if one system failed or creating any further lag in the match-curing system. Figure 3-18 shows the match-curing system in use beside the tarp-covered girder once curing had begun.

Figure 3-18: Match Curing System Alongside Tarp-Covered Girder

3.2.2.2 Tarp-Cured Specimens

The specimens designated to undergo tarp curing were cast into molds then sealed in accordance with the Standard Method of Test for Making and Curing Concrete Test Specimens in the Laboratory, AASHTO T126 (2001). These specimens were then moved to a shelf built in the web of the girder formwork and the whole system was covered with weatherproof tarps and curing blankets that were used to seal in the heat and moisture during the steam curing process. This allowed the test specimens to essentially experience similar curing conditions and temperatures as the parent girders. This covering with the tarp can be observed in Figure 3-19.

Figure 3-19: Covering the Girders and Test Cylinders for Tarp Curing

After curing under the tarp for approximately 18 to 20 hours, the cylinders were then transported two hours to the laboratory in an insulated container which was used to prolong the curing process for as long as possible during transport. The 24-hour (or "release") specimens were match-cured approximately 18 to 20 hours, and then insulated for another two hours during transport, and then exposed to the room temperature conditions for another two to four hours during preparation for loading. The 26-hour, tarp-cured specimens were transported with the match-cured specimens and then released into the room-temperature laboratory conditions for another four to six hours before being loaded. After stripping and preparing the cylinders for testing, all of the specimens (loaded or not), were placed into a climate-controlled room, which maintains a humidity of 50% ± 10%. Here, the drying process and creep testing ensued.

3.3 GIRDER CONCRETE PROPERTIES

The material properties of each of the concrete girders and the concrete test specimens are discussed in this section. The materials used include both self-consolidated and conventionally-vibrated concretes.

3.3.1 CONCRETE MIXTURE PROPORTIONS

Four concrete mixtures were designed by the contractor to satisfy the special provisions that were required for the prestressed bridge girders. These provisions are reported by Dunham (2011). Each batch of concrete was mixed on site at Hanson Pipe & Precast concrete prestressing plant located in Pelham, Alabama. The four mixtures, all containing Type III portland cement, comprised an SCC and CVC mixture for both the 54-inch girders and the 72-inch girders. The components of each mixture are summarized in Table 3-4.

Table 3-4: Concrete Mixture Proportions

	BT-54		BT-72	
Item	**SCC**	**CVC**	**SCC**	**CVC**
Total Air Content (%)*	4.1	4.2	4.0	3.2
Water Content (pcy)	266	238	265	234
Cement Content (pcy)	758	696	760	708
Slag Cement Content (pcy)	134	124	135	125
w/cm	0.30	0.29	0.30	0.28
SSD Coarse Agg. #78 (pcy)	1528	0	1550	0
SSD Coarse Agg. #67 (pcy)	0	1923	0	1950
SSD Fine Agg. (pcy)	1384	1163	1370	1179
***s/agg* (by weight)**	0.48	0.38	0.47	0.38
Air-Entraining Admixture (oz/cy)	0.3	0.3	0.2	0.2
HRWR Admixture (oz/cy)	11	8	11	7
Viscosity-Modifying Admixture (oz/cy)	2	0	4	0
Hydration-Stabilizing Admixture (oz/cy)	2	1	2	1

*Average air content was determined from fresh test results.

The admixtures, supplied by W.R. Grace and presented in ounces per cubic yard, included an air-entraining admixture (Darex AEA EH), a high-range water-reducing admixture (ADVA Cast 575), a viscosity-modifying admixture (V-Mar 3), and a hydration-stabilizing admixture (Recover). The SCC mixtures contained #78 limestone as coarse aggregate, whereas the CVC mixtures contained #67 limestone coarse aggregate.

3.3.2 Fresh and Hardened Concrete Properties

Because of the large quantities of each mixture that were batched each day of production, representative samples were taken at the beginning, middle, and end of casting for each

mixture each day. Fresh concrete properties were then tested from each sample in order to determine the quality and consistency of each mixture. Each of these tests was done by the concrete producer with the assistance of Auburn University Highway Research Center (AUHRC) researchers and was overseen by an ALDOT inspector. These properties can be observed in Table 3-5; however, it should be noted that the properties listed here are ones that are relevant to the batches subjected to creep and shrinkage testing and not a complete list of all concrete tested during the project.

Table 3-5: Fresh Concrete Properties

Mixture	Sample No.	Batch Temp (°C)	Slump (in.)	Slump Flow (in.)	Air (%)
54-03S	2	25	NA	26.0	3.0
54-07S	2	24	NA	26.0	4.2
72-03S	2	27	NA	26.0	4.3
54-12C	2	31	9.0	NA	4.5
72-11C	2	23	9.0	NA	3.1

Concrete test cylinders representative of each mixture were made and tested at certain benchmark ages to determine the hardened properties. The age of the concrete at prestress transfer ("release") as well as the average of the compressive strength, f_c, and the elastic modulus, E_c, can be seen in Table 3-6. It should be noted that this table contains values that were obtained from tests performed on cylinders that were cast simultaneously to the cylinders used for creep and shrinkage testing. The "release" values were obtained through tests conducted at the prestressed plant at the actual time of prestress transfer. The 28-day

values were obtained from cylinders that were transported to AUHRC and allowed to dry outdoors. The elastic modulus for each mixture was obtained using the compressometer shown in Figure 3-20. This test was conducted in accordance with ASTM C469 Standard Test Method for Static Modulus of Elasticity and Poisson's Ratio of Concrete in Compression (2002) and was performed after a companion cylinder was used to obtain the compressive strength.

Table 3-6: Girder Concrete Hardened Properties

	Release			**28 Days**	
Mixture	**Age (hrs)**	**f_{ci} (psi)**	**E_{ci} (ksi)**	**f_c (psi)**	**E_c (ksi)**
54-03S	24	8680	6300	10800	6600
54-07S	24	7940	6100	10180	6200
72-03S	20	7860	5900	10770	6400
54-12C	24	7860	6700	9670	6900
72-11C	20	8320	6800	11050	7700

Figure 3-20: Modulus of Elasticity Test

A specified compressive strength at release was set at 5200 psi for the 54-inch girders and 5800 psi for the 72-inch girders. This required strength was well surpassed for all of the mixtures, which can be partially attributed to the actual time of release. The approximate industry standard is set for release to occur 18 hours after casting.

3.4 CREEP AND SHRINKAGE TESTING PROCEDURES

For this research, the hardened properties of interest consisted of the compressive strength, modulus of elasticity, creep, and total shrinkage exhibited by each concrete mixture. This section gives a description of the equipment and procedures that were used to gather the data necessary for the testing of creep and shrinkage.

3.4.1 PREPARING THE SPECIMENS FOR TESTING

Once the girders and specimens were cast and prepared for curing, they were left overnight for either match or tarp curing. At approximately 18 to 20 hours of curing, the test cylinders were removed from under the tarp or from the match-curing system and were transported to the laboratory at Auburn University for testing. In order to maintain curing conditions as best as possible during the two-hour travel period, they were kept in their molds with the lids sealed and placed in insulated containers that were created specifically for this purpose. This ensured a more gradual loss of heat in an attempt to replicate the parent girder's temperature change as the tarps were removed. Meanwhile at the prestressing plant, the curing blankets and tarps were rolled up and the side forms were removed from the girders as shown in Figure 3-21.

Figure 3-21: Removal of Side Forms from Girders

Once the cylinders arrived at Auburn University laboratory, the plastic molds were stripped from the cylinders and preparation for testing began.

To ensure that the concrete cylinders are flat and smooth on their ends, a common practice is to sulfur-cap each specimen in accordance with AASHTO T231 Standard Practice for Capping Cylindrical Concrete Specimens (2003). However, most sulfur capping compounds require at least a two-hour set time and can cause unwanted delay of creep testing. As an alternative to sulfur capping, a concrete grinder was used to achieve a smooth, level surface in order to meet the planeness requirements. The Auburn University laboratory houses a MARUI concrete cylinder grinder, seen in Figure 3-22, that made it possible to grind two specimens in a single preset operating cycle. Using this machine, an output of 45 units per hour was achievable, which made grinding a valuable tool because of the time restriction.

Figure 3-22: MARUI Concrete Cylinder Grinder

After both ends of each cylinder were ground, demountable, mechanical (DEMEC) locating discs for strain measurements were attached to the specimens. First, lines were measured and drawn in 120-degree intervals around the perimeter of each specimen. Each line was labeled with A, B, or C in the clockwise direction. Next, the top DEMEC discs were applied two inches from the top of the cylinder with 5-minute epoxy. After the epoxy hardened adequately, the bottom discs were located and applied using the DEMEC spacing bar, seen in Figure 3-23. Figure 3-24 shows a finished specimen set with lines drawn and labeled and DEMEC locating discs applied.

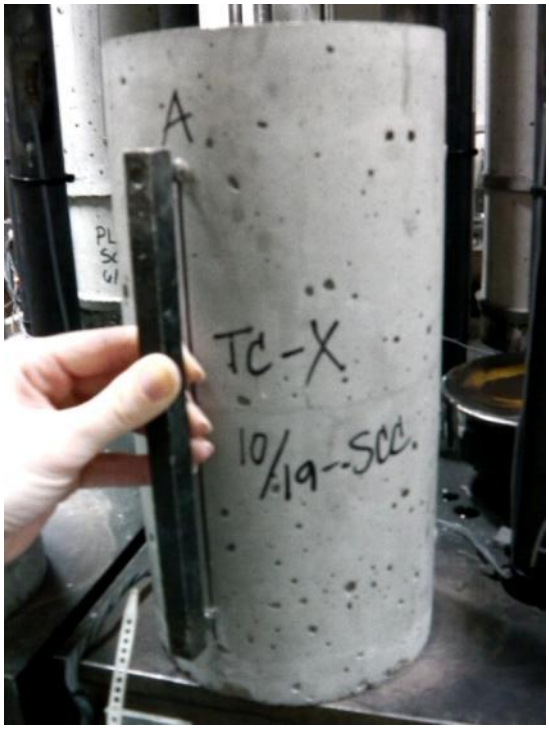

Figure 3-23: Applying DEMEC Locating Discs Using Spacing Bar

Figure 3-24: Complete Shrinkage Specimen Set with Labels and DEMEC Locating Discs

Once the cylinders were prepared, two cylinders were tested in the laboratory to obtain the average compressive strength. The compressive strength was then used to determine the required load that was to be applied to the creep frames. This load is further explained in Section 3.4.2. At this time, the prestressing force was transferred to the girders in the prestressing plant by cutting flame-cutting the prestressing strands. This can be seen in Figure 3-25. While this process took place at the plant, AUHRC researchers began loading the "at release" creep test specimens in the laboratory. The tarp-cured specimens were loaded later at an age of 26 hours.

Figure 3-25: Flame-Cutting the Prestressing Strands

3.4.2 DETERMINATION OF TEST LOAD

The compressive strength for each sample and curing type had to be measured before creep testing could begin. Prior to obtaining the compressive strength, the specimens were ground smooth on each end as an alternative to sulfur capping. Each specimen was tested in accordance to the ASTM C39 Standard Test Method for Compressive Strength of Cylindrical Concrete Specimens (2005).

Each cylinder was placed into a Forney FX600 compressive testing machine, which can be seen in Figure 3-26, and was loaded at a target rate of 60,000 lbs/min. until failure was reached on the 600-kip capacity compression machine. This process was done immediately prior to loading and was repeated for two specimens with the average taken as the compressive strength. Table 3-7 shows the acquired compressive strengths from each of the

trials. If one test resulted in an extremely lower strength than the other for a test set, the low-strength value was discarded and only one was used.

Figure 3-26: Forney FX 600 Compression Testing Machine Used in This Study

Table 3-7: Compressive Strength prior to Creep Loading

Specimen	Trial	Compressive Strength (psi)	Average (psi)
54-03S-M*	1	7230	7230
	2	-	
54-03S-T	1	9090	8930
	2	8770	
54-07S-M	1	7850	7880
	2	7900	
54-07S-T	1	7360	7490
	2	7620	
72-03S-M	1	7390	7060
	2	6740	
72-03S-T-U	1	7630	7680
	2	7740	
54-12C-M	1	7030	7110
	2	7190	
54-12C-T	1	-	8120
	2	8120	
72-11C-M	1	8120	7980
	2	7850	
72-11C-T-U	1	8720	8880
	2	9030	

It should be noted that test loads were determined and applied at release for the match-cured sets of specimens and the entire process was repeated at 26 hours for the tarp-cured sets of specimens. Also note that the values in this table are from the laboratory testing of specimens created for the creep and shrinkage testing for this particular research and should

not be confused with the on-site compressive strength testing of cylinders which were created from the same batches of concrete.

3.4.3 CREEP TESTING

All equipment and procedures used in conducting this research satisfied the requirements implemented by ASTM C512 (2002), which is the governing specification for standard creep testing in the United States. In this section, the entire testing program is described including details about the equipment and test methods that were used during the process of testing and data collection.

3.4.3.1 Creep Frames

This research required the use of ten creep testing frames in order to test the five concrete samples for the two curing conditions of interest. A basic description of a standard creep frame is provided by ASTM C 512 (2002). A basic requirement is that the frame must maintain the applied load within ±2% of the target load despite length changes within the test specimens. In order to accomplish this, the specification recommends the use of springs which are flexible enough to allow small length changes without a significant loss of load.

The creep testing facility at Auburn University is equipped with twenty-five such creep frames that were designed and fabricated for a previous research project reported by Kavanaugh (2008). These frames are able to withstand the forces required to load 6 in. x 12 in. concrete cylinders, having a compressive strength of 16,000 psi, to 40% of their ultimate strength. This means that each frame has a maximum service-load capacity of approximately 180 kips. Schematics of the configuration of each frame can be seen in Figure 3-27 and

Figure 3-28, and a photograph of an actual frame used during the course of research can be seen in Figure 3-29.

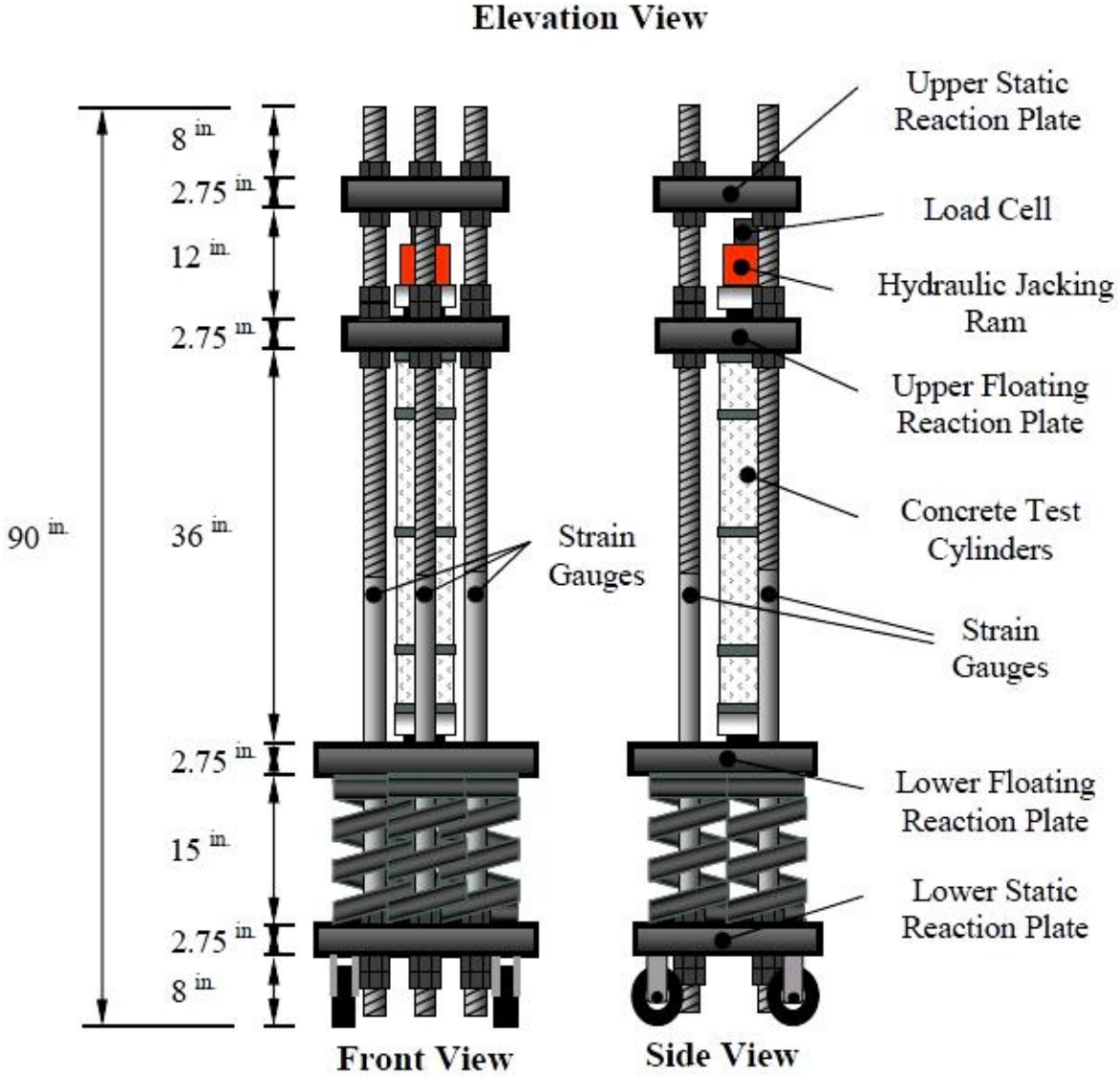

Figure 3-27: Elevation Schematic of Creep Frames (Kavanaugh 2008)

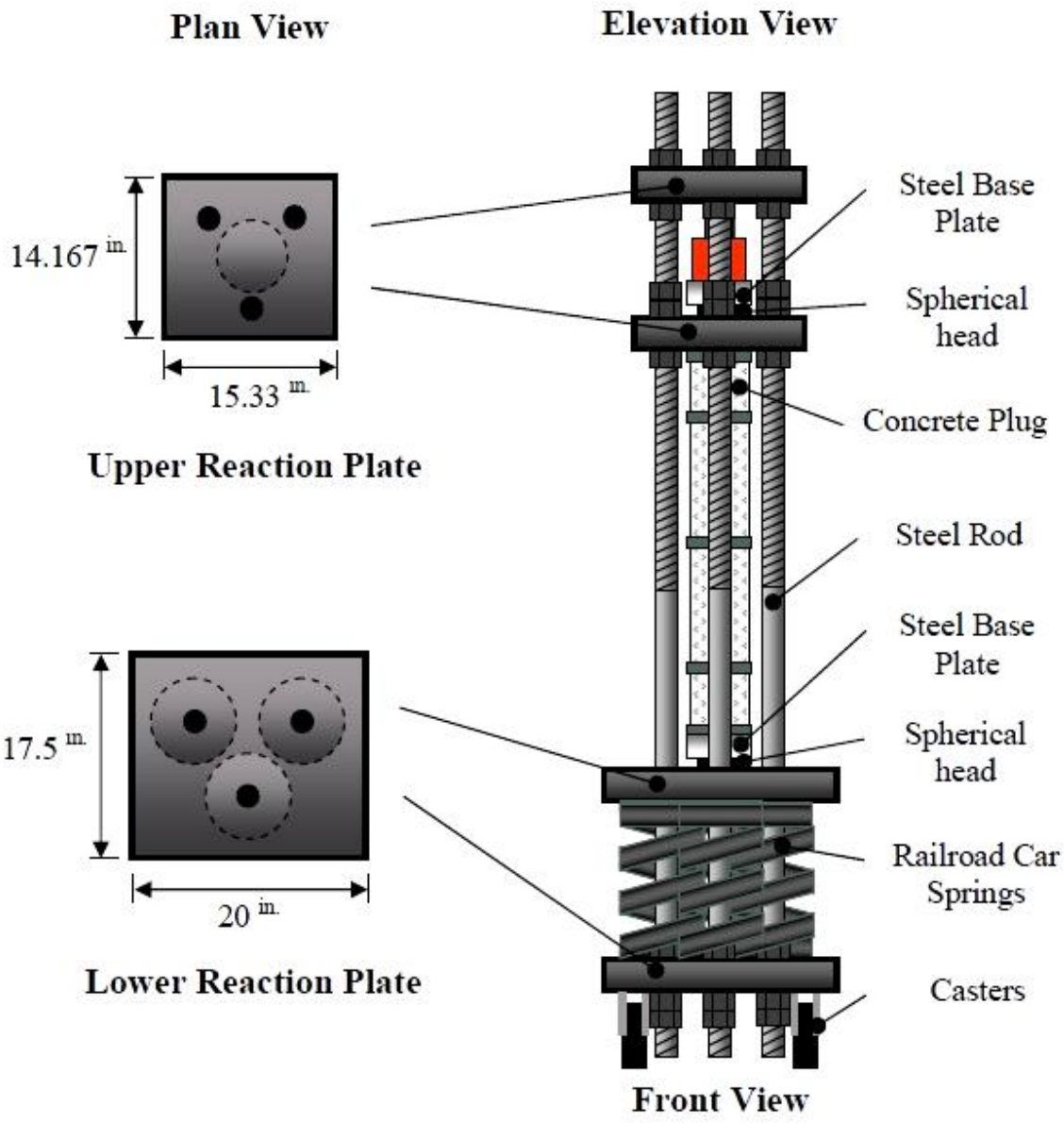

Figure 3-28: Plan Views of Reaction Plates on Creep Frame (Kavanaugh 2008)

Figure 3-29: Creep Frames

Every frame houses three railroad car springs, each of which has a spring constant of 25,000 lbs/in. These springs were designed and constructed specifically for Auburn University by Duer/Carolina Coil, Inc. of Reidville, South Carolina. Each spring is made from ASTM A304, Grade 220 steel, and is 15 in. high with an 8½ in. outer diameter (Kavanaugh 2008). The springs are sandwiched between two steel plates that transfer the applied load into the test specimens. In total, there are four of these 2¾ in.-thick Grade 50 steel plates on each frame.

Holding the entire mechanism together are three 90 in. steel rods that are able to safely hold 60 kips of force while experiencing minimal relaxation. This is accomplished using 1¾ in. diameter steel which has a yield stress of 65 ksi and an ultimate stress of 80 ksi. Grade 8, heavy-duty, 1¾ in. hex nuts are threaded onto the rods to hold the plates in the proper locations. Each frame has eight of these nuts, which are made from C 1045 steel having a minimum Rockwell hardness of C24 and a minimum ultimate tensile stress of 150 ksi (Kavanaugh 2008).

Used in monitoring the load, strain gauges are affixed on the unthreaded portion of each bar at a distance of no less than two bar diameters away from the end of the threads. This location allows the stress distribution in each bar to be fully distributed across the cross section and provides the most accurate strain reading possible.

Each frame was calibrated during previous research and can be recalibrated, if necessary, to determine that the gauges are working properly. This calibration process is used to relate the strain gauge readings to a known level of applied force.

3.4.3.2 Creep Room

Because creep is dependent on temperature and humidity conditions, ASTM C512 requires that both temperature and relative humidity be controlled at 73°F ±2°F and 50% ±4%, respectively during any creep testing. The Auburn University Creep Room was constructed with the sole purpose of providing an environment for conducting creep testing. Figure 3-30 shows a plan view of the 18 ft x 11 ft room located within the Auburn University Structural Research Laboratory. Locations of the individual creep frames as they are positioned within the room are also indicated.

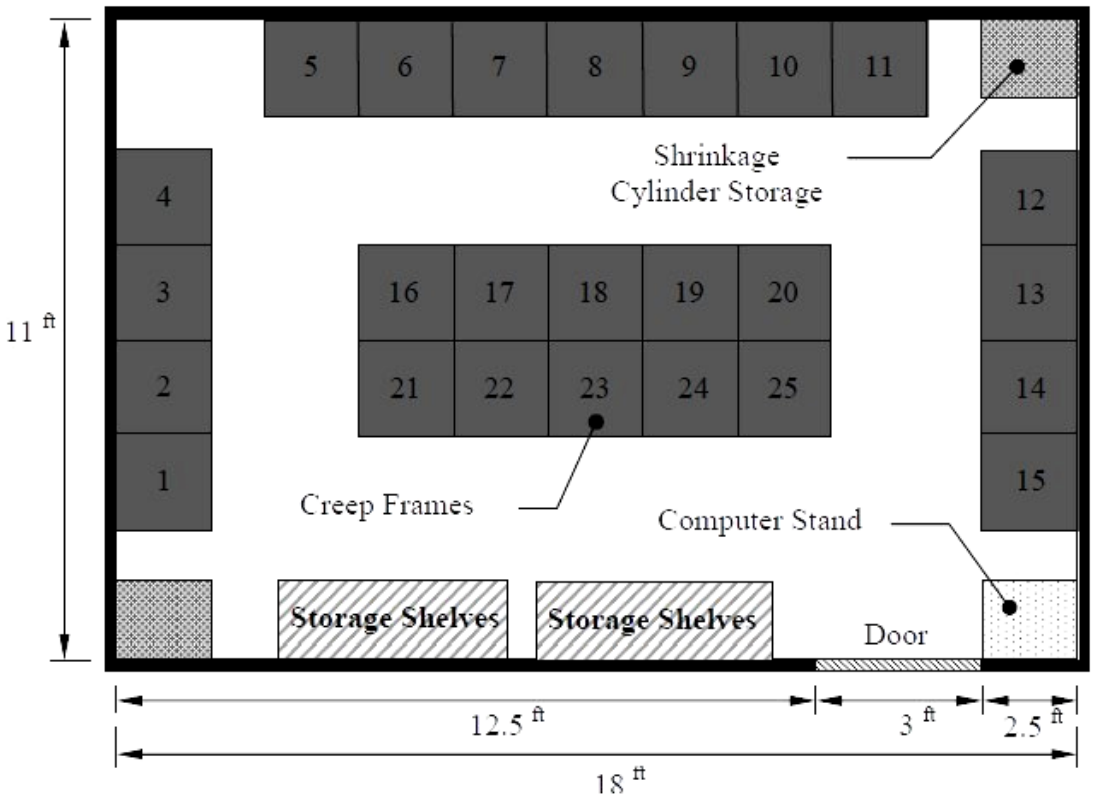

Figure 3-30: Layout of Environmentally-Controlled Creep Testing Room (Kavanaugh 2008)

This is a climate-controlled room, which has a dedicated air-conditioning unit and humidifier that are automatically controlled to meet the requirements of ASTM C512. These environmental conditions are recorded through the use of a datalogger and can be referenced for up to six months. Each time readings are taken in the creep room, the temperature and humidity should also be recorded manually as a back-up or cross-reference to the data logger.

3.4.3.3 Creep Testing Procedure

After the appropriate curing regime and preparation for each set of specimens was complete, the specimens were each loaded in uniaxial compression. All creep testing procedures were conducted in accordance with the specifications set forth by ASTM C512 (2002) and with the most consistency possible. Below, the entire procedure that was used in the creep testing process is presented in sum. Several steps are also explained in further detail afterward.

1. Remove all specimens from their curing conditions and strip from molds.
2. Grind each specimen until a level, smooth surface is achieved.
3. Using 5-minute epoxy, apply DEMEC points around the perimeter of each specimen (except strength specimens) at 120-degree intervals. Allow epoxy to fully harden.
4. In order to determine the target load, obtain the average compressive strength of two specimens.
5. Raise the upper floating reaction plate to allow ample space for necessary cylinders.

6. Making sure proper alignment is achieved, insert the test cylinders into the appropriate creep frame.
7. Lower the upper floating reaction plate to hold cylinders in place.
8. Record reference resistor strain indicator values then attach the strain gauge wiring to the strain gauge indicator and take initial strain readings from frame bars.
9. Take and record initial DEMEC readings on creep and shrinkage specimens
10. Position the hydraulic cylinder on top of the upper floating reaction plate taking care that the ram is centered to minimize eccentricity.
11. Position the load cell on top of the hydraulic cylinder taking care that the entire setup is centered.
12. Attach the load cell wiring to the strain indicator leaving the strain gauge wiring still attached also.
13. Using the hydraulic pump, apply the target load which is approximately 40% of the ultimate compressive strength as found in Step 4.
14. Apply load until 102% of the target load is reached.
15. Lock the load into place by making sure all nuts on the top side of the upper floating reaction plate are hand-tight.
16. Retract the hydraulic cylinder to transfer load to frame.
17. After hydraulic pressure is released, ensure the load was held within ±2% of desired value by checking the bar strains. Repeat loading process if load is inadequate.

18. Once load is sufficient, record all concrete DEMEC strain measurements as soon as possible after initial loading. This includes readings from both the loaded cylinders and the corresponding shrinkage cylinders. Also record all bar strain readings.

When inserting the cylinders into the creep frames, as in Step 6, two test cylinders and two high-strength half cylinder "caps" were needed. Figure 3-31 depicts how this process was accomplished. During loading, alignment is extremely important within the frames. It was crucial that the specimens be in good alignment with both the frame itself and each other. Otherwise, the possibility of eccentricity was increased. If eccentricities are allowed, erratic strain measurements will ensue. For this reason, properly determining the best alignment of the test specimens is of the utmost importance. Alignment marks are located on the floating reaction plates for reference.

Figure 3-31: Example of Loading the Creep Frames

As mentioned in Steps 10 and 11, the hydraulic cylinder and load cell were placed on top of the upper floating reaction plate in order to apply load to the frame. The hydraulic cylinder used in the creep room is a single-stage cylinder with a stroke of approximately two inches. Often, steel plates were stacked beneath the cylinder so that the entire load could be applied without exceeding the stroke of the cylinder. Figure 3-32 shows the items mentioned and their arrangement in the load-application column.

Figure 3-32: Arrangement of Loading Mechanisms

After the loading equipment was set up, the load cell was connected to the strain indicator with the wires arranged in the configuration that is seen in Figure 3-33. As mentioned in Step 8, reference resistor measurements must be taken prior to bar strain measurements and

must be read from Inputs 1, 2, and 3. The resistor may be seen attached to one channel in Figure 3-34. After the resistor readings were taken, the bar strain wires were attached as in Figure 3-35 in order to obtain the strains in each bar. Each wire must be inserted into the proper slot to obtain accurate readings.

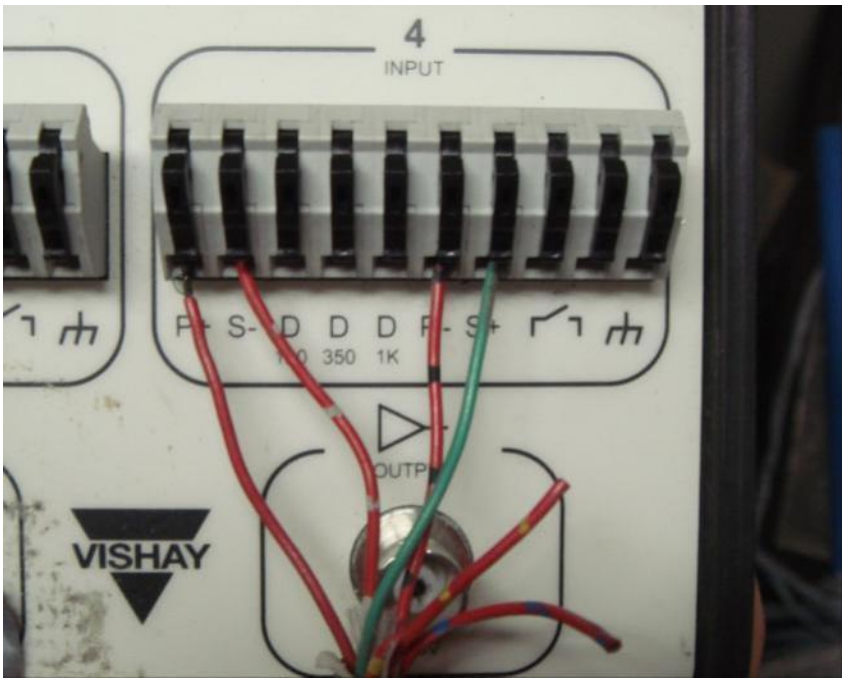

Figure 3-33: Load Cell Wiring Arrangement on Strain Indicator

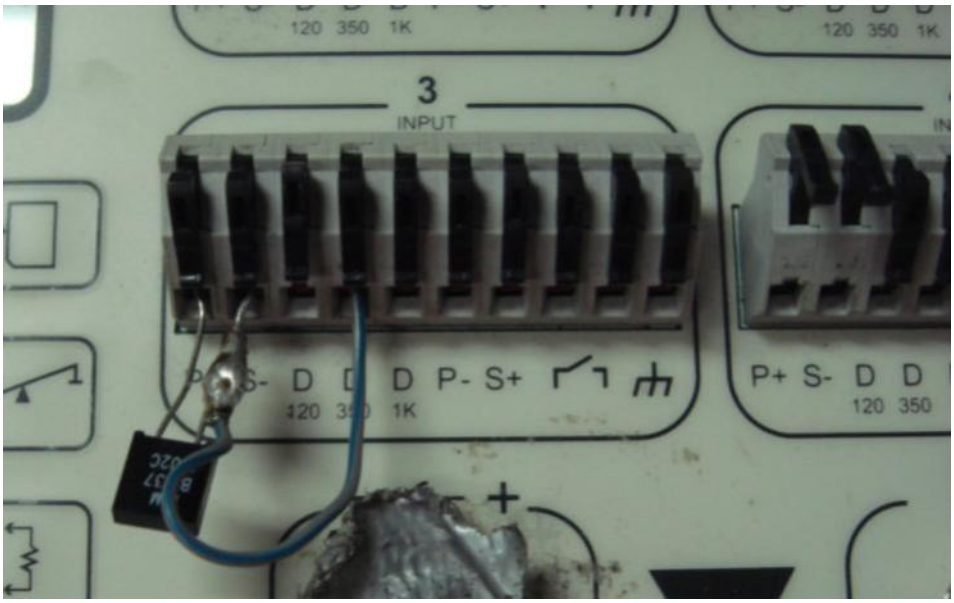

Figure 3-34: Reference Resistor Attached to Strain Indicator

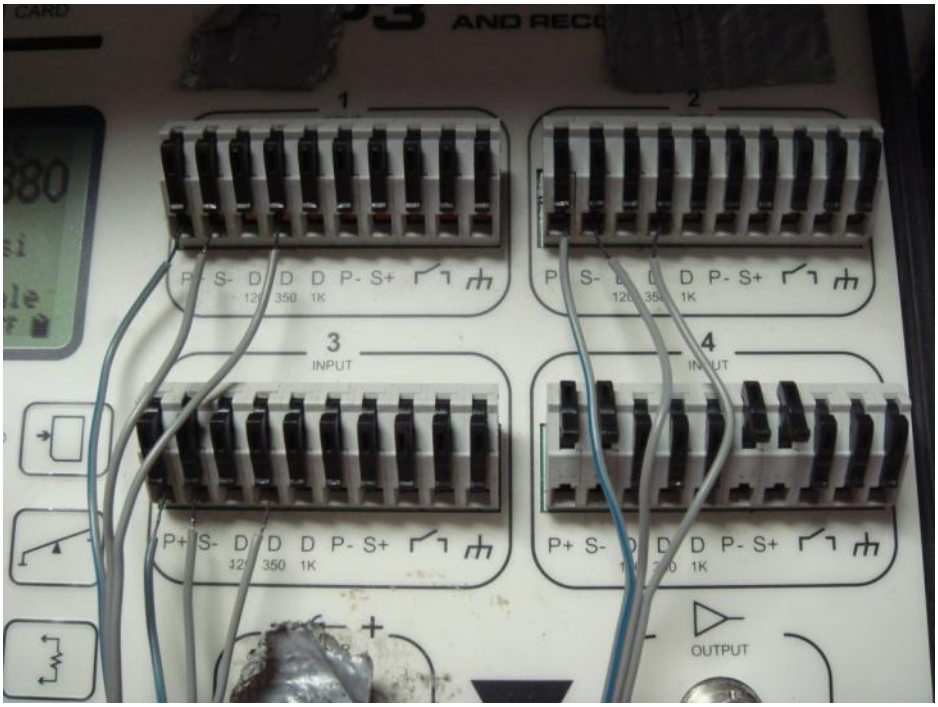

Figure 3-35: Bar Strain Gauges Attached to Strain Indicator

When applying the load, as in Steps 13 and 14, the target load for the frame was set at 40% of the compressive strength, the maximum recommended by ASTM C512 (2002). In the time it took to finish the remaining steps to secure the load, a small percent of load was lost and because of this, it was determined that a good practice was to load to approximately 102% of the target load (40% of the compressive strength) in order to account for the loss. Over time, the load within the frame itself may also change and ASTM C512 (2002) requires the applied load to remain within ±2% of the original target load. To track any change in the load, bar strain readings were taken, as seen in Figure 3-36, immediately prior to all creep strain readings. The measured bar strains were then compared to the initial bar strains prior to loading in order to calculate the percent change in load. If the load moved outside of the 2% specified range, the load was adjusted as necessary and the creep strain measurements were taken.

Figure 3-36: Taking Bar Strain Measurements Using Strain Indicator

In order to measure the total strain in a specimen, strain measurements were taken using the DEMEC strain reading gauge that can be seen in Figure 3-37. This process is shown in Figure 3-38 where the top cylinder strains were measured twice at each of the three points around the specimen, and then the process was repeated for the bottom cylinder. The time intervals required for strain measurements by ASTM C512 (2002) include readings immediately before loading (pre-load), immediately after loading (post lock-down), 2 to 6 hours after loading, then daily for the first week, weekly until the end of the first month, and monthly for the for the first year. Aside from what the specification required, it was determined that for this research, readings after the first year would be taken every 90 days or approximately every three months. In an effort to provide uniform results, each reading was

takes as close to the required time as possible. Also, as with the reference resistor readings that must be taken prior to measuring the bar strains, a reference bar was also measured prior to each time the DEMEC gauge was used to measure concrete strains. This reference bar as well as the DEMEC point-spacing bar is pictured in Figure 3-39.

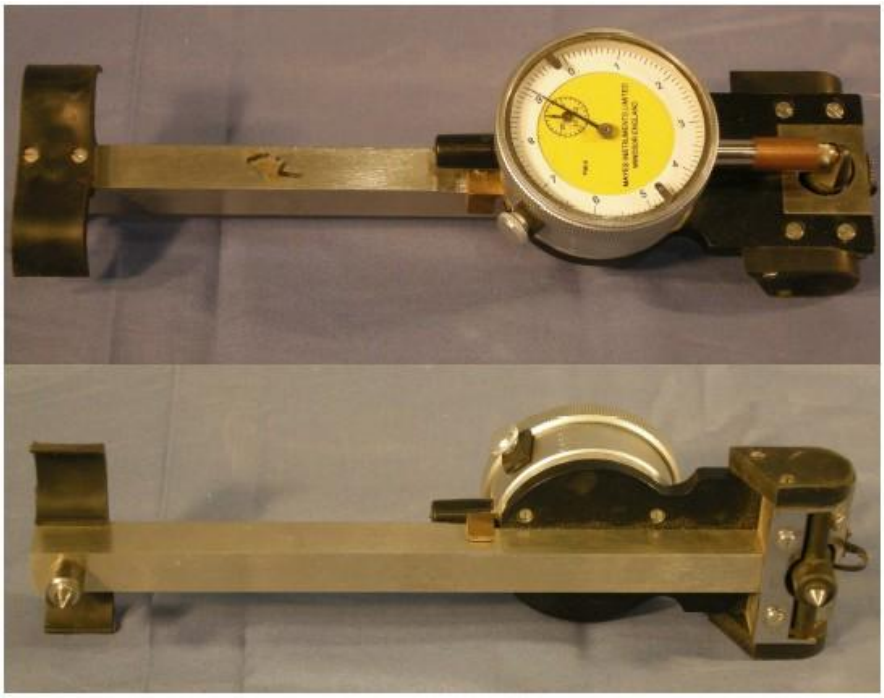

Figure 3-37: Demountable, Mechanical **(**DEMEC) Strain Gauge

Figure 3-38: Total Strain Measurements Taken With DEMEC Gauge

Figure 3-39: DEMEC Spacing Bar (Top) and Reference Bar (Bottom)

3.4.4 SHRINKAGE MEASUREMENTS

In attempt to isolate the strain associated exclusively with creep, corresponding shrinkage strain measurements were taken as is required by ASTM C512 (2002). For this research, the drying shrinkage was measured using the same Demountable, Mechanical (DEMEC) strain gauge on three 6 in. x 12 in. concrete cylinder specimens for each test group. These "shrinkage" or "control" cylinders were free of any load or restraint and were housed in the same environment as the creep test cylinders. The measurements for shrinkage strain were taken in the same manner and in identical time intervals as the measurements for creep strain. These intervals included measurements taken immediately before and after applying the load on creep test specimens, 2 to 6 hours after loading, every day for one week, every week for one month, and every month for one year, then every three months thereafter until the desired time was reached. Figure 3-40 illustrates measuring the shrinkage strains using the DEMEC gauge.

Figure 3-40: Taking Shrinkage Strain Measurements Using DEMEC Gauge

The procedures for preparing the specimens, equipment used in data collection, and schedule used for gathering shrinkage data was unchanged from the creep testing procedures and are more thoroughly detailed in the previous section. This consistency was made use of in an attempt to limit errors in data collection and to establish uniformity across the study.

CHAPTER 4
APPLICATION OF PREDICTION METHODS

4.1 INTRODUCTION

One of the main objectives of this study was to evaluate the nine prediction methods detailed in Chapter 2 to determine their effectiveness for estimating creep and shrinkage of both SCC and CVC mixtures using both tarp- and match-curing regimes. This was accomplished by determining the creep and shrinkage strains (ε_{cr} and ε_{sh} respectively) of the experimental specimens and comparing this data against strains predicted using each method.

Each method requires concrete properties, environmental conditions, and other details about testing in order to predict the desired strains. Often, a prescribed method requires interpretation or assumptions to be made where sufficient information is not available. This chapter is organized first by the general assumptions or decisions that were applied to implement several or all of the prediction methods for this study. Second, this chapter indicates how each method was applied and details any specific assumptions that were needed to use that particular method in the prediction of creep and shrinkage strain.

4.2 GENERAL CONSIDERATIONS

This section outlines the general assumptions or decisions that were applied to more than one prediction model. Here, the assumptions are categorized by topic.

4.2.1 ENVIRONMENTAL CONDITIONS

All creep and shrinkage prediction models set forth specific limits for temperature and humidity. Since testing was conducted in a climate-controlled room, as described in Section 3.4.3.2, the ambient conditions within this room were monitored and recorded using a data collection unit. During the course of this year-long study, the creep room maintained temperature values within a range of 69 to 74°F (20 to 23°C). On the other hand, the humidity control unit in the creep testing room malfunctioned for approximately 90 days starting in the first month of testing. During this period, the average relative humidity was 38% with individual readings ranging from 20 to 54%. After equipment repair, the relative humidity fluctuated only slightly over the remaining testing period, with daily averages ranging from 54 to 58%. It was assumed that by averaging the temperature and humidity data that were collected throughout this research, a representative value of the temperature and relative humidity could be used for the strain predictions. The average temperature and relative humidity readings used were 72°F and 50%, respectively. The percent difference in the correction factor for relative humidity when moving from 50% to 38% relative humidity varies from 4 to 8% for the various prediction models employed in this study. Thus, prediction inaccuracies in the 5 to 10% range could be at least partially attributable to humidity variations, particularly for the results during the first three months of testing.

4.2.2 CEMENT CLASS

Each of the European methods (i.e. all the Model Codes including MC-KAV and Eurocode) require the selection of a “cement class” for the calculation of the cement type coefficient which ultimately determines the notional shrinkage coefficient. For these

European methods plus NCHRP 628, this is also used in determining the creep deformations; the European methods use it for the modified time factor and NCHRP utilizes the cement type for the calculation of the ultimate creep coefficient. MC 2010 refers to this input as the "cement strength class" and, here, the choices are defined in more detail according to the European Committee for Standardization (CEN) cement classes. Since the values for these strength classes corresponded with the values for the cement class in other methods, it was assumed that the three choices in MC 2010 were equivalent to the more simplified classes represented in earlier methods. Table 4-1 lists each of the cement classes and shows the corresponding "strength class" in MC 2010 and the general definition of what the terms represent. In all cases, the cement class that most represented the Type III used in this study was the rapid-hardening, high-strength cement. This equivalency assumption is confirmed in the *Guide for Modeling and Calculating Shrinkage and Creep in Hardened Concrete* (ACI 2008), which indicates that Type III cement is equivalent to the RS cement class. This factor is also used in the determining the modified age for creep calculations as described in Section 2.3.5.1.

Table 4-1: Cement Classification for European Methods

Cement Class (MC 90, 99,KAV, EC2)	Cement Strength Class (MC 2010)	Definition
SL	32.5N	Slowly-hardening cements
N or R	32.5R, 42.5N	Normal or Rapid-hardening cements
RS	42.5R, 52.5 N, 52.5R	Rapid-hardening, High-strength cements

The NCHRP 628 method also requires an input termed the "cement type factor". Here, the choices are given for "Type I/II cement" or "Type III + 20% FA binder which may be

used for P(SCC)". Since there is no clear commentary on whether the Type III cement can be separated from the addition of the 20% fly ash binder, it was assumed that this was a particular type of cement used in the research for the NCHRP report and there was not an option for Type III cement alone or Type III combined with slag cement, as was used in this study. Although this option did not directly correspond to the type of cement used in this research, the Type III cement with fly ash binder was the closest match and was selected.

4.2.3 MODULUS OF ELASTICITY

The elastic modulus for each mixture was obtained through testing that was conducted at the precast plant. However, because this test was not conducted on the actual specimens used for creep testing in the laboratory, it was determined that a relationship could be established to estimate an elastic modulus for the laboratory creep specimens based on the available test data. One property of the elastic modulus is that for the same concrete mixture in the normal range of concrete strength, the elastic modulus is proportional to the square root of the compressive strength (Caldarone 2009). Accordingly, the relationship seen in Equation 4-1 was used to determine a modulus of elasticity from the laboratory data at loading based on the proportion from the field data. The calculated modulus of elasticity for each mixture can be seen in Equation 4-1.

$$E_l = \mathrm{E_f}\left(\frac{\sqrt{(\mathrm{f_c})_\mathrm{l}}}{\sqrt{(\mathrm{f_c})_\mathrm{f}}}\right) \qquad \textbf{Equation 4-1}$$

where,

E_l is the modulus of elasticity based on laboratory strength testing

E_f is the modulus of elasticity measured in the prestress plant

$(f_c)_l$ is the compressive strength measured in the laboratory, and

$(f_c)_f$ is the compressive strength measured in the plant.

4.2.4 TEMPERATURE EFFECTS

For this research, an elevated-temperature curing cycle was used for each specimen that was tested. In order to account for these accelerated curing methods, several prediction models implement a temperature-adjusted age in the prediction of creep strain. This is because any deviation from the mean concrete temperature can have an effect on the maturity ("equivalent age") of the concrete. Thus, the concrete's chronological age must be adjusted. This equivalent age concept, which is outlined in Section 2.3.5.1, is employed in the following methods employed in this study:

- MC 90
- MC 90-KAV
- MC 90-99
- MC 2010, and
- Eurocode.

While at the prestressing plant, the test cylinders were cured via either match- or tarp-curing processes. A temperature profile was collected from representative steam-cured and match-cured cylinders using thermocouple wire. However, the specimens had to be transported two hours from the plant to the laboratory where testing was conducted. In order to do this, the cylinders had to be disconnected from the datalogging equipment. Since the temperatures of the test specimens were not monitored through the final few hours prior to

loading, several assumptions had to be made to estimate the temperature-adjusted age of these specimens.

After removal of the specimens from their respective curing conditions, their temperature gradually began to move towards the ambient temperature. This was assumed to occur slowly during transportation while in the insulated plastic containers, and then more rapidly once they were stripped and exposed to the laboratory conditions during test preparation. This principle was based on a simplified assumption of Newton's Law of Cooling, which states that the rate at which heat flows from a hot body to a colder one is proportional to the temperature difference between the two (Sastry 2009). The assumed rate of heat loss for the cylinders was 0.1°C per hour per temperature differential (°C) relative to the outdoor ambient temperature while in the insulated containers. The rate of heat loss when stripped in the laboratory was assumed to be 1.0°C per hour per temperature differential (°C) relative to the laboratory temperature. Equation 4-2 and Equation 4-3 depict how the calculated portion of the temperature profiles was created while the cylinders were insulated and exposed to the atmosphere, respectively. These equations were used for both two-minute and five-minute intervals.

$$T_{i,t} = T_{x-1} - R_i(T_{x-1} - T_a)(t_x - t_{x-1}) \qquad \textbf{Equation 4-2}$$

where,

$T_{i,t}$ is the temperature of the insulated cylinders at time t (°C)

T_{x-1} is the temperature of the cylinders at time t_{x-1} (°C)

R_i is the assumed rate of change for the insulated cylinders; 0.1°C per °C per hour

T_a is the ambient temperature (°C)

t_x is the time at the moment considered (hours), and

t_{x-1} is the time one interval before the moment considered (hours).

$$T_{e,t} = T_{x-1} - R_e(T_{x-1} - T_l)(t_x - t_{x-1}) \quad \textbf{Equation 4-3}$$

where,

$T_{e,t}$ is the temperature of the exposed cylinders at time t (°C)

T_{x-1} is the temperature of the cylinders at time t_{x-1} (°C)

R_e is the assumed rate of change for the exposed cylinders; 1.0°C per °C per hour

T_l is the laboratory temperature (°C)

t_x is the time at the moment considered (hours), and

t_{x-1} is the time one interval before the moment considered (hours).

These temperatures were calculated in small intervals until the time of loading. One example of the temperature profiles created can be seen in Figure 4-1, which graphs the temperature profile over time for one set of specimens. This plot shows one mixture with the two different curing methods that were implemented. The first portion of the graph shows solid lines that represent the measured temperatures from the thermocouples, and the latter portion of the graph shows dotted lines which represent the calculated temperatures using the assumed rates of cooling.

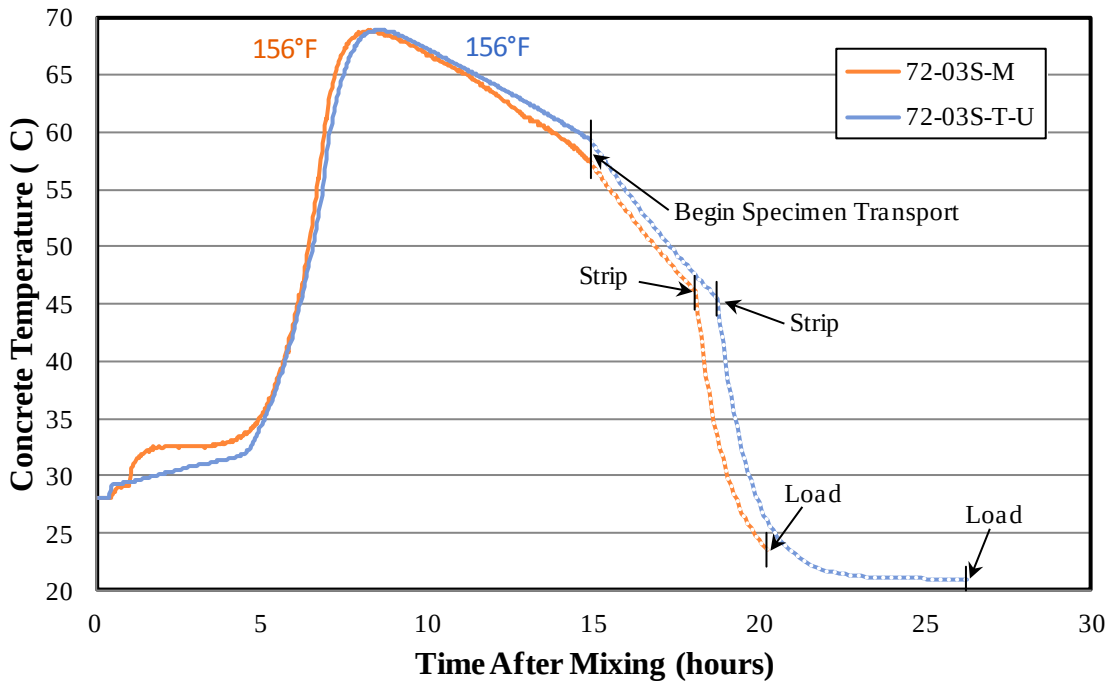

Figure 4-1: Temperature Profile for Batch 72-03S

Figure 4-2 and Figure 4-3 each represent one of the curing types from the mixture in the previous example. This graph depicts the maturity of concrete over time for each particular set of specimens and shows the chronological age of the concrete as well as the adjusted age to account for the elevated curing cycles. The "EU Modified (for Temp & Cement) Age" represents the maturity computed in accordance with the European methods: MC 90, MC 90-99, MC 2010, and Eurocode. Also shown is the "EU Temperature-Adjusted Age" that represents the first step in the two-step process given by the European methods. This two-step process is represented by Equation 2-32 and Equation 2-33 in Section 2.3.5.1. The second step includes the correction factor for cement type. The "Temperature-Adjusted Age (KAV)" represents the maturity computed in accordance with MC 90-KAV, as seen in Table 2-1 in Section 2.3.6. Although the MC 90-KAV age adjustment is only a one-step process,

the resulting maturity is intended for use as the loading age and therefore corresponds to the entire two-step European process. These graphs point out the major milestones for testing. These include the point at which transportation began, the time at which the cylinders were stripped from their plastic molds, and the time at which the cylinders were loaded. For a complete set of both the temperature profiles and the maturity plots, refer to Appendix B.

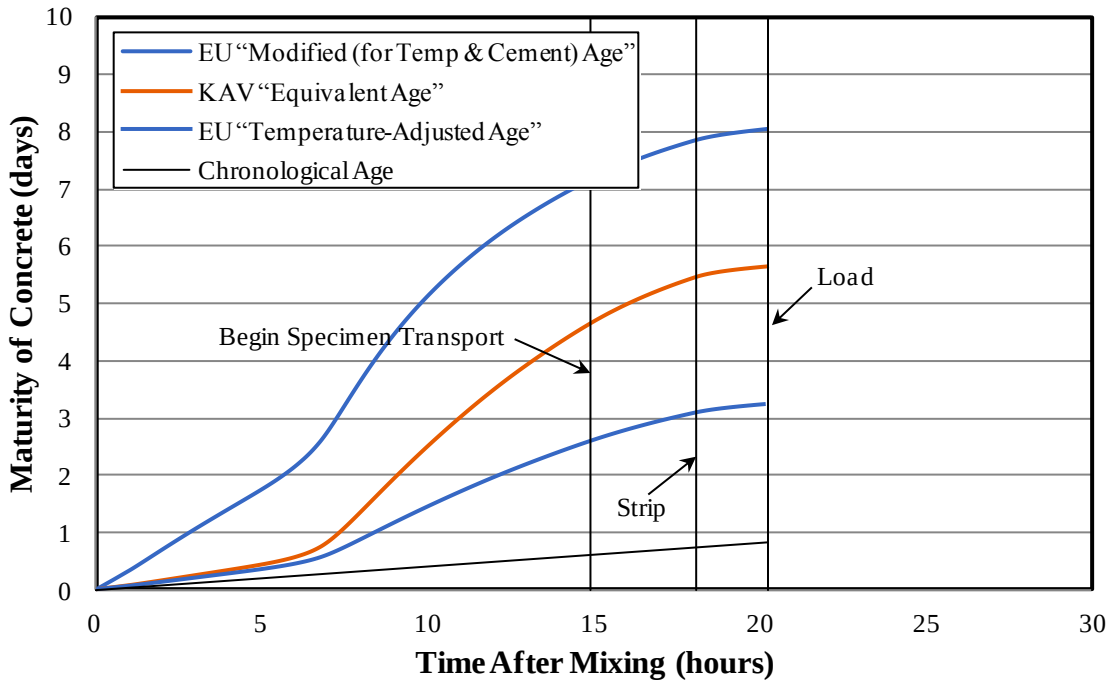

Figure 4-2: Maturity of Specimens 72-03S-M

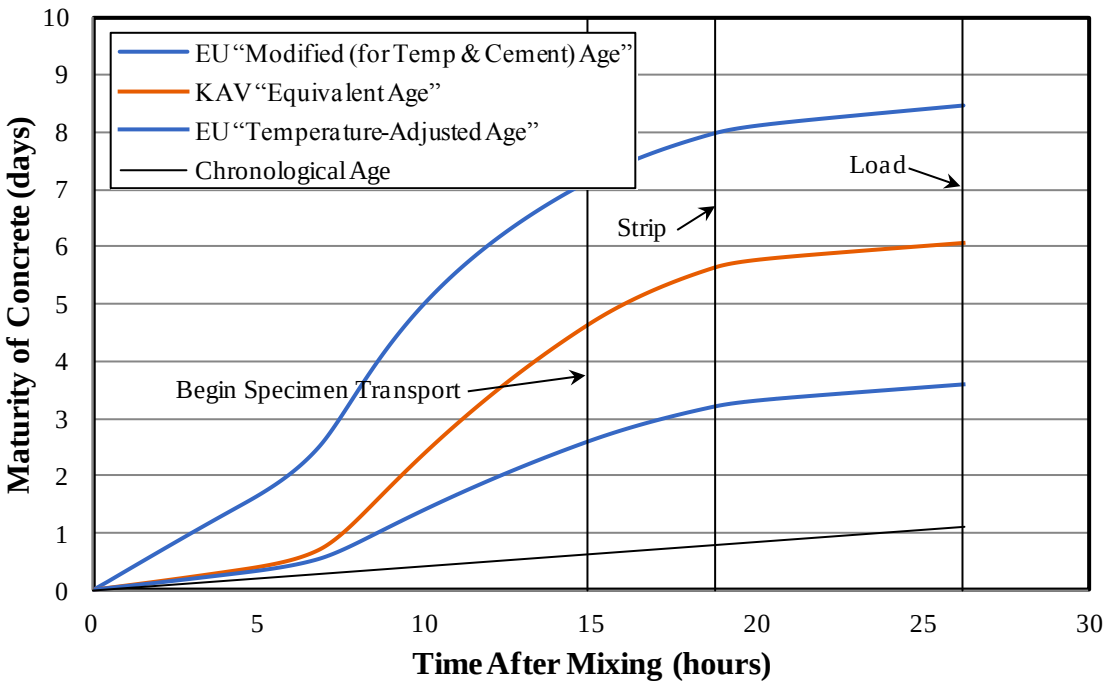

Figure 4-3: Maturity of Specimens 72-03S-T-U

4.2.5 Age at Loading and Duration of Curing

For the purpose of this research, three distinct chronological milestones were identified. The chronological curing age was the time from adding water to the cement until stripping the test specimens from their molds. The chronological loading age was the time from the start of mixing the concrete to applying a load on the test specimens. Lastly, the drying age at loading was taken as the time between stripping and loading the specimens. These events are extremely significant to the effects of creep and shrinkage on concrete.

In ACI 209, the creep correction factor is given for non-accelerated-cured concrete at loading ages later than 7 days, and also for accelerated-cured concrete at loading ages later than 1 to 3 days. However, there is no mention of ages less than 7 days for non-accelerated-cured concrete, or less than 1 day for accelerated-cured concrete. ACI 209 is also unclear in

regards to the shrinkage correction factor for curing age. A table is given for non-accelerated-cured concrete that is cured for a time other than the recommended 7 days and interpolation is allowed. However, there is no mention of what to do about accelerated-cured concrete for times other than the standard 1 to 3 days. Lastly, the shrinkage shape and size factor used in ACI 209 is also dependent on the 7 days for non-accelerated curing and 1 to 3 days for accelerated curing rules. Again, there is no mention of what to do outside of these parameters. Several of the specimens used in this research were cured just shy of the 1 day limitation for the creep loading age and the shrinkage curing age correction factors. For both of these cases, an assumption was made that the standard equation for accelerated-cured concrete was to be applied.

AASHTO 2004 does not explicitly state if the loading age is based on accelerated or non-accelerated curing. However, the statement is made that "one day of accelerated curing by steam or radiant heat may be taken as equal to seven days of normal curing". This implies that accelerated, or steam curing requires modification, but again, does not explicitly state whether this should be an addition of 6 days or a multiplication by a factor of 7. Commentary in AASHTO 2004 indicates that this method is adapted from Collins and Mitchell (1991), who refer to "adding" days to compensate for accelerated curing. However, at one day of curing, there is no difference to the loading age when adding 6 days or multiplying by 7; and, for accelerated-curing periods of 18 to 24 hours, the difference in the resulting loading age correction factor is less than 3 percent. Thus, since all the concrete for this research was cured for a period close to one day, the assumption was made that the loading age for accelerated curing should be multiplied by 7 to get an equivalent number of non-accelerated

curing days. AASHTO 2010, on the other hand, is based on the number of *accelerated-curing* days and therefore, no correction was necessary.

AASHTO 2004 and AASHTO 2010 both specify an increase in shrinkage of 20 percent for concrete "exposed to drying before 5 days of curing have elapsed." The code does not clarify if these days are for accelerated or non-accelerated curing. Since the term "normal" is used throughout the text to differentiate from accelerated curing, the assumption was made that the above mentioned 5 days are for non-accelerated curing. Thus, for non-accelerated concrete cured for less than 5 days, the shrinkage should be increased by 20 percent. Using the same AASHTO logic relating accelerated-curing days to non-accelerated-curing days as discussed above, 17 hours of accelerated curing is roughly equivalent to 5 days of non-accelerated curing. Therefore, this shrinkage correction was not used for the AASHTO predictions in this study.

4.3 SPECIFIC CONSIDERATIONS

This section outlines the specific assumptions or decisions that were applied to each individual prediction model. Here, the assumptions are categorized by method.

4.3.1 ACI 209

The ACI 209 prediction method originated before the introduction of water-reducing admixtures, and thus changes were necessary to account for the increased slumps that occurred in both the SCC and CVC mixtures due to these chemical admixtures. These high slump values could not be used because unrealistic creep and shrinkage correction factors resulted and thus produced unrealistic strain predictions. Experimental results and analyses reported by Schrantz (2012) showed that using the actual slump in the ACI 209 prediction

models can result in significant errors in time-dependent deformations and therefore, an adjusted slump should be used. In order to estimate the slump values before any admixtures were added to the concrete mixtures, an adjusted "water slump" was set as zero inches for all SCC mixtures and 0.5 inches for all CVC mixtures. This adjusted slump was estimated based on the water content, nominal maximum aggregate size, and air content of the concrete mixtures. More precise adjusted-slump estimates were not warranted because the correction factor is relatively insensitive to small changes in low slump values such as these.

In addition, an assumption was made that the cement content should be taken as the total cementitious material. This meant that the cement content consisted of the portland cement plus the slag cement.

With these assumptions made, as well as decisions about the elastic modulus and curing duration discussed in previous sections, the predictions for creep and shrinkage were conducted according to the ACI 209 model which is outlined in Sections 2.3.1 and 2.5.1, respectively.

4.3.2 AASHTO 2004 AND 2010

Unlike the ACI 209 method, both AASHTO methods that were studied were developed with high-strength concrete in mind; although, AASHTO 2010 is geared toward high-strength concrete moreso than AASHTO 2004. Furthermore, no assumptions specific to these methods had to be made in order to predict the creep or shrinkage. It should be noted, however, that AASHTO 2010 is the only prediction model to estimate the creep and shrinkage based on the compressive strength at transfer. Otherwise, the prediction for creep and shrinkage for AASHTO 2004 was completed in the manner described in Section 2.3.2

and Section 2.5.2, respectively. The prediction for creep and shrinkage for AASHTO 2010 was completed in the manner described in Section 2.3.3 and Section 2.5.3, respectively.

4.3.3 NCHRP 628

The NCHRP Report 628 was created to address the need to better understand the influence of the materials used in SCC on the properties of fresh and hardened concrete used in prestressed concrete construction. This project sought to accomplish this by identifying reliable test methods and performance specifications for mix design and quality control of SCC specifically. The NCHRP 628 predicts creep by modifying the AASHTO 2010 model and shrinkage by modifying the AASHTO 2004 model. Since the NCHRP 628 modifications were targeted at SCC, this model could only be applied to the SCC mixtures used in this research. Otherwise, if CVC mixtures were used, the creep was calculated by means of AASHTO 2010, and the shrinkage was calculated by means of AASHTO 2004. Furthermore, it should be noted that AASHTO 2010 estimates the creep and shrinkage based on the compressive strength at transfer and thus, the NCHRP 628 model does also.

With these assumptions made, as well as decisions discussed in previous sections, the predictions for creep and shrinkage were conducted according to the NCHRP 628 model outlined in Sections 2.3.4 and 2.5.4, respectively.

4.3.4 MC 90, MC 90-99, AND MC 2010

The language in the model codes is relatively clear and other than the general assumptions made in the previous sections, there were no other assumptions made specifically to these methods in order to predict the creep or shrinkage. Section 4.2.2 describes the cement class that was chosen with further details in Table 4-1. The prediction

of creep for MC 90, MC 90-99, and MC 2010 are detailed in Section 2.3.5, Section 2.3.7, and Section 2.3.8, respectively. The prediction of shrinkage for these methods is detailed in Section 2.5.5, Section 2.5.7, and Section 2.5.8, respectively.

4.3.5 MC 90-KAV

The modifications made by Kavanaugh to the MC 90 creep prediction method are detailed in Section 2.3.6. However, it should be noted that the temperature-adjusted concrete age, t_T , shown in Table 2-1, was developed to include the effects of the type of cement within this equation itself. This means that when calculating the temperature effects on maturity at loading, as in Section 2.3.5.1, the Kavanaugh t_T is *not* then modified again by Equation 2-33; but rather, is meant to directly replace the loading age, t_o.

4.3.6 EUROCODE

In order to calculate the development of drying shrinkage over time for the Eurocode model, the coefficient that depends on notional size must first be found. This coefficient, k_h , is determined according to Table 2-3. However, the Eurocode does not specify what to do if the notional size is outside of the range of this table (100 to 500 mm) or does not fall on one of the values represented (increments of 100 mm). For the cylindrical specimens in this study, the notional size was 76.2 mm, which was outside the scope of the given table. It was assumed that any number less than the notional sizes represented in the table would be taken as the previous value for k_h with 1.0 being the maximum value. Thus, k_h was taken as 1.0.

With this assumption made, as well as decisions discussed in previous sections, the predictions for creep and shrinkage were conducted according to the Eurocode model, which is discussed in Sections 2.3.9 and 2.5.9, respectively.

4.4 SUMMARY OF PREDICTION METHOD INPUTS

Table 4-2 is a summary of all the parameters that were utilized in the prediction of creep and shrinkage deformations for the various methods investigated. The parameters in this table are defined such that:

- t_{cure} is the amount of time since curing began; from mixing to stripping (days)
- t_i is the age at which the load was applied; from mixing to loading (days)
- $t_i - t_{cure}$ is the amount of time since drying began until loading (days)
- $t_{T,EU}$ is the European age at loading modified for temperature (days)
- $t_{o,EU}$ is the European age at loading modified for temperature and cement (days)
- $t_{o,\,KAV}$ is the MC 90-KAV modified age at loading (days)
- f_{ci} is the compressive strength at transfer (ksi)
- $f_{c,28}$ is the compressive strength at 28 days (ksi)
- E_{ci} is the estimated elastic modulus at transfer (ksi)
- C is the total cement content; portland cement plus slag cement (lbs/yd^3)
- S is the adjusted slump (in.), and
- F is the applied compressive force at loading (kips).

Table 4-2: Inputs Used in Creep and Shrinkage Prediction Calculations

Specimen	t_{cure} (days)	t_i (days)	$t_i - t_{cure}$ (days)	$t_{T,EU}$ (days)	$t_{o,EU}$ (days)	$t_{o,KAV}$ (days)	f_{ci} (ksi)	$f_{c,28}$ (ksi)	E_{ci} (ksi)	C (lbs/yd^3)	*Air* (%)	*S* (in.)	% Fine Aggregate	*F* (kips)
54-03S-M*	0.94	1.08	0.15	2.63	7.19	3.87	7.23	10.80	5700	892	3.0	0.0	48	82.0
54-03S-T	0.99	1.15	0.15	4.55	9.57	8.07	8.93	10.80	6400	892	3.0	0.0	48	103.0
54-07S-M	0.89	0.99	0.10	3.86	8.78	6.63	7.88	10.18	6100	892	4.2	0.0	48	87.0
54-07S-T	0.91	1.12	0.21	3.10	7.84	4.78	7.49	10.18	5900	892	4.2	0.0	48	81.0
72-03S-M	0.75	0.84	0.09	3.26	8.04	5.63	7.06	10.77	7680	895	4.3	0.0	47	84.0
72-03S-T-U	0.78	1.09	0.31	3.60	8.47	6.07	7.68	10.77	5800	895	4.3	0.0	47	35.0
54-12C-M	0.81	0.90	0.09	2.41	6.86	3.51	7.11	9.67	6400	820	4.5	0.5	38	82.0
54-12C-T	0.85	1.06	0.21	3.06	7.79	4.67	8.12	9.67	6800	820	4.5	0.5	38	87.0
72-11C-M	0.77	0.86	0.10	2.39	6.83	3.56	7.98	11.05	6700	833	3.1	0.5	38	90.0
72-11C-T-U	0.79	1.14	0.35	2.83	7.48	4.15	8.88	11.05	7000	833	3.1	0.5	38	32.5

CHAPTER 5
PRESENTATION AND ANALYSIS OF RESULTS

5.1 INTRODUCTION

One of the primary objectives of this research was to evaluate the performance of the nine creep and shrinkage prediction methods detailed in Chapter 2 in order to determine their efficiency at determining time-dependent deformations of SCC and CVC. This was achieved by comparing the measured time-dependent strains from each test sample with the strains estimated in accordance with the following creep and shrinkage models:

- ACI 209
- AASHTO 2004
- AASHTO 2010
- NCHRP 628
- MC 90
- MC 90-99
- MC 90-KAV
- MC 2010, and
- Eurocode.

This chapter first presents all of the results from the creep testing that was conducted for this research up to one year. These results include both measured strains from the laboratory

and predicted strains from each of the nine prediction methods that were tested. Later, a discussion of the accuracy of each method is included and a summary of all conclusions is given at the close of the chapter.

5.2 MEASURED STRAIN

This section presents the strains that were calculated using the measured data up to one year. Figure 5-1 illustrates the strain cases that were evaluated where the following was assumed:

- *Initial Strain* is the strain that is measured immediately after application of the load. Also called *Instantaneous Strain*.
- *Creep Strain* (ε_{cr}) is the additional strain that occurs over time due to sustained loads.
- *Load-Induced Strain* (ε_{li}) is the total strain due to the applied load, which is the sum of the Initial and Creep Strains. Also called *Load-Dependent Strain*.
- *Shrinkage Strain* (ε_{sh}) is the strain that occurs without any applied load.
- *Total Strain* (ε_t) is the total of all strains.

These concrete strains were calculated from the DEMEC measurements taken from the concrete cylinders. The cylinders loaded in the creep frames were used to measure the total strain in the concrete, which includes the strain due to the induced load and the shrinkage strain. This procedure was done for each DEMEC measurement distance on the cylinder (A, B, and C), and for both the top and bottom cylinders in the frame. The result was six different strains for each frame. These strains were then used to find the average strain per cylinder

and the average strain per frame. The unloaded shrinkage cylinders exhibit only the shrinkage strain. The DEMEC measurements were taken for each of the three shrinkage cylinders just as with the cylinders in the creep frames. This resulted in nine strains for each specimen set. Three strains per cylinder were averaged to find the strain per cylinder and the resulting three averages were averaged to find the shrinkage strain per group. Once the total strain and shrinkage strain were found for a specimen set, the shrinkage strain was subtracted from the total strain to compute the load-induced strain. In these results, a negative strain indicates a contraction or shortening of a specimen and a positive strain indicates a stretching or expansion of a specimen.

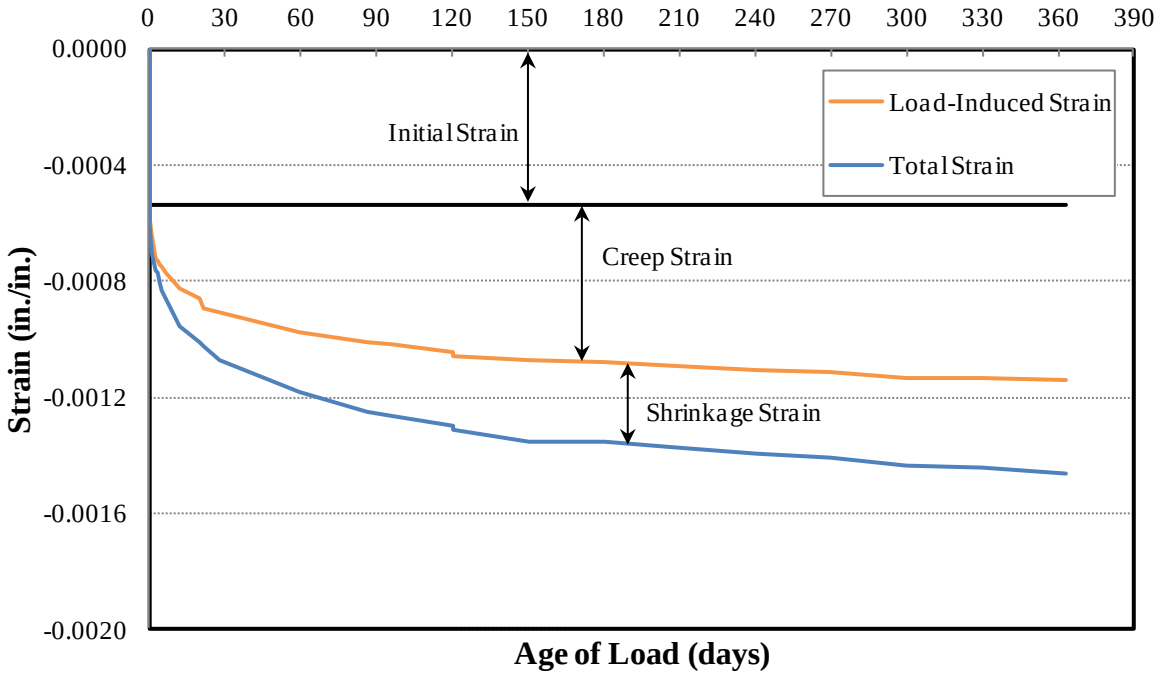

Figure 5-1: Illustration of Strain Cases

It is difficult to precisely determine where the instantaneous strain ends and the creep strain begins because it takes several minutes to execute the cylinder loading process

described in Section 3.4.3.3. Therefore, the initial strain *measurement* can include a creep component that is impossible to accurately quantify in practice. Experimental determination of the creep *coefficient*, which is traditionally defined as the ratio of creep strain to elastic strain, is particularly sensitive to slight inaccuracies in the initial strain measurement. Because of this, creep effects were assessed for this thesis by considering the *load-induced* strain, which represents the summation of the initial strain and the creep strain.

The total strain (ε_t), shrinkage strain (ε_{sh}), load-induced strain (ε_{li}), and creep strain (ε_{cr}) are presented in Table 5-1 through Table 5-10 as well as the age of load, which indicates when the strain occurred. The tables are organized according to concrete type where the first six samples are of SCC and the last four samples are CVC.

Table 5-1: First-Year Strains of Specimen 54-03S-M*

Target Age	Age of Load (days)	Age since Zero-Strain (days)	Total Strain (in./in.)	Shrinkage Strain (in./in.)	Strain due to Load (in./in.)	Creep Strain (in./in.)
Pre-Load	NA	0.00	0.000000	0.000000	0.000000	0.000000
Post-Load	0.00	0.03	-0.000536	0.000000	-0.000536	0.000000
2-6 Hours	0.19	0.22	-0.000612	-0.000028	-0.000584	-0.000048
1 Day	1.0	1.0	-0.000705	-0.000064	-0.000640	-0.000104
2 Day	2.3	2.3	-0.000762	-0.000039	-0.000723	-0.000187
3 Day	3.3	3.3	-0.000769	-0.000040	-0.000729	-0.000192
4 Day	4.4	4.4	-0.000803	-0.000060	-0.000743	-0.000207
5 Day	5.1	5.2	-0.000832	-0.000082	-0.000750	-0.000213
6 Day	6.2	6.2	-0.000859	-0.000088	-0.000771	-0.000235
7 Day	12.1	12.1	-0.000955	-0.000127	-0.000828	-0.000292
2 Week	20	20	-0.001013	-0.000150	-0.000862	-0.000326
3 Week	21	21	-0.001028	-0.000136	-0.000892	-0.000355
4 Week	28	28	-0.001073	-0.000162	-0.000910	-0.000374
2 Month	59	59	-0.001185	-0.000211	-0.000974	-0.000438
3 Month[1]	86	86	-0.001255	-0.000242	-0.001012	-0.000476
3 Month[2]	96	96	-0.001263	-0.000245	-0.001018	-0.000481
4 Month	120	120	-0.001299	-0.000254	-0.001045	-0.000508
4 Month[3]	120	120	-0.001310	-0.000254	-0.001056	-0.000520
5 Month	150	150	-0.001355	-0.000279	-0.001076	-0.000539
6 Month	180	180	-0.001357	-0.000276	-0.001081	-0.000545
7 Month	210	210	-0.001375	-0.000283	-0.001092	-0.000555
8 Month	240	240	-0.001394	-0.000289	-0.001105	-0.000569
9 Month	270	270	-0.001408	-0.000294	-0.001114	-0.000577
10 Month	300	300	-0.001438	-0.000300	-0.001137	-0.000601
11 Month	330	330	-0.001446	-0.000314	-0.001132	-0.000595
12 Month	363	363	-0.001467	-0.000329	-0.001138	-0.000602

NOTE: [1] Measurements were taken before scheduled time

[2] Measurements were taken again after scheduled time

[3] Measurements were retaken after frame force was re-adjusted to original magnitude

Table 5-2: First-Year Strains of Specimen 54-03S-T

Target Age	Age of Load (days)	Age since Zero-Strain (days)	Total Strain (in./in.)	Shrinkage Strain (in./in.)	Strain due to Load (in./in.)	Creep Strain (in./in.)
Pre-Load	NA	0.00	0.000000	0.000000	0.000000	0.000000
Post-Load	0.00	0.03	-0.000717	0.000002	-0.000719	0.000000
2-6 Hours	0.13	0.17	-0.000775	-0.000014	-0.000760	-0.000041
1 Day	0.9	0.9	-0.000876	-0.000036	-0.000840	-0.000120
2 Day	2.2	2.2	-0.000929	-0.000005	-0.000923	-0.000204
3 Day	3.2	3.2	-0.000941	-0.000013	-0.000928	-0.000209
4 Day	4.3	4.4	-0.000969	-0.000020	-0.000950	-0.000231
5 Day	5.1	5.1	-0.001008	-0.000028	-0.000980	-0.000261
6 Day	6.1	6.1	-0.001031	-0.000046	-0.000984	-0.000265
7 Day	12.0	12.1	-0.001169	-0.000092	-0.001077	-0.000358
2 Week	20	20	-0.001251	-0.000119	-0.001132	-0.000412
3 Week	21	21	-0.001250	-0.000117	-0.001133	-0.000414
4 Week	28	28	-0.001311	-0.000148	-0.001163	-0.000444
2 Month	59	59	-0.001472	-0.000207	-0.001265	-0.000546
3 Month[1]	86	86	-0.001555	-0.000244	-0.001311	-0.000592
3 Month[2]	96	96	-0.001572	-0.000247	-0.001325	-0.000606
4 Month	120	120	-0.001615	-0.000252	-0.001364	-0.000645
4 Month[3]	120	120	-0.001622	-0.000252	-0.001370	-0.000651
5 Month	150	150	-0.001677	-0.000279	-0.001398	-0.000679
6 Month	180	180	-0.001685	-0.000276	-0.001409	-0.000690
7 Month	210	210	-0.001705	-0.000274	-0.001431	-0.000712
8 Month	240	240	-0.001733	-0.000286	-0.001447	-0.000728
9 Month	270	270	-0.001752	-0.000285	-0.001467	-0.000748
10 Month	300	300	-0.001774	-0.000290	-0.001485	-0.000765
11 Month	330	330	-0.001786	-0.000304	-0.001482	-0.000763
12 Month	363	363	-0.001809	-0.000319	-0.001490	-0.000771

NOTE: [1] Measurements were taken before scheduled time

[2] Measurements were taken again after scheduled time

[3] Measurements were retaken after frame force was re-adjusted to original magnitude

Table 5-3: First-Year Strains of Specimen 54-07S-M

Target Age	Age of Load (days)	Age since Zero-Strain (days)	Total Strain (in./in.)	Shrinkage Strain (in./in.)	Strain due to Load (in./in.)	Creep Strain (in./in.)
Pre-Load	NA	0.00	0.000000	0.000000	0.000000	0.000000
Post-Load	0.00	0.02	-0.000658	-0.000016	-0.000642	0.000000
2-6 Hours	0.14	0.16	-0.000767	-0.000062	-0.000705	-0.000063
1 Day	1.2	1.2	-0.000865	-0.000106	-0.000760	-0.000118
2 Day	2.3	2.3	-0.000924	-0.000109	-0.000815	-0.000173
3 Day	3.1	3.1	-0.000966	-0.000119	-0.000847	-0.000205
4 Day	4.3	4.3	-0.000990	-0.000139	-0.000851	-0.000209
5 Day	5.2	5.3	-0.001017	-0.000129	-0.000888	-0.000246
6 Day	6.2	6.2	-0.001031	-0.000143	-0.000889	-0.000247
7 Day	7.0	7.1	-0.001081	-0.000168	-0.000913	-0.000271
2 Week	14	14	-0.001183	-0.000185	-0.000997	-0.000355
3 Week	21	21	-0.001267	-0.000228	-0.001039	-0.000397
4 Week	28	28	-0.001308	-0.000239	-0.001069	-0.000427
2 Month	58	58	-0.001487	-0.000339	-0.001148	-0.000506
3 Month	93	93	-0.001604	-0.000375	-0.001229	-0.000587
4 Month	120	120	-0.001625	-0.000376	-0.001249	-0.000607
4 Month[1]	120	120	-0.001658	-0.000376	-0.001282	-0.000640
5 Month	150	150	-0.001715	-0.000400	-0.001315	-0.000673
6 Month	180	180	-0.001744	-0.000410	-0.001334	-0.000692
7 Month	210	210	-0.001755	-0.000408	-0.001347	-0.000705
8 Month	240	240	-0.001782	-0.000401	-0.001382	-0.000740
9 Month	270	270	-0.001799	-0.000410	-0.001389	-0.000747
10 Month	307	307	-0.001824	-0.000424	-0.001399	-0.000757
11 Month	331	331	-0.001848	-0.000439	-0.001409	-0.000767
12 Month	363	363	-0.001866	-0.000447	-0.001418	-0.000776

NOTE: [1] Measurements were retaken after frame force was re-adjusted to original magnitude

Table 5-4: First-Year Strains of Specimen 54-07S-T

Target Age	Age of Load (days)	Age since Zero-Strain (days)	Total Strain (in./in.)	Shrinkage Strain (in./in.)	Strain due to Load (in./in.)	Creep Strain (in./in.)
Pre-Load	NA	0.00	0.000000	0.000000	0.000000	0.000000
Post-Load	0.00	0.04	-0.000581	-0.000018	-0.000564	0.000000
2-6 Hours	0.17	0.21	-0.000663	-0.000027	-0.000637	-0.000073
1 Day	1.6	1.6	-0.000726	-0.000040	-0.000686	-0.000123
2 Day	2.7	2.7	-0.000777	-0.000050	-0.000728	-0.000164
3 Day	3.5	3.5	-0.000823	-0.000068	-0.000755	-0.000191
4 Day	4.7	4.7	-0.000855	-0.000072	-0.000783	-0.000219
5 Day	6.1	6.1	-0.000885	-0.000073	-0.000811	-0.000248
6 Day	7.1	7.1	-0.000892	-0.000083	-0.000809	-0.000246
7 Day	7.9	8.0	-0.000938	-0.000103	-0.000835	-0.000272
2 Week	15	15	-0.001032	-0.000122	-0.000910	-0.000346
3 Week	22	22	-0.001115	-0.000161	-0.000954	-0.000390
4 Week	29	29	-0.001151	-0.000169	-0.000982	-0.000419
2 Month	59	59	-0.001319	-0.000250	-0.001068	-0.000505
3 Month	94	94	-0.001410	-0.000289	-0.001121	-0.000557
4 Month	121	121	-0.001446	-0.000292	-0.001154	-0.000591
4 Month[1]	121	121	-0.001463	-0.000292	-0.001172	-0.000608
5 Month	151	151	-0.001516	-0.000315	-0.001201	-0.000638
6 Month	181	181	-0.001544	-0.000324	-0.001220	-0.000656
7 Month	211	211	-0.001559	-0.000324	-0.001235	-0.000672
8 Month	241	241	-0.001570	-0.000327	-0.001243	-0.000679
9 Month	271	271	-0.001593	-0.000336	-0.001256	-0.000693
10 Month	308	308	-0.001614	-0.000349	-0.001265	-0.000701
11 Month	332	332	-0.001638	-0.000363	-0.001275	-0.000711
12 Month	364	364	-0.001656	-0.000365	-0.001291	-0.000727

NOTE: [1] Measurements were retaken after frame force was re-adjusted to original magnitude

Table 5-5: First-Year Strains of Specimen 72-03S-M

Target Age	Age of Load (days)	Age since Zero-Strain (days)	Total Strain (in./in.)	Shrinkage Strain (in./in.)	Strain due to Load (in./in.)	Creep Strain (in./in.)
Pre-Load	NA	0.00	0.000000	0.000000	0.000000	0.000000
Post-Load	0.00	0.08	-0.000782	-0.000027	-0.000755	0.000000
2-6 Hours	0.25	0.33	-0.000920	-0.000076	-0.000844	-0.000088
1 Day	1.2	1.3	-0.001068	-0.000128	-0.000940	-0.000185
2 Day	2.1	2.2	-0.001110	-0.000139	-0.000971	-0.000216
3 Day	3.0	3.1	-0.001162	-0.000129	-0.001033	-0.000278
4 Day	4.4	4.5	-0.001217	-0.000145	-0.001072	-0.000317
5 Day	5.2	5.3	-0.001253	-0.000156	-0.001097	-0.000342
6 Day	6.2	6.3	-0.001261	-0.000172	-0.001089	-0.000334
7 Day	7.1	7.2	-0.001296	-0.000176	-0.001120	-0.000365
2 Week	14	14	-0.001391	-0.000207	-0.001184	-0.000428
3 Week	21	21	-0.001469	-0.000246	-0.001223	-0.000468
4 Week	28	28	-0.001509	-0.000277	-0.001231	-0.000476
2 Month	58	58	-0.001653	-0.000336	-0.001317	-0.000561
3 Month	90	90	-0.001727	-0.000380	-0.001348	-0.000592
4 Month	120	120	-0.001772	-0.000388	-0.001384	-0.000629
4 Month[1]	120	120	-0.001799	-0.000388	-0.001411	-0.000655
5 Month	150	150	-0.001847	-0.000408	-0.001440	-0.000684
6 Month	180	180	-0.001879	-0.000409	-0.001470	-0.000714
7 Month	210	210	-0.001910	-0.000426	-0.001483	-0.000728
8 Month	240	240	-0.001923	-0.000425	-0.001498	-0.000743
9 Month	270	270	-0.001946	-0.000441	-0.001505	-0.000749
10 Month	301	301	-0.001970	-0.000451	-0.001520	-0.000764
11 Month	330	330	-0.001993	-0.000456	-0.001537	-0.000782
12 Month	358	358	-0.002005	-0.000469	-0.001537	-0.000781

NOTE: [1] Measurements were retaken after frame force was re-adjusted to original magnitude

Table 5-6: First-Year Strains of Specimen 72-03S-T-U

Target Age	Age of Load (days)	Age since Zero-Strain (days)	Total Strain (in./in.)	Shrinkage Strain (in./in.)	Strain due to Load (in./in.)	Creep Strain (in./in.)
Pre-Load	NA	0.00	0.000000	0.000000	0.000000	0.000000
Post-Load	0.00	0.02	-0.000262	-0.000011	-0.000251	0.000000
2-6 Hours	0.10	0.13	-0.000277	-0.000018	-0.000260	-0.000009
1 Day	1.0	1.0	-0.000325	-0.000026	-0.000299	-0.000048
2 Day	1.8	1.9	-0.000349	-0.000036	-0.000314	-0.000063
3 Day	2.8	2.8	-0.000358	-0.000040	-0.000318	-0.000067
4 Day	4.2	4.2	-0.000380	-0.000053	-0.000327	-0.000076
5 Day	4.9	4.9	-0.000388	-0.000062	-0.000326	-0.000075
6 Day	5.9	5.9	-0.000401	-0.000072	-0.000329	-0.000078
7 Day	6.9	7.0	-0.000415	-0.000086	-0.000329	-0.000078
2 Week	14	14	-0.000489	-0.000114	-0.000375	-0.000124
3 Week	21	21	-0.000548	-0.000153	-0.000395	-0.000144
4 Week	28	28	-0.000579	-0.000173	-0.000406	-0.000155
2 Month	58	58	-0.000689	-0.000240	-0.000448	-0.000197
3 Month	90	90	-0.000741	-0.000270	-0.000470	-0.000220
4 Month	120	120	-0.000759	-0.000276	-0.000483	-0.000232
4 Month[1]	120	120	-0.000771	-0.000276	-0.000495	-0.000244
5 Month	150	150	-0.000801	-0.000308	-0.000494	-0.000243
6 Month	180	180	-0.000818	-0.000312	-0.000506	-0.000255
7 Month	210	210	-0.000830	-0.000320	-0.000510	-0.000259
8 Month	240	240	-0.000838	-0.000327	-0.000511	-0.000260
9 Month	270	270	-0.000856	-0.000341	-0.000515	-0.000264
10 Month	301	301	-0.000870	-0.000350	-0.000520	-0.000269
11 Month	330	330	-0.000882	-0.000363	-0.000519	-0.000268
12 Month	358	358	-0.000893	-0.000372	-0.000521	-0.000270

NOTE: [1] Measurements were retaken after frame force was re-adjusted to original magnitude

Table 5-7: First-Year Strains of Specimen 54-12C-M

Target Age	Age of Load (days)	Age since Zero-Strain (days)	Total Strain (in./in.)	Shrinkage Strain (in./in.)	Strain due to Load (in./in.)	Creep Strain (in./in.)
Pre-Load	NA	0.00	0.000000	0.000000	0.000000	0.000000
Post-Load	0.00	0.02	-0.000562	-0.000035	-0.000527	0.000000
2-6 Hours	0.17	0.19	-0.000637	-0.000045	-0.000592	-0.000065
1 Day	1.3	1.3	-0.000733	-0.000050	-0.000682	-0.000155
2 Day	2.3	2.3	-0.000756	-0.000068	-0.000688	-0.000160
3 Day	3.4	3.5	-0.000807	-0.000072	-0.000735	-0.000207
4 Day	4.2	4.2	-0.000828	-0.000084	-0.000744	-0.000217
5 Day	5.2	5.3	-0.000875	-0.000105	-0.000770	-0.000242
6 Day	6.1	6.1	-0.000882	-0.000107	-0.000775	-0.000248
7 Day	12.2	12.2	-0.000955	-0.000124	-0.000830	-0.000303
2 Week	19	19	-0.001024	-0.000152	-0.000872	-0.000345
3 Week	21	21	-0.001047	-0.000163	-0.000884	-0.000356
4 Week	28	28	-0.001079	-0.000167	-0.000912	-0.000385
2 Month	59	59	-0.001199	-0.000217	-0.000982	-0.000455
3 Month[1]	85	85	-0.001269	-0.000249	-0.001020	-0.000492
3 Month[2]	95	95	-0.001280	-0.000250	-0.001030	-0.000503
4 Month	120	120	-0.001317	-0.000265	-0.001052	-0.000524
4 Month[3]	120	120	-0.001322	-0.000265	-0.001057	-0.000530
5 Month	150	150	-0.001364	-0.000281	-0.001083	-0.000555
6 Month	180	180	-0.001371	-0.000277	-0.001093	-0.000566
7 Month	210	210	-0.001395	-0.000280	-0.001115	-0.000587
8 Month	240	240	-0.001415	-0.000285	-0.001129	-0.000602
9 Month	270	270	-0.001422	-0.000292	-0.001130	-0.000603
10 Month	300	300	-0.001458	-0.000298	-0.001160	-0.000633
11 Month	331	331	-0.001462	-0.000311	-0.001150	-0.000623
12 Month	362	362	-0.001486	-0.000329	-0.001157	-0.000630

NOTE: [1] Measurements were taken before scheduled time

[2] Measurements were taken again after scheduled time

[3] Measurements were retaken after frame force was re-adjusted to original magnitude

Table 5-8: First-Year Strains of Specimen 54-12C-T

Target Age	Age of Load (days)	Age since Zero-Strain (days)	Total Strain (in./in.)	Shrinkage Strain (in./in.)	Strain due to Load (in./in.)	Creep Strain (in./in.)
Pre-Load	NA	0.00	0.000000	0.000000	0.000000	0.000000
Post-Load	0.00	0.02	-0.000591	-0.000024	-0.000567	0.000000
2-6 Hours	0.12	0.14	-0.000655	-0.000045	-0.000610	-0.000043
1 Day	1.2	1.2	-0.000805	-0.000023	-0.000782	-0.000216
2 Day	2.2	2.2	-0.000826	-0.000041	-0.000785	-0.000218
3 Day	3.3	3.3	-0.000857	-0.000036	-0.000821	-0.000254
4 Day	4.0	4.0	-0.000891	-0.000047	-0.000845	-0.000278
5 Day	5.1	5.1	-0.000929	-0.000056	-0.000873	-0.000306
6 Day	5.9	5.9	-0.000951	-0.000067	-0.000884	-0.000317
7 Day	12.1	12.1	-0.001017	-0.000076	-0.000940	-0.000374
2 Week	19	19	-0.001096	-0.000116	-0.000980	-0.000413
3 Week	21	21	-0.001114	-0.000120	-0.000994	-0.000427
4 Week	28	28	-0.001155	-0.000129	-0.001026	-0.000459
2 Month	59	59	-0.001276	-0.000177	-0.001099	-0.000532
3 Month[1]	85	85	-0.001353	-0.000211	-0.001142	-0.000575
3 Month[2]	95	95	-0.001361	-0.000217	-0.001144	-0.000578
4 Month	120	120	-0.001399	-0.000217	-0.001182	-0.000616
4 Month[3]	120	120	-0.001402	-0.000217	-0.001185	-0.000618
5 Month	150	150	-0.001449	-0.000242	-0.001207	-0.000640
6 Month	180	180	-0.001454	-0.000239	-0.001215	-0.000649
7 Month	210	210	-0.001469	-0.000241	-0.001228	-0.000661
8 Month	240	240	-0.001488	-0.000241	-0.001248	-0.000681
9 Month	270	270	-0.001503	-0.000248	-0.001256	-0.000689
10 Month	300	300	-0.001531	-0.000251	-0.001280	-0.000714
11 Month	331	331	-0.001545	-0.000263	-0.001282	-0.000716
12 Month	362	362	-0.001563	-0.000279	-0.001284	-0.000717

NOTE: [1] Measurements were taken before scheduled time

[2] Measurements were taken again after scheduled time

[3] Measurements were retaken after frame force was re-adjusted to original magnitude

Table 5-9: First-Year Strains of Specimen 72-11C-M

Target Age	Age of Load (days)	Age since Zero-Strain (days)	Total Strain (in./in.)	Shrinkage Strain (in./in.)	Strain due to Load (in./in.)	Creep Strain (in./in.)
Pre-Load	NA	0.00	0.000000	0.000000	0.000000	0.000000
Post-Load	0.00	0.02	-0.000609	-0.000011	-0.000598	0.000000
2-6 Hours	0.15	0.17	-0.000708	-0.000086	-0.000622	-0.000024
1 Day	1.3	1.3	-0.000789	-0.000105	-0.000684	-0.000086
2 Day	2.2	2.2	-0.000819	-0.000104	-0.000715	-0.000117
3 Day	3.3	3.3	-0.000847	-0.000107	-0.000740	-0.000142
4 Day	4.2	4.2	-0.000868	-0.000109	-0.000759	-0.000161
5 Day	5.3	5.4	-0.000884	-0.000111	-0.000773	-0.000175
6 Day	6.3	6.4	-0.000907	-0.000123	-0.000785	-0.000187
7 Day	7.4	7.4	-0.000926	-0.000119	-0.000807	-0.000209
2 Week	14	14	-0.001014	-0.000147	-0.000867	-0.000269
3 Week	21	21	-0.001058	-0.000156	-0.000902	-0.000304
4 Week	28	28	-0.001092	-0.000174	-0.000918	-0.000320
2 Month	58	58	-0.001205	-0.000218	-0.000987	-0.000389
3 Month	90	90	-0.001241	-0.000230	-0.001011	-0.000413
4 Month	120	120	-0.001278	-0.000254	-0.001024	-0.000426
4 Month[1]	120	120	-0.001292	-0.000254	-0.001038	-0.000440
5 Month	150	150	-0.001306	-0.000260	-0.001046	-0.000448
6 Month	180	180	-0.001332	-0.000274	-0.001058	-0.000460
7 Month	210	210	-0.001342	-0.000273	-0.001068	-0.000470
8 Month	240	240	-0.001350	-0.000277	-0.001074	-0.000476
9 Month	270	270	-0.001379	-0.000289	-0.001090	-0.000492
10 Month	300	300	-0.001390	-0.000291	-0.001099	-0.000501
11 Month	330	330	-0.001408	-0.000305	-0.001104	-0.000506
12 Month	357	357	-0.001426	-0.000316	-0.001110	-0.000512

NOTE: [1] Measurements were retaken after frame force was re-adjusted to original magnitude

Table 5-10: First-Year Strains of Specimen 72-11C-T-U

Target Age	Age of Load (days)	Age since Zero-Strain (days)	Total Strain (in./in.)	Shrinkage Strain (in./in.)	Strain due to Load (in./in.)	Creep Strain (in./in.)
Pre-Load	NA	0.00	0.000000	0.000000	0.000000	0.000000
Post-Load	0.00	0.09	-0.000244	-0.000027	-0.000217	0.000000
2-6 Hours	0.17	0.25	-0.000265	-0.000038	-0.000226	-0.000009
1 Day	1.0	1.1	-0.000269	-0.000051	-0.000219	-0.000001
2 Day	1.9	2.0	-0.000285	-0.000056	-0.000229	-0.000012
3 Day	2.9	3.0	-0.000294	-0.000059	-0.000235	-0.000018
4 Day	3.9	4.0	-0.000301	-0.000063	-0.000239	-0.000021
5 Day	5.0	5.1	-0.000312	-0.000066	-0.000246	-0.000029
6 Day	6.1	6.1	-0.000318	-0.000072	-0.000246	-0.000029
7 Day	7.1	7.2	-0.000333	-0.000076	-0.000257	-0.000040
2 Week	14	14	-0.000381	-0.000112	-0.000269	-0.000052
3 Week	21	21	-0.000407	-0.000124	-0.000282	-0.000065
4 Week	28	28	-0.000437	-0.000138	-0.000299	-0.000082
2 Month	58	58	-0.000503	-0.000187	-0.000317	-0.000099
3 Month	90	90	-0.000531	-0.000207	-0.000324	-0.000107
4 Month	120	120	-0.000571	-0.000236	-0.000335	-0.000118
4 Month[1]	120	120	-0.000585	-0.000236	-0.000349	-0.000132
5 Month	150	150	-0.000596	-0.000237	-0.000359	-0.000142
6 Month	180	180	-0.000615	-0.000251	-0.000364	-0.000146
7 Month	210	210	-0.000619	-0.000252	-0.000367	-0.000150
8 Month	240	240	-0.000631	-0.000259	-0.000371	-0.000154
9 Month	255	255	-0.000649	-0.000268	-0.000382	-0.000164
10 Month	300	300	-0.000655	-0.000273	-0.000382	-0.000165
11 Month	330	330	-0.000670	-0.000285	-0.000385	-0.000168
12 Month	357	357	-0.000682	-0.000298	-0.000384	-0.000167

NOTE: [1] Measurements were retaken after frame force was re-adjusted to original magnitude

Table 5-11 presents the averages of the SCC, CVC, tarp-, and match-cured specimens excluding the underloaded specimens and the specimens with questionable curing.

Table 5-11: Measured Strain Averages at 1 Year (microstrain)

Average	ε_{li}	ε_{sh}	ε_{t}
SCC	-1434	-400	-1834
CVC	-1184	-308	-1492
Match	-1306	-390	-1696
Tarp	-1355	-321	-1676

Based on these averages, the SCC specimens experienced greater total strain than the CVC specimens at 1 year. The SCC specimens also experienced greater average shrinkage and load-induced strains than the CVC specimens. However, examining the data on an average basis does not yield equitable comparisons due to different actual concrete strengths, actual concrete stiffnesses, applied stresses, and temperature histories for each specimen set. Because of this, further analysis was required to investigate whether these strains are comparable or consistent with expected behavior.

Figure 5-2 through Figure 5-11 graphically illustrate the data presented in the previous tables along with the initial strain. It should be noted that in these figures, the underloaded specimens, denoted by "U", appear to exhibit less strain than the other specimens. As expected, the load-induced strain experienced by the specimens is approximately proportional to the load applied. In many of these figures, there is a slight increase in the

load-induced strains at an age of approximately 120 days. This is because these readings reflect the change due to the reloading process that was done in order to maintain the load within 2% of the original load that was applied.

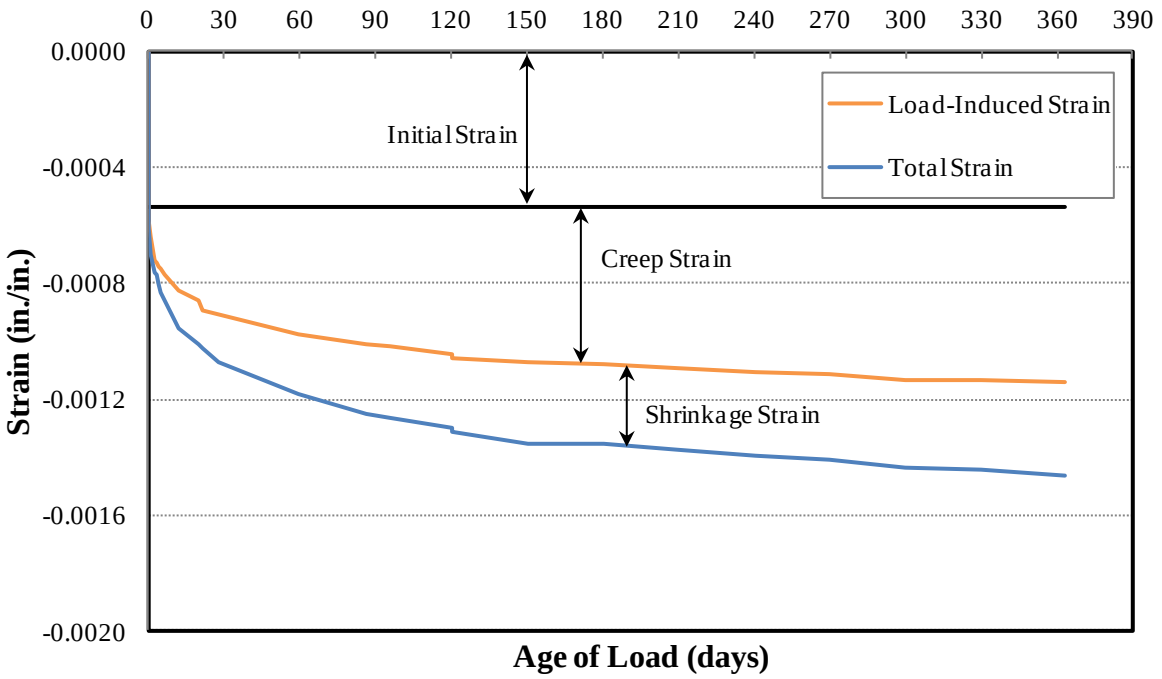

Figure 5-2: First Year Strains of Specimen 54-03S-M*

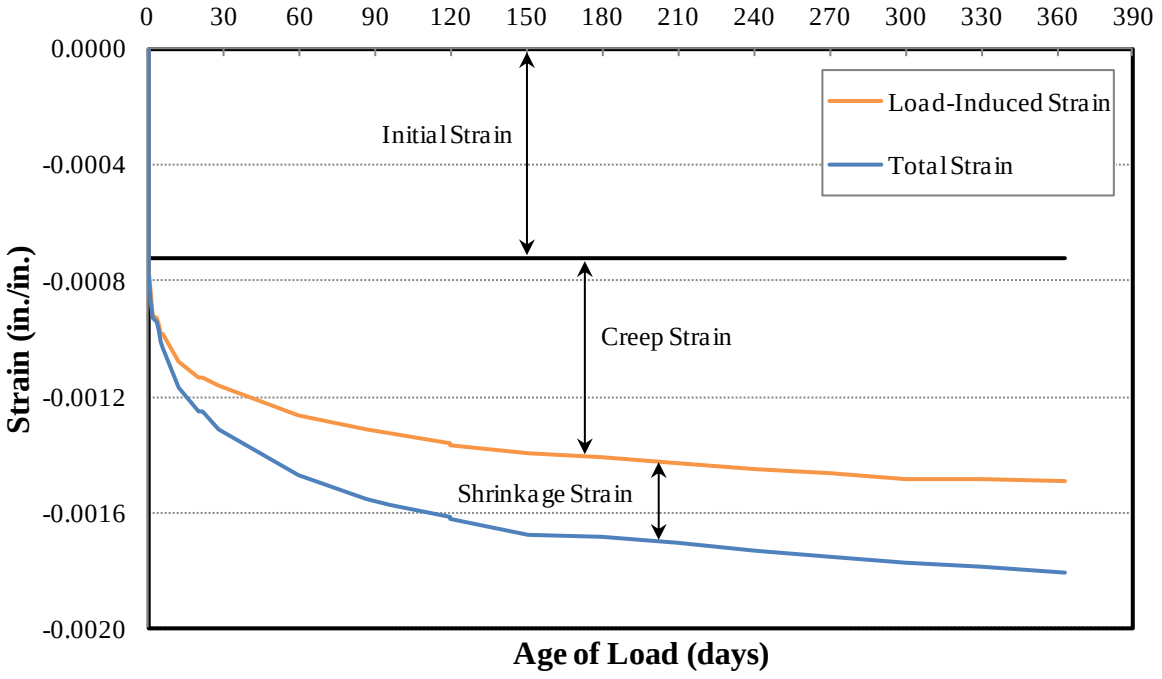

Figure 5-3: First Year Strains of Specimen 54-03S-T

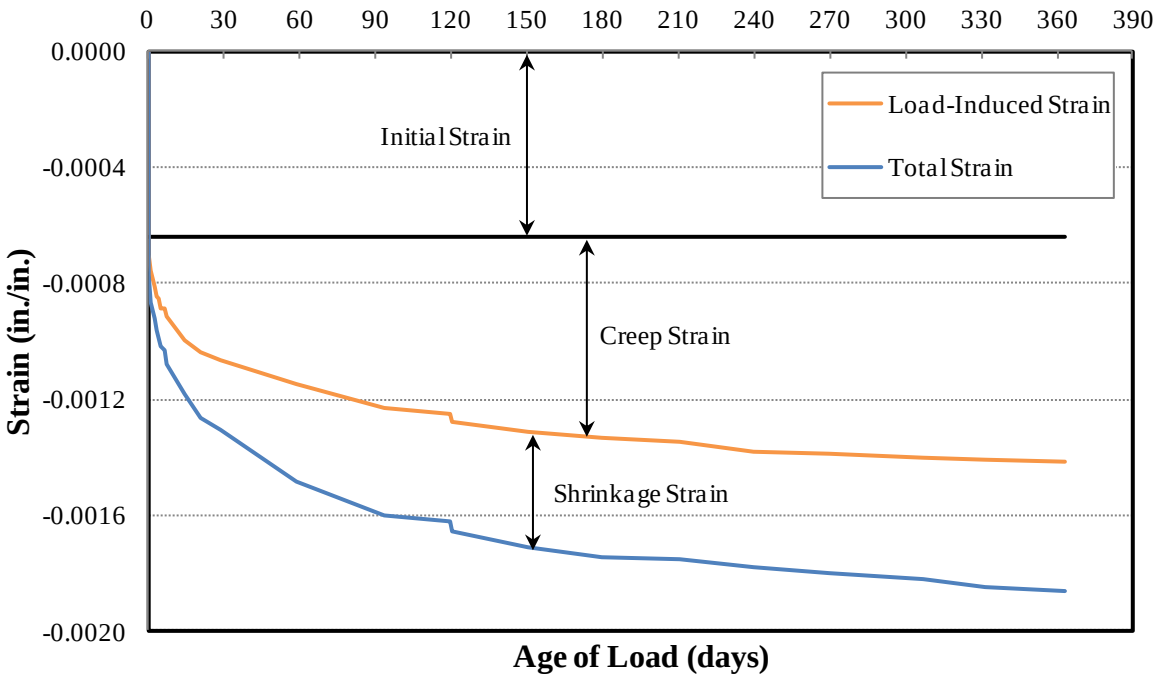

Figure 5-4: First Year Strains of Specimen 54-07S-M

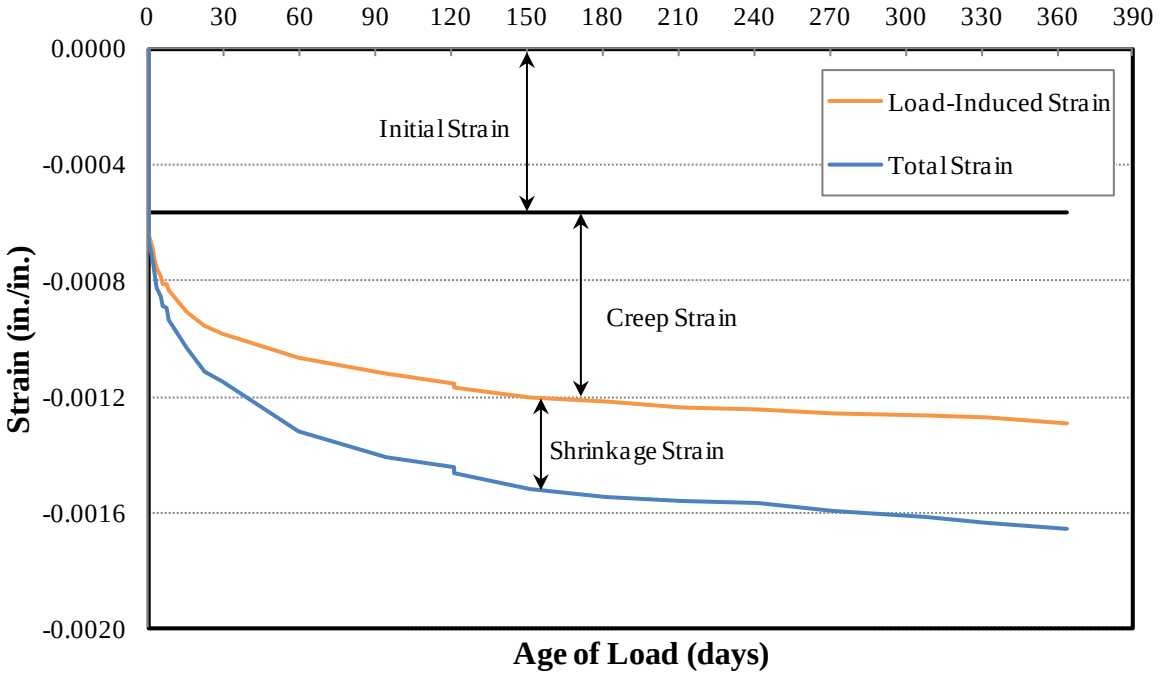

Figure 5-5: First Year Strains of Specimen 54-07S-T

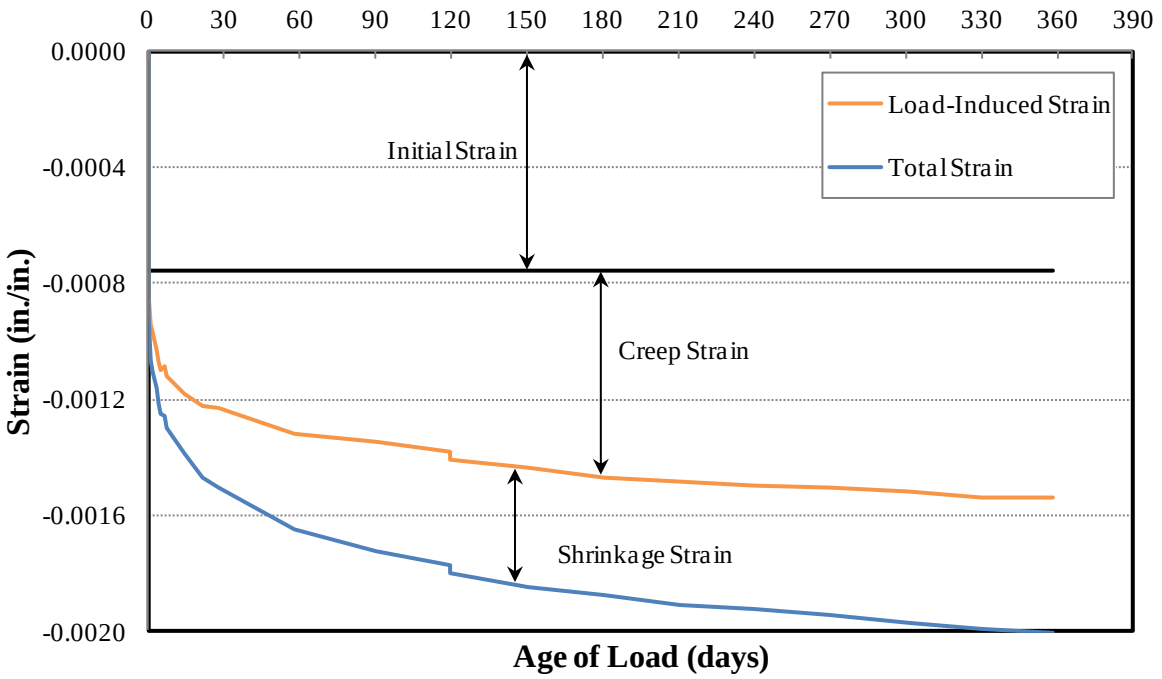

Figure 5-6: First Year Strains of Specimen 72-03S-M

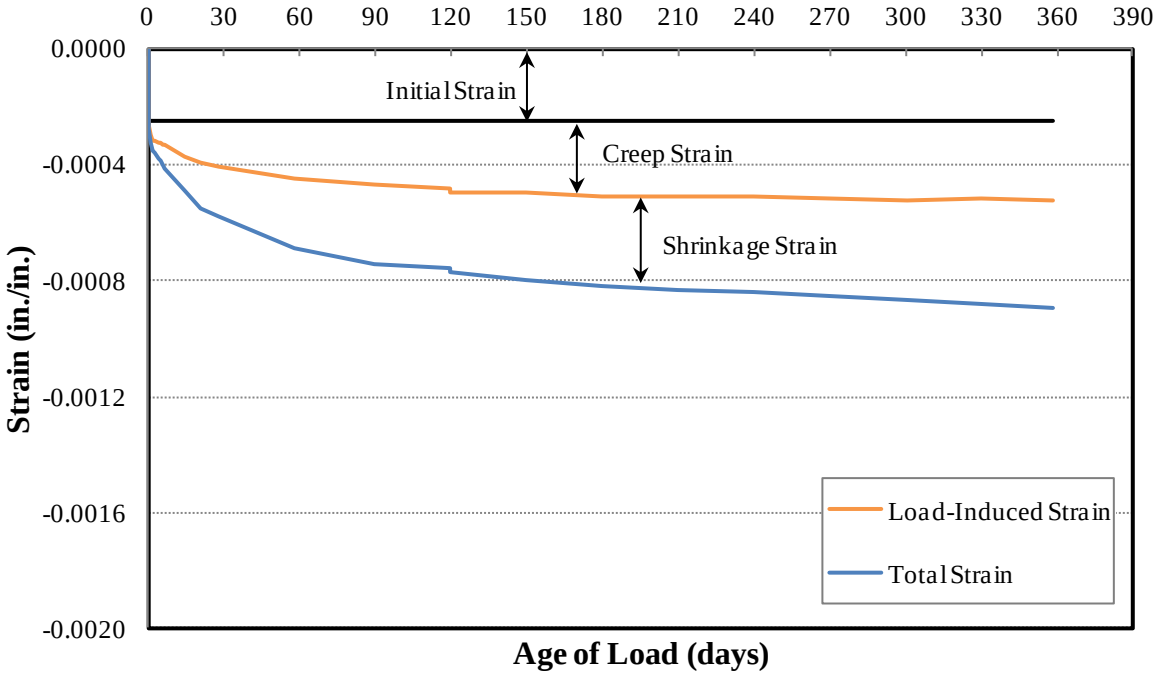

Figure 5-7: First Year Strains of Specimen 72-03S-T-U

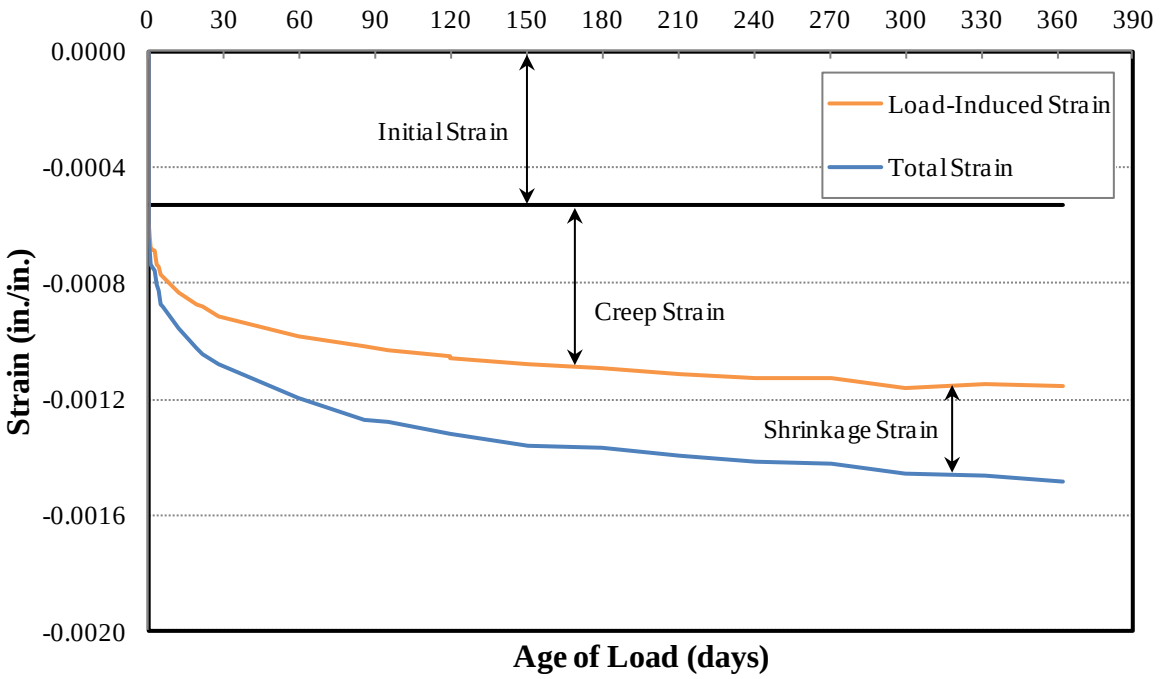

Figure 5-8: First Year Strains of Specimen 54-12C-M

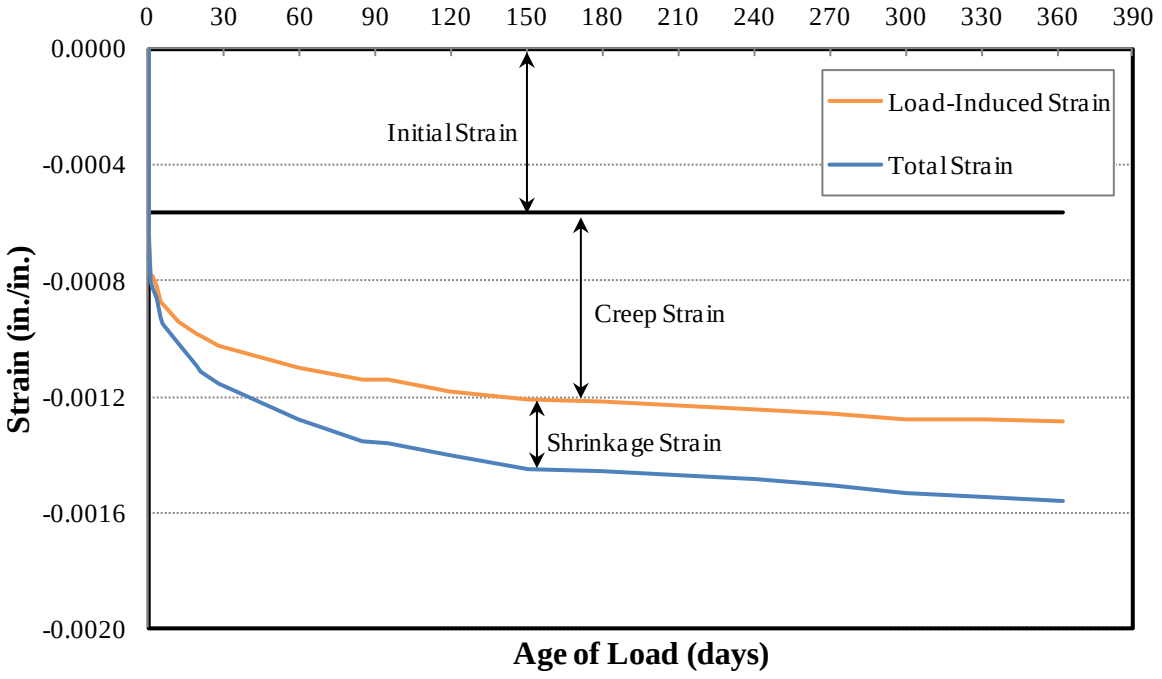

Figure 5-9: First Year Strains of Specimen 54-12C-T

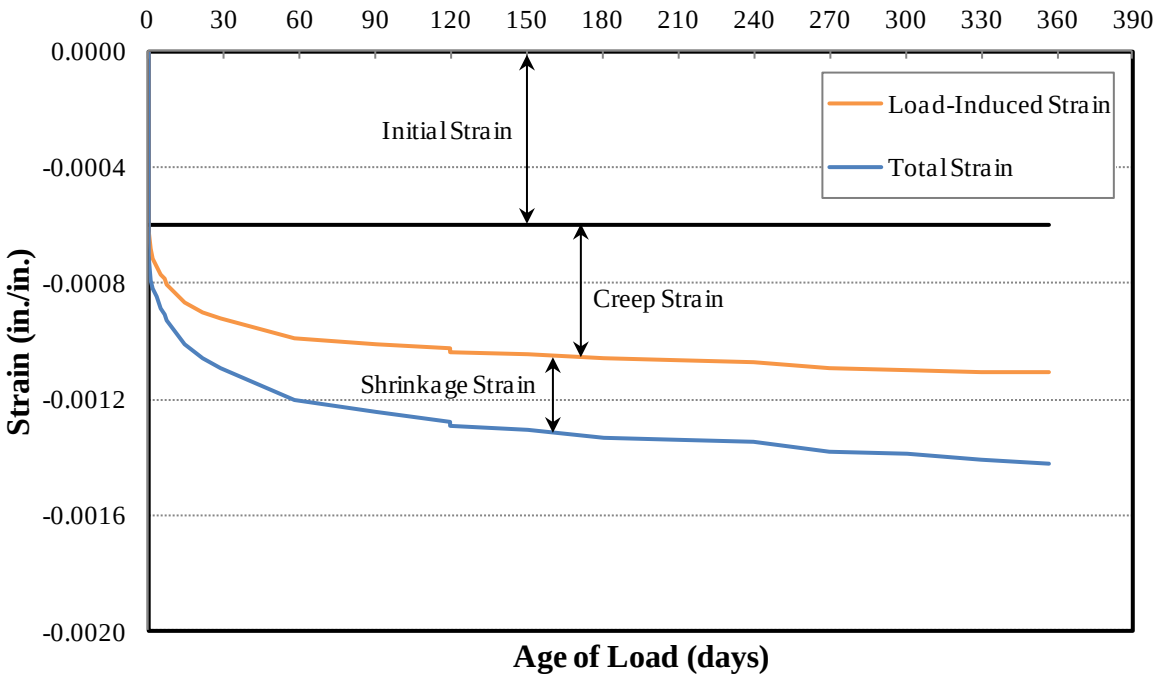

Figure 5-10: First Year Strains of Specimen 72-11C-M

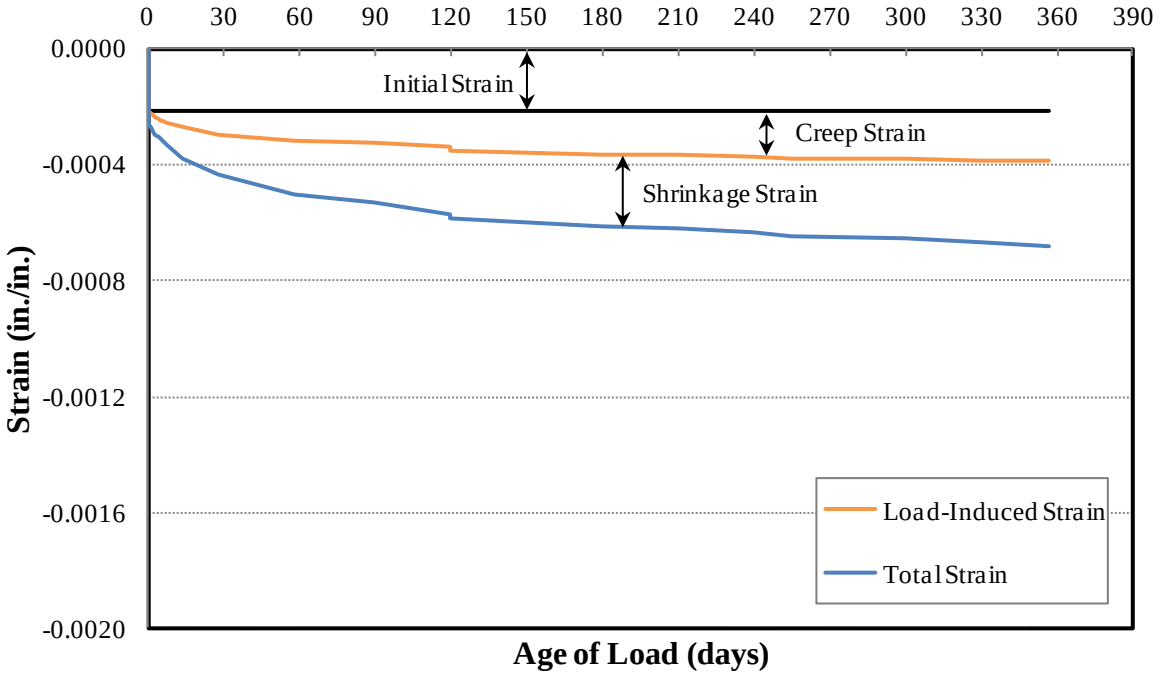

Figure 5-11: First Year Strains of Specimen 72-11C-T-U

5.3 STRAIN PREDICTIONS

This section presents the strains predicted using the nine prediction models presented in Chapter 2 and compares them with the measured values.

5.3.1 PREDICTED CREEP STRAIN

The predicted load-induced strains are detailed in this section. As mentioned earlier, because it is difficult to isolate the instantaneous elastic deformation from the *true* creep deformation, the two strains are combined in this research for a more accurate measure of strain. The load-induced strain (ε_{li}) predicted using each of the nine methods as well as the measured load-induced strain can be seen in Figure 5-12 through Figure 5-31 for up to 56 or 365 days. These milestones were chosen because 56 days is a typical estimate of the age at which the girders and deck would be placed during bridge construction and 1 year is a reasonable time for long-term testing and the practical boundary for the scope of this thesis research. It should be noted that for load-induced strain predictions, MC 90-99 and Eurocode are equivalent to MC 2010 and thus are not shown separately. Also, NCHRP 628 is only compared to other methods when SCC is used; otherwise, NCHRP 628 defaults to AASHTO 2010 where CVC is used.

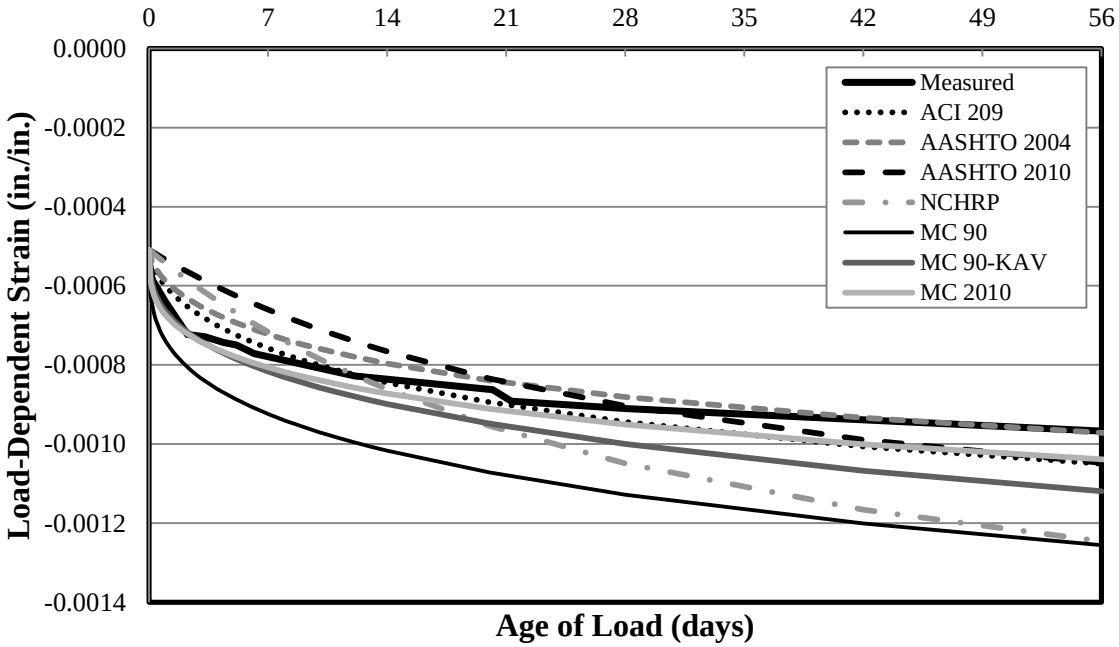

Figure 5-12: Load-Induced Strain for Specimen 54-03S-M* up to 56 Days

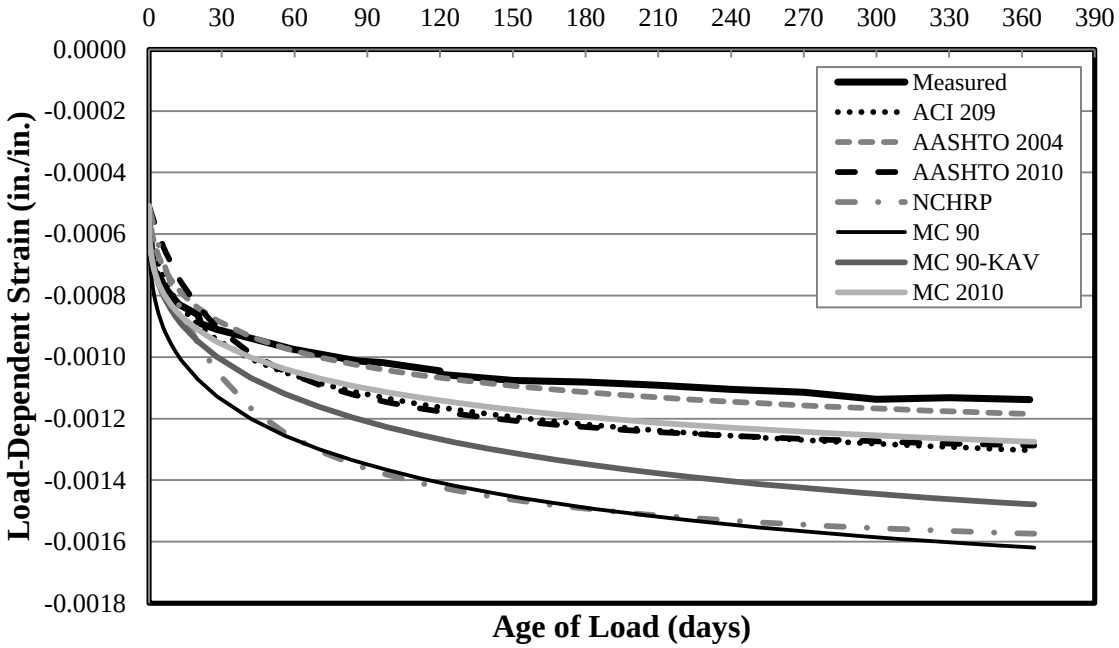

Figure 5-13: Load-Induced Strain for Specimen 54-03S-M* up to 1 Year

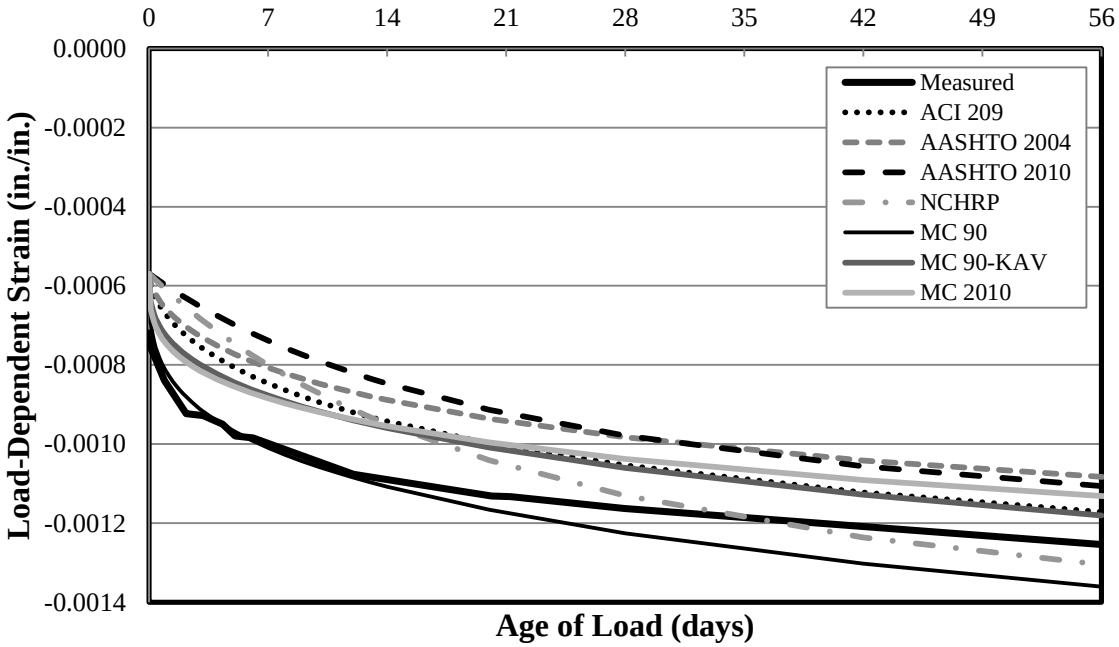

Figure 5-14: Load-Induced Strain for Specimen 54-03S-T up to 56 Days

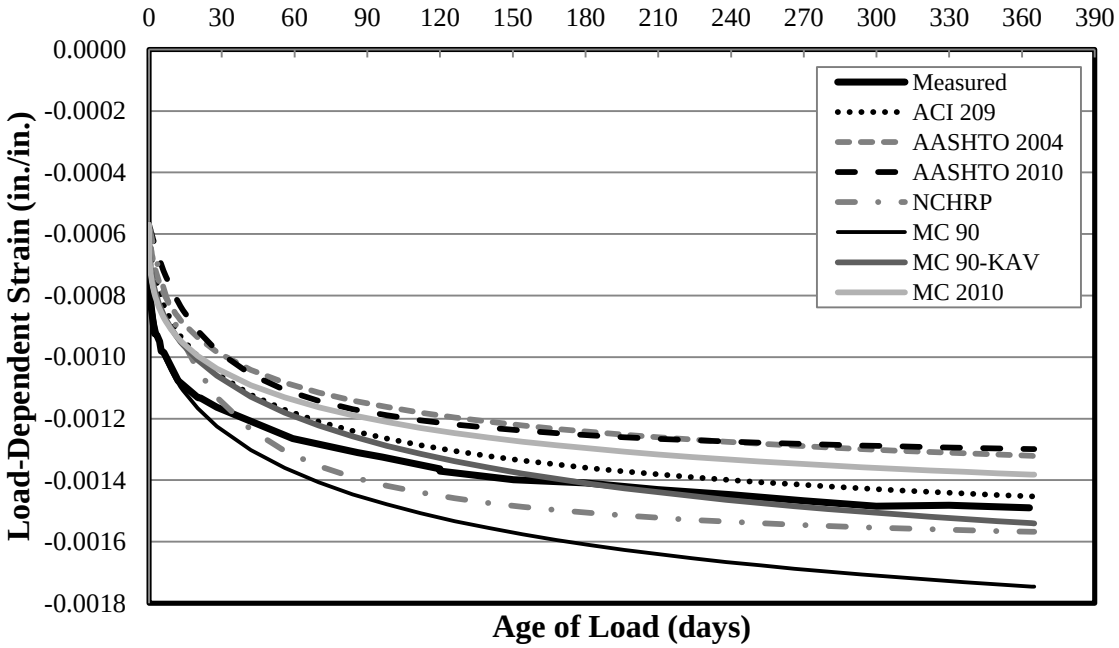

Figure 5-15: Load-Induced Strain for Specimen 54-03S-T up to 1 Year

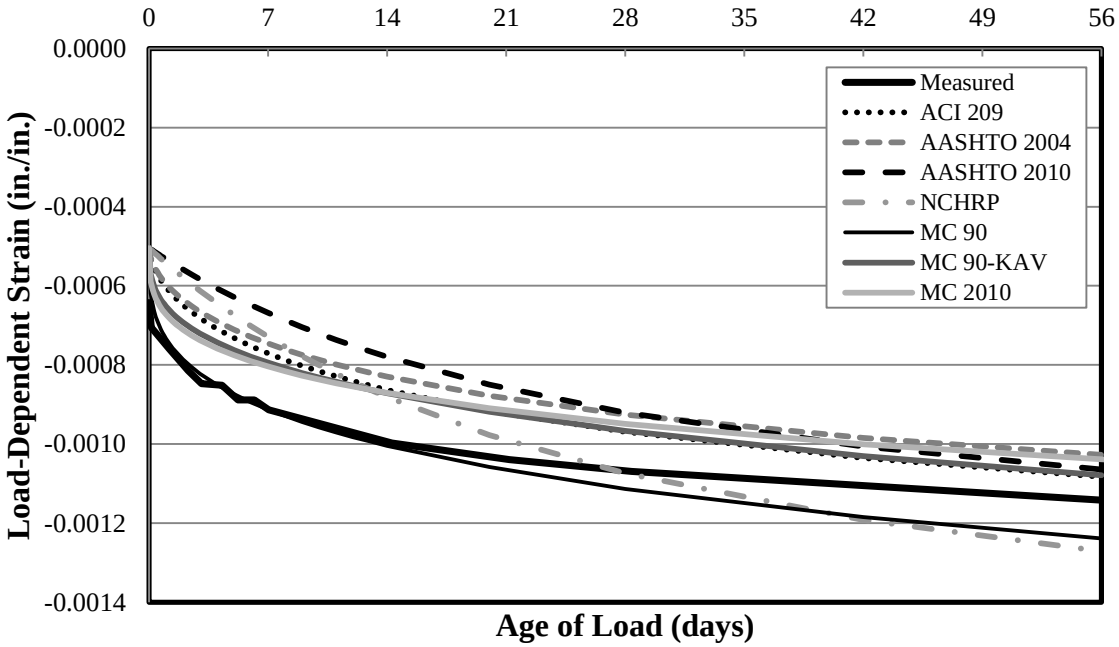

Figure 5-16: Load-Induced Strain for Specimen 54-07S-M up to 56 Days

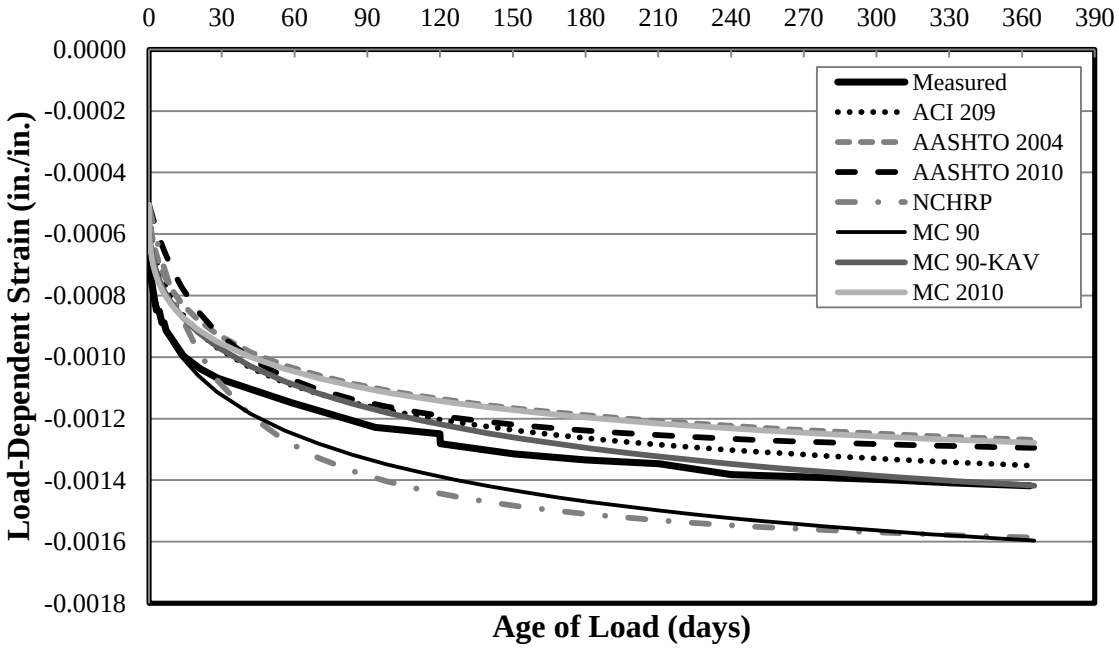

Figure 5-17: Load-Induced Strain for Specimen 54-07S-M up to 1 Year

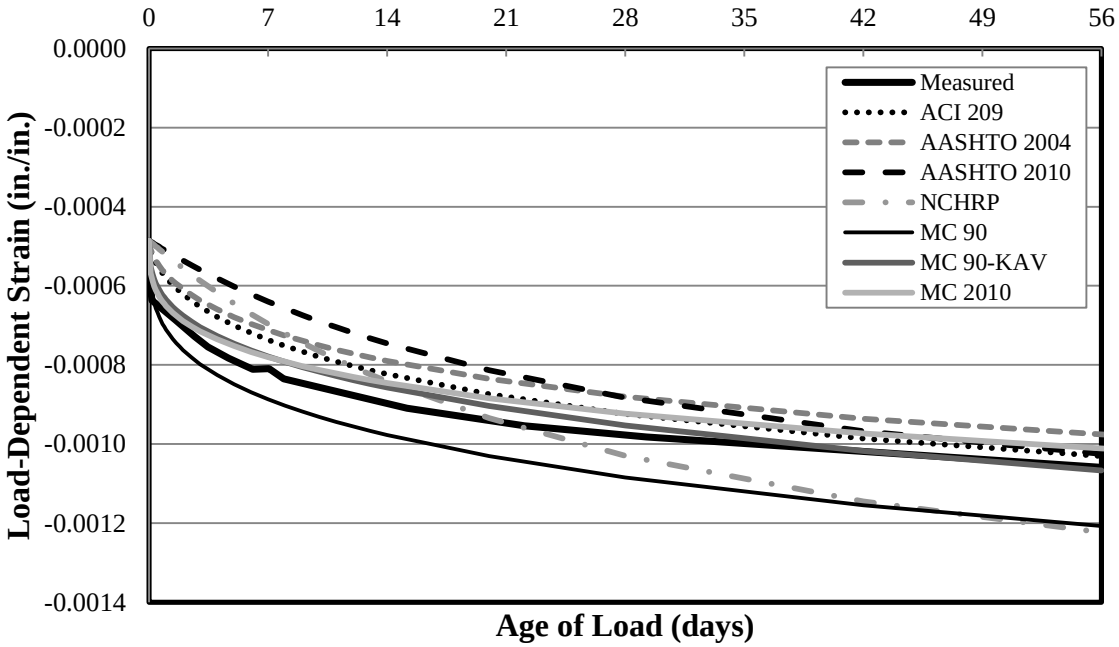

Figure 5-18: Load-Induced Strain for Specimen 54-07S-T up to 56 Days

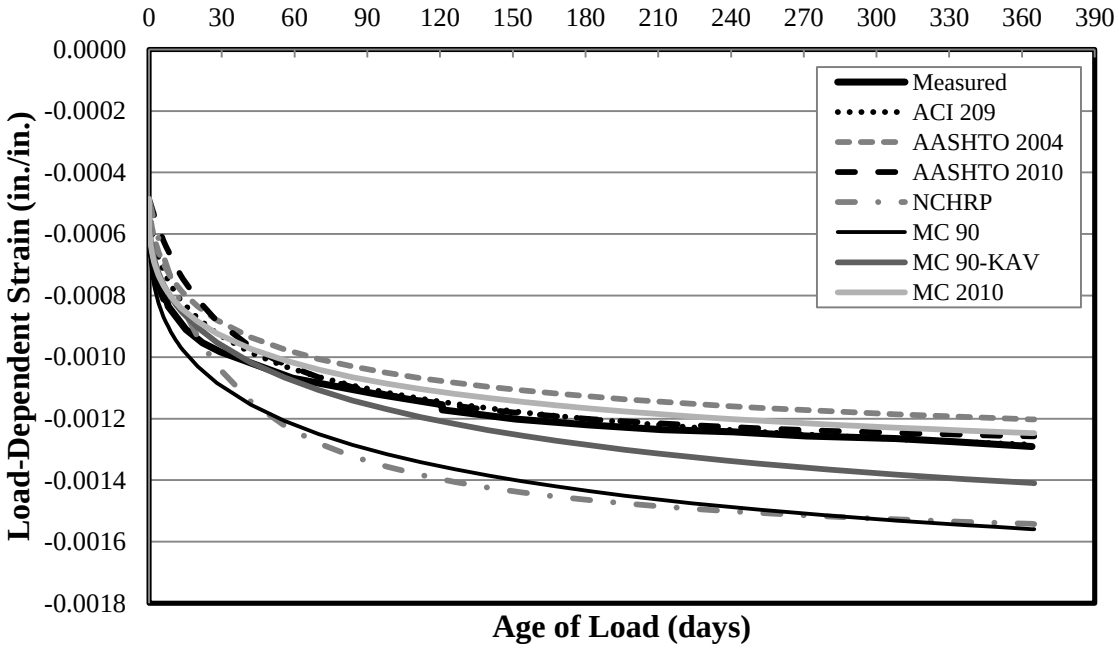

Figure 5-19: Load-Induced Strain for Specimen 54-07S-T up to 1 Year

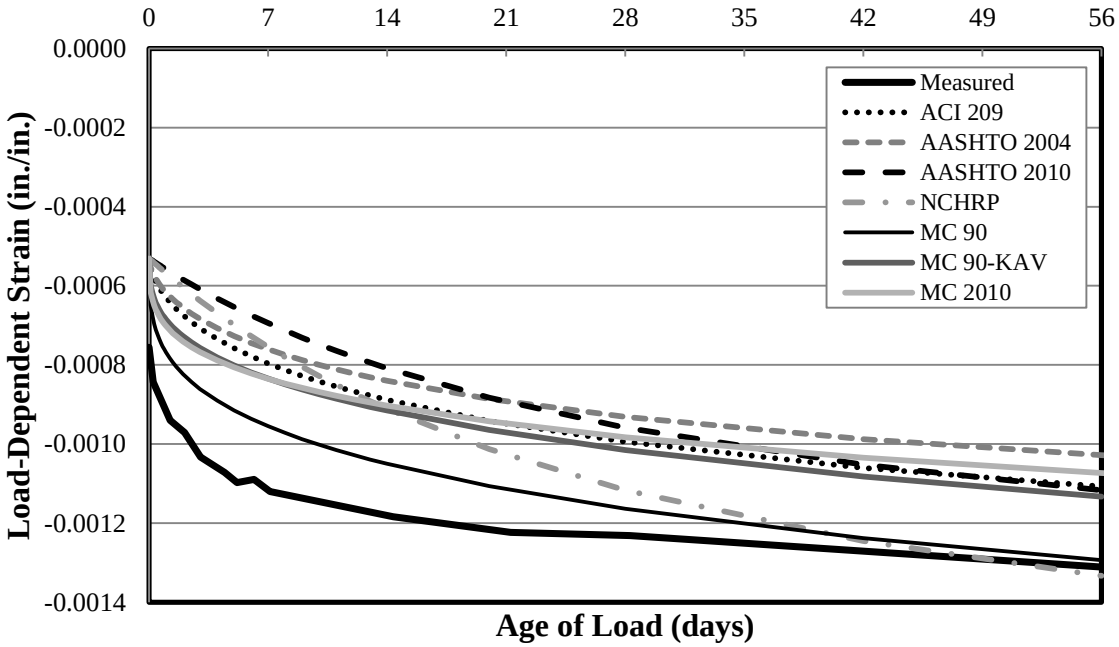

Figure 5-20: Load-Induced Strain for Specimen 72-03S-M up to 56 Days

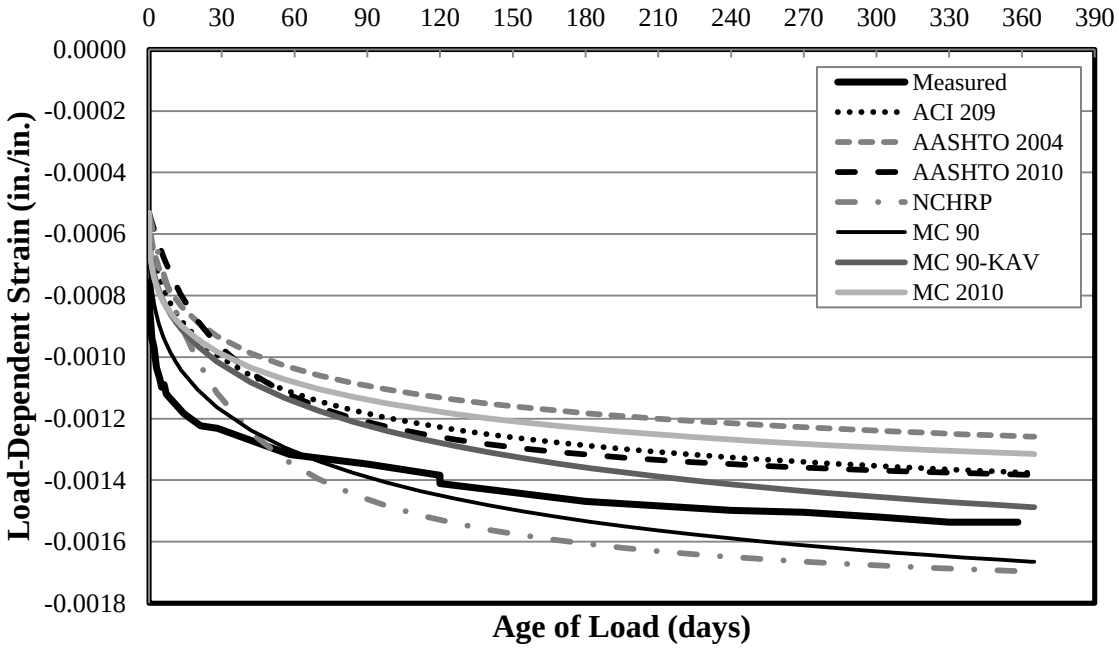

Figure 5-21: Load-Induced Strain for Specimen 72-03S-M up to 1 Year

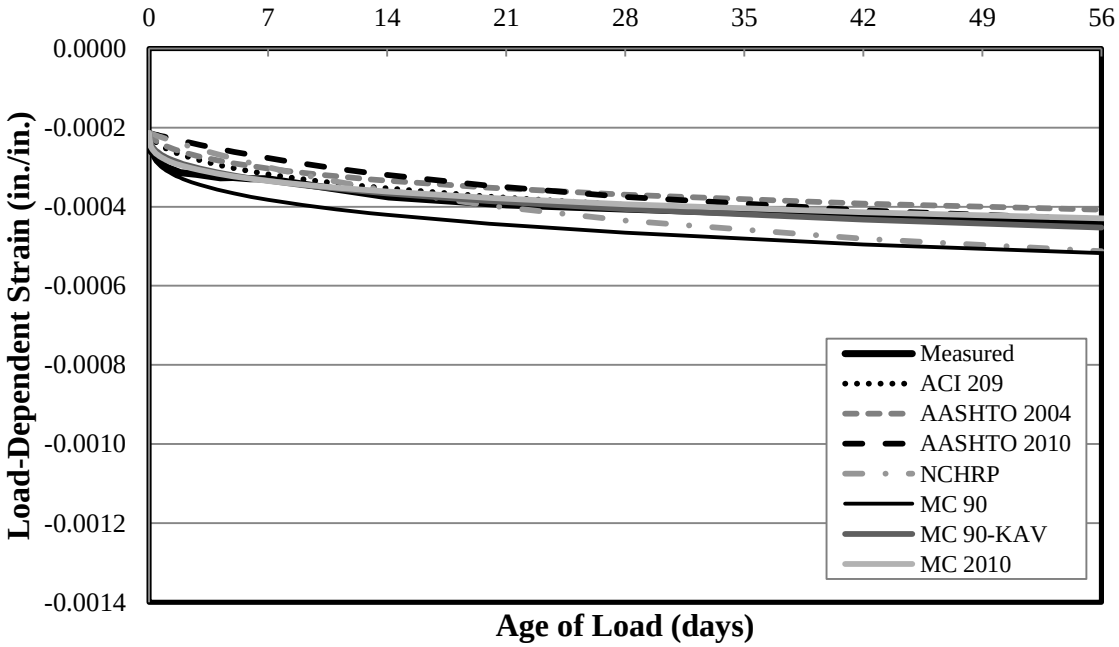

Figure 5-22: Load-Induced Strain for Specimen 72-03S-T-U up to 56 Days

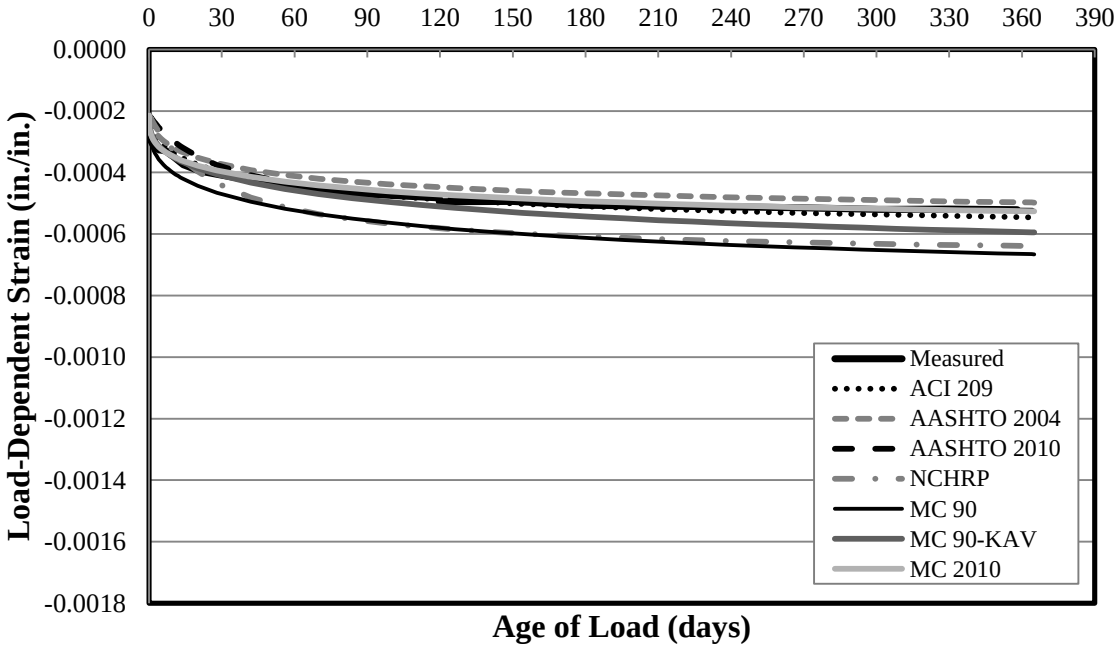

Figure 5-23: Load-Induced Strain for Specimen 72-03S-T-U up to 1 Year

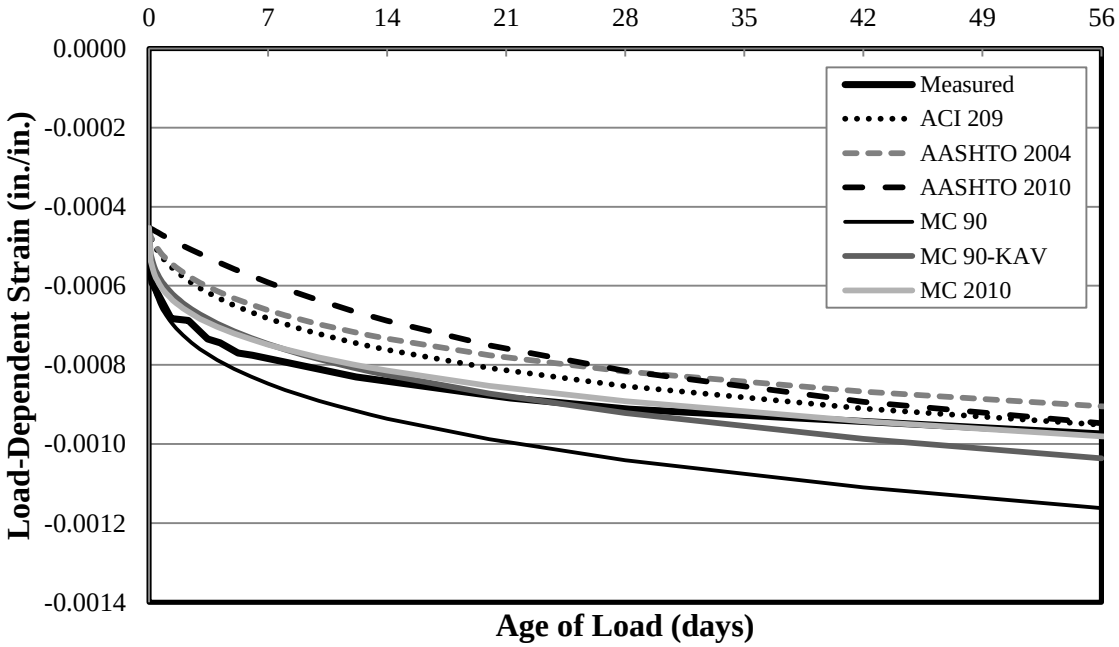

Figure 5-24: Load-Induced Strain for Specimen 54-12C-M up to 56 Days

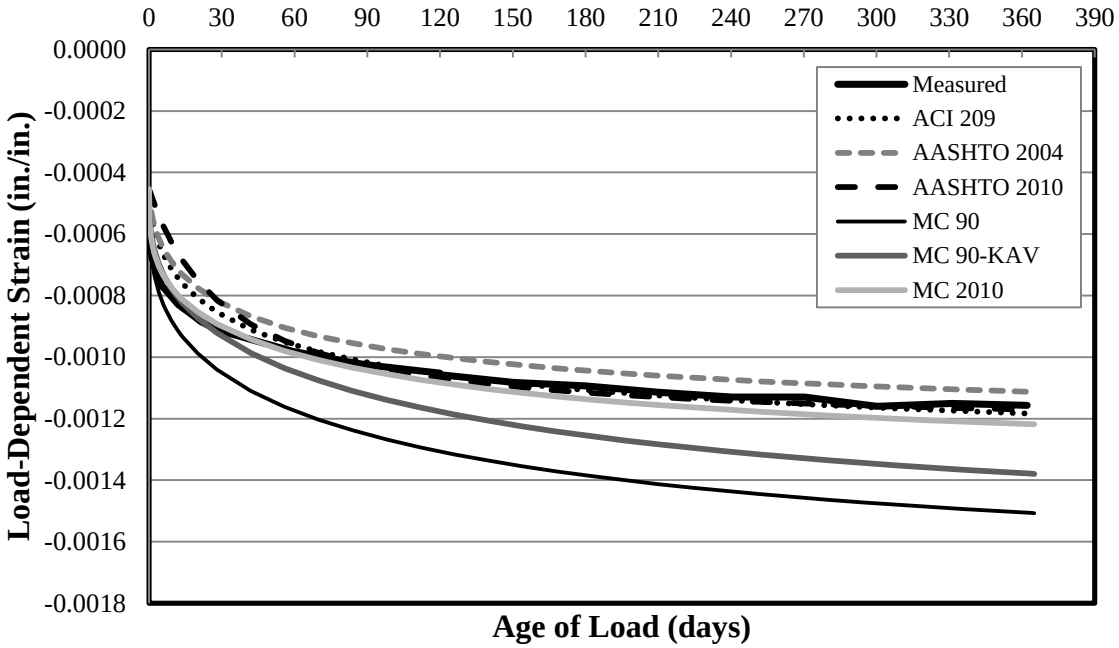

Figure 5-25: Load-Induced Strain for Specimen 54-12C-M up to 1 Year

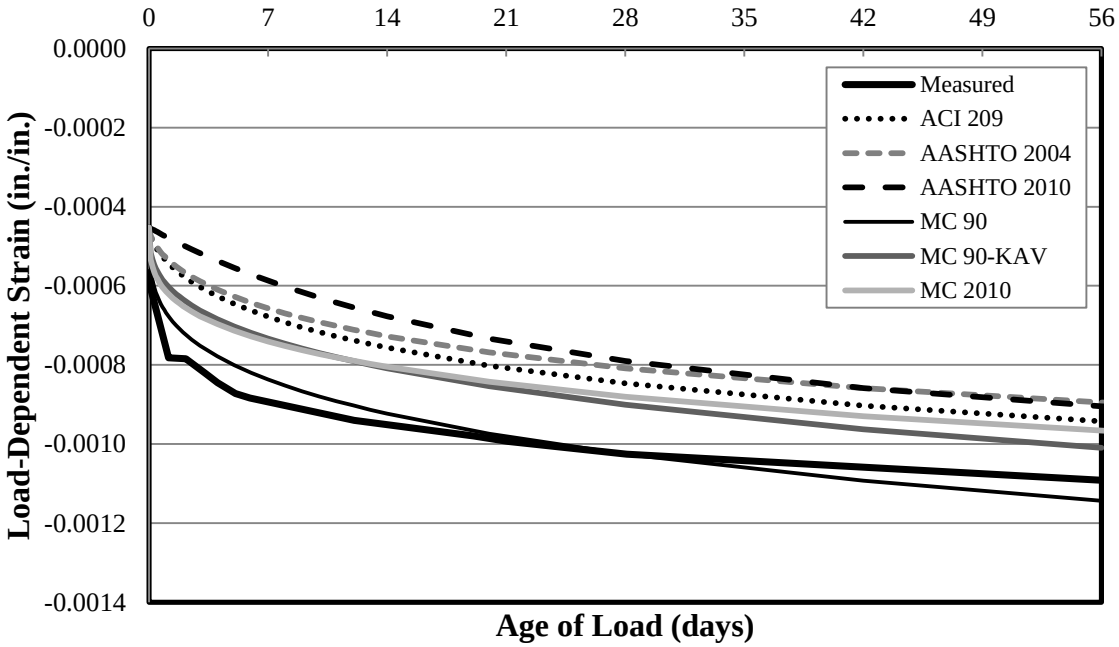

Figure 5-26: Load-Induced Strain for Specimen 54-12C-T up to 56 Days

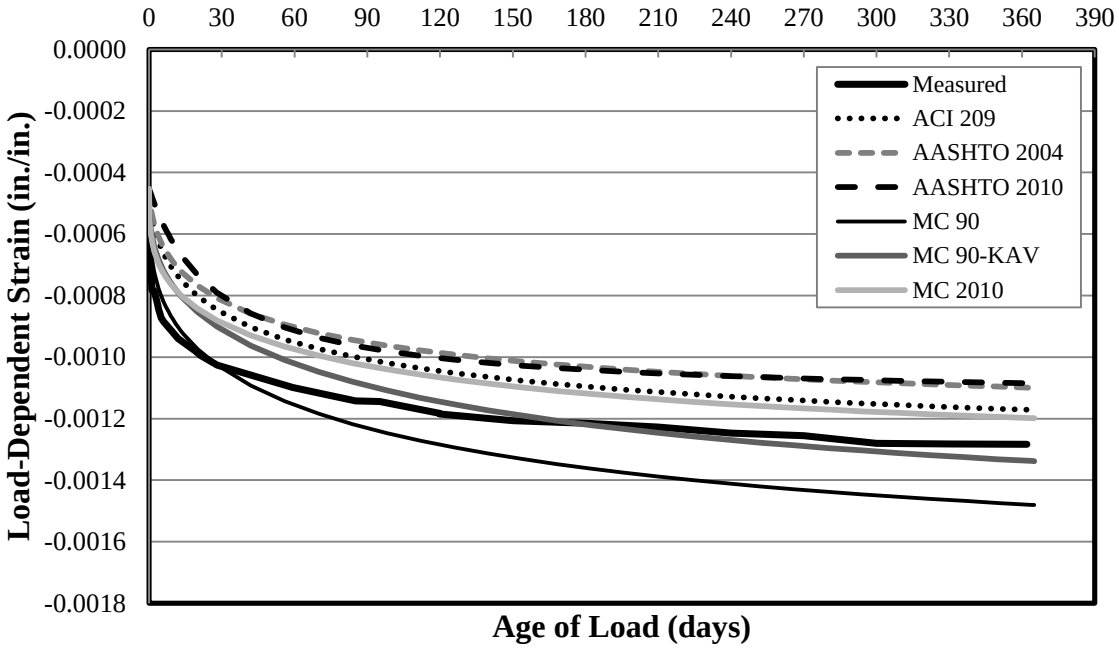

Figure 5-27: Load-Induced Strain for Specimen 54-12C-T up to 1 Year

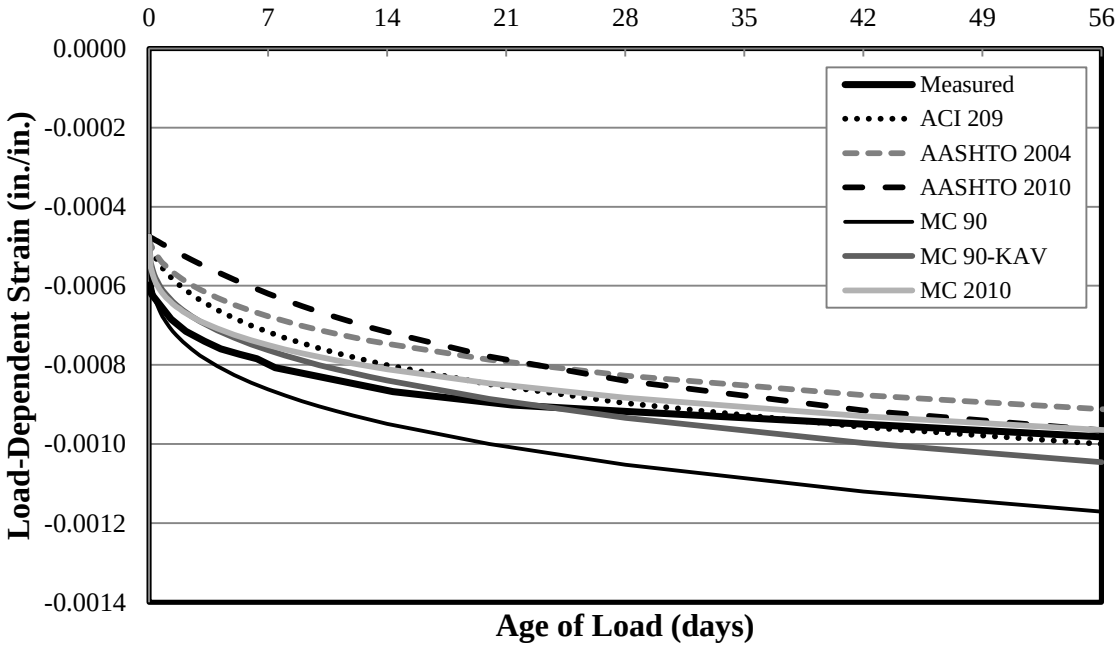

Figure 5-28: Load-Induced Strain for Specimen 72-11C-M up to 56 Days

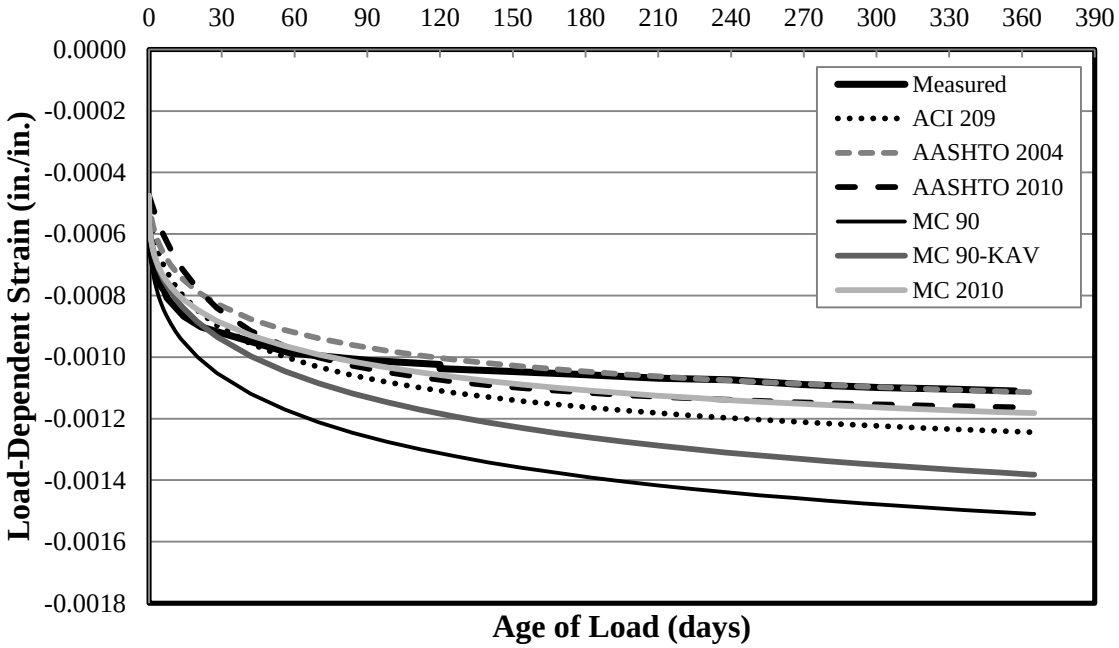

Figure 5-29: Load-Induced Strain for Specimen 72-11C-M up to 1 Year

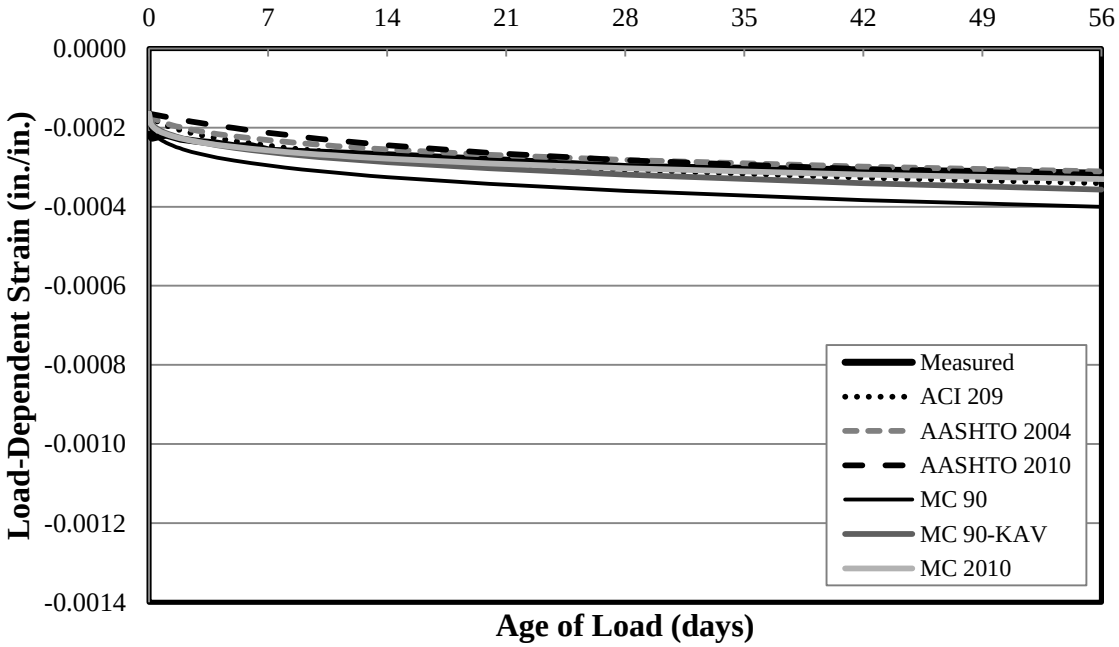

Figure 5-30: Load-Induced Strain for Specimen 72-11C-T-U up to 56 Days

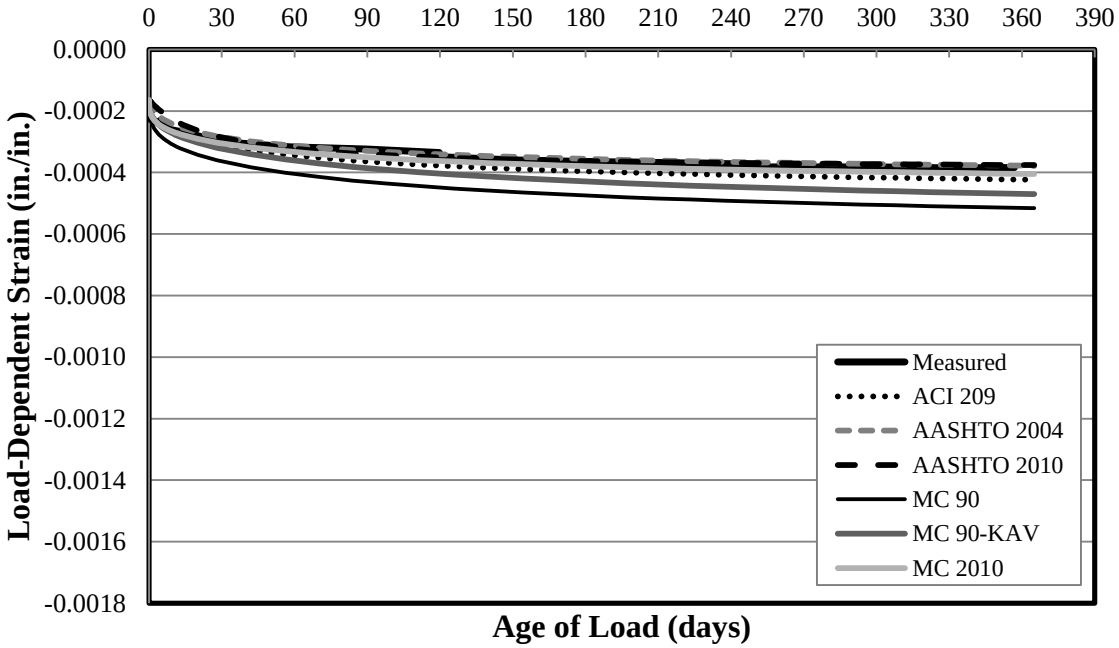

Figure 5-31: Load-Induced Strain for Specimen 72-11C-T-U up to 1 Year

Table 5-12 shows the average load-induced strains at 56 days and 1 year for each prediction method evaluated. These averages are shown for SCC only, CVC only, and the averages of all specimens. The averages do not include specimens that were underloaded or improperly cured. It should also be noted that the average of the CVC specimens for NCHRP 628 is identical to AASHTO 2010 for load-induced strains.

Table 5-12: Average Load-Induced Strain Predictions by Method

Prediction Method	Average SCC (microstrain)		Average CVC (microstrain)		Average ALL (microstrain)	
	56 Days	1 Year	56 Days	1 Year	56 Days	1 Year
ACI 209	-1081	-1342	-965	-1200	-1031	-1281
AASHTO 2004	-1010	-1235	-904	-1109	-964	-1181
AASHTO 2010	-1058	-1280	-939	-1140	-1007	-1220
NCHRP 628	-1255	-1559	N/A	N/A	-1120	-1380
MC 90	-1275	-1642	-1159	-1499	-1225	-1580
MC 90-KAV	-1115	-1464	-1031	-1366	-1079	-1422
MC 2010	-1063	-1305	-970	-1200	-1023	-1260

From the above figures and table, it can be seen that the predicted 56-day and 365-day load-induced strain values range between -976 and -1361 microstrain, and -1202 and -1746 microstrain, respectively for SCC mixtures. For CVC at 56 and 365 days, the ε_{li} ranges from -895 to -1171 microstrain and from -1085 to -1509 microstrain, respectively. As was observed in the measured data, the predicted load-induced strains of SCC specimens are generally larger than the load-induced strains experienced by CVC specimens. There is no comparison given between the tarp- and match-cured specimens because no prediction method differentiates between different types of accelerated curing; the models only

differentiate between accelerated and non-accelerated curing methods. With this observation noted, some of the models do take into account the equivalent age, which *is* different between match- and tarp-cured specimens based on the fact that the match-curing temperature history is different than the tarp-curing temperature history.

From these plots alone, several general observations can also be made about the prediction of load-induced strain:

For ACI 209,

- ACI 209 fluctuates between over- and underpredicting load-induced strains at 1 year for both SCC and CVC.

For AASHTO models,

- AASHTO 2004 underpredicts load-induced strains for both concrete types at 1 year.
- AASHTO 2010 tends to underpredict load-induced strains for both types of concrete but is more accurate for CVC at 1 year.
- NCHRP 628 slightly overpredicts load-induced strains for SCC at 1 year due to the amplification factor based on the cement type.

For European models,

- MC 90 and MC 90-KAV consistently overpredict load-induced strains for both types of concrete at 1 year but are more inaccurate for CVC than SCC.
- MC 2010 generally underpredicts load-induced strains for SCC at 1 year but appears fairly accurate for CVC.
- MC 90-KAV and MC 2010 both offer an improvement over MC 90 for both concrete types at 1 year.

- For both concrete types, there is no clear trend whether MC 90-KAV or MC 2010 predicts more accurate strains at 1 year.

As discussed in Section 5.2, the measured load-induced strains were greater for SCC mixtures than for CVC mixtures on average. However, the larger measured creep for SCC appears to have been reflected by the various prediction methods based on the input parameters unique to each set of specimens.

5.3.2 PREDICTED SHRINKAGE STRAIN

The predicted shrinkage strains are detailed in this section. The predicted shrinkage strain by each of the nine methods as well as the measured ε_{sh} can be seen in Figure 5-32 through Figure 5-51 for up to 56 or 365 days. It should be noted that for shrinkage strain, MC 90-99 is equivalent to MC 2010. Furthermore, MC 90-KAV was not evaluated for shrinkage and thus this method is not shown. Unlike creep, Eurocode is not equivalent to MC 2010 for shrinkage; therefore, they are presented as two distinct predictions here.

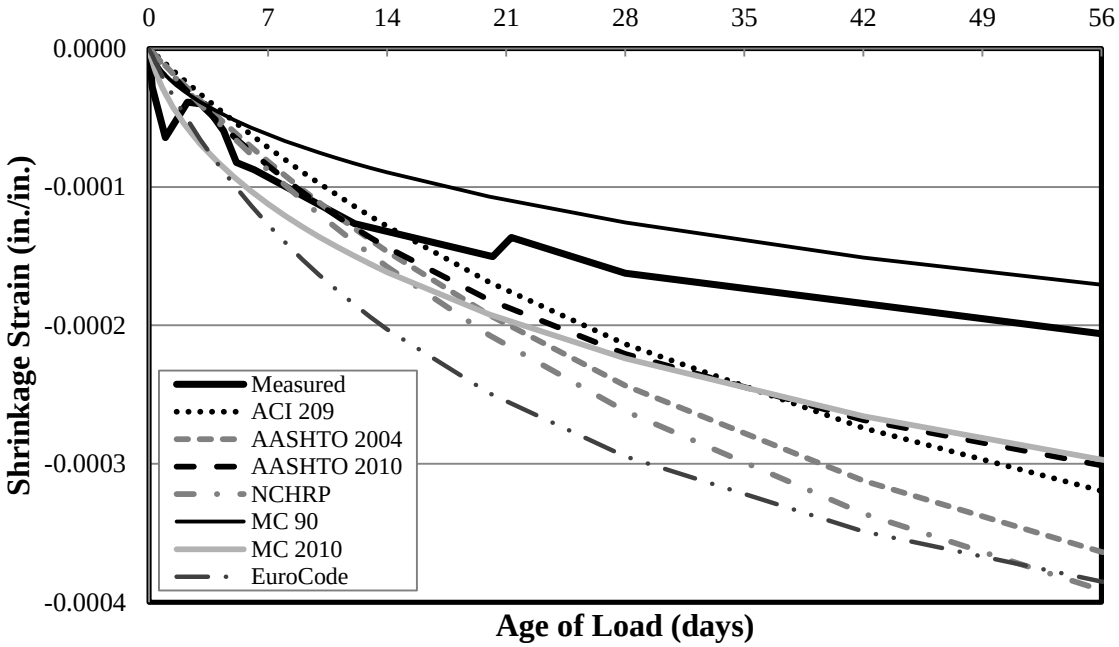

Figure 5-32: Shrinkage Strain for Specimen 54-03S-M* up to 56 Days

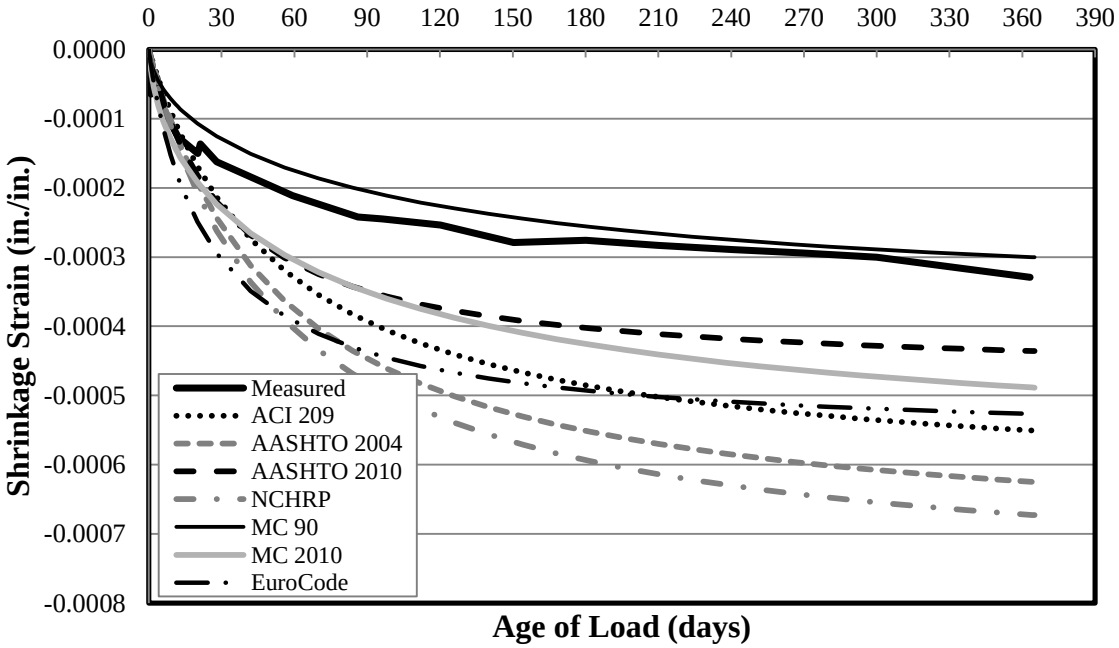

Figure 5-33: Shrinkage Strain for Specimen 54-03S-M* up to 1 Year

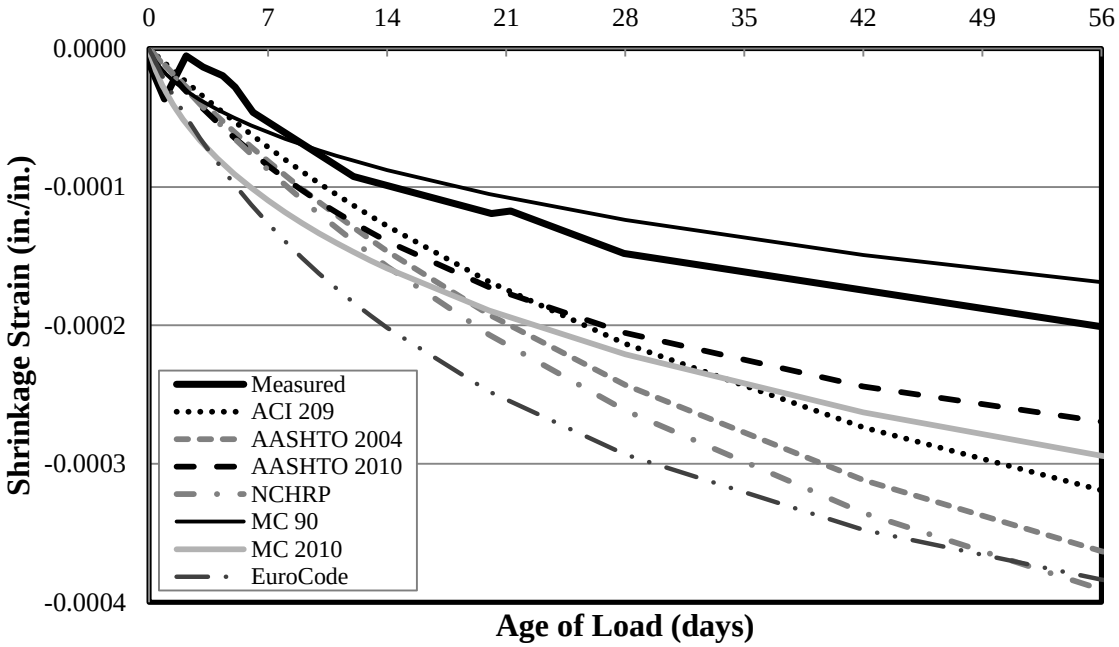

Figure 5-34: Shrinkage Strain for Specimen 54-03S-T up to 56 Days

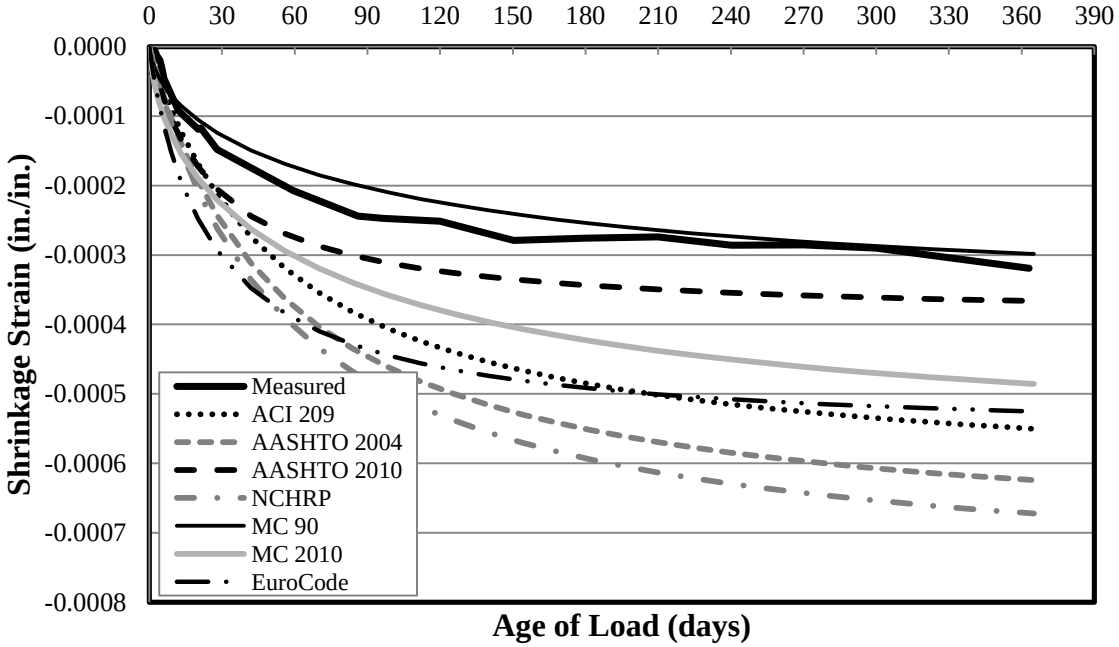

Figure 5-35: Shrinkage Strain for Specimen 54-03S-T up to 1 Year

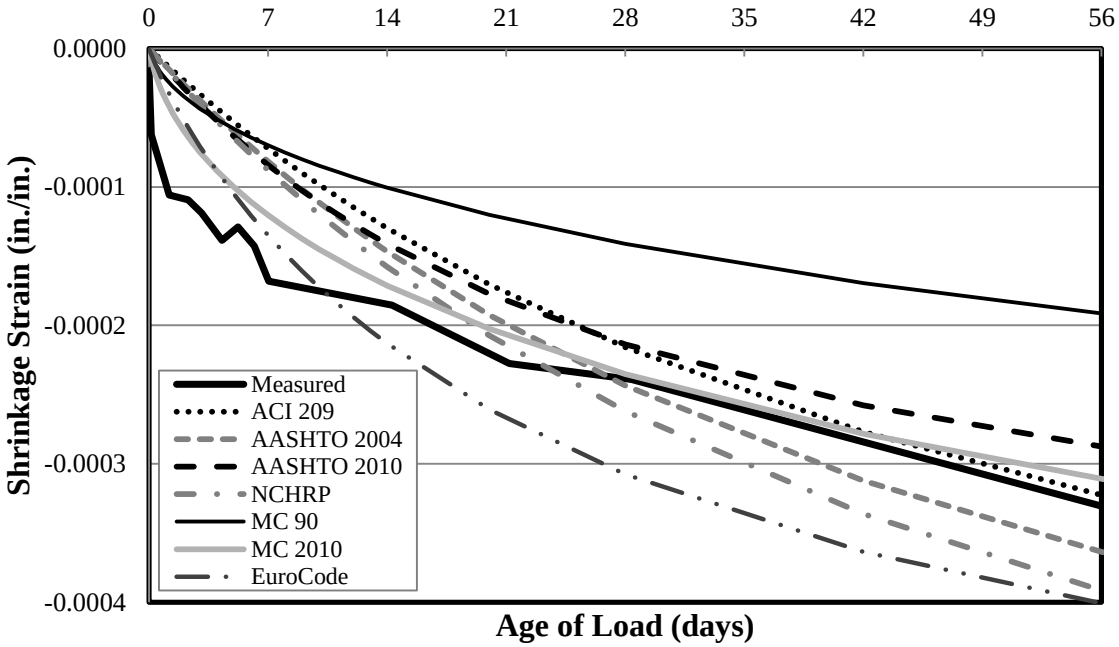

Figure 5-36: Shrinkage Strain for Specimen 54-07S-M up to 56 Days

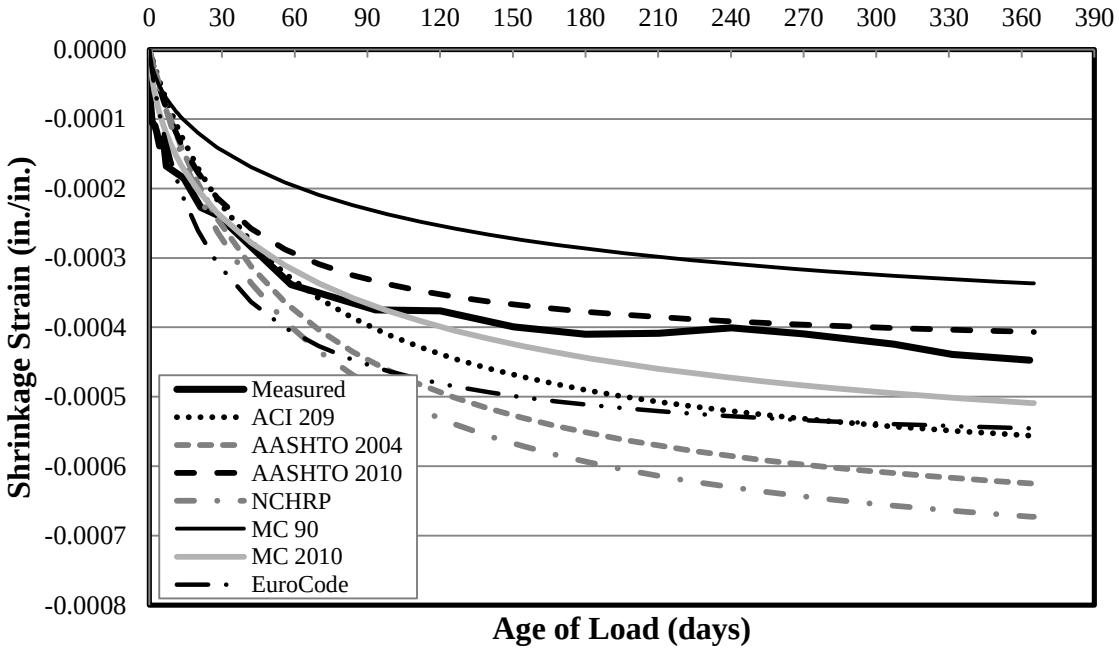

Figure 5-37: Shrinkage Strain for Specimen 54-07S-M up to 1 Year

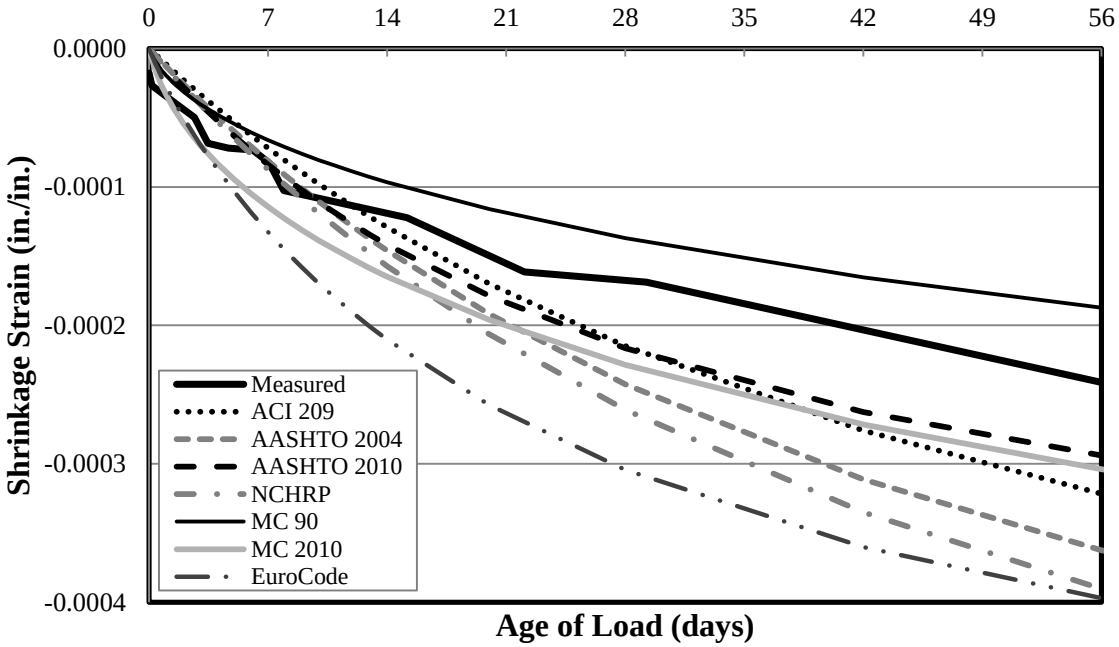

Figure 5-38: Shrinkage Strain for Specimen 54-07S-T up to 56 Days

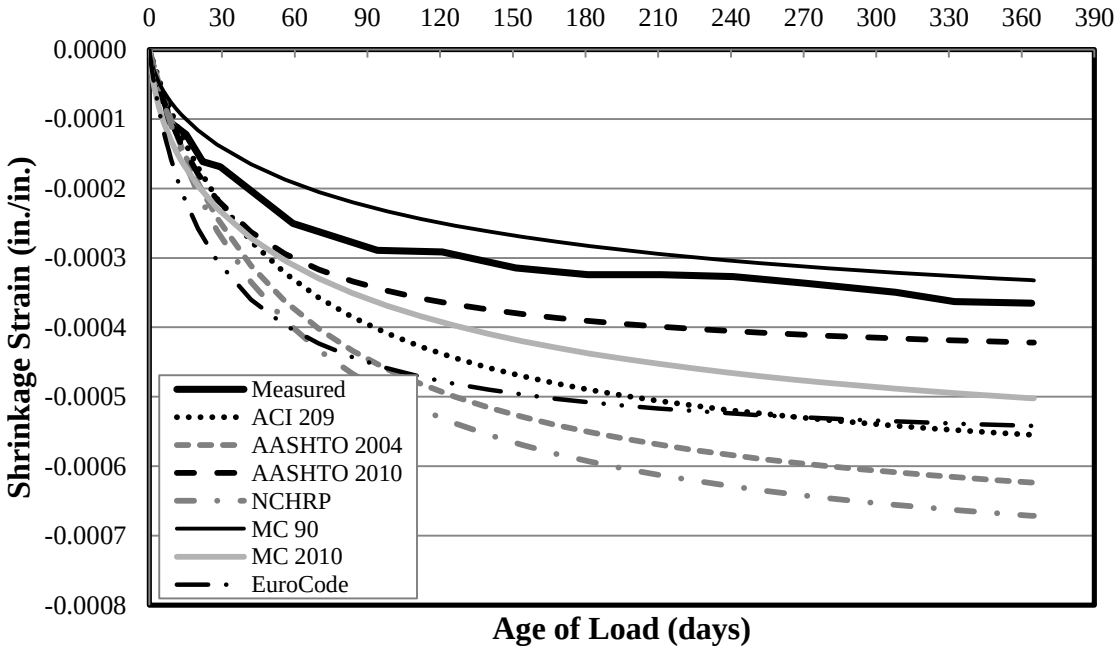

Figure 5-39: Shrinkage Strain for Specimen 54-07S-T up to 1 Year

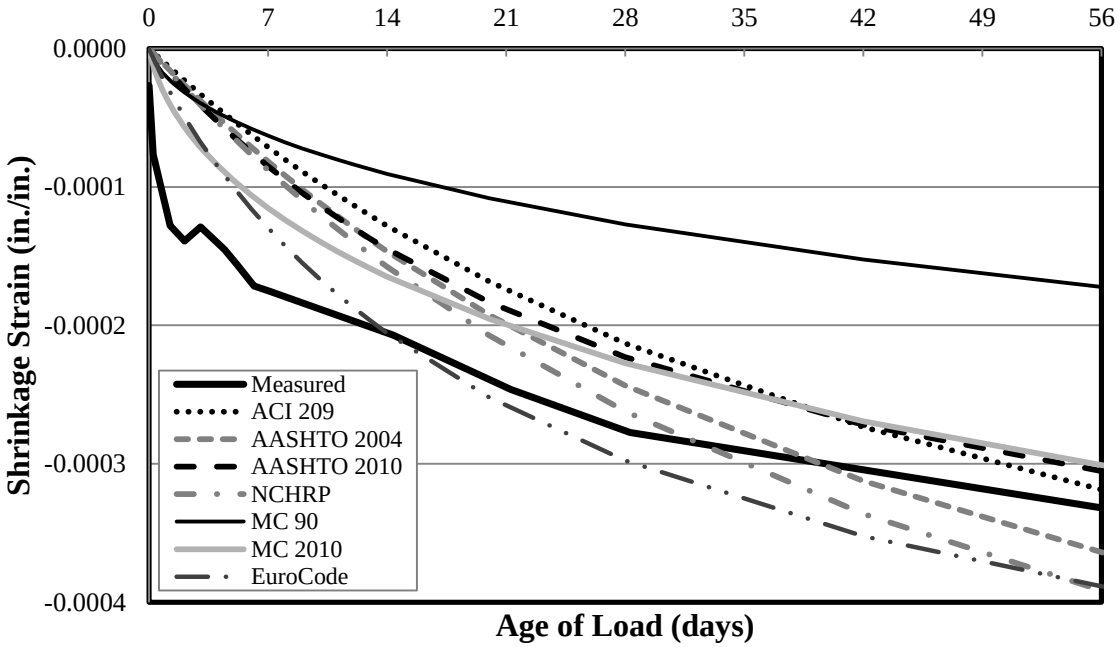

Figure 5-40: Shrinkage Strain for Specimen 72-03S-M up to 56 Days

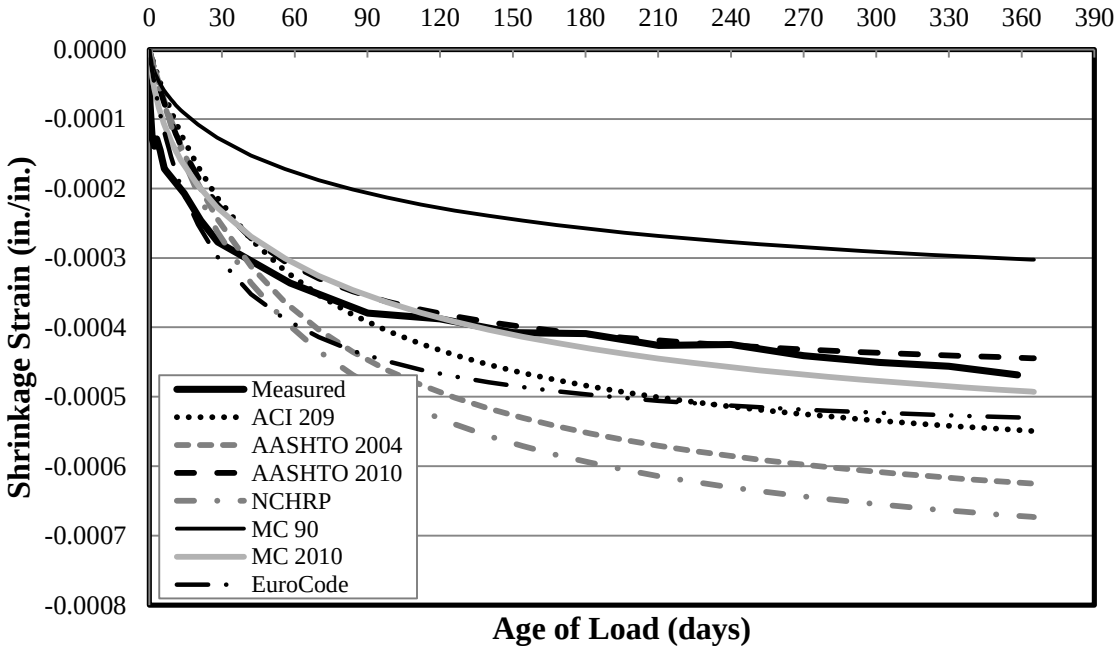

Figure 5-41: Shrinkage Strain for Specimen 72-03S-M up to 1 Year

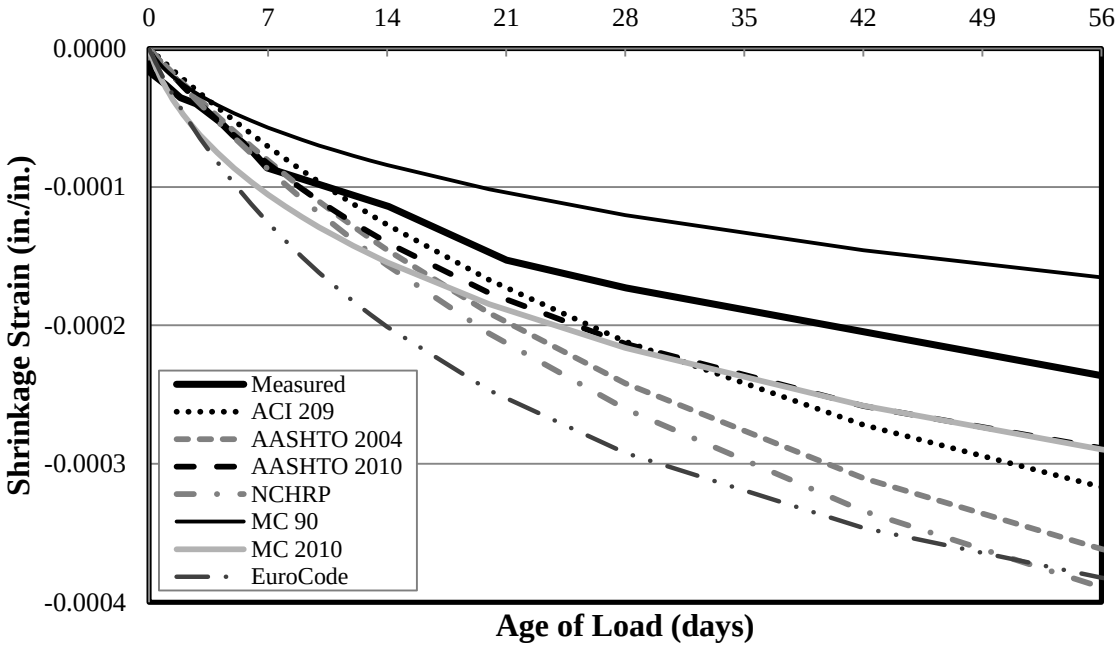

Figure 5-42: Shrinkage Strain for Specimen 72-03S-T-U up to 56 Days

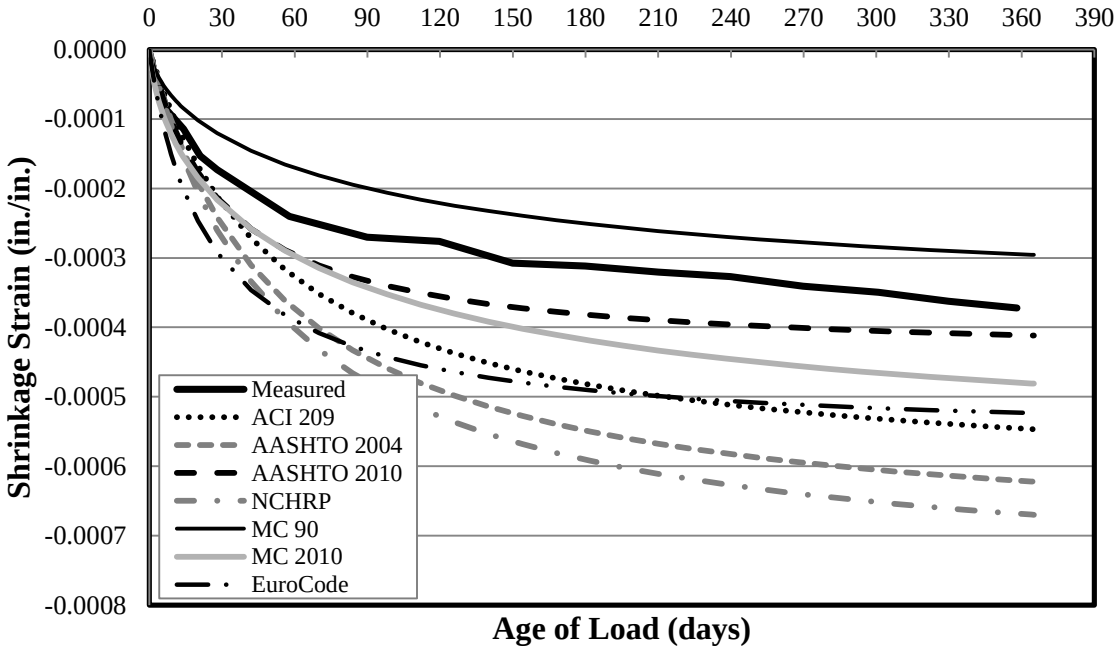

Figure 5-43: Shrinkage Strain for Specimen 72-03S-T-U up to 1 Year

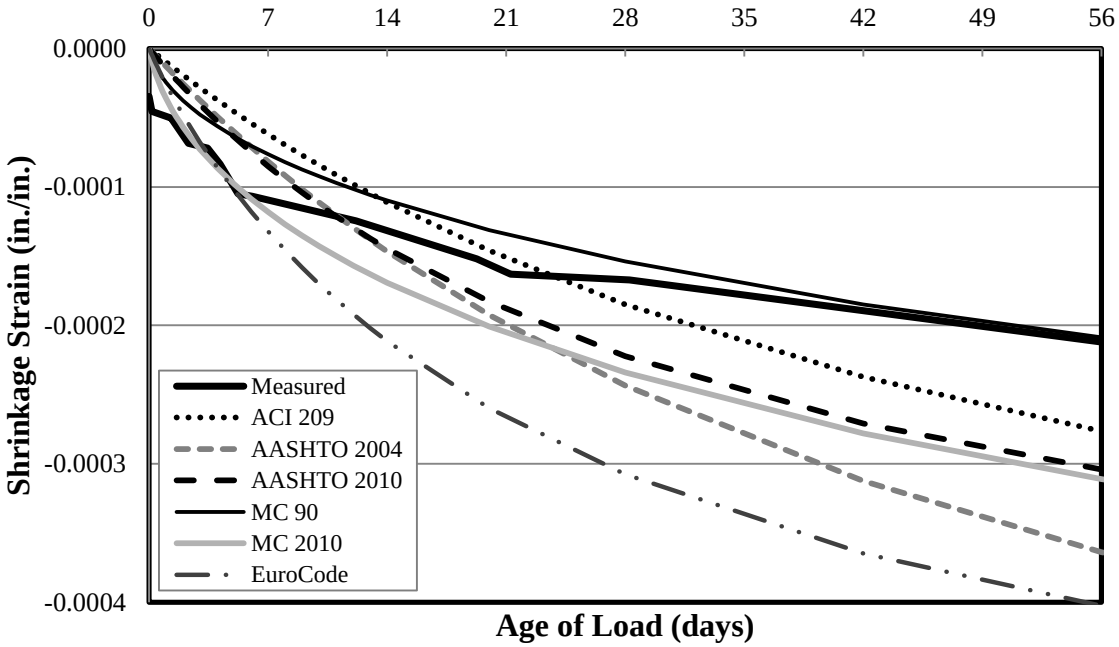

Figure 5-44: Shrinkage Strain for Specimen 54-12C-M up to 56 Days

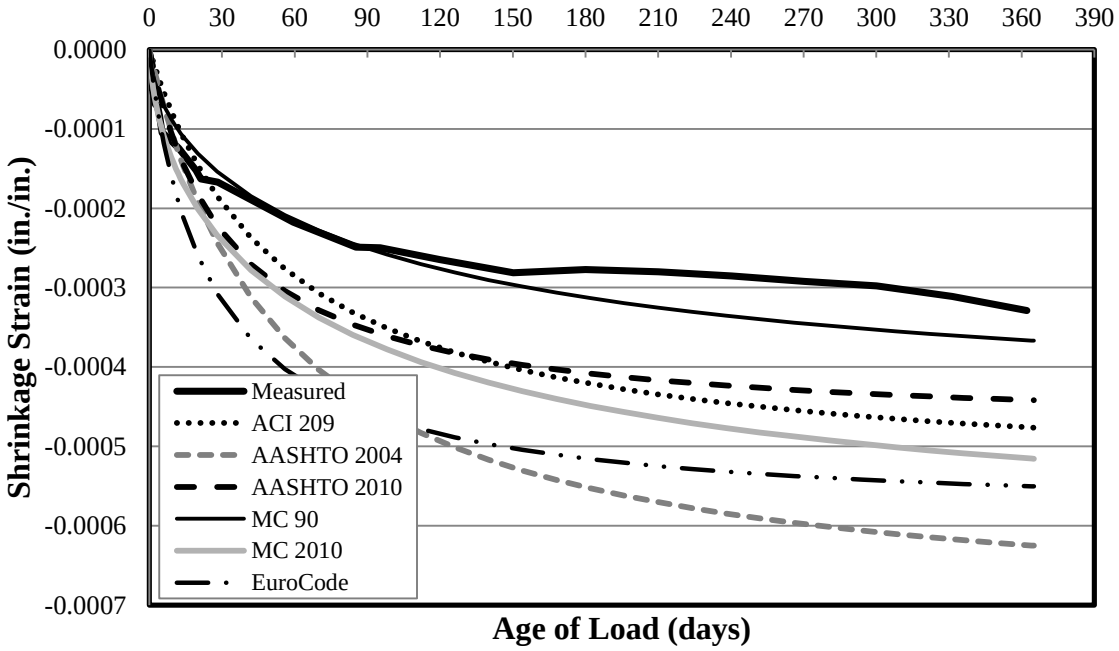

Figure 5-45: Shrinkage Strain for Specimen 54-12C-M up to 1 Year

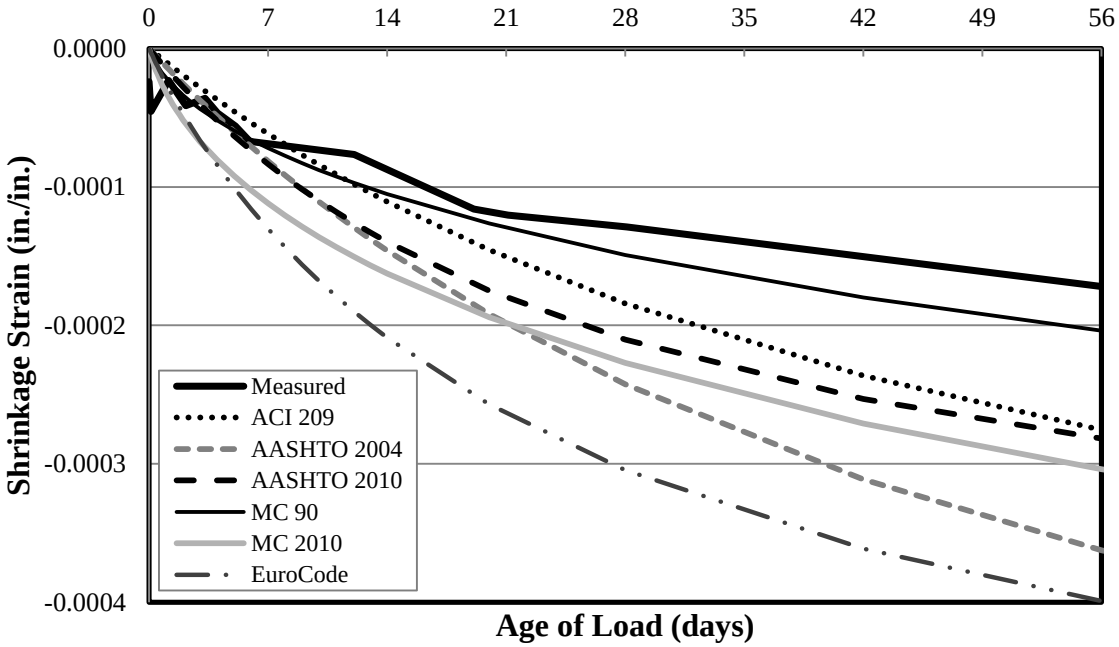

Figure 5-46: Shrinkage Strain for Specimen 54-12C-T up to 56 Days

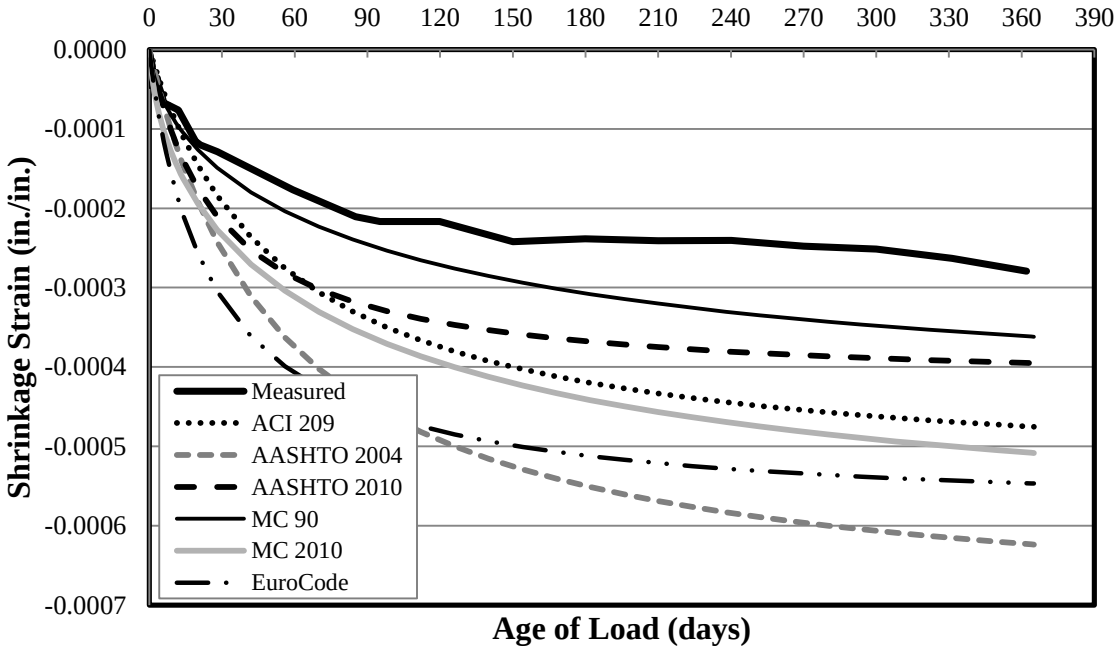

Figure 5-47: Shrinkage Strain for Specimen 54-12C-T up to 1 Year

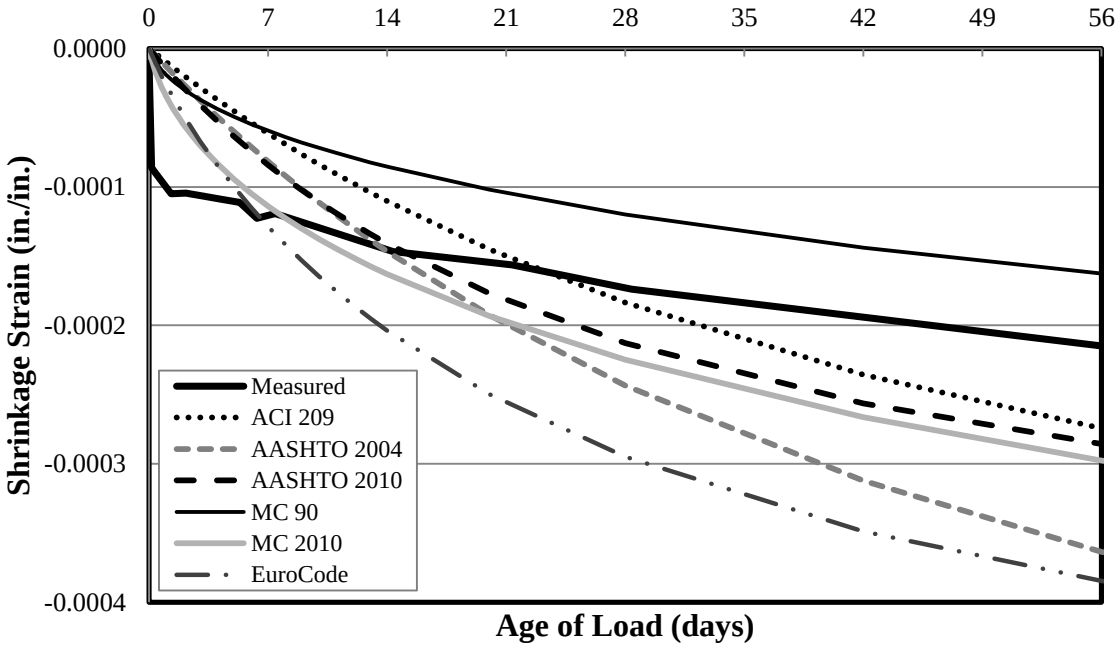

Figure 5-48: Shrinkage Strain for Specimen 72-11C-M up to 56 Days

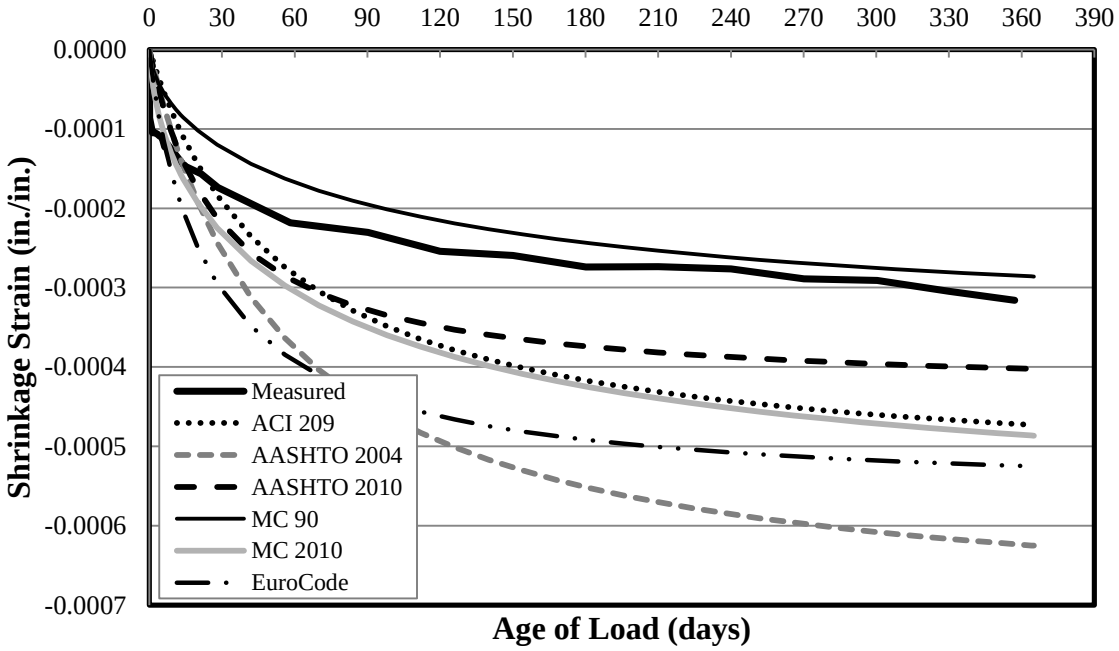

Figure 5-49: Shrinkage Strain for Specimen 72-11C-M up to 1 Year

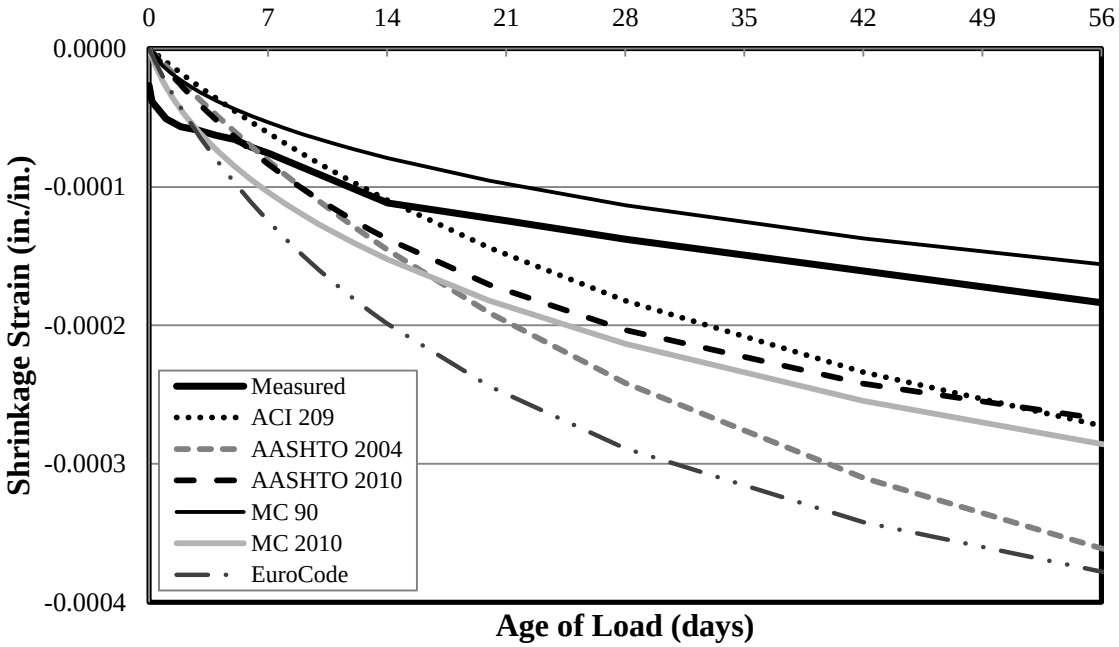

Figure 5-50: Shrinkage Strain for Specimen 72-11C-T-U up to 56 Days

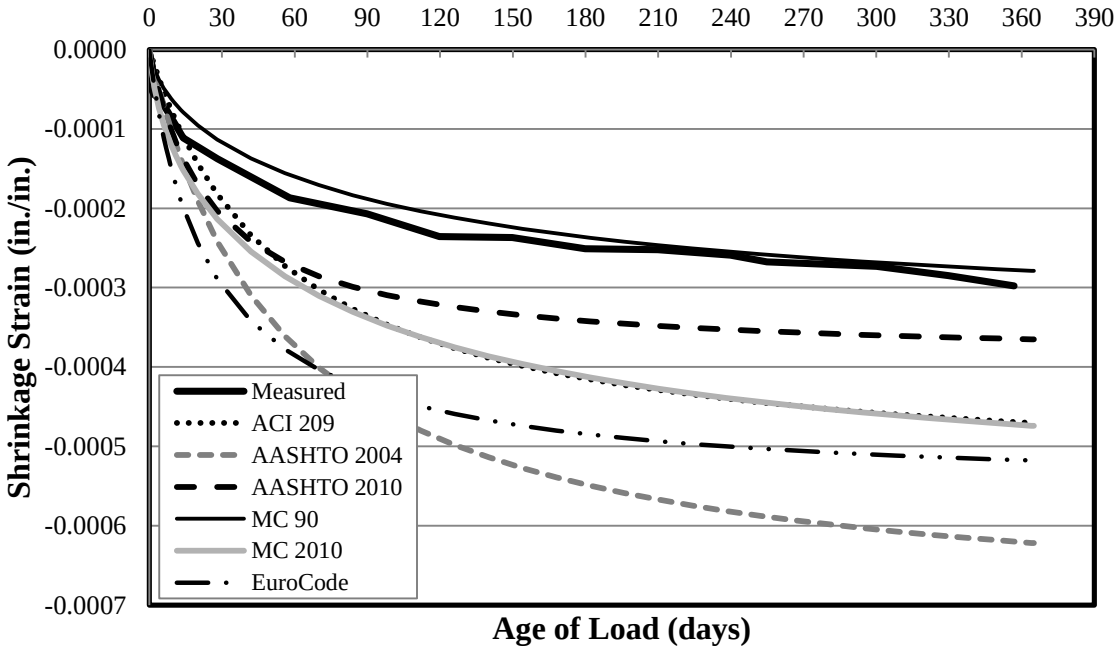

Figure 5-51: Shrinkage Strain for Specimen 72-11C-T-U up to 1 Year

Table 5-13 shows the average shrinkage strains at 56 days and 1 year for each prediction method evaluated. These averages are shown for SCC only, CVC only, and the averages of all specimens. The averages do not include specimens that are underloaded or improperly cured. It should also be noted that the average of the CVC specimens for NCHRP 628 is identical to AASHTO 2004 for shrinkage strains.

Table 5-13: Average Shrinkage Strain Predictions by Method

Prediction Method	Average SCC (microstrain)		Average CVC (microstrain)		Average ALL (microstrain)	
	56 Days	1 Year	56 Days	1 Year	56 Days	1 Year
ACI 209	-321	-552	-276	-475	-301	-519
AASHTO 2004	-363	-624	-363	-624	-363	-624
AASHTO 2010	-289	-410	-291	-413	-290	-411
NCHRP 628	-391	-672	N/A	N/A	-379	-652
Eurocode	-389	-533	-395	-541	-392	-536
MC 90	-180	-317	-192	-338	-185	-326
MC 2010	-299	-494	-304	-503	-301	-498

From the above figures and table it can be seen that the predicted 56-day and 365-day shrinkage strain values for SCC mixtures range between -169 and -401 microstrain, and -298 and -673 microstrain, respectively. For conventional concrete at 56 and 365 days, the ε_{sh} ranges from -163 to -403 microstrain and from -286 to -625 microstrain, respectively. Although the predicted load-induced strains for each method were greater in magnitude for SCC specimens than CVC specimens, there is no consistent pattern between SCC and CVC for the predicted shrinkage strains.

From the plots alone, several general observations can also be made about the shrinkage predictions. Most strikingly, the prediction of shrinkage strain is much less accurate than the prediction of load-induced strain. Some method-specific observations follow:

For ACI 209,

- ACI 209 greatly overpredicts shrinkage strains at 1 year for both SCC and CVC.

For AASHTO models,

- AASHTO 2004 overpredicts shrinkage strains for both SCC and CVC at 1 year.
- AASHTO 2010 overpredicts shrinkage strains for some SCC specimens but is close to the measured data for others. For CVC, AASHTO 2010 generally overpredicts slightly.
- NCHRP 628 grossly overpredicts shrinkage strains for SCC at 1 year. NCHRP 628 predicts more than AASHTO 2004 and significantly more than AASHTO 2010 due to the amplification factor based on cement type. NCHRP 628 produces the largest shrinkage predictions of any method at 1 year.

For European models,

- MC 90 underpredicts or is reasonably close to the measured shrinkage for SCC, but overpredicts or is reasonably close to the measured shrinkage for CVC. MC 90 has the slowest growth rate and always produces the smallest shrinkage predictions.
- MC 2010 overpredicts shrinkage strain for both SCC and CVC, but is slightly more accurate for SCC.
- Eurocode overpredicts shrinkage strain for SCC and significantly overpredicts shrinkage strain for CVC. Eurocode has the fastest early growth rate and produces the largest shrinkage predictions early on.

5.4 EVALUATION OF PREDICTION METHODS

Although some generalizations on the prediction of creep and shrinkage can be made based on the specimens alone, it is difficult to make direct comparisons between the methods while looking at a single specimen. Because each specimen was loaded to 40% of its compressive strength, a slightly weaker specimen would have been loaded slightly less which could mean less load-induced strain. This is especially true with regards to creep where the strains are directly related to the applied load. Because of this, a comparison of all specimens in relation to a single method was also evaluated.

Once all creep and shrinkage data were collected, several comparisons of the results were made to determine which methods proved to be the most reliable. This was accomplished first by plotting the measured values against the predicted values in order to compare each method individually. Afterwards, statistical analyses were conducted in order to evaluate the accuracy of each of the methods investigated.

5.4.1 MEASURED VERSUS PREDICTED STRAIN

The following sections present the measured strains in comparison to the predicted strains for creep and shrinkage. If a prediction method accurately predicts the strain, each point will line up perfectly along the line of equality. The preferred range of error for the prediction models evaluated in this research was selected as ±20%. By plotting the predicted value on the vertical axis and the measured value on the horizontal axis, and by plotting ±20% error margins, the specimens that fall within the acceptable range can easily be seen. Points that are outside the 20% error margins represent test cases that are not accurately predicted.

5.4.1.1 Measured Versus Predicted Creep Strain

In this section, the measured load-induced strains are plotted against the predicted load-induced strains in an effort to evaluate creep predictions. Figure 5-52 through Figure 5-59 plot each prediction method individually with data markers differentiating match- and tarp-curing conditions for SCC and CVC specimens. For each instance, there are data for 1 day, 7 days, 56 days, and 365 days shown. It should be noted that for load-induced strain, MC 90-99 and Eurocode are equivalent to MC 2010, and thus are not shown independently.

5.4.1.1.1 ACI 209

Figure 5-52 shows the comparison of the measured load-induced strain to the estimated load-induced strain that was calculated using the ACI 209 prediction method. This figure shows each strain measurement as a separate data point. It may be seen that ACI 209 predicts both SCC and CVC load-induced strains with relatively good accuracy.

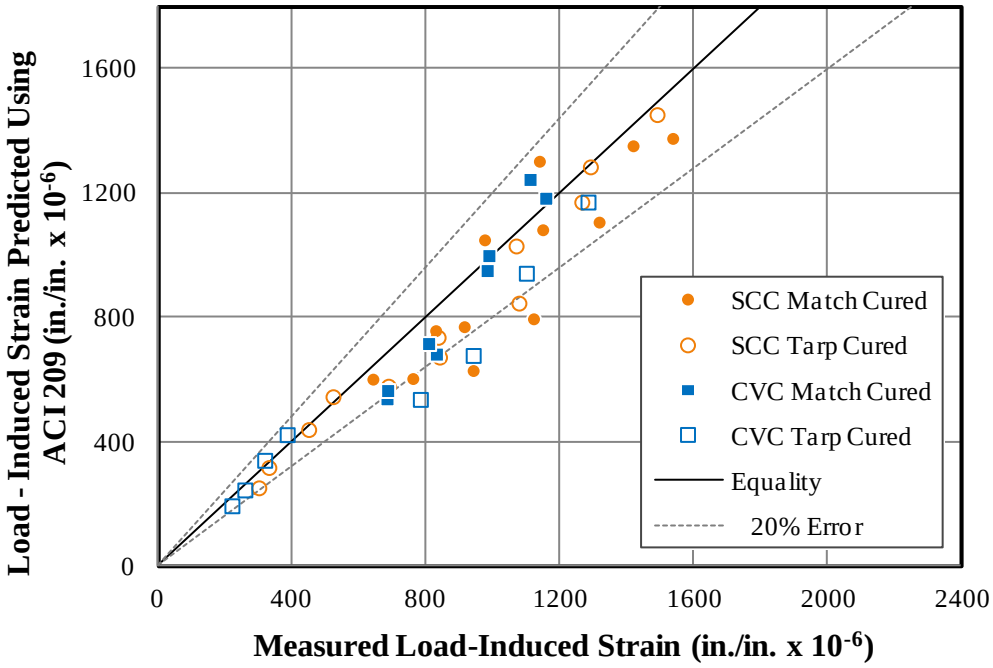

Figure 5-52: Measured Versus Predicted Load-Induced Strain Using ACI 209

As seen from this figure, at one year, all the specimens fell within the ±20% range with no real distinction between the accuracy of SCC versus CVC or match-cured versus tarp-cured. All of the predictions that fell outside of the ±20% error margins were early-age strains.

It should be noted that in the previous figure, the smallest strains are not necessarily the early-age strains. For clarification, Figure 5-53 plots just the 56 day and 1 year strains where it can be seen that for the under-loaded specimens, the strains are small even at these later ages. This will also occur for all other load-induced plots like Figure 5-52. This is not an issue for plots of shrinkage strain as shrinkage does not depend on the applied load.

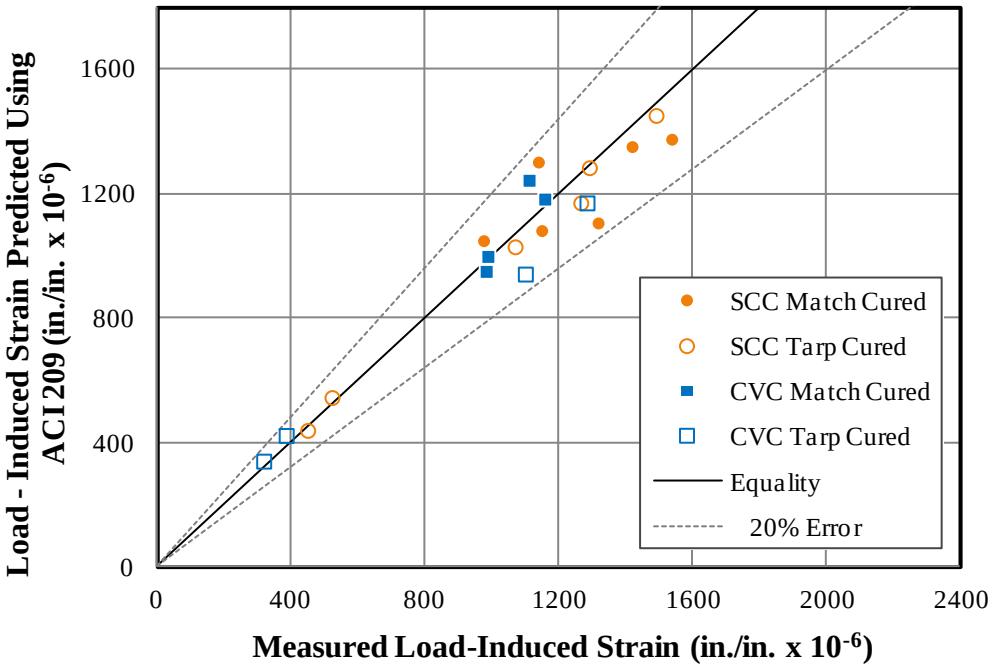

Figure 5-53: Measured Versus Predicted Load-Induced Strain at 56 Days and 1 Year Using ACI 209

It can be seen from Figure 5-53 that the load-induced strain predictions for ACI 209 at later ages were not only within the error boundaries but were also heavily concentrated around the line of equality. This is also verified through findings by Kavanaugh (2008) who showed that ACI 209 was a reliable method for accelerated-cured, conventional-slump concrete. When comparing the other methods that follow, it can also be seen that ACI 209 is one of the most accurate prediction methods overall for load-induced strain.

5.4.1.1.2 AASHTO 2004

The measured load-induced strain compared to the estimated load-induced strain that was calculated using the AASHTO 2004 prediction method can be seen in Figure 5-54. It may be seen that AASHTO 2004 predicts both SCC and CVC load-induced strains with relatively fair accuracy with no apparent difference between the two mixtures visible from this figure.

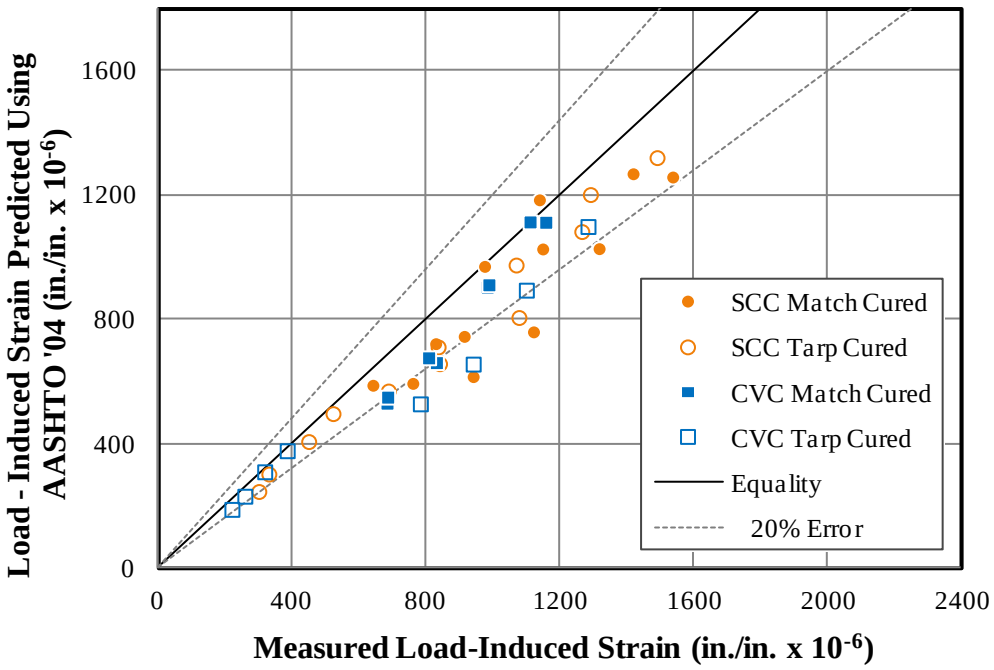

Figure 5-54: Measured Versus Predicted Load-Induced Strain Using AASHTO 2004

AASHTO 2004 method does tend to underestimate ε_{li} at every age for all specimens, except one, at or below the line of equality. However, even with this underestimation, the majority of specimens still fell within the error margin with the only errors outside the ±20% range occurring in early ages. Excluding any specimens that were underloaded or cured improperly, at one year and at 56 days, all of the specimens fell within the ±20% range with only one exception. Also, a distinct pattern may be observed where there is a tendency for low predictions at early ages then a slight increase in accuracy of predictions in later ages. This pattern indicates that the rate function needs to be adjusted. For the prediction of load-induced strain for AASHTO 2004, the growth rate at early ages is too slow.

5.4.1.1.3 AASHTO 2010

Figure 5-55 shows the AASHTO 2010 estimated ε_{li} values versus the ε_{li} values collected during the research phase of this study. AASHTO 2010 depicts similar trends to that of AASHTO 2004. The distinctive low prediction can be seen at early ages then the jump at later ages is much more pronounced. As with AASHTO 2004, this pattern indicates that the rate function needs to be adjusted for the prediction of load-induced strain where the rate at early ages is increased and is decreased at later ages. The majority of the specimens are within the error lines at later ages, but this method proves to be especially inaccurate early on where the predictions are low and most of the values fall outside of the preferable ± 20% error range.

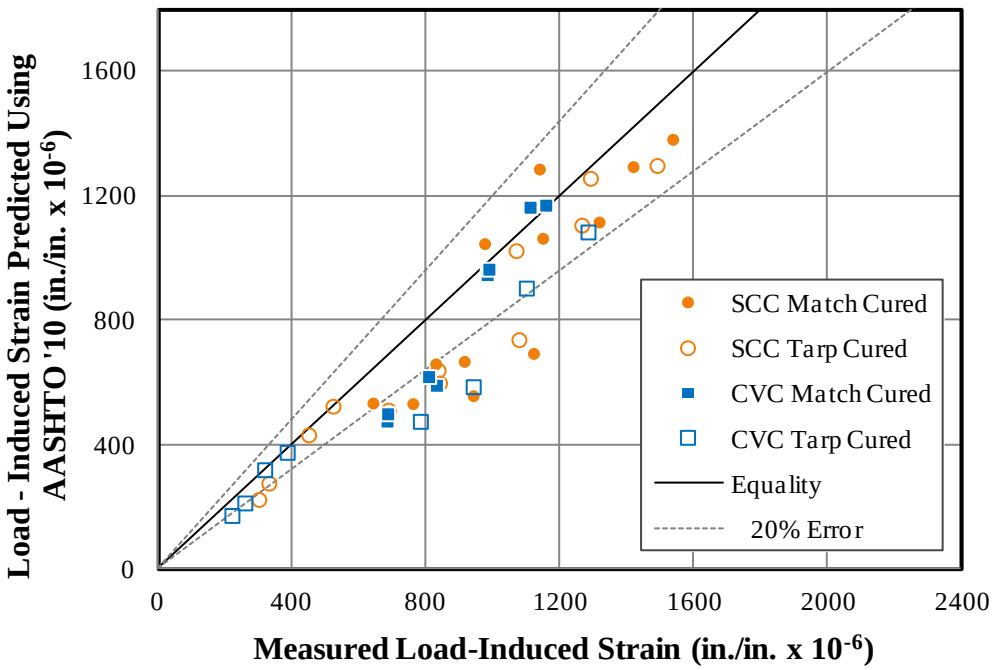

Figure 5-55: Measured Versus Predicted Load-Induced Strain Using AASHTO 2010

As with the previous methods, AASHTO 2010 shows no apparent bias towards SCC or CVC.. It can be seen that, at one year, all the specimens fell within the ±20% range with a good balance around the line of equality. Overall, the accuracy of this method for the prediction of load-induced strain is relatively good at later ages.

5.4.1.1.4 NCHRP 628

Figure 5-56 depicts the ε_{li} that was estimated by NCHRP 628 versus the measured ε_{li} that was collected during this study. Because this report is formulated from the AASHTO methods, the pattern is very similar to the pattern of prediction values for both AASHTO methods. Here however, the underprediction at early ages is so extreme that most of the specimens fall outside of the -20% error and the jump at later ages causes an over-prediction

where most of the specimens are above the line of equality and some are even above the +20% error line.

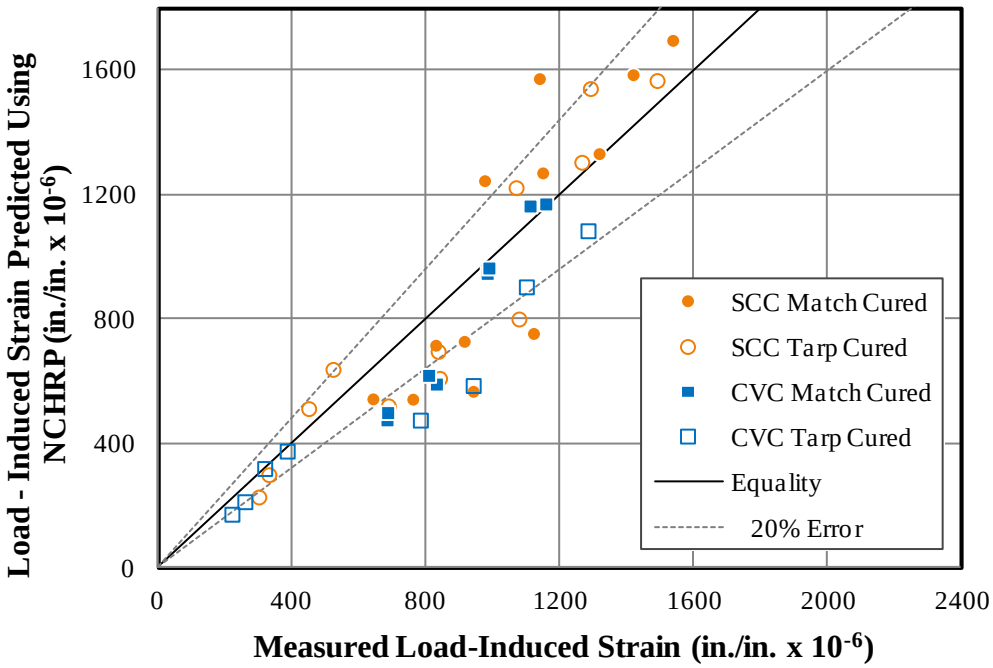

Figure 5-56: Measured Versus Predicted Load-Induced Strain Using NCHRP 628

The extreme spread of predictions seen here makes this method much less reliable than either of the AASHTO models. In fact, the NCHRP 628 method predicts more results outside of the ±20% range than any other method which is an indication of the poor accuracy of this method for load-induced strains especially at early ages. It should also be noted that the NCHRP method reverts to AASHTO 2010 when CVC is used.

As described in Chapter 2, the prediction of creep by NCHRP 628 is based on the AASHTO model with an additional amplification factor, *A*, that can be seen in Equation 2-20. Because this method was tailored to a specific type of concrete, the NCHRP 628 may

yield more accurate results if used in conjunction with a concrete that is more similar to the one used specifically for that report. For example, if fly ash were used instead of slag for this research, the NCHRP 628 method may have been more relevant. Based on the results of *this* study, it appears that the AASHTO 2010 method does not require the same amplification for SCC as was used in the NCHRP 628 method.

5.4.1.1.5 MC 90

Figure 5-57 illustrates the comparison of the measured load-induced strain to the estimated load-induced strain that was calculated using the MC 90 prediction method. The performance of this method is excellent at early ages; however, at later ages, it does tend to overestimate load-induced strains. As can be seen in the load-induced strain plots at 56 days in the previous section, the rate of creep at early ages is fairly accurate but continues to grow throughout later ages causing an overestimation. If this rate was slowed for later ages, this method might produce excellent predictions.

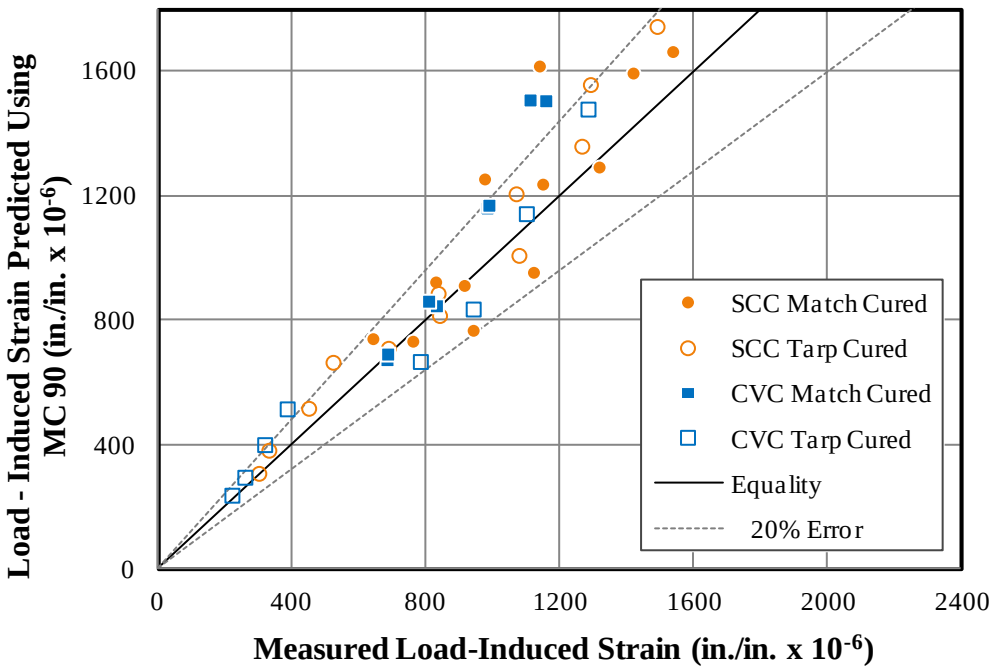

Figure 5-57: Measured Versus Predicted Load-Induced Strain Using MC 90

Although the data are predominately within the +20% boundary at one year, this figure shows that some data points are well over the upper boundary for SCC and CVC match-cured specimens. Figure 5-57 also shows that most of the data points at later ages are above the line of equality with only a few exceptions. In fact, this method produces the most overestimated later-age predictions of any of the methods. This is a direct contradiction to the results found by Kavanaugh (2008) that claim that MC 90 was the best prediction model for the estimation of creep for SCC mixtures. However, as mentioned in Section 2.7, Kavanaugh failed to apply the two-step modification for equivalent age at loading, described in Section 2.3.5.1, that is prescribed in MC 90. The apparent contradiction in results seen here can be directly attributed to Kavanaugh's error in application of the creep prediction model outlined in MC 90.

5.4.1.1.6 MC 90-KAV

The comparison of the measured load-induced strain to the estimated load-induced strain that was calculated using the Kavanaugh modification of MC 90 (MC 90-KAV) is depicted in Figure 5-58. From this figure, it can be seen that the overall pattern of predictions is the same as MC 90, but the entire plot is shifted down to correct the overprediction problem experienced by MC 90.

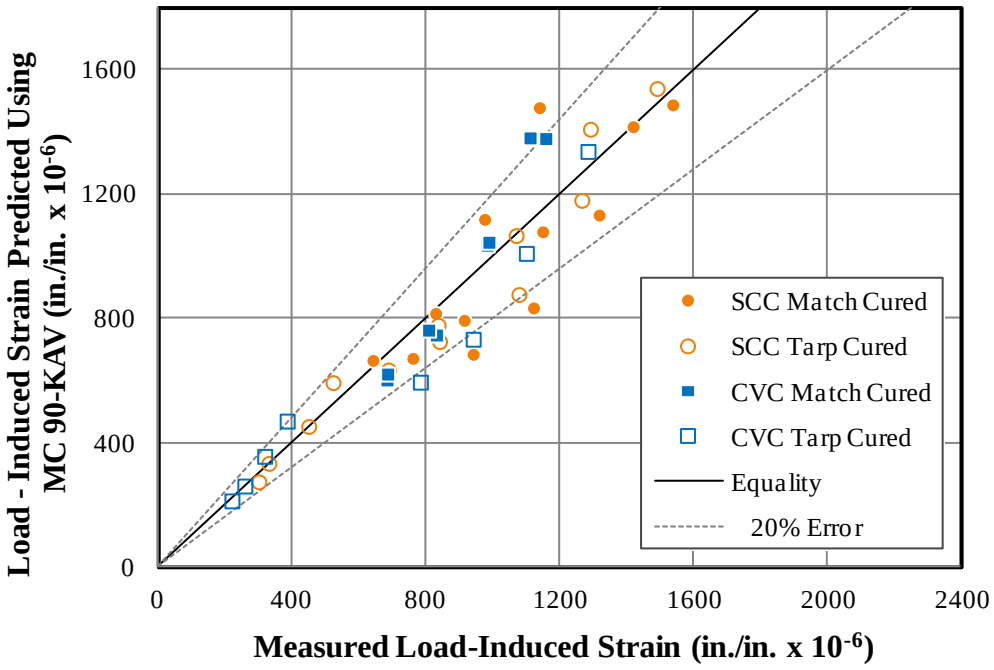

Figure 5-58: Measured Versus Predicted Load-Induced Strain Using MC 90-KAV

Here, the data are much more balanced about the line of equality and there are fewer points outside of the ±20% error margins where the largest errors are from the CVC match-cured specimens. Even these points outside of the boundaries are within close proximity of the preferred tolerance.. At early ages, the data are concentrated under the line of equality

which indicates the method is under prediction strains early on. The modification of MC 90 seems to have corrected the later age rate problem discussed in the previous section; however, the rate at early ages was also affected and is now less accurate. Nevertheless, MC 90-KAV is a definite improvement over the MC 90 model.

5.4.1.1.7 MC 2010 (also MC 90-99 and Eurocode)

Figure 5-59 depicts the ε_{li} that was estimated by MC 2010 versus the measured ε_{li} that was collected during this study. As seen in this figure, MC 2010 produced the most concentrated pattern of prediction points within the ±20% boundary lines. For this method, there seems to be a much smaller difference between early-age prediction and later predictions than was noticed in other methods such as ACI 209, both AASHTO methods, and NCHRP 628. This is a clear indication that the growth rate of this method is one of the most accurate of the methods investigated.

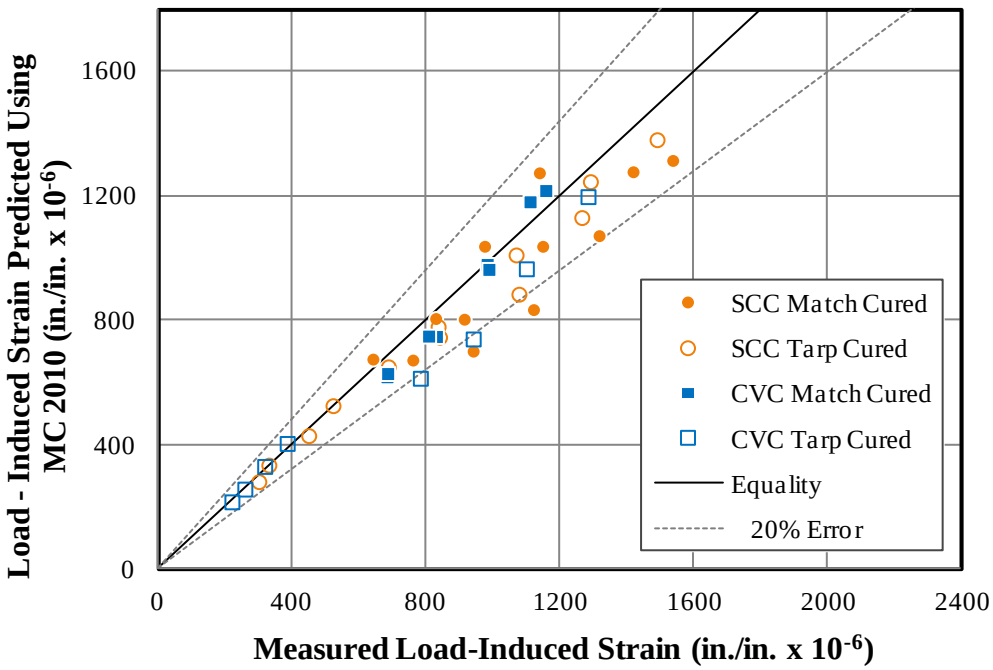

Figure 5-59: Measured Versus Predicted Load-Induced Strain Using MC 2010

According to this figure, at one year, all the specimens fell within the ±20% range with an excellent balance of prediction points around the line of equality. Any points that appear to be outside of the 20% boundary lines are under-loaded specimens or specimens with questionable curing. It may be observed that, overall, this method predicts load-induced strains with a relatively high degree of accuracy.

5.4.1.2 Measured Versus Predicted Shrinkage Strain

In this section, the measured shrinkage strains are plotted against the predicted shrinkage strains. Figure 5-60 through Figure 5-66 plots each prediction method individually with data points for match and tarp curing conditions for both SCC and CVC specimens. For each instance, there are results for 1 day, 7 days, 56 days, and 365 days which are shown in much more distinguishable groups than with load-induced strain. This is due to the fact that

shrinkage strain is not dependent on the applied load. It should be noted that for shrinkage strain, MC 90-99 is equivalent to MC 2010 and MC 90-KAV was not evaluated for shrinkage and thus, these methods are not shown. Also, unlike creep, Eurocode is not equivalent to MC 2010 for shrinkage.

5.4.1.2.1 ACI 209

Figure 5-60 shows the comparison of the measured shrinkage strain to the estimated shrinkage strain that was calculated using the ACI 209 prediction method. This figure shows each specimen as a separate data point. It may be seen that ACI 209 predicts both SCC and CVC mixtures with relatively poor accuracy. However, this figure shows a clear separation between SCC specimens and CVC specimens at later ages. This pattern indicates that ACI 209 predicts the same shrinkage strain for all the SCC specimens and the same shrinkage strain for all the CVC specimens. This is because the model is based largely on concrete mixture proportions.

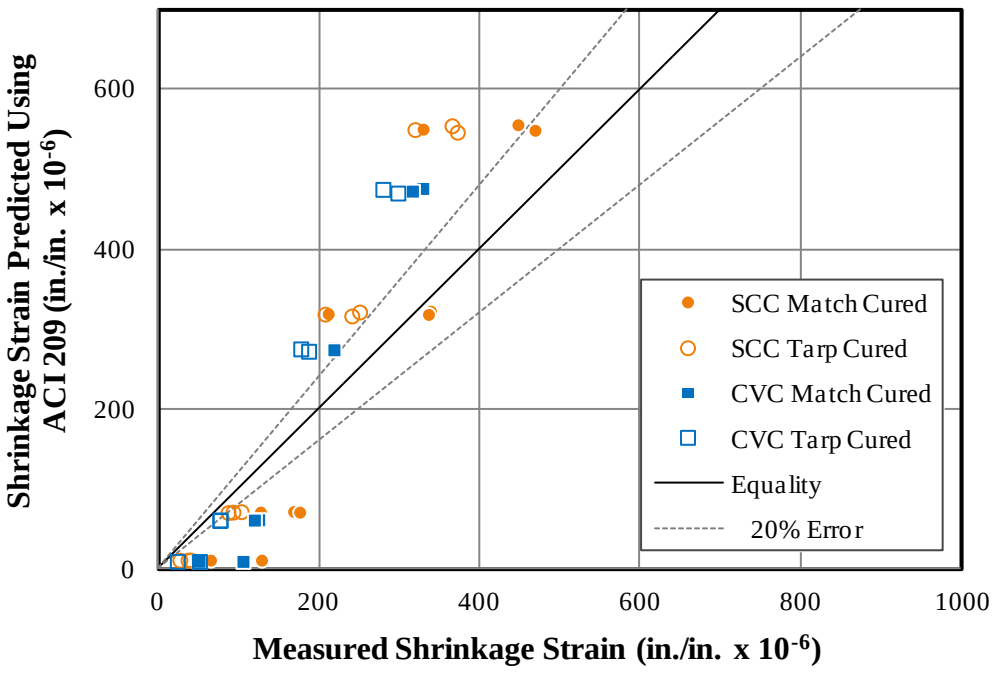

Figure 5-60: Measured Versus Predicted Shrinkage Strain Using ACI 209

This method tends to underestimate the shrinkage strains at early ages and overestimate long-term strains. There is only one SCC match-cured specimen as an exception at one year that fell within the ±20% range. In comparison to load-induced strains, the prediction of shrinkage is much more problematic for ACI 209 and the errors are much greater. This figure clearly indicates that shrinkage for neither SCC nor CVC is well estimated by this method.

5.4.1.2.2 AASHTO 2004

A comparison of the measured ε_{sh} to the estimated ε_{sh} that was calculated using the AASHTO 2004 prediction method is shown in Figure 5-61. Unlike ACI 209, AASHTO 2004 shows no divergence between SCC and CVC because the model does not consider concrete strength or composition.

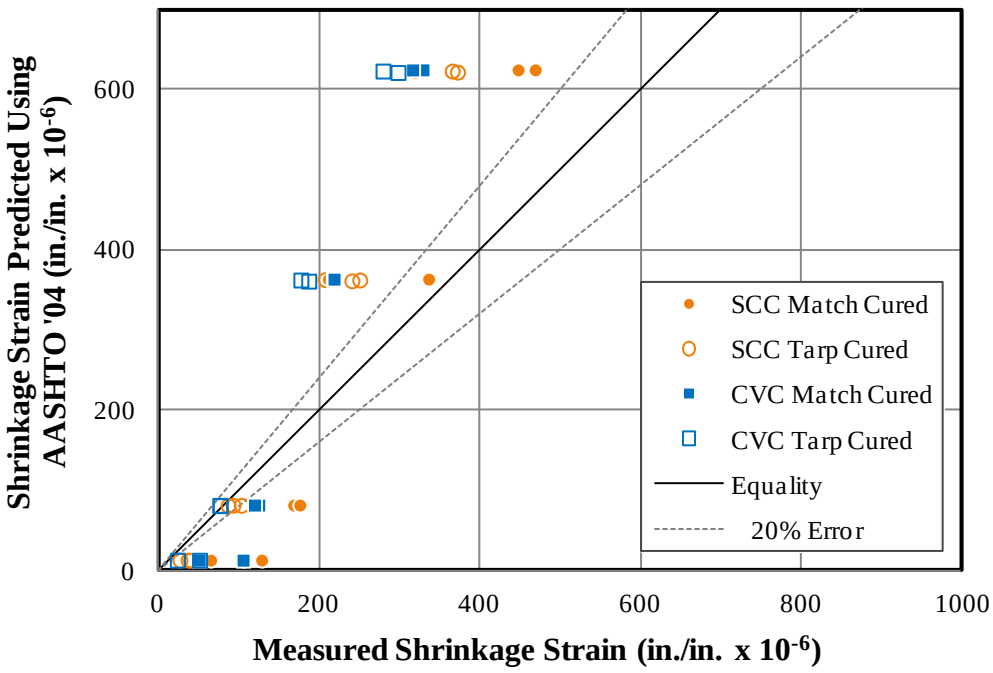

Figure 5-61: Measured Versus Predicted Shrinkage Strain Using AASHTO 2004

In this figure, both mixture types are shown on one horizontal line, indicating that the predictions were the same for all specimens at each age regardless of mixture type or curing conditions. From this figure, it can be seen that shrinkage predictions by AASHTO 2004 are especially inaccurate. Because the model is independent of concrete composition, the relative accuracy is different for SCC than for CVC. Like ACI 209, this method tends to underestimate the shrinkage strains at early ages and overestimate strains at later ages with every point above the line of equality at 56 days and one year. None of the data at one year is within reasonable proximity of the ±20% range and only one specimen was within the acceptable range at 56 days. In comparison to load-induced strains predicted by AASHTO 2004, the prediction of shrinkage is far less accurate.

5.4.1.2.3 AASHTO 2010

Figure 5-62 provides a comparison of the measured ε_{sh} to the estimated ε_{sh} that was predicted using AASHTO 2010. Like AASHTO 2004, AASHTO 2010 predicts the same shrinkage strain for all the SCC specimens and the same shrinkage strain for all the CVC specimens at early ages (1 and 7 days). However, at later ages (56 and 365 days), the pattern tends to be more scattered indicating that the method differentiates between different concrete types at later ages.

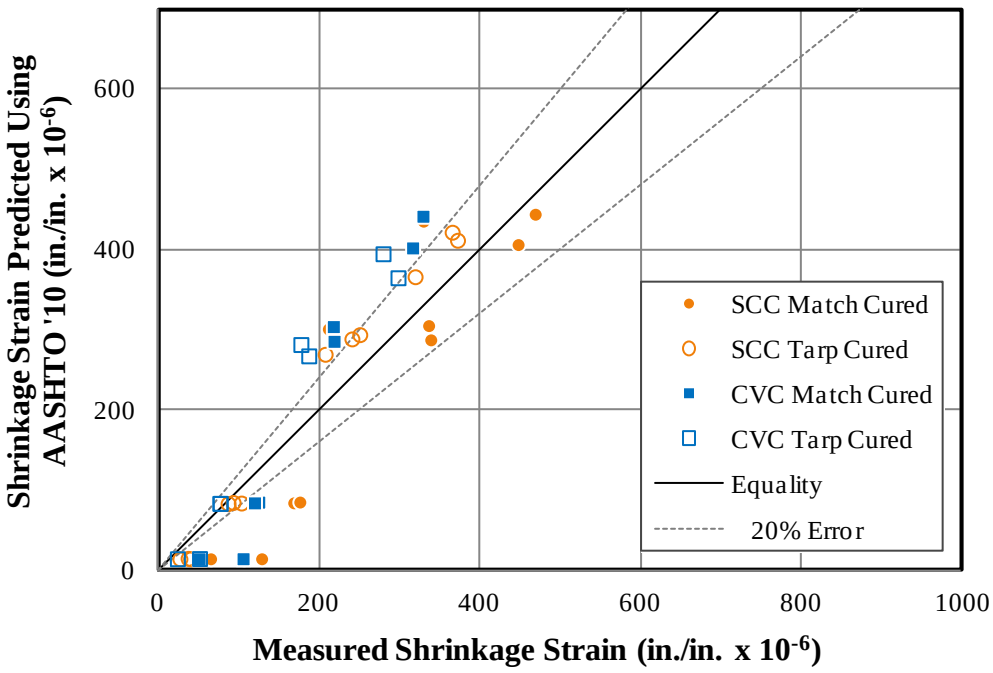

Figure 5-62: Measured Versus Predicted Shrinkage Strain Using AASHTO 2010

From this figure, it can be seen that SCC shrinkage predictions by AASHTO 2010 are actually within the ±20% error boundaries with only a few exceptions. SCC predictions are also well distributed around the line of equality at one year. On the other hand, CVC

predictions are all outside of the desired range. Like the other methods discussed, this method also tends to underestimate the shrinkage strains at early ages. As was seen with the load-induced strains as well, the growth rate of shrinkage predictions is too slow early on.

Overall, AASHTO 2010 predicts ε_{sh} with comparatively good accuracy for SCC at later ages (56 days and 1 year), and less so for CVC. Unlike many of the other methods, this figure shows definite separation between the SCC and CVC specimens where SCC is predicted with greater accuracy by this model.

5.4.1.2.4 NCHRP 628

Figure 5-63 compares the measured ε_{sh} to the estimated ε_{sh} that was predicted using the NCHRP 628. Showing patterns much like ACI 209, this method tends to underestimate the shrinkage strains at early ages and over-estimate strains at later ages with every point above the line of equality at 56 days and one year. Also like ACI 209, NCHRP 628 shows some separation between SCC specimens and CVC specimens at later ages. This pattern indicates that NCHRP 628 predicts the same shrinkage strain for all the SCC specimens and the same shrinkage strain for all the CVC specimens regardless of curing conditions for either mixture type. This separation between mixture types is due to the fact that the NCHRP method reverts to AASHTO 2004 when CVC is used.

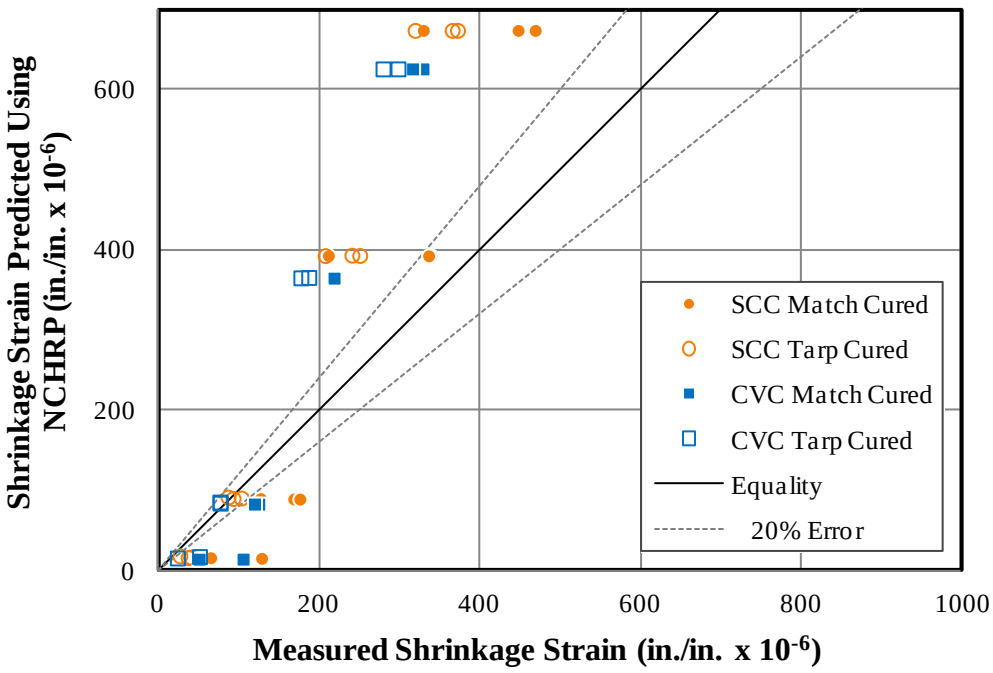

Figure 5-63: Measured Versus Predicted Shrinkage Strain Using NCHRP 628

Here, the SCC predictions are slightly higher than the CVC predictions. The poor accuracy of this method is indicated by the fact that only two specimens are within the acceptable range at 56 days and none of the data at one year are within reasonable proximity of the ±20% error boundaries. When excluding any underloaded specimens or specimens that were cured improperly, this figure also indicates that for NCHRP 628, the errors increase from match- to tarp-cured specimens.

As described in Chapter 2, the prediction of shrinkage by NCHRP 628 is based on the AASHTO 2004 method with an additional modification factor, *A*, as can be seen in Equation 2-68. Because this method was tailored to a specific type of concrete, the NCHRP 628 may yield more accurate results if used in conjunction with a concrete that is more similar to the one used specifically for that report. For example, because the SCC used in NCHRP

contained 20% fly ash, if SCC mixtures with fly ash were used instead of slag cement for this research, the NCHRP 628 method may have been more relevant. However, other research on SCC mixtures similar to those in this study indicates that there is little difference between the shrinkage strains of SCC containing fly ash and SCC containing similar amounts of slag cement (Levy, Barnes, and Schindler 2010).

5.4.1.2.5 MC 90

Figure 5-64 provides a comparison of the measured ε_{sh} to the estimated ε_{sh} that was predicted using MC 90. Like AASHTO 2010, MC 90 has a more scattered pattern indicating that the method differentiates between different concrete types at all ages.

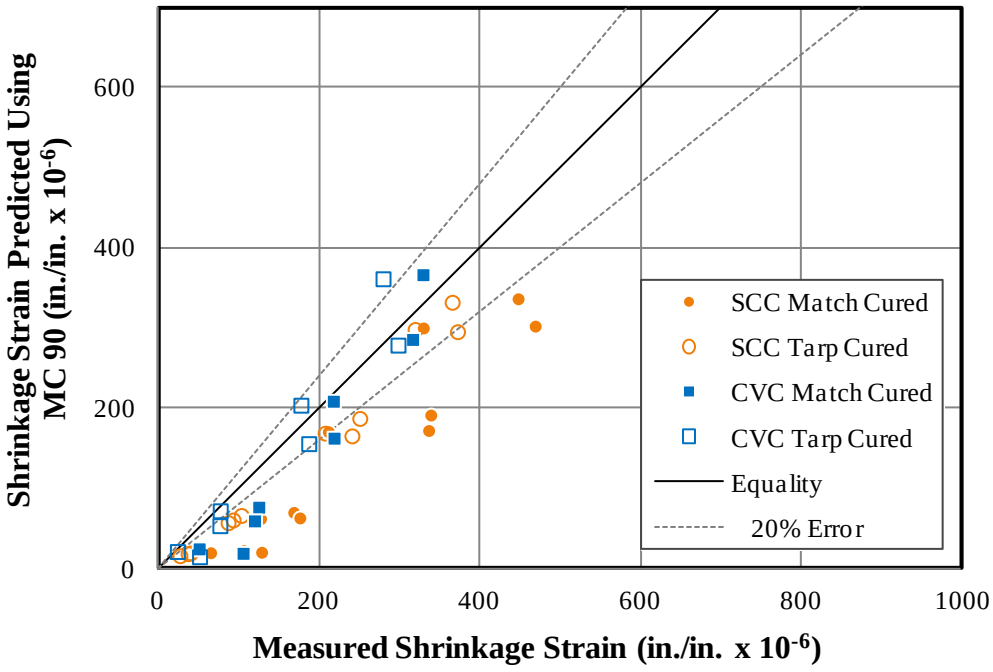

Figure 5-64: Measured Versus Predicted Shrinkage Strain Using MC 90

From this figure, it can be seen that MC 90 predicts the most concentrated pattern of results than any other of the methods studied in this research. MC 90 also produces the lowest shrinkage predictions of any other method and is the only method that underestimates shrinkage long-term. At one year, several SCC and CVC shrinkage predictions by are actually within the ±20% error boundaries with only a few exceptions.

5.4.1.2.6 MC 2010 (also MC 90-99)

Figure 5-65 shows the comparison of the measured shrinkage strain to the estimated shrinkage strain that was calculated using the MC 2010 prediction method. The MC 2010 predictions look strikingly similar to those of ACI 209 with the exception of the CVC specimens being separate from the SCC specimens in ACI 209.

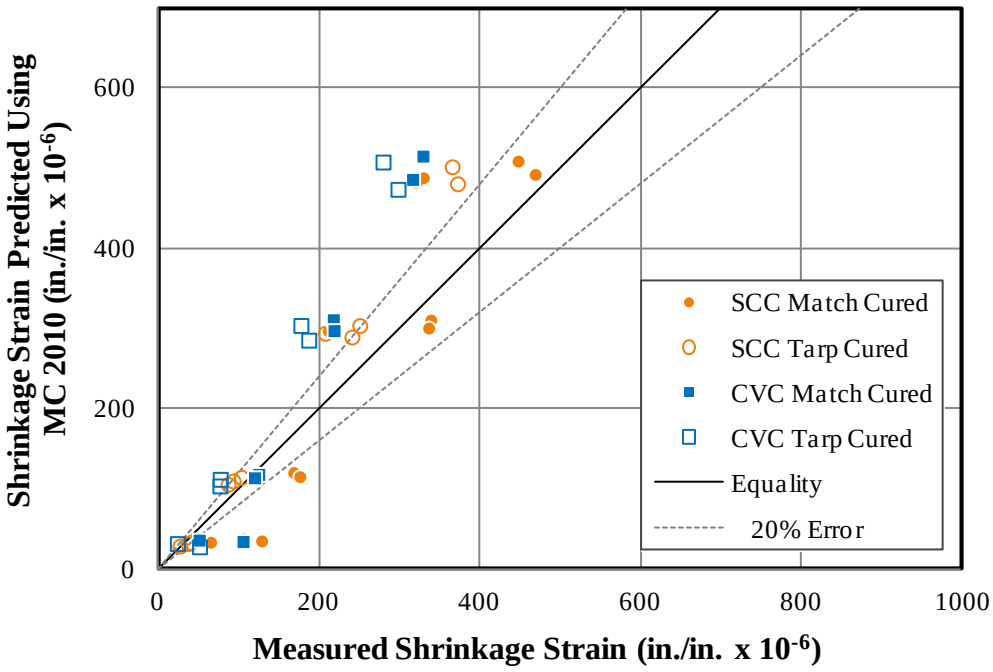

Figure 5-65: Measured Versus Predicted Shrinkage Strain Using MC 2010

It may be seen from this figure that most of the estimated shrinkage values fall outside of the preferable ± 20% error range with only two exceptions at 56 days and one year. Nearly all of the shrinkage strains are overestimated at 56 days and one year attesting to the poor accuracy of this method. At earlier ages however, more accuracy can be seen than at 1 year.This figure also indicates that shrinkage predictions for CVC specimens are higher and more inaccurate than those of SCC specimens.

5.4.1.2.7 Eurocode

Figure 5-66 compares the measured ε_{sh} to the estimated ε_{sh} that was predicted using Eurocode. This method, like most of the prediction methods studied, does not predict shrinkage with any great degree of accuracy.

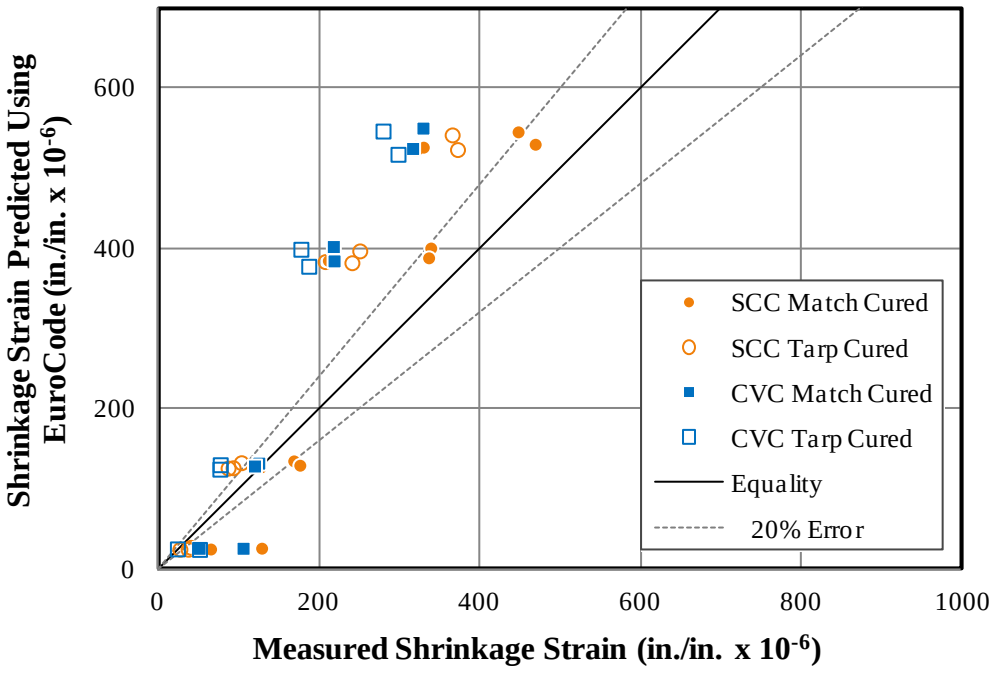

Figure 5-66: Measured Versus Predicted Shrinkage Strain Using Eurocode

As with MC 2010, this method tends to over-estimate shrinkage strains at later ages with every point above the line of equality at 56 days and one year. The poor accuracy of this method is indicated by the fact that only two specimens are within the acceptable range at 56 days and only one specimen is within the ±20% error margin at one year. This figure also indicates that at later ages, Eurocode is more accurate for the prediction of shrinkage using SCC than CVC and more accurate for match curing than tarp curing.

5.4.2 ACCURACY OF PREDICTION METHODS

Once the methods were compared individually by plotting the measured strains against the predicted strains, the methods were compared simultaneously to evaluate the overall performance of the methods. This was accomplished by conducting statistical analyses on the data and plotting these values in order to provide further evidence of the accuracy of each prediction method.

5.4.2.1 Statistical Analysis Of Prediction Methods

In order to calculate the percent error, Δ, for each case and method, the measured value was subtracted from the predicted value and the difference was divided by the measured value then multiplied by 100. This calculation can be seen in the following equation.

$$\Delta = \left(\frac{\hat{y} - \bar{y}}{\bar{y}}\right) \times 100 \qquad \textbf{Equation 5-1}$$

where,

$\hat{y}$ is the predicted value, and

$\bar{y}$ is the measured value.

A second analysis was also conducted to evaluate the error between the predicted and measured values. The unbiased estimate of the standard deviation of the percent error of the predicted time-dependent strains was calculated utilizing the percent error from Equation 5-1 and Equation 5-2 taken from McCuen (1985).

$$S = \sqrt{\frac{1}{n-1}\sum_{i}^{n}\Delta_i^2} \qquad \textbf{Equation 5-2}$$

where,

S is the unbiased estimate of the standard deviation of the percent error

n is the number of data points, and

Δ is the percent error.

These error statistics were calculated by concrete type and by curing method for each prediction model used. A value closer to zero corresponds to a smaller absolute error of the predicted time-dependent strains relative to the measured quantities.

5.4.2.1.1 Results From Statistical Analysis

Using the error calculations previously described, each prediction method was compared to the measured value in order to evaluate each method's performance. Table 5-14 through Table 5-17 shows the percent error values for the four parameters evaluated: load-induced strains, shrinkage strains, creep strains, and creep coefficients. These values are shown at 56 days, which is representative of the approximate time that girders are typically installed during construction of a bridge, and 1 year, which is the best available indication of long-term effects. The tables are arranged by concrete type (SCC or CVC) and cylinder curing

regime (match or tarp). For the percent error, positive errors indicate the predicted values are larger than the measured values and negative errors indicate the predicted values are less than the measured values.

Table 5-14: Percent Error of Prediction Methods for SCC, Match-Cured Specimens

Mix	Method	Load-Induced Δ (%)		Shrinkage Δ (%)		Creep Δ (%)		Creep Coefficient Δ (%)	
		Day 56	Year 1	Day 56	Year 1	Day 56	Year 1	Day 56	Year 1
54-03S-M*	ACI 209	8	14	51	67	24	32	30	39
	AASHTO '04	0	4	72	90	6	12	11	19
	AASHTO '10	8	13	42	32	23	29	30	36
	NCHRP 628	28	38	86	105	68	77	78	87
	MC 90	29	42	-20	-9	71	84	80	94
	MC 90-KAV	15	30	N/A	N/A	39	61	47	70
	MC 2010	7	12	40	48	21	27	28	34
	Eurocode	7	12	82	60	21	27	28	34
54-07S-M	ACI 209	-9	-8	-5	24	7	2	45	39
	AASHTO '04	-14	-15	7	40	-5	-9	32	25
	AASHTO '10	-11	-13	-15	-9	2	-6	41	30
	NCHRP 628	5	6	16	51	39	28	93	77
	MC 90	8	13	-43	-25	45	41	85	79
	MC 90-KAV	-6	0	N/A	N/A	14	18	45	50
	MC 2010	-10	-10	-10	12	6	0	34	27
	Eurocode	-10	-10	16	21	6	0	34	27
72-03S-M	ACI 209	-16	-10	-5	17	3	8	46	54
	AASHTO '04	-22	-18	8	33	-11	-7	26	33
	AASHTO '10	-15	-10	-9	-5	4	9	49	55
	NCHRP 628	1	10	17	44	43	49	104	113
	MC 90	-2	8	-49	-35	36	45	94	107
	MC 90-KAV	-14	-3	N/A	N/A	7	22	53	74
	MC 2010	-19	-14	-10	5	-3	0	38	43
	Eurocode	-19	-14	16	13	-3	0	38	43

Table 5-15: Percent Error of Prediction Methods for SCC, Tarp-Cured Specimens

Mix	Method	Load-Induced Δ (%)		Shrinkage Δ (%)		Creep Δ (%)		Creep Coefficient Δ (%)	
		Day 56	Year 1	Day 56	Year 1	Day 56	Year 1	Day 56	Year 1
54-03S-T	ACI 209	-7	-2	54	72	10	15	39	45
	AASHTO '04	-14	-11	75	96	-6	-2	19	23
	AASHTO '10	-13	-13	30	15	-2	-5	24	20
	NCHRP 628	3	5	89	111	35	30	70	64
	MC 90	8	17	-18	-7	45	53	83	93
	MC 90-KAV	-7	3	N/A	N/A	12	26	42	59
	MC 2010	-11	-7	42	52	3	5	30	33
	Eurocode	-11	-7	85	65	3	5	30	33
54-07S-T	ACI 209	-6	-4	29	52	2	4	25	28
	AASHTO '04	-12	-11	45	71	-10	-8	13	14
	AASHTO '10	-8	-7	18	15	0	-1	24	23
	NCHRP 628	10	14	57	85	36	35	70	69
	MC 90	13	21	-25	-9	43	48	66	71
	MC 90-KAV	0	9	N/A	N/A	15	27	34	47
	MC 2010	-5	-3	19	36	4	5	21	22
	Eurocode	-5	-3	56	47	4	5	21	22
72-03S-T-U	ACI 209	-2	5	32	47	15	23	35	45
	AASHTO '04	-9	-4	50	67	-2	5	16	24
	AASHTO '10	-4	1	20	11	11	15	30	35
	NCHRP 628	14	23	62	80	52	58	78	85
	MC 90	15	28	-31	-21	54	67	81	97
	MC 90-KAV	1	14	N/A	N/A	21	41	43	66
	MC 2010	-4	1	20	29	10	16	29	36
	Eurocode	-4	1	59	41	10	16	29	36

Table 5-16: Percent Error of Prediction Methods for CVC, Match-Cured Specimens

Mix	Method	Load-Induced Δ (%)		Shrinkage Δ (%)		Creep Δ (%)		Creep Coefficient Δ (%)	
		Day 56	Year 1	Day 56	Year 1	Day 56	Year 1	Day 56	Year 1
54-12C-M	ACI 209	-3	2	27	45	10	16	28	35
	AASHTO '04	-8	-4	67	90	-1	5	15	22
	AASHTO '10	-3	1	40	34	9	14	27	33
	NCHRP 628	-3	1	67	90	9	14	27	33
	MC 90	18	30	-4	11	56	67	81	95
	MC 90-KAV	6	19	N/A	N/A	28	47	49	71
	MC 2010	0	5	43	57	16	21	35	41
	Eurocode	0	5	85	67	16	21	35	41
72-11C-M	ACI 209	1	12	26	50	35	50	70	89
	AASHTO '04	-8	0	67	98	12	25	41	57
	AASHTO '10	-2	5	31	27	26	35	58	69
	NCHRP 628	-2	5	67	98	26	35	58	69
	MC 90	19	36	-25	-10	79	102	125	154
	MC 90-KAV	6	24	N/A	N/A	47	77	85	123
	MC 2010	-2	6	36	54	26	38	58	74
	Eurocode	-2	6	76	66	26	38	58	74

Table 5-17: Percent Error of Prediction Methods for CVC, Tarp-Cured Specimens

Mix	Method	Load-Induced Δ (%)		Shrinkage Δ (%)		Creep Δ (%)		Creep Coefficient Δ (%)	
		Day 56	Year 1	Day 56	Year 1	Day 56	Year 1	Day 56	Year 1
54-12C-T	ACI 209	-14	-9	56	70	-8	0	15	26
	AASHTO '04	-19	-14	105	123	-17	-10	4	13
	AASHTO '10	-18	-15	59	41	-15	-12	6	10
	NCHRP 628	-18	-15	105	123	-15	-12	6	10
	MC 90	4	15	15	29	30	43	63	80
	MC 90-KAV	-8	4	N/A	N/A	5	24	31	55
	MC 2010	-12	-7	72	82	-3	4	21	30
	Eurocode	-12	-7	126	96	-3	4	21	30
72-11C-T-U	ACI 209	8	10	46	58	78	56	135	106
	AASHTO '04	-2	-2	93	109	47	28	95	70
	AASHTO '10	1	-2	43	23	57	27	107	68
	NCHRP 628	1	-2	93	109	57	27	107	68
	MC 90	27	34	-17	-6	138	111	215	179
	MC 90-KAV	13	23	N/A	N/A	94	84	157	143
	MC 2010	4	5	53	59	67	44	122	91
	Eurocode	4	5	102	74	67	44	122	91

In these tables, the large errors associated with creep strain as opposed to load-induced strain relay the previously mentioned idea that measured creep strain is highly sensitive to the initial elastic strain, which is difficult to accurately determine. Because of this, creep strain alone was determined to be an unreliable measure of strain for this research. Also, shrinkage strain errors are significantly larger than load-induced strain errors and could indicate that the prediction of shrinkage is not accurately done by any model with regards to the test cases used in this research.

Table 5-19 through Table 5-21 show the average percent error and the unbiased estimate of the standard deviation of the percent error for each of the prediction models based on SCC and CVC specimens at 56 days and 1 year. Table 5-18 and Table 5-19 are arranged by mixture type and Table 5-20 and Table 5-21 are arranged by curing method. These tables only show the two main evaluated strain cases: load-induced strains and shrinkage strains.

Table 5-18: Average Percent Error and Unbiased Estimate of the Standard Deviation of the Percent Error for Prediction Methods at 56 Days (by Mixture Type)

Method	Load-Induced Δ (%)		Shrinkage Δ (%)		Load-Induced *S* (%)		Shrinkage *S* (%)	
	SCC	CVC	SCC	CVC	SCC	CVC	SCC	CVC
ACI 209	-10	-5	18	36	12	10	36	48
AASHTO '04	-16	-11	34	80	18	15	51	100
AASHTO '10	-12	-8	6	43	14	13	23	55
NCHRP 628	5	N/A	44	N/A	7	N/A	62	N/A
MC 90	7	14	-34	-5	10	19	42	21
MC 90-KAV	-7	1	N/A	N/A	10	8	N/A	N/A
MC 2010	-11	-5	10	50	14	9	28	65
Eurocode	-11	-5	43	96	14	9	60	120

Table 5-19: Average Percent Error and Unbiased Estimate of the Standard Deviation of the Percent Error for Prediction Methods at 1 Year (by Mixture Type)

Method	Load-Induced Δ (%)		Shrinkage Δ (%)		Load-Induced *S* (%)		Shrinkage *S* (%)	
	SCC	CVC	SCC	CVC	SCC	CVC	SCC	CVC
ACI 209	-6	2	41	55	8	11	54	69
AASHTO '04	-14	-6	60	104	16	10	75	128
AASHTO '10	-11	-3	4	34	13	12	14	43
NCHRP 628	9	N/A	72	N/A	11	N/A	89	N/A
MC 90	15	27	-19	10	18	35	26	23
MC 90-KAV	2	16	N/A	N/A	6	22	N/A	N/A
MC 2010	-9	2	26	64	11	8	37	80
Eurocode	-9	2	36	76	11	8	48	95

Table 5-20: Average Percent Error and Unbiased Estimate of the Standard Deviation of the Percent Error for Prediction Methods at 56 Days (by Curing Method)

Method	Load-Induced Δ (%)		Shrinkage Δ (%)		Load-Induced *S* (%)		Shrinkage *S* (%)	
	Match	Tarp	Match	Tarp	Match	Tarp	Match	Tarp
ACI 209	-7	-9	11	46	11	12	22	59
AASHTO '04	-13	-15	37	75	16	19	55	97
AASHTO '10	-8	-13	12	36	11	16	31	49
NCHRP 628	0	-2	42	83	4	15	56	105
MC 90	11	8	-30	-9	16	11	41	25
MC 90-KAV	-2	-5	N/A	N/A	10	7	N/A	N/A
MC 2010	-8	-9	15	44	12	12	34	60
Eurocode	-8	-9	48	89	12	12	67	115

Table 5-21: Average Percent Error and Unbiased Estimate of the Standard Deviation of the Percent Error for Prediction Methods at 1 Year (by Curing Method)

Method	Load-Induced Δ (%)		Shrinkage Δ (%)		Load-Induced *S* (%)		Shrinkage *S* (%)	
	Match	Tarp	Match	Tarp	Match	Tarp	Match	Tarp
ACI 209	-1	-5	34	65	11	7	42	80
AASHTO '04	-9	-12	65	96	14	15	82	121
AASHTO '10	-4	-12	12	24	10	15	26	33
NCHRP 628	6	1	70	106	7	15	86	131
MC 90	22	18	-15	5	28	22	26	22
MC 90-KAV	10	6	N/A	N/A	18	8	N/A	N/A
MC 2010	-3	-6	32	57	11	7	46	73
Eurocode	-3	-6	42	69	11	7	56	88

It should be noted that the unbiased estimate of the standard deviation is a more appropriate comparison when trying to compare all specimens simultaneously. This is due to the fact that a prediction method could be deceivingly accurate when an overpredicted specimen is averaged with an underpredicted specimen. On the other hand, the average error *is* valuable when attempting to compute a single modification factor to "correct" a prediction method to improve prediction accuracy *on average*.

5.4.2.2 Accuracy of Creep Prediction Methods

This section provides further review of the accuracy of the creep prediction models described in this research. As discussed in previous sections, creep prediction is evaluated by means of load-induced strain in order to minimize error caused by separating the initial strain from the *true* creep strain.

Figure 5-67 depicts the predicted load-induced strain divided by the measured load-induced strain for each of the ten specimen sets and for each prediction model studied at 1 year. In this figure, the difference from 1 graphically indicates the percent errors that were tabulated in Section 5.4.2.1.1 for the load-induced strain. This plot may be seen at 56 days and for all other strain cases in Appendix E.

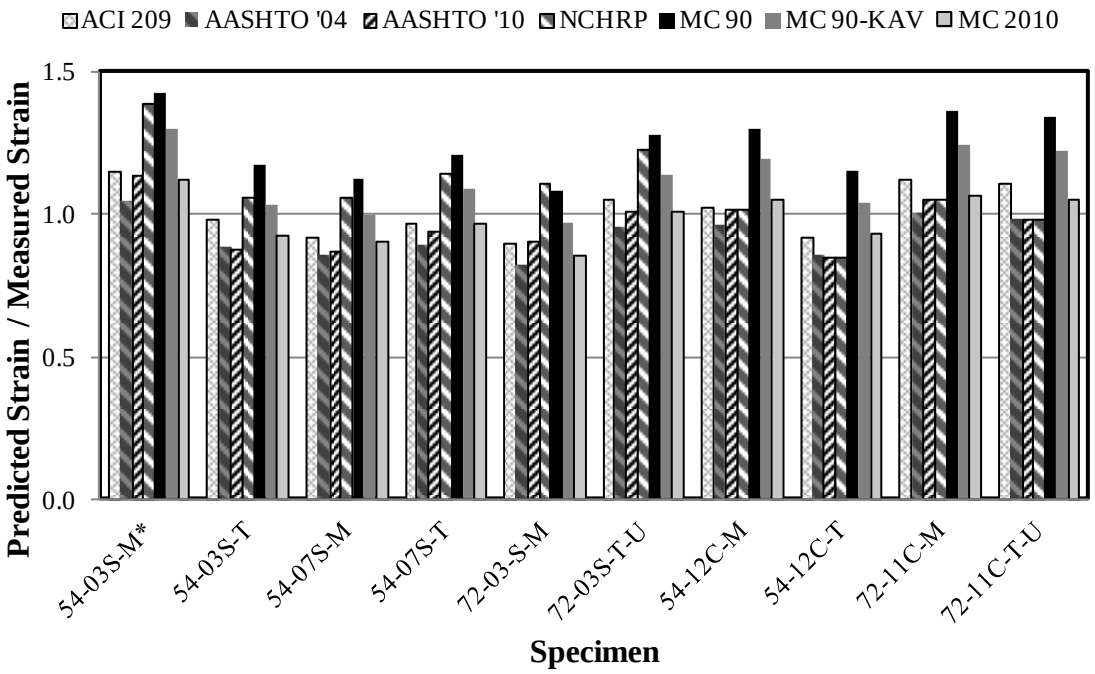

Figure 5-67: Accuracy of Predicted Load-Induced Strains at 1 Year

Figure 5-68 graphically indicates the average percent error for load-induced strain, and Figure 5-69 shows the unbiased estimate of the standard deviation of the percent error. Both of these figures are sorted by the mixture type: either SCC or CVC. Finally, Figure 5-70 and Figure 5-71 also show the average percent error and the unbiased estimate of the standard deviation of the percent error, respectively, and are sorted by the curing method employed: either match-cured or tarp-cured. Each of these figures shows the accuracy of the prediction models at 1 year. For the average percent error, no specimen that was underloaded or cured improperly was included for the average and any model predicting strains within the boundaries of 0.8 and 1.2 were deemed sufficiently accurate. For the standard deviation, the closer the method is to zero, the more accurate the method is. These plots may be seen at 56 days and for all other strain cases in Appendix E.

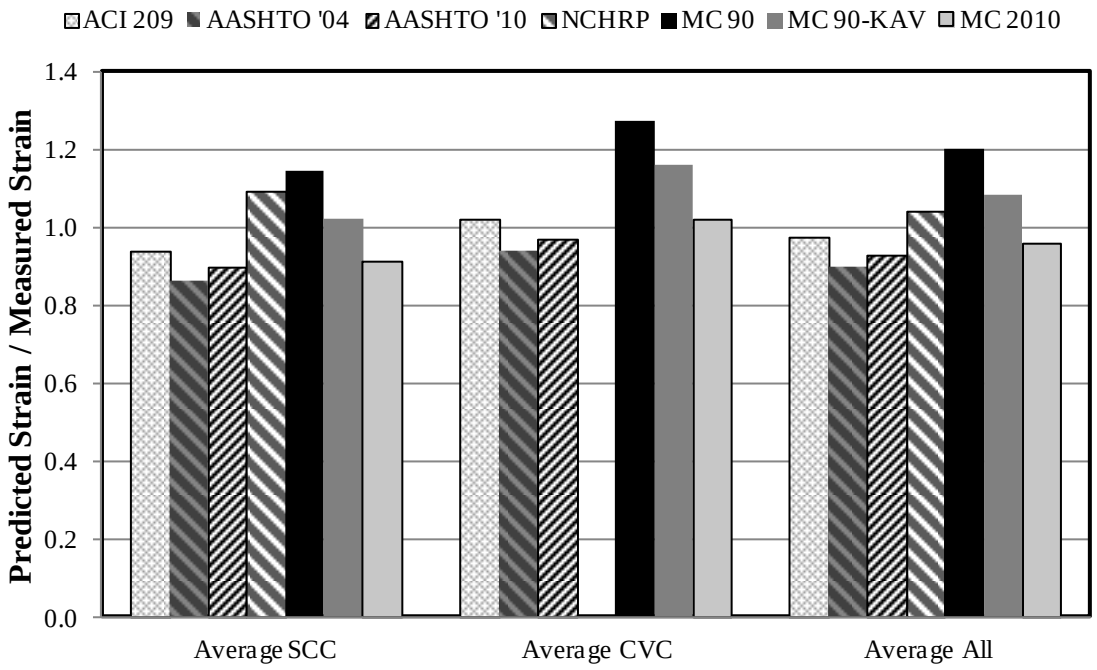

Figure 5-68: Accuracy of Predicted Load-Induced Strains at 1 Year (by Mixture Type)

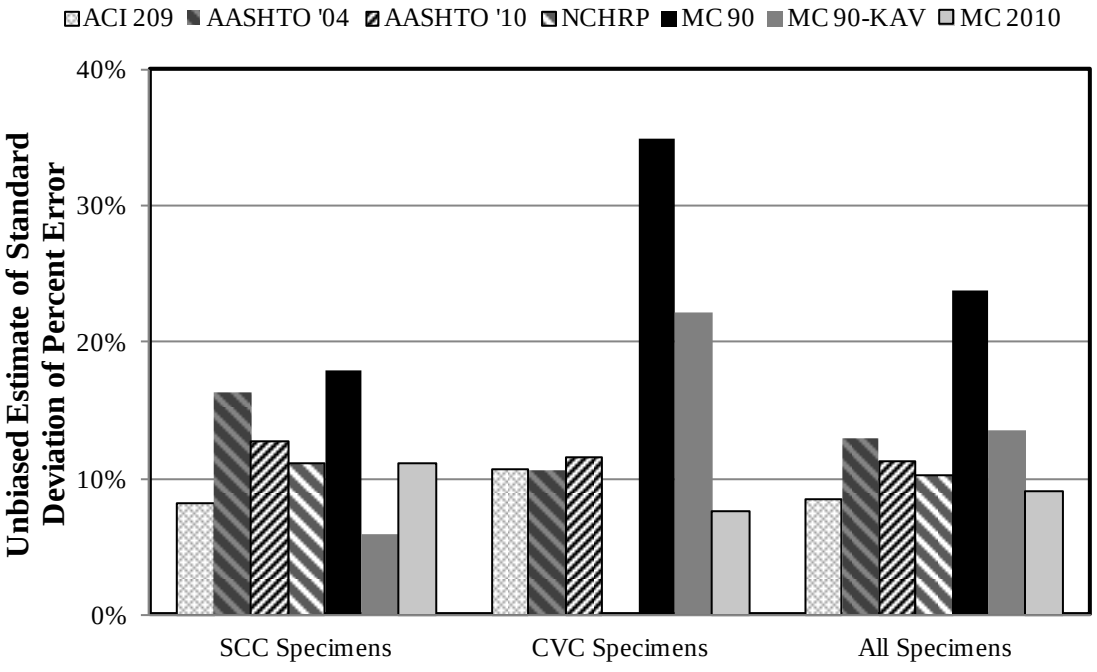

Figure 5-69: Unbiased Estimate of Standard Deviation of Percent Error for Load-Induced Strains at 1 Year (by Mixture Type)

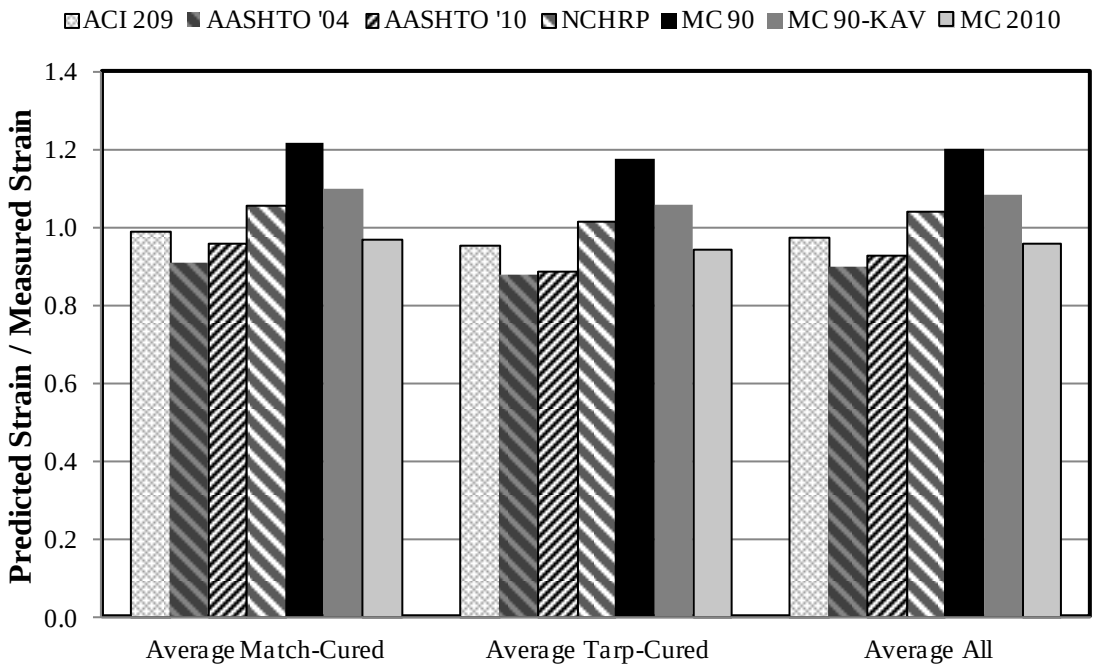

Figure 5-70: Accuracy of Predicted Load-Induced Strains at 1 Year by Curing Method

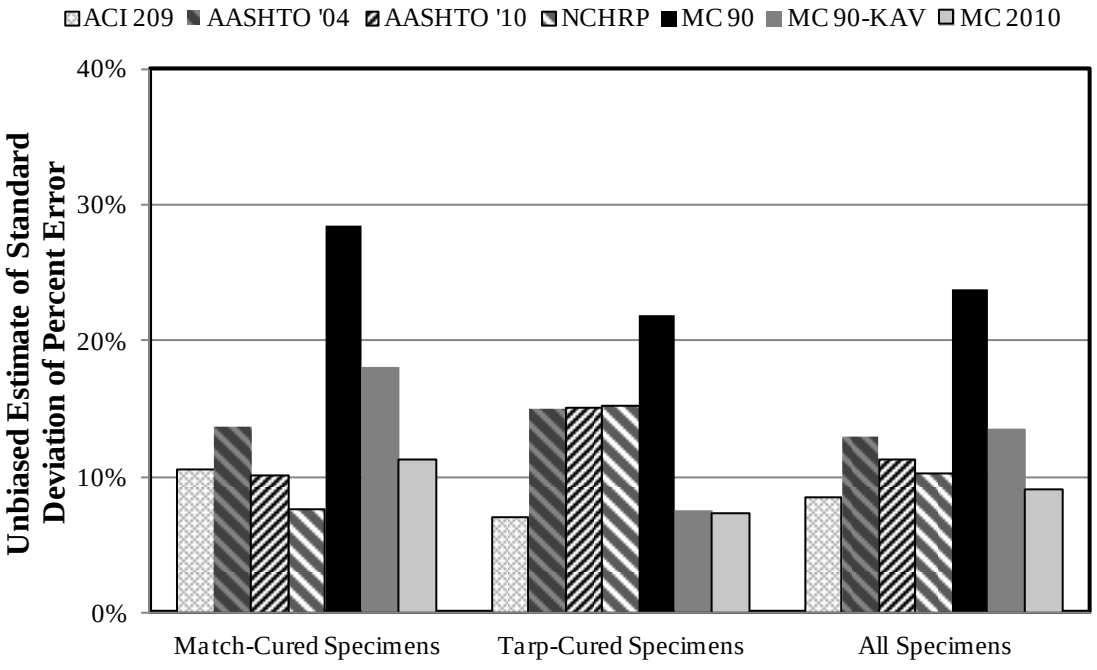

Figure 5-71: Unbiased Estimate of Standard Deviation of Percent Error for Load-Induced Strains at 1 Year (by Curing Method)

From Figure 5-68 and Figure 5-69, it can be seen that some methods are largely affected by mixture type whereas others are not. AASHTO 2010 shows the smallest difference between SCC and CVC prediction error statistics, whereas MC 90 and MC 90-KAV show the largest differences between SCC and CVC for load-induced predictions. For example, MC 90-KAV appears to be the most accurate method for SCC specimens based on the standard deviation statistic (6%) in Figure 5-69, but is significantly more erroneous when considering CVC specimens (22%).This difference in error statistic from one mixture type to the next makes MC 90-KAV unreliable when a single method is desired for predicting strains for both CVC and SCC. On the other hand, the AASHTO 2010 error statistics indicate that it predicts load-induced deformations with consistent accuracy for both SCC and CVC.

NCHRP 628 is not shown for CVC specimens due to the fact that the prediction of load-induced strain defaults to AASHTO 2010 when any other concrete besides SCC is used. Figure 5-68 indicates that, on average, AASHTO 2010 underpredicts load-induced strains for SCC at 1 year. This figure also indicates that the amplification factor used by NCHRP 628 results in an overprediction of SCC. This is an indication that amplification to AASHTO 2010 may be warranted, but the specific value used in NCHRP 628 is not accurate for the SCC used in this research.

From Figure 5-70, it may appear that there is only a slight difference between the average of tarp-cured specimens and that of match-cured specimens; however, Figure 5-71 shows a much larger distinction using the standard deviation approach. Here, there appears to be a vast improvement in accuracy for tarp-cured specimens as opposed to match-cured specimens for the European models and a slight improvement for ACI 209, but a decrease in accuracy for all methods in the AASHTO family.

Kavanaugh (2008) made modifications to MC 90 based on findings that MC 90 provided the most accurately predicted ε_{li} values for all the SCC mixtures used in that study. However, the findings here do not agree. At one year, Figure 5-69 indicates that MC 90 produces the highest error for SCC and CVC specimens. These error statistics were 18% and 35%, respectively. As previously mentioned, the Kavanaugh study did not correctly employ the modified age at loading parameters in the MC 90 creep prediction model, which is probably what accounts for this apparent disagreement.

Like research conducted by Mokhtarzadeh and French (2000), which found that the ACI 209 creep model was a good predictor of creep strain, these figures also reveal that ACI 209 was the top performing method for the prediction of load-induced strain at one year with an average error of only -3%, and a standard deviation of the percent error of only 8%. For the European model codes and AASHTO methods, which were investigated for two different versions, there seems to be no reason to use the older versions instead of the newer version for the prediction of load-induced strain. Both AASHTO 2010 and MC 2010 show relatively equal or improved predictions as compared to AASHTO 2004 and MC 90, respectively.

In summary, when solely considering the standard deviation analysis for all specimens in Figure 5-69 and Figure 5-71, all methods with the exception of MC 90 offer fairly good predictions of load-induced strains. ACI 209 produces the lowest error, AASHTO 2010 shows slight improvement over AASHTO 2004 (particularly for SCC), NCHRP 628 offers a slight improvement over AASHTO 2010, and both MC 90-KAV and MC 2010 show improvement over MC 90. Therefore, creep of both self-consolidating and conventional mixtures is predicted well enough by ACI 209, AASHTO 2010, and MC 2010 to be implemented in practice with an acceptable degree of accuracy.

5.4.2.3 Accuracy of Shrinkage Prediction Methods

This section provides further review of the accuracy of the shrinkage prediction models described in this research. Figure 5-72 depicts the predicted shrinkage strain divided by the measured shrinkage strain for each of the ten specimen sets and for each prediction model studied at 1 year. In this figure, the difference from 1 is the same as the percent errors that were tabulated in Section 5.4.2.1.1 for the shrinkage strain. This plot may be seen at 56 days and for all other strain cases in Appendix E.

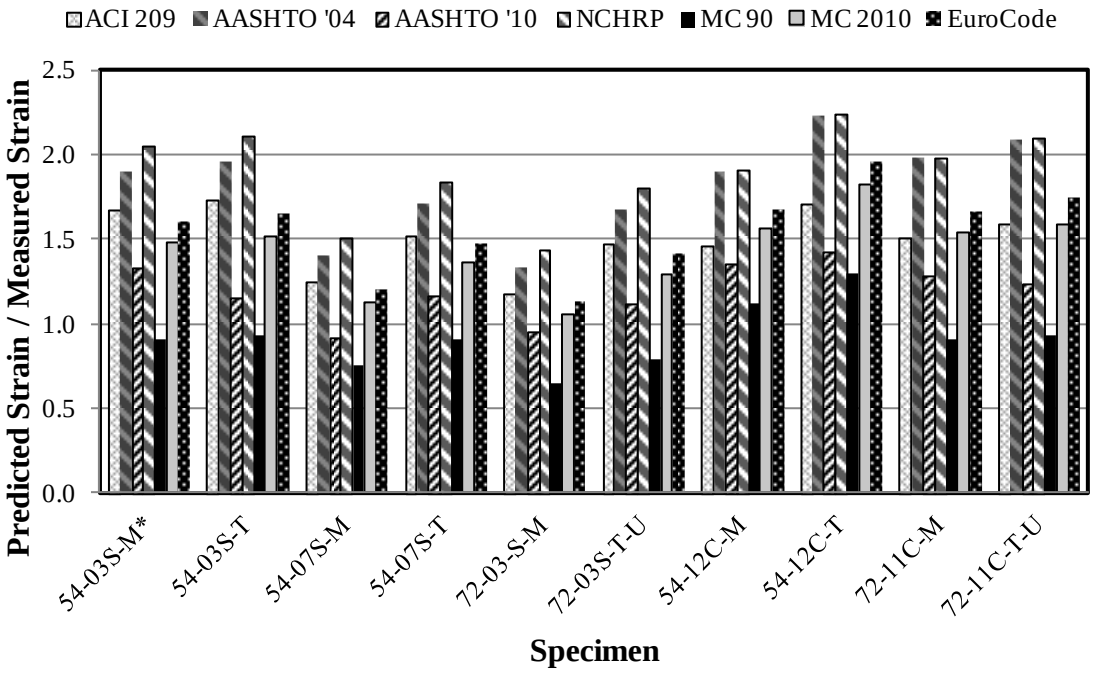

Figure 5-72: Accuracy of Predicted Shrinkage Strains at 1 Year

Figure 5-73 shows the average percent error and Figure 5-74 shows the unbiased estimate of the standard deviation of the percent error for shrinkage. Both of these figures are sorted by the mixture type: either SCC or CVC. Finally, Figure 5-75 and Figure 5-76 also show the

average percent error and the unbiased estimate of the standard deviation of the percent error, respectively, and are sorted by the curing method employed: either match-cured or tarp-cured. Each of these figures is a measure of accuracy of the prediction models at 1 year. For the average percent error, no specimen that was underloaded or cured improperly was included for the average and any model predicting strains within the boundaries of 0.8 and 1.2 were deemed sufficiently accurate. For the standard deviation, the closer the method is to zero, the more accurate the method is. These plots may be seen at 56 days and for all other strain cases in Appendix E.

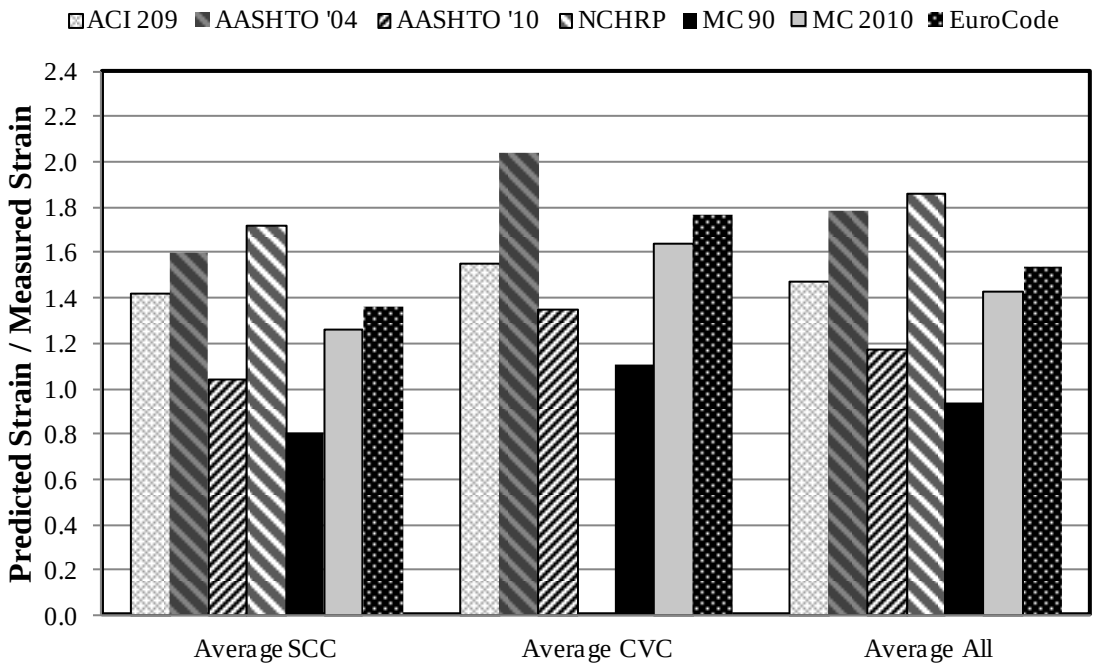

Figure 5-73: Accuracy of Predicted Shrinkage Strains at 1 Year by Mixture Type

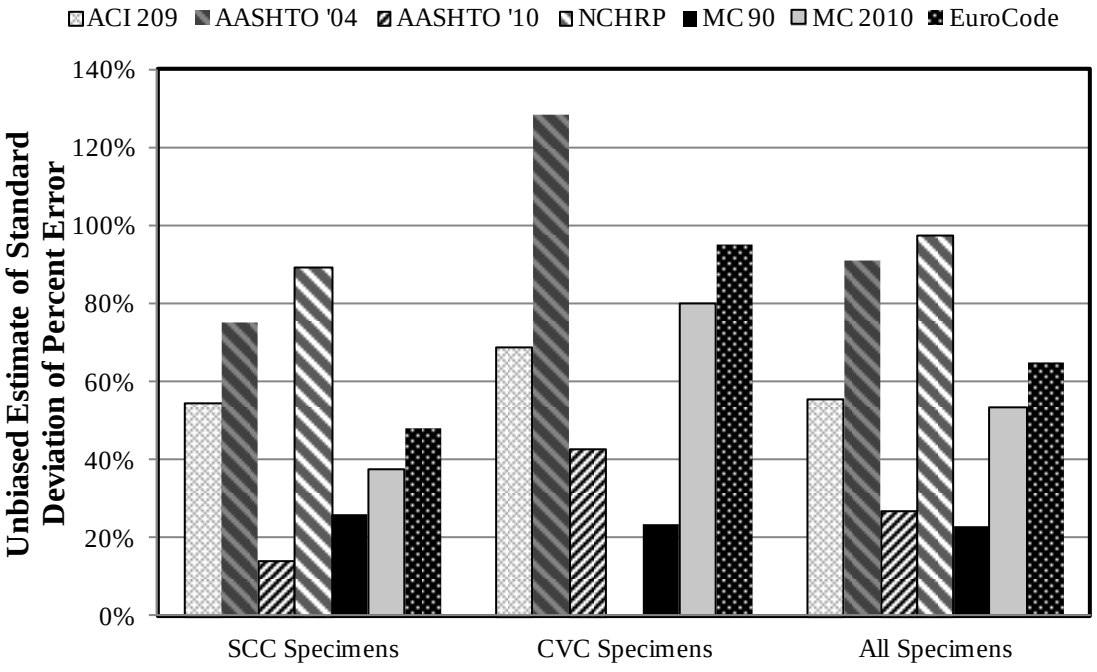

Figure 5-74: Unbiased Estimate of Standard Deviation of Percent Error for Shrinkage Strains at 1 Year (by Mixture Type)

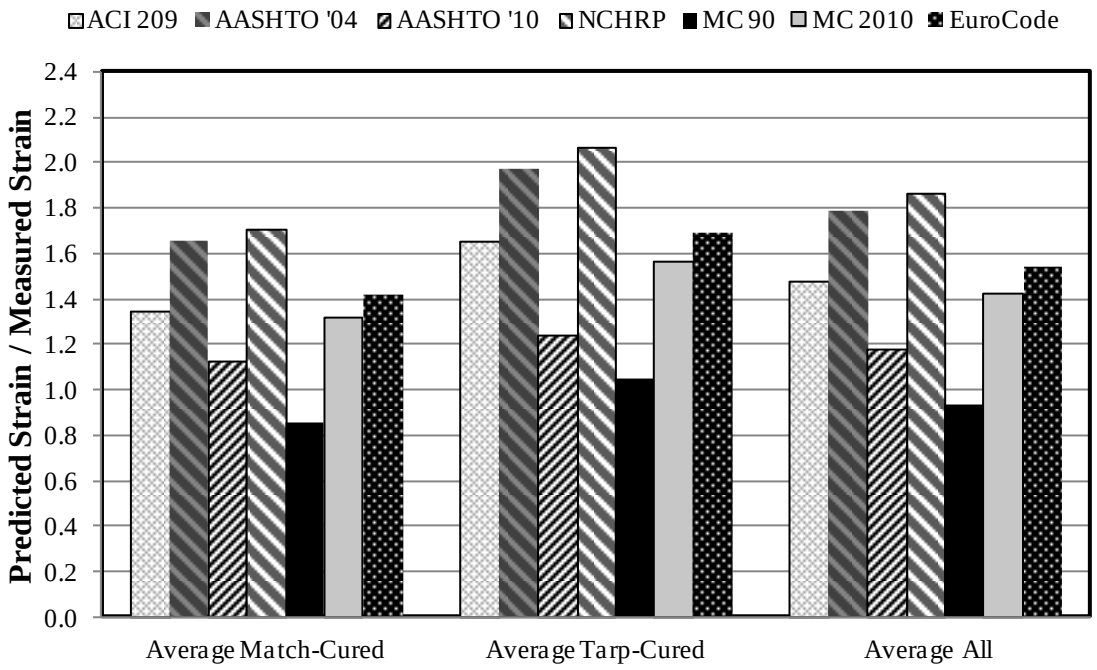

Figure 5-75: Accuracy of Predicted Shrinkage Strains at 1 Year by Curing Method

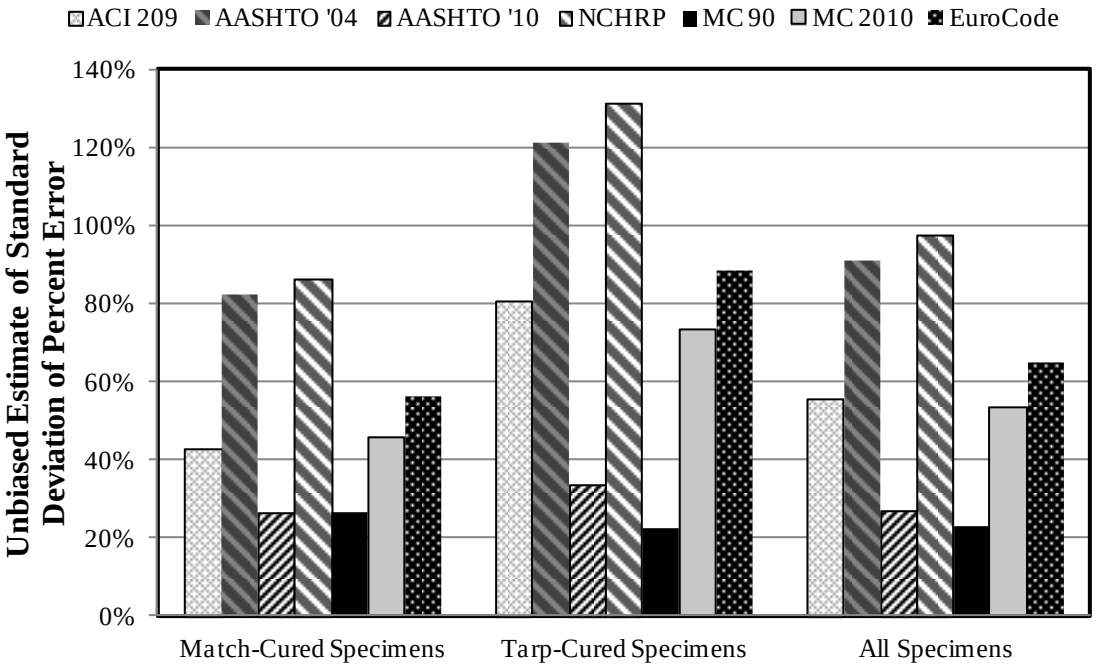

Figure 5-76: Unbiased Estimate of Standard Deviation of Percent Error for Shrinkage Strains at 1 Year (by Curing Method)

From Figure 5-73 and Figure 5-74, it can be seen that the prediction of shrinkage for some methods is largely affected by mixture type, whereas others are not. Using the standard deviation approach, at one year, MC 90 experiences the smallest change from SCC to CVC with difference of approximately 2%. AASHTO 2004 appears to be the most affected by mixture type with an increase of 53% when moving from SCC to CVC. When comparing SCC and CVC separately, AASHTO 2010 and MC 90 appear to be the best methods in those respective categories with error statistics of only 14% and 23%, respectively when considering the standard deviation approach. Both of these methods also produce the smallest errors overall when considering both mixture types.

NCHRP 628 is not shown for CVC specimens due to the fact that the prediction of shrinkage strain defaults to AASHTO 2004 when any other concrete besides SCC is used. Figure 5-73 indicates that, on average, AASHTO 2004 significantly overpredicts shrinkage and the amplification for SCC in NCHRP 628 only exacerbates the error produced by this method. The average percent error increases from 60% to 72% making NCHRP 628 the worst method for the prediction of shrinkage for SCC. Therefore, the NCHRP 628 amplification factor for the AASHTO 2004 method is unwarranted for the SCC used in this research. When referring to the SCC average percent errors or standard deviations, it can be seen that between the AASHTO models, the 2010 model is the most accurate method for SCC. Thus, why AASHTO 2004 was chosen for NCHRP 628 shrinkage modification is unclear based on the concrete used in this study. Unlike load-induced strains, from Figure 5-75 and Figure 5-76, there appears to be a much larger difference between the average of tarp-cured specimens and that of match-cured specimens. This difference between the curing methods seen here as compared to differences observed for load-induced strain could

possibly be attributed to the fact that for shrinkage prediction, the maturity and strength are not considered when drying shrinkage begins. Instead, these parameters are evaluated at loading or 28 days. Figure 5-74 shows that the only methods that do not significantly increase in error from match to tarp curing are AASHTO 2010 and MC 90.

As was seen with load-induced strain, the most inaccurate methods for match and tarp curing are the same as the most inaccurate methods seen for mixture types. Similarly, the most accurate methods based on the curing type are the same as the most accurate methods based on mixture type. At one year, Figure 5-76 indicates that the most inaccurate method for predicting shrinkage strain based on match or tarp curing alone was NCHRP 628, which produced a standard deviation error statistic of 86% for match-cured specimens and 131% for tarp-cured specimens. However, as mentioned previously, these averages include some CVC specimens, which default to predictions made by AASHTO 2004. With this consideration, AASHTO 2004 was the most inaccurate method for curing type. The best methods based on match-cured specimens alone were AASHTO 2010 and MC 90, which both had an error statistic of 26%. For tarp-cured specimens alone MC 90 was the most accurate with a 22% value.

When comparing the overall performance at one year using either approach, it can be seen that although MC 90 slightly underestimates SCC and slightly overestimates CVC, this models is the most accurate prediction model overall for ε_{sh} with an average percent error of only -6% and a standard deviation of the percent error of 23%. This is a stark contrast to the prediction of load-induced strains, for which MC 90 was the most inaccurate method overall.

For the model codes and AASHTO methods, which were investigated for two different versions, there seems to be no reason to use the older version of AASHTO (2004)

instead of the newer version (2010) for the prediction of shrinkage strain. However, MC 2010 did not show any improvement over MC 90; rather, it showed a decrease in accuracy for the updated method where shrinkage is concerned. However, the addition of slag cement may have reduced the shrinkage of the high-strength concrete used in this research. Because MC 2010 was updated to include increased shrinkage from high-strength cement, and also does not reflect the possible reduction from the slag cement, MC 2010 shows a larger net error than MC 90.

In summary, when solely considering the standard deviation analysis for all specimens in Figure 5-74 and Figure 5-76, none of the methods offer enough accuracy to fall within the 20% standard deviation range. This is completely opposite of the findings from the load-induced strain where all except one method fell within this range. Even though none of the methods are particularly accurate, shrinkage of SCC seems to be predicted more accurately than CVC. ACI 209 is not accurate for the prediction of shrinkage. AASHTO 2010 shows significant improvement over AASHTO 2004. The NCHRP 628 amplification is not warranted for the SCC used in this research. The MC 2010 is more accurate than Eurocode but does not show improvement over MC 90. For the prediction of shrinkage strain, MC 90 is the most accurate method investigated in this study.

CHAPTER 6
CONCLUSIONS AND RECOMMENDATIONS

6.1 INTRODUCTION

This chapter is a summary of all the work and findings from this research. This includes a brief description of the experimental work, the lessons learned through creep testing, and a summary of all conclusions, and recommendations for future research. The conclusions consist of a comparison between SCC and CVC as well as match-curing versus tarp-curing, and the accuracy of the prediction methods investigated for the estimation of creep and shrinkage.

6.2 SUMMARY OF EXPERIMENTAL WORK

For this research, two SCC mixtures and two conventional-slump mixtures were tested to determine the creep and shrinkage behavior of each. All mixtures were comprised of Type III portland cement, several types of chemical admixtures, and the supplementary cementing material slag cement. One SCC mixture and one CVC mixture was used for each of the two girder sizes that were tested. Representative 6 in. x 12 in. cylindrical test specimens were cast from each of the mixtures and cured using two different accelerated-curing regimes. The specimens were then loaded to 40% of their compressive strength (at the time of insertion into the creep-testing frames) and creep and shrinkage data were gathered. The compressive strength testing was conducted in accordance with ASTM C39 (2005) and the creep and shrinkage testing was conducted according to ASTM C512 (2002). The laboratory data were

then compared to the following nine creep and shrinkage prediction models to determine their accuracy:

- ACI 209 (1992)
- AASHTO 2004
- AASHTO 2010
- NCHRP 628 (2009)
- MC 90
- MC 90-99
- MC 90-KAV
- MC 2010, and
- Eurocode (2004).

6.3 LESSONS LEARNED THROUGH TESTING

This section details experience that was gained over the course of performing the tests outlined in ASTM C512. Here, the reader will find information regarding lessons learned while preparing the test specimens and conducting creep testing.

6.3.1 SPECIMEN PREPARATION

Many lessons were learned while preparing the concrete specimens for testing. This section discusses that experience and includes information on casting and final preparation before testing.

After curing was complete, all specimens needed to have a flat, smooth top and bottom surface before testing could begin. Because this research paralleled actual bridge girders being constructed at a precast plant, the loading of the specimens needed to be conducted as close to simultaneously as possible to the release of the prestress. For this reason, time was of the utmost importance and sulfer-capping was not possible so the ends were ground using a concrete cylinder grinder. In order to keep the process running smoothly and to allow ample time for the epoxy that was used to attach the DEMEC points to dry, the grinding and gluing of the DEMEC points needed to be one fluent process. As soon as a cylinder was ground, the cylinder was immediately measured and epoxy was applied around the cylinder at the necessary locations. This allowed the epoxy to begin setting before the points were then applied, in the same order at the epoxy, to the epoxy spots. All the while, another set of cylinders were being ground. When this process was complete for all the cylinders, the epoxy was set enough to begin testing.

After the specimens were prepared, the compressive strength of each specimen set was determined. ASTM C512 requires that at least two specimens be tested for compressive strength and because of the limited number of specimens cast, only the minimum were able to be tested. Because only two cylinders were broken, if one seemed to be in error that left only one specimen used as the compressive strength of that particular group instead of the recommended average. Having an extra cylinder available in case of errors may have produced more reliable strengths.

6.3.2 CONDUCTING CREEP TESTING

Because ASTM C512 is not a test that is run with any great regularity, there is a certain level of uncertainty involved. Many of the "kinks" that were encountered were only worked

out after going through the process several times. This section outlines lessons learned regarding the creep testing procedure.

The first lesson learned was with regard to the test set up. Inserting the cylinders into the creep testing frames was a difficult process to master but is an extremely important part of obtaining accurate measurements. The alignment of the cylinders within the frame is crucial to ensure that no eccentricities are allowed. If eccentricities do occur, erratic strain measurements may result. During this process, a level was used to ensure that each cylinder surface was ground properly before being placed into the creep testing frame. Once placed inside the frame, a level was also used to ensure that the entire stack of cylinders (two specimens sandwiched between two half-cylinder plugs) was level. The cylinders also had to be in alignment with the frame itself and the alignment marks, mentioned in Chapter 3, made this process easier and more uniform. Where the alignment marks were not enough, a level was also used as a spacer to ensure that each of the bars around the apparatus was an equal distance from the cylinders themselves.

Another important lesson learned was with regard to data collection. This test requires that many data points be collected for each specimen at many different intervals. These intervals were often overlapping for several specimen sets at once. This made the process very difficult to keep up with without proper tracking. This is why a spreadsheet was made to keep track of all the collection dates and times.

6.4 CONCLUSIONS

This section contains conclusions that may be drawn based on the results from this research. This includes conclusions on the general creep and shrinkage behavior of SCC

versus CVC as well as the reliability of the creep and shrinkage prediction models that were investigated.

6.4.1 General Conclusions

From the results obtained through the analysis discussed research, the following general conclusions can be drawn:

- Relative to the time-dependent strains predicted using the most current AASHTO (2010) creep and shrinkage prediction methods, the CVC used in this project performed no better than the SCC used in this project.
- All models except AASHTO 2004 and MC 2010 produced more accurate load-induced strain predictions for SCC than for CVC.
- All models except MC 90 produced more accurate shrinkage strain predictions for SCC than for CVC.
- Based on the models investigated in this research, the prediction of shrinkage strain is much less reliable than the prediction of creep strain.

6.4.2 Conclusions on Creep Prediction Methods

Based on the results obtained through this research, the following conclusions can be drawn on the creep prediction models that were investigated:

For ACI 209,

- In general, ACI 209 provided the most accurate estimate of load-induced strains of any of the nine methods investigated and was mainly attributed to the high accuracy of SCC.

For AASHTO models,

- In general, the AASHTO 2004 creep prediction model underestimates load-induced strains for all concrete types and curing conditions investigated.
- In general, the AASHTO 2010 creep prediction method underestimates load-induced strains especially at early ages and is slightly more accurate for CVC than SCC.
- Relative to AASHTO 2010, NCHRP 628 predicts significantly more load-induced strain for SCC due to the amplification factor based on the cement type. The underprediction of AASHTO 2010 for SCC shows that amplification may be warranted, but the specific value from NCHRP 628 is not accurate for the SCC used in this research.

For European models,

- In general, MC 90 overestimates and provides the most inaccurate load-induced strains for all concrete types and curing conditions investigated. Subsequently, MC 90 was the most inaccurate model for the prediction of load -induced strains of any of the nine methods investigated.
- In general, MC 90-KAV showed a dramatic improvement over MC 90 and was the most accurate model when considering SCC alone.
- In general, MC 2010 was one of the most accurate creep prediction models overall investigated in this research and was slightly more accurate for CVC than SCC. MC 2010 also provided the most accurate load-induced strain predictions of any other method investigated when CVC alone was considered.

Overall, the AASHTO 2010, MC 2010, or ACI 209 methods for predicting creep behavior provide acceptable predictions of load-induced strains for both SCC and CVC produced in accordance with ALDOT specifications for precast/prestressed concrete girders.

6.4.3 Conclusions on Shrinkage Prediction Methods

Based on the results obtained through this research, the following conclusions can be drawn about the shrinkage prediction methods:

For ACI 209,

- In general, ACI 209 overestimates shrinkage strain for both concrete types but more for CVC than SCC.

For AASHTO models,

- In general, the AASHTO 2004 shrinkage prediction model greatly overestimates shrinkage strains (especially at later ages) and produces some of the highest errors in predictions especially when considering CVC alone.
- AASHTO 2010 provided the second most accurate prediction of shrinkage strain overall and was the most accurate for SCC specimens alone.
- NCHRP 628 grossly overestimates shrinkage strains and provided the most inaccurate shrinkage strain predictions of any of the methods investigated for SCC and thus is not warranted for the SCC used in this research.

For European models,

- On average, MC 90 was the only method to underestimate shrinkage strains and, overall, provided the most accurate estimate of shrinkage strains of any of the methods investigated.

- In general, MC 2010 overpredicts shrinkage strain but was more accurate for SCC than it was for CVC. For the prediction of shrinkage, MC 2010 was the only method to not show improvement over its predecessor (MC 90).
- In general, Eurocode overpredicts shrinkage strain and was one of the least accurate creep prediction models investigated in this research especially for CVC.

Overall, none of the methods for predicting shrinkage behavior provided accurate predictions of shrinkage strains for SCC or CVC produced in accordance with ALDOT specifications for precast/prestressed concrete girders. All methods except the original MC 90 overpredict the shrinkage strains; however, the SCC strain predictions from these same methods are more accurate than the CVC strain predictions. Of the most current methods, AASHTO 2010 is the most accurate method for estimating shrinkage strains. The original MC 90 method is the only method that was more accurate than AASHTO 2010 for the concretes tested in this project.

6.5 RECOMMENDATIONS FOR FUTURE RESEARCH

Although implementation of SCC into prestressed construction has recently gained popularity, further research is still needed to gain better understanding of its properties and behavior. Based on the research detailed in this report, the following recommendations can be made:

1. Further research is necessary to determine the long-term creep and shrinkage behavior of SCC past one year.

2. With more data, there is greater potential for proposing an accurate modification to the prediction models in order to adapt them to the typical concrete mixtures used in Alabama bridges.
3. Creep and shrinkage testing should be performed on full-scale prestressed elements to determine the real-world behavior of SCC.

REFERENCES

AASHTO T 126. 2001. "Standard Method of Test for Making and Curing Concrete Specimen in the Laboratory". In *Standard Specifications for Transportation Materials and Methods of Sampling and Testing*. Washington, DC: American Association of State Highway and Transportation Officials.

AASHTO T 231. 2003. "Capping Cylindrical Concrete Specimens". In *Standard Specifications for Transportation Materials and Methods of Sampling and Testing*. Washington, DC: American Association of State Highway and Transportation Officials.

AASHTO. 2004. *AASHTO LRFD Bridge Design Specifications.* 3rd ed. Washington, D.C.: American Association of State Highway and Transportation Officials (AASHTO).

AASHTO. 2010. *AASHTO LRFD Bridge Design Specifications.* 5th ed. Washington D.C.: American Association of State Highway and Transportation Officials (AASHTO), 5.14-5.17.

ACI 209. 1992. *Prediction of Creep, Shrinkage, and Temperature Effects in Concrete Structures* (ACI 209R-92). Farmington Hills, Michigan: American Concrete Institute, 209R-92 (Reapproved 1997).

ACI Committee 209. 1997. "Prediction of Creep, Shrinkage, and Temperature Effects in concrete Structures (ACI 209R-97)". In *ACI Manual of Concrete Practice 2001: Part 1*. Farmington Hills, Michigan: American Concrete Institute, 209R-1-209R-47.

ACI Committee 209. 2008. *Guide for Modeling and Calculating Shrinkage and Creep in Hardened Concrete* (ACI 209.2R-08). Farmington Hills, Michigan: American Concrete Institute, 209.2R-08.

Al-Manaseer, A., Lam, J. P. 2005. Statistical Evaluation of Shrinkage and Creep Models. *ACI Materials Journal* 102, no.3: 170-176

Aly, Tarek. and Jay G. Sanjayan. 2008. Factors Contributing to Early Age Shrinkage Cracking of Slag Concretes Subjected to 7-days Moist Curing. *Materials and Structures Journal*. Vol. 41, No. 4: 633-642.

ASTM C192. 2005. Standard Practice for Making and Curing Concrete Test Specimens in the Laboratory. *Annual Book of ASTM Standards*. Vol 4: Concrete and Aggregates: 130-137.

ASTM C39. 2005. "Standard Test Method for Compressive Strength of Cylindrical Concrete Specimens". *Annual Book of ASTM Standards*. Vol 4: Concrete and Aggregates: 21-25.

ASTM C469. 2002. Standard Test Method for Static Modulus of Elasticity and Poisson's Ratio of Concrete in Compression. *Annual Book of ASTM Standards*. Vol 4: Concrete and Aggregates.

ASTM C512. 2002. Standard Test Method for Creep of Concrete in Compression. *Annual Book of ASTM Standards*. Vol 4: Concrete and Aggregates.

Bažant, Zdenek P., Gianluca Cusatis, and Luigi Cedolin. 2004. "Temperature Effect on Concrete Creep Modeled by Microprestress-Solidification Theory". *ASCE Journal of Engineering Mechanics*. Vol. 130, No. 6: 691-699.

Bui, Van Khanh and Dennis Montgomery. 1999. "Drying Shrinkage of Self-Compacting Concrete Containing Miller Limestone". In *1st International RILEM Symposium on*

Self-Compacting Concrete. Stockholm, Sweden. ed. A. Skarendal and O. Petersson. Cachan, France: RILEM Publications.

Caldarone, Michael A. 2009. High-Strength Concrete: A Practical Guide. New York, NY: Taylor & Francis.

CEB. 1990. "Creep and Shrinkage". In CEB-FIP *Model Code 1990*. Lausanne, Switzerland: Comite Euro-International du Beton (CEB), 52-65.

CEN. 2004. "Creep and Shrinkage". In *Eurocode 2: Design of Concrete Structures*. British Standards (BSi), 30-33.

Collins, Michael P. and Dennis Mitchell. 1991. Prestressed Concrete Structures. Englewood Cliffs, N.J.: Prentice Hall.

Cramer, Steven and Oliva, Michael G. 2008. Self Consolidating Concrete: Creep and Shrinkage Characteristics. Report, University of Wisconsin.

Dunham, Emily L. 2011. Transfer Length in Blub-Tee Girders Constructed with Self-Consolidating Concrete. M.S. Thesis, Auburn University.

fib. 2010. "Creep and Shrinkage". In *fib Model Code 2010: First Complete Draft*. Lausanne, Switzerland: fédération internationale du béton (*fib*), 52-65.

Ganesh Babu, K., and V. Sree Rama Kumar. 2000. "Efficiency of GGBS in Concrete." *Journal of Cement and Concrete Research*. Vol. 30, Issue 7: 1031- 1036.

Gilbert, R.I. 2001. "Shrinkage, Cracking and Deflection-the Serviceability of Concrete Structures". *Electronic Journal of Structural Engineering*. Vol. 1, No. 1: 2-14.

Hans-Eric, Gram and Piiparinen Pentti. 1999. "Properties of SCC – Especially Early Age and Long Term Shrinkage and Salt Frost Resistance". In *1st International RILEM*

Symposium on Self-Compacting Concrete. Stockholm, Sweden. ed. A. Skarendal and O. Petersson. Cachan, France: RILEM Publications.

Hassoun, M. N. and A. Al-Manaseer. 2012. Structural Concrete Theory and Design. 5th ed. John Wiley & Sons, Inc. Hoboken, New Jersey.

Hauke B. (2001) Self-Compacting Concrete for Precast Concrete Products in Germany. In *Proceedings of the 2nd International RILEM Symposium on Self-Compacting Concrete*. Tokyo, Japan. ed. Ozawa K. and Ouchi M. COMS Engineering Corporation: 633-642.

Hinkle, Stephen D. 2006. Investigation of Time-Dependent Deflection in Long Span, High Strength, Prestressed Concrete Bridge Beams. M.S. Thesis, Virginia Polytechnic Institute and State University.

Horta, Alen. 2005. Evaluation of Self-Consolidating Concrete for Bridge Structure Applications. M.S. Thesis, Georgia Institute of Technology.

Jianyong, Li and Yan Yao. 2001. "A Study on Creep and Drying Shrinkage of High Performance Concrete". *Journal of Cement and Concrete Research*. Vol. 31, No. 8: 1203–1206.

Jianyong, Li. and Tian Pei. 1997. "Effects of Slag and Silica Fume on the Mechanical Properties of High Strength Concrete". *Journal of Cement and Concrete Research*. Vol. 27, Issue 6: 833– 837.

Kavanaugh, Bryan P. 2008. Creep Behavior of Self-Consolidating Concrete. M.S. Thesis, Auburn University.

Khayat, K. H. 1999. Workability, Testing, and Performance of Self-Consolidating Concrete. *ACI Materials Journal* 96, no. 3: 346-353.

Khayat, K., Hu, C. and Monty, H. 1999. "Stability of Self-Consolidating Concrete, Advantages and Potential Applications". In *1st International RILEM Symposium on Self-Compacting Concrete.* Stockholm, Sweden. ed. A. Skarendahl and O. Petersson. Cachan, France: RILEM Publications: 143-152.

Levy, K.R., R. W. Barnes, and A. K. Schindler. 2010. Time-dependent deformations of pretensioned, self-consolidating concrete. In *Think Globally, Build Locally: Proceedings of the Third International fib (International Federation for Structural Concrete) Congress and Exhibition* in Washington, D.C., 29 May-2 June 2010. Chicago: Precast/Prestressed Concrete Institute.

Long, W.J. and K. H. Khayat. 2011. Creep of Prestressed Self-Consolidating Concrete. *ACI Materials Journal* 108, no. 5: 476-484.

McCuen, R.H. 1985. *Statistical Methods for Engineers*. Prentice-Hall: 439.

Mokhtarzadeh, A. and C. French. 2000. Time-Dependent Properties of High-Strength Concrete with Consideration for Precast Applications. ACI Materials Journal, Vol. 97, No. 3: 263-271.

Muller, H. S. and Hillsdorf, H. K. 1990. "Evaluation of the Time-Dependent Behavior of Concrete, Summary Report on the Work of General Task Force 9". *CEB Bulletin d'Information*, No. 199: 290

Nawy, Edward G. 1996. *Prestressed Concrete: A Fundamental Approach*. 2nd ed. Prentice Hall, Inc.

Nawy, Edward G. 2001. *Fundamentals of High-Performance Concrete*. 2nd ed. John Wiley & Sons, Inc.

NCHRP 628. 2009. Self-Consolidating Concrete for Precast, Prestressed Concrete Bridge Elements (NCHRP Report 628). Washington D.C.: Transportation Research Board.

Neville, Adam M. 1997. "Aggregate Bond and Modulus of Elasticity of Concrete". ACI Materials Journal. Vol. 94, No. 1: 71 – 74.

Okamura, H. and M. Ouchi. 1999. "Self-Compacting Concrete. Development, Present Use and Future". In *1st International RILEM Symposium on Self-Compacting Concrete.* Stockholm, Sweden. ed. A. Skarendal and O. Petersson. Cachan, France: RILEM Publications, 3-14.

Persson, Bertil. 1999. "Creep, Shrinkage, and Elastic Modulus of Self-Compacting Concrete". In *1st International RILEM Symposium on Self-Compacting Concrete.* Stockholm, Sweden. ed. A. Skarendahl and O. Petersson. Cachan, France: RILEM Publications: 239-250.

Persson, Bertil. 2001. "A Comparison Between Mechanical Properties of Self-Compacting Concrete and the Corresponding Properties of Normal Concrete". *Journal of Cement and Concrete Research*. Vol. 31: 193-198.

Saric-Coric, M. and Pierre-Claude Aïtcin. 2003. "Influence of Curing Conditions on Shrinkage of Blended Cements Containing Various Amounts of Slag". *ACI Materials Journal.* Vol. 100, Issue 6: 477-484.

Sastry, S. S. 2009. Engineering Mathematics. Connaught Circus, New Delhi: PHI Learning Private Limited.

Schindler, A. K., R. W. Barnes, J. B. Roberts, and S. Rodriguez. 2007. Properties of Self-Consolidating Concrete for Prestressed Members. *ACI Materials Journal 104*, no. 1: 53 – 61.

Schrantz, Claire E. 2012. Development of a User-Guided Program for Prediction Time-Dependent Deformations in Prestressed Bridge Girders. M.S. Thesis, Auburn University.

Shams, M. and Kahn, L.F. 2000. "Time-Dependent Behavior of High-Performance Concrete". Georgia Tech Structural Engineering, Mechanics and Materials Research Report No. 00-5, Georgia Department of Transportation Research Project No. 9510, April 2000: 395.

Valcuende, M., E. Marco, C. Parra, and P. Serna. 2012. Influence of Limestone Filler and Viscosity-Modifying Admixture on the Shrinkage of Self-Compacting Concrete. Cement and Concrete Research Journal. Vol. 42, Issue 4: 583–592.

APPENDICES

APPENDIX A
FIRST YEAR STRAINS OF CREEP SPECIMENS

Table A-1 through Table A-10 contains all specimen strains, up to one year, due to creep and shrinkage that were measured and calculated from test data collected during this study. Each table contains the total strain, drying shrinkage strain, load-induced strain, and the creep strain at each target age for each of the ten sets of tested specimens. Furthermore, the date of when the target age was reached and the DEMEC reading was taken is also provided and the age of the load and the age since the zero-strain measurement was taken are also given.

Table A-1: First Year Strains of Specimen 54-03S-M*

Target Age	Reading Date	Age of Load (days)	Age since Zero-Strain (days)	Total Strain (in./in.)	Shrinkage Strain (in./in.)	Strain due to Load (in./in.)	Creep Strain (in./in.)
Pre-Load	9/29/2010	NA	0.00	0.000000	0.000000	0.000000	0.000000
Post-Load	9/29/2010	0.00	0.03	-0.000536	0.000000	-0.000536	0.000000
2-6 Hours	9/29/2010	0.19	0.22	-0.000612	-0.000028	-0.000584	-0.000048
1 Day	9/30/2010	1.0	1.0	-0.000705	-0.000064	-0.000640	-0.000104
2 Day	10/1/2010	2.3	2.3	-0.000762	-0.000039	-0.000723	-0.000187
3 Day	10/2/2010	3.3	3.3	-0.000769	-0.000040	-0.000729	-0.000192
4 Day	10/3/2010	4.4	4.4	-0.000803	-0.000060	-0.000743	-0.000207
5 Day	10/4/2010	5.1	5.2	-0.000832	-0.000082	-0.000750	-0.000213
6 Day	10/5/2010	6.2	6.2	-0.000859	-0.000088	-0.000771	-0.000235
7 Day	10/11/2010	12.1	12.1	-0.000955	-0.000127	-0.000828	-0.000292
2 Week	10/19/2010	20	20	-0.001013	-0.000150	-0.000862	-0.000326
3 Week	10/20/2010	21	21	-0.001028	-0.000136	-0.000892	-0.000355
4 Week	10/27/2010	28	28	-0.001073	-0.000162	-0.000910	-0.000374
2 Month	11/27/2010	59	59	-0.001185	-0.000211	-0.000974	-0.000438
3 Month[1]	12/24/2010	86	86	-0.001255	-0.000242	-0.001012	-0.000476
3 Month[2]	1/3/2011	96	96	-0.001263	-0.000245	-0.001018	-0.000481
4 Month	1/27/2011	120	120	-0.001299	-0.000254	-0.001045	-0.000508
4 Month[3]	1/27/2011	120	120	-0.001310	-0.000254	-0.001056	-0.000520
5 Month	2/26/2011	150	150	-0.001355	-0.000279	-0.001076	-0.000539
6 Month	3/28/2011	180	180	-0.001357	-0.000276	-0.001081	-0.000545
7 Month	4/27/2011	210	210	-0.001375	-0.000283	-0.001092	-0.000555
8 Month	5/27/2011	240	240	-0.001394	-0.000289	-0.001105	-0.000569
9 Month	6/26/2011	270	270	-0.001408	-0.000294	-0.001114	-0.000577
10 Month	7/26/2011	300	300	-0.001438	-0.000300	-0.001137	-0.000601
11 Month	8/25/2011	330	330	-0.001446	-0.000314	-0.001132	-0.000595
12 Month	9/27/2011	363	363	-0.001467	-0.000329	-0.001138	-0.000602

NOTE:
[1] Measurements were taken before scheduled time
[2] Measurements were taken again after scheduled time
[3] Measurements were retaken after frame force was adjusted to target magnitude

Table A-2: First Year Strains of Specimen 54-03S-T

Target Age	Reading Date	Age of Load (days)	Age since Zero-Strain (days)	Total Strain (in./in.)	Shrinkage Strain (in./in.)	Strain due to Load (in./in.)	Creep Strain (in./in.)
Pre-Load	9/29/2010	NA	0.00	0.000000	0.000000	0.000000	0.000000
Post-Load	9/29/2010	0.00	0.03	-0.000717	0.000002	-0.000719	0.000000
2-6 Hours	9/29/2010	0.13	0.17	-0.000775	-0.000014	-0.000760	-0.000041
1 Day	9/30/2010	0.9	0.9	-0.000876	-0.000036	-0.000840	-0.000120
2 Day	10/1/2010	2.2	2.2	-0.000929	-0.000005	-0.000923	-0.000204
3 Day	10/2/2010	3.2	3.2	-0.000941	-0.000013	-0.000928	-0.000209
4 Day	10/3/2010	4.3	4.4	-0.000969	-0.000020	-0.000950	-0.000231
5 Day	10/4/2010	5.1	5.1	-0.001008	-0.000028	-0.000980	-0.000261
6 Day	10/5/2010	6.1	6.1	-0.001031	-0.000046	-0.000984	-0.000265
7 Day	10/11/2010	12.0	12.1	-0.001169	-0.000092	-0.001077	-0.000358
2 Week	10/19/2010	20	20	-0.001251	-0.000119	-0.001132	-0.000412
3 Week	10/20/2010	21	21	-0.001250	-0.000117	-0.001133	-0.000414
4 Week	10/27/2010	28	28	-0.001311	-0.000148	-0.001163	-0.000444
2 Month	11/27/2010	59	59	-0.001472	-0.000207	-0.001265	-0.000546
3 Month[1]	12/24/2010	86	86	-0.001555	-0.000244	-0.001311	-0.000592
3 Month[2]	1/3/2011	96	96	-0.001572	-0.000247	-0.001325	-0.000606
4 Month	1/27/2011	120	120	-0.001615	-0.000252	-0.001364	-0.000645
4 Month[3]	1/27/2011	120	120	-0.001622	-0.000252	-0.001370	-0.000651
5 Month	2/26/2011	150	150	-0.001677	-0.000279	-0.001398	-0.000679
6 Month	3/28/2011	180	180	-0.001685	-0.000276	-0.001409	-0.000690
7 Month	4/27/2011	210	210	-0.001705	-0.000274	-0.001431	-0.000712
8 Month	5/27/2011	240	240	-0.001733	-0.000286	-0.001447	-0.000728
9 Month	6/26/2011	270	270	-0.001752	-0.000285	-0.001467	-0.000748
10 Month	7/26/2011	300	300	-0.001774	-0.000290	-0.001485	-0.000765
11 Month	8/25/2011	330	330	-0.001786	-0.000304	-0.001482	-0.000763
12 Month	9/27/2011	363	363	-0.001809	-0.000319	-0.001490	-0.000771

NOTE:
[1] Measurements were taken before scheduled time
[2] Measurements were taken again after scheduled time
[3] Measurements were retaken after frame force was adjusted to target magnitude

Table A-3: First Year Strains of Specimen 54-07S-M

Target Age	Reading Date	Age of Load (days)	Age since Zero-Strain (days)	Total Strain (in./in.)	Shrinkage Strain (in./in.)	Strain due to Load (in./in.)	Creep Strain (in./in.)
Pre-Load	10/6/2010	NA	0.00	0.000000	0.000000	0.000000	0.000000
Post-Load	10/6/2010	0.00	0.02	-0.000658	-0.000016	-0.000642	0.000000
2-6 Hours	10/6/2010	0.14	0.16	-0.000767	-0.000062	-0.000705	-0.000063
1 Day	10/7/2010	1.2	1.2	-0.000865	-0.000106	-0.000760	-0.000118
2 Day	10/8/2010	2.3	2.3	-0.000924	-0.000109	-0.000815	-0.000173
3 Day	10/9/2010	3.1	3.1	-0.000966	-0.000119	-0.000847	-0.000205
4 Day	10/10/2010	4.3	4.3	-0.000990	-0.000139	-0.000851	-0.000209
5 Day	10/11/2010	5.2	5.3	-0.001017	-0.000129	-0.000888	-0.000246
6 Day	10/12/2010	6.2	6.2	-0.001031	-0.000143	-0.000889	-0.000247
7 Day	10/13/2010	7.0	7.1	-0.001081	-0.000168	-0.000913	-0.000271
2 Week	10/20/2010	14	14	-0.001183	-0.000185	-0.000997	-0.000355
3 Week	10/27/2010	21	21	-0.001267	-0.000228	-0.001039	-0.000397
4 Week	11/3/2010	28	28	-0.001308	-0.000239	-0.001069	-0.000427
2 Month	12/3/2010	58	58	-0.001487	-0.000339	-0.001148	-0.000506
3 Month	1/7/2011	93	93	-0.001604	-0.000375	-0.001229	-0.000587
4 Month	2/3/2011	120	120	-0.001625	-0.000376	-0.001249	-0.000607
4 Month[1]	2/3/2011	120	120	-0.001658	-0.000376	-0.001282	-0.000640
5 Month	3/5/2011	150	150	-0.001715	-0.000400	-0.001315	-0.000673
6 Month	4/4/2011	180	180	-0.001744	-0.000410	-0.001334	-0.000692
7 Month	5/4/2011	210	210	-0.001755	-0.000408	-0.001347	-0.000705
8 Month	6/3/2011	240	240	-0.001782	-0.000401	-0.001382	-0.000740
9 Month	7/3/2011	270	270	-0.001799	-0.000410	-0.001389	-0.000747
10 Month	8/9/2011	307	307	-0.001824	-0.000424	-0.001399	-0.000757
11 Month	9/2/2011	331	331	-0.001848	-0.000439	-0.001409	-0.000767
12 Month	10/4/2011	363	363	-0.001866	-0.000447	-0.001418	-0.000776

NOTE: [1] Measurements were retaken after frame force was adjusted to target magnitude

Table A-4: First Year Strains of Specimen 54-07S-T

Target Age	Reading Date	Age of Load (days)	Age since Zero-Strain (days)	Total Strain (in./in.)	Shrinkage Strain (in./in.)	Strain due to Load (in./in.)	Creep Strain (in./in.)
Pre-Load	10/5/2010	NA	0.00	0.000000	0.000000	0.000000	0.000000
Post-Load	10/5/2010	0.00	0.04	-0.000581	-0.000018	-0.000564	0.000000
2-6 Hours	10/5/2010	0.17	0.21	-0.000663	-0.000027	-0.000637	-0.000073
1 Day	10/7/2010	1.6	1.6	-0.000726	-0.000040	-0.000686	-0.000123
2 Day	10/8/2010	2.7	2.7	-0.000777	-0.000050	-0.000728	-0.000164
3 Day	10/9/2010	3.5	3.5	-0.000823	-0.000068	-0.000755	-0.000191
4 Day	10/10/2010	4.7	4.7	-0.000855	-0.000072	-0.000783	-0.000219
5 Day	10/11/2010	6.1	6.1	-0.000885	-0.000073	-0.000811	-0.000248
6 Day	10/12/2010	7.1	7.1	-0.000892	-0.000083	-0.000809	-0.000246
7 Day	10/13/2010	7.9	8.0	-0.000938	-0.000103	-0.000835	-0.000272
2 Week	10/20/2010	15	15	-0.001032	-0.000122	-0.000910	-0.000346
3 Week	10/27/2010	22	22	-0.001115	-0.000161	-0.000954	-0.000390
4 Week	11/3/2010	29	29	-0.001151	-0.000169	-0.000982	-0.000419
2 Month	12/3/2010	59	59	-0.001319	-0.000250	-0.001068	-0.000505
3 Month	1/7/2011	94	94	-0.001410	-0.000289	-0.001121	-0.000557
4 Month	2/3/2011	121	121	-0.001446	-0.000292	-0.001154	-0.000591
4 Month[1]	2/3/2011	121	121	-0.001463	-0.000292	-0.001172	-0.000608
5 Month	3/5/2011	151	151	-0.001516	-0.000315	-0.001201	-0.000638
6 Month	4/4/2011	181	181	-0.001544	-0.000324	-0.001220	-0.000656
7 Month	5/4/2011	211	211	-0.001559	-0.000324	-0.001235	-0.000672
8 Month	6/3/2011	241	241	-0.001570	-0.000327	-0.001243	-0.000679
9 Month	7/3/2011	271	271	-0.001593	-0.000336	-0.001256	-0.000693
10 Month	8/9/2011	308	308	-0.001614	-0.000349	-0.001265	-0.000701
11 Month	9/2/2011	332	332	-0.001638	-0.000363	-0.001275	-0.000711
12 Month	10/4/2011	364	364	-0.001656	-0.000365	-0.001291	-0.000727

NOTE: [1] Measurements were retaken after frame force was adjusted to target magnitude

Table A-5: First Year Strains of Specimen 72-03S-M

Target Age	Reading Date	Age of Load (days)	Age since Zero-Strain (days)	Total Strain (in./in.)	Shrinkage Strain (in./in.)	Strain due to Load (in./in.)	Creep Strain (in./in.)
Pre-Load	10/20/2010	NA	0.00	0.000000	0.000000	0.000000	0.000000
Post-Load	10/20/2010	0.00	0.08	-0.000782	-0.000027	-0.000755	0.000000
2-6 Hours	10/20/2010	0.25	0.33	-0.000920	-0.000076	-0.000844	-0.000088
1 Day	10/21/2010	1.2	1.3	-0.001068	-0.000128	-0.000940	-0.000185
2 Day	10/22/2010	2.1	2.2	-0.001110	-0.000139	-0.000971	-0.000216
3 Day	10/23/2010	3.0	3.1	-0.001162	-0.000129	-0.001033	-0.000278
4 Day	10/24/2010	4.4	4.5	-0.001217	-0.000145	-0.001072	-0.000317
5 Day	10/25/2010	5.2	5.3	-0.001253	-0.000156	-0.001097	-0.000342
6 Day	10/26/2010	6.2	6.3	-0.001261	-0.000172	-0.001089	-0.000334
7 Day	10/27/2010	7.1	7.2	-0.001296	-0.000176	-0.001120	-0.000365
2 Week	11/3/2010	14	14	-0.001391	-0.000207	-0.001184	-0.000428
3 Week	11/10/2010	21	21	-0.001469	-0.000246	-0.001223	-0.000468
4 Week	11/17/2010	28	28	-0.001509	-0.000277	-0.001231	-0.000476
2 Month	12/17/2010	58	58	-0.001653	-0.000336	-0.001317	-0.000561
3 Month	1/18/2011	90	90	-0.001727	-0.000380	-0.001348	-0.000592
4 Month	2/17/2011	120	120	-0.001772	-0.000388	-0.001384	-0.000629
4 Month[1]	2/17/2011	120	120	-0.001799	-0.000388	-0.001411	-0.000655
5 Month	3/19/2011	150	150	-0.001847	-0.000408	-0.001440	-0.000684
6 Month	4/18/2011	180	180	-0.001879	-0.000409	-0.001470	-0.000714
7 Month	5/18/2011	210	210	-0.001910	-0.000426	-0.001483	-0.000728
8 Month	6/17/2011	240	240	-0.001923	-0.000425	-0.001498	-0.000743
9 Month	7/17/2011	270	270	-0.001946	-0.000441	-0.001505	-0.000749
10 Month	8/17/2011	301	301	-0.001970	-0.000451	-0.001520	-0.000764
11 Month	9/15/2011	330	330	-0.001993	-0.000456	-0.001537	-0.000782
12 Month	10/13/2011	358	358	-0.002005	-0.000469	-0.001537	-0.000781

NOTE: [1] Measurements were retaken after frame force was adjusted to target magnitude

Table A-6: First Year Strains of Specimen 72-03S-T-U

Target Age	Reading Date	Age of Load (days)	Age since Zero-Strain (days)	Total Strain (in./in.)	Shrinkage Strain (in./in.)	Strain due to Load (in./in.)	Creep Strain (in./in.)
Pre-Load	10/20/2010	NA	0.00	0.000000	0.000000	0.000000	0.000000
Post-Load	10/20/2010	0.00	0.02	-0.000262	-0.000011	-0.000251	0.000000
2-6 Hours	10/20/2010	0.10	0.13	-0.000277	-0.000018	-0.000260	-0.000009
1 Day	10/21/2010	1.0	1.0	-0.000325	-0.000026	-0.000299	-0.000048
2 Day	10/22/2010	1.8	1.9	-0.000349	-0.000036	-0.000314	-0.000063
3 Day	10/23/2010	2.8	2.8	-0.000358	-0.000040	-0.000318	-0.000067
4 Day	10/24/2010	4.2	4.2	-0.000380	-0.000053	-0.000327	-0.000076
5 Day	10/25/2010	4.9	4.9	-0.000388	-0.000062	-0.000326	-0.000075
6 Day	10/26/2010	5.9	5.9	-0.000401	-0.000072	-0.000329	-0.000078
7 Day	10/27/2010	6.9	7.0	-0.000415	-0.000086	-0.000329	-0.000078
2 Week	11/3/2010	14	14	-0.000489	-0.000114	-0.000375	-0.000124
3 Week	11/10/2010	21	21	-0.000548	-0.000153	-0.000395	-0.000144
4 Week	11/17/2010	28	28	-0.000579	-0.000173	-0.000406	-0.000155
2 Month	12/17/2010	58	58	-0.000689	-0.000240	-0.000448	-0.000197
3 Month	1/18/2011	90	90	-0.000741	-0.000270	-0.000470	-0.000220
4 Month	2/17/2011	120	120	-0.000759	-0.000276	-0.000483	-0.000232
4 Month[1]	2/17/2011	120	120	-0.000771	-0.000276	-0.000495	-0.000244
5 Month	3/19/2011	150	150	-0.000801	-0.000308	-0.000494	-0.000243
6 Month	4/18/2011	180	180	-0.000818	-0.000312	-0.000506	-0.000255
7 Month	5/18/2011	210	210	-0.000830	-0.000320	-0.000510	-0.000259
8 Month	6/17/2011	240	240	-0.000838	-0.000327	-0.000511	-0.000260
9 Month	7/17/2011	270	270	-0.000856	-0.000341	-0.000515	-0.000264
10 Month	8/17/2011	301	301	-0.000870	-0.000350	-0.000520	-0.000269
11 Month	9/15/2011	330	330	-0.000882	-0.000363	-0.000519	-0.000268
12 Month	10/13/2011	358	358	-0.000893	-0.000372	-0.000521	-0.000270

NOTE: [1] Measurements were retaken after frame force was adjusted to target magnitude

Table A-7: First Year Strains of Specimen 54-12C-M

Target Age	Reading Date	Age of Load (days)	Age since Zero-Strain (days)	Total Strain (in./in.)	Shrinkage Strain (in./in.)	Strain due to Load (in./in.)	Creep Strain (in./in.)
Pre-Load	9/30/2010	NA	0.00	0.000000	0.000000	0.000000	0.000000
Post-Load	9/30/2010	0.00	0.02	-0.000562	-0.000035	-0.000527	0.000000
2-6 Hours	9/30/2010	0.17	0.19	-0.000637	-0.000045	-0.000592	-0.000065
1 Day	10/1/2010	1.3	1.3	-0.000733	-0.000050	-0.000682	-0.000155
2 Day	10/2/2010	2.3	2.3	-0.000756	-0.000068	-0.000688	-0.000160
3 Day	10/3/2010	3.4	3.5	-0.000807	-0.000072	-0.000735	-0.000207
4 Day	10/4/2010	4.2	4.2	-0.000828	-0.000084	-0.000744	-0.000217
5 Day	10/5/2010	5.2	5.3	-0.000875	-0.000105	-0.000770	-0.000242
6 Day	10/6/2010	6.1	6.1	-0.000882	-0.000107	-0.000775	-0.000248
7 Day	10/12/2010	12.2	12.2	-0.000955	-0.000124	-0.000830	-0.000303
2 Week	10/19/2010	19	19	-0.001024	-0.000152	-0.000872	-0.000345
3 Week	10/21/2010	21	21	-0.001047	-0.000163	-0.000884	-0.000356
4 Week	10/28/2010	28	28	-0.001079	-0.000167	-0.000912	-0.000385
2 Month	11/28/2010	59	59	-0.001199	-0.000217	-0.000982	-0.000455
3 Month[1]	12/24/2010	85	85	-0.001269	-0.000249	-0.001020	-0.000492
3 Month[2]	1/3/2011	95	95	-0.001280	-0.000250	-0.001030	-0.000503
4 Month	1/28/2011	120	120	-0.001317	-0.000265	-0.001052	-0.000524
4 Month[3]	1/28/2011	120	120	-0.001322	-0.000265	-0.001057	-0.000530
5 Month	2/27/2011	150	150	-0.001364	-0.000281	-0.001083	-0.000555
6 Month	3/29/2011	180	180	-0.001371	-0.000277	-0.001093	-0.000566
7 Month	4/28/2011	210	210	-0.001395	-0.000280	-0.001115	-0.000587
8 Month	5/28/2011	240	240	-0.001415	-0.000285	-0.001129	-0.000602
9 Month	6/27/2011	270	270	-0.001422	-0.000292	-0.001130	-0.000603
10 Month	7/27/2011	300	300	-0.001458	-0.000298	-0.001160	-0.000633
11 Month	8/27/2011	331	331	-0.001462	-0.000311	-0.001150	-0.000623
12 Month	9/27/2011	362	362	-0.001486	-0.000329	-0.001157	-0.000630

NOTE:
[1] Measurements were taken before scheduled time
[2] Measurements were taken again after scheduled time
[3] Measurements were retaken after frame force was adjusted to target magnitude

Table A-8: First Year Strains of Specimen 54-12C-T

Target Age	Reading Date	Age of Load (days)	Age since Zero-Strain (days)	Total Strain (in./in.)	Shrinkage Strain (in./in.)	Strain due to Load (in./in.)	Creep Strain (in./in.)
Pre-Load	9/30/2010	NA	0.00	0.000000	0.000000	0.000000	0.000000
Post-Load	9/30/2010	0.00	0.02	-0.000591	-0.000024	-0.000567	0.000000
2-6 Hours	9/30/2010	0.12	0.14	-0.000655	-0.000045	-0.000610	-0.000043
1 Day	10/1/2010	1.2	1.2	-0.000805	-0.000023	-0.000782	-0.000216
2 Day	10/2/2010	2.2	2.2	-0.000826	-0.000041	-0.000785	-0.000218
3 Day	10/3/2010	3.3	3.3	-0.000857	-0.000036	-0.000821	-0.000254
4 Day	10/4/2010	4.0	4.0	-0.000891	-0.000047	-0.000845	-0.000278
5 Day	10/5/2010	5.1	5.1	-0.000929	-0.000056	-0.000873	-0.000306
6 Day	10/6/2010	5.9	5.9	-0.000951	-0.000067	-0.000884	-0.000317
7 Day	10/12/2010	12.1	12.1	-0.001017	-0.000076	-0.000940	-0.000374
2 Week	10/19/2010	19	19	-0.001096	-0.000116	-0.000980	-0.000413
3 Week	10/21/2010	21	21	-0.001114	-0.000120	-0.000994	-0.000427
4 Week	10/28/2010	28	28	-0.001155	-0.000129	-0.001026	-0.000459
2 Month	11/28/2010	59	59	-0.001276	-0.000177	-0.001099	-0.000532
3 Month[1]	12/24/2010	85	85	-0.001353	-0.000211	-0.001142	-0.000575
3 Month[2]	1/3/2011	95	95	-0.001361	-0.000217	-0.001144	-0.000578
4 Month	1/28/2011	120	120	-0.001399	-0.000217	-0.001182	-0.000616
4 Month[3]	1/28/2011	120	120	-0.001402	-0.000217	-0.001185	-0.000618
5 Month	2/27/2011	150	150	-0.001449	-0.000242	-0.001207	-0.000640
6 Month	3/29/2011	180	180	-0.001454	-0.000239	-0.001215	-0.000649
7 Month	4/28/2011	210	210	-0.001469	-0.000241	-0.001228	-0.000661
8 Month	5/28/2011	240	240	-0.001488	-0.000241	-0.001248	-0.000681
9 Month	6/27/2011	270	270	-0.001503	-0.000248	-0.001256	-0.000689
10 Month	7/27/2011	300	300	-0.001531	-0.000251	-0.001280	-0.000714
11 Month	8/27/2011	331	331	-0.001545	-0.000263	-0.001282	-0.000716
12 Month	9/27/2011	362	362	-0.001563	-0.000279	-0.001284	-0.000717

NOTE:
[1] Measurements were taken before scheduled time
[2] Measurements were taken again after scheduled time
[3] Measurements were retaken after frame force was adjusted to target magnitude

Table A-9: First Year Strains of Specimen 72-11C-M

Target Age	Reading Date	Age of Load (days)	Age since Zero-Strain (days)	Total Strain (in./in.)	Shrinkage Strain (in./in.)	Strain due to Load (in./in.)	Creep Strain (in./in.)
Pre-Load	10/27/2010	NA	0.00	0.000000	0.000000	0.000000	0.000000
Post-Load	10/27/2010	0.00	0.02	-0.000609	-0.000011	-0.000598	0.000000
2-6 Hours	10/27/2010	0.15	0.17	-0.000708	-0.000086	-0.000622	-0.000024
1 Day	10/28/2010	1.3	1.3	-0.000789	-0.000105	-0.000684	-0.000086
2 Day	10/29/2010	2.2	2.2	-0.000819	-0.000104	-0.000715	-0.000117
3 Day	10/30/2010	3.3	3.3	-0.000847	-0.000107	-0.000740	-0.000142
4 Day	10/31/2010	4.2	4.2	-0.000868	-0.000109	-0.000759	-0.000161
5 Day	11/1/2010	5.3	5.4	-0.000884	-0.000111	-0.000773	-0.000175
6 Day	11/2/2010	6.3	6.4	-0.000907	-0.000123	-0.000785	-0.000187
7 Day	11/3/2010	7.4	7.4	-0.000926	-0.000119	-0.000807	-0.000209
2 Week	11/10/2010	14	14	-0.001014	-0.000147	-0.000867	-0.000269
3 Week	11/17/2010	21	21	-0.001058	-0.000156	-0.000902	-0.000304
4 Week	11/24/2010	28	28	-0.001092	-0.000174	-0.000918	-0.000320
2 Month	12/24/2010	58	58	-0.001205	-0.000218	-0.000987	-0.000389
3 Month	1/25/2011	90	90	-0.001241	-0.000230	-0.001011	-0.000413
4 Month	2/24/2011	120	120	-0.001278	-0.000254	-0.001024	-0.000426
4 Month[1]	2/24/2011	120	120	-0.001292	-0.000254	-0.001038	-0.000440
5 Month	3/26/2011	150	150	-0.001306	-0.000260	-0.001046	-0.000448
6 Month	4/25/2011	180	180	-0.001332	-0.000274	-0.001058	-0.000460
7 Month	5/25/2011	210	210	-0.001342	-0.000273	-0.001068	-0.000470
8 Month	6/24/2011	240	240	-0.001350	-0.000277	-0.001074	-0.000476
9 Month	7/24/2011	270	270	-0.001379	-0.000289	-0.001090	-0.000492
10 Month	8/23/2011	300	300	-0.001390	-0.000291	-0.001099	-0.000501
11 Month	9/22/2011	330	330	-0.001408	-0.000305	-0.001104	-0.000506
12 Month	10/19/2011	357	357	-0.001426	-0.000316	-0.001110	-0.000512

NOTE: [1] Measurements were retaken after frame force was adjusted to target magnitude

Table A-10: First Year Strains of Specimen 72-11C-T-U

Target Age	Reading Date	Age of Load (days)	Age since Zero-Strain (days)	Total Strain (in./in.)	Shrinkage Strain (in./in.)	Strain due to Load (in./in.)	Creep Strain (in./in.)
Pre-Load	10/27/2010	NA	0.00	0.000000	0.000000	0.000000	0.000000
Post-Load	10/27/2010	0.00	0.09	-0.000244	-0.000027	-0.000217	0.000000
2-6 Hours	10/27/2010	0.17	0.25	-0.000265	-0.000038	-0.000226	-0.000009
1 Day	10/28/2010	1.0	1.1	-0.000269	-0.000051	-0.000219	-0.000001
2 Day	10/29/2010	1.9	2.0	-0.000285	-0.000056	-0.000229	-0.000012
3 Day	10/30/2010	2.9	3.0	-0.000294	-0.000059	-0.000235	-0.000018
4 Day	10/31/2010	3.9	4.0	-0.000301	-0.000063	-0.000239	-0.000021
5 Day	11/1/2010	5.0	5.1	-0.000312	-0.000066	-0.000246	-0.000029
6 Day	11/2/2010	6.1	6.1	-0.000318	-0.000072	-0.000246	-0.000029
7 Day	11/3/2010	7.1	7.2	-0.000333	-0.000076	-0.000257	-0.000040
2 Week	11/10/2010	14	14	-0.000381	-0.000112	-0.000269	-0.000052
3 Week	11/17/2010	21	21	-0.000407	-0.000124	-0.000282	-0.000065
4 Week	11/24/2010	28	28	-0.000437	-0.000138	-0.000299	-0.000082
2 Month	12/24/2010	58	58	-0.000503	-0.000187	-0.000317	-0.000099
3 Month	1/25/2011	90	90	-0.000531	-0.000207	-0.000324	-0.000107
4 Month	2/24/2011	120	120	-0.000571	-0.000236	-0.000335	-0.000118
4 Month[1]	2/24/2011	120	120	-0.000585	-0.000236	-0.000349	-0.000132
5 Month	3/26/2011	150	150	-0.000596	-0.000237	-0.000359	-0.000142
6 Month	4/25/2011	180	180	-0.000615	-0.000251	-0.000364	-0.000146
7 Month	5/25/2011	210	210	-0.000619	-0.000252	-0.000367	-0.000150
8 Month	6/24/2011	240	240	-0.000631	-0.000259	-0.000371	-0.000154
9 Month	7/9/2011	255	255	-0.000649	-0.000268	-0.000382	-0.000164
10 Month	8/23/2011	300	300	-0.000655	-0.000273	-0.000382	-0.000165
11 Month	9/22/2011	330	330	-0.000670	-0.000285	-0.000385	-0.000168
12 Month	10/19/2011	357	357	-0.000682	-0.000298	-0.000384	-0.000167

NOTE: [1] Measurements were retaken after frame force was adjusted to target magnitude

APPENDIX B
TEMPERATURE EFFECTS

B.1. MEASURED AND ASSUMED TEMPERATURE PROFILES

Figure B-1 to Figure B-5 graphs the temperature profile over time for each set of specimens. Each graph shows one sample with the two different curing methods that were implemented. The first portion of the graph shows solid lines that represent the measured temperatures from the thermocouples and the latter portion of the graph shows dotted lines which represent the calculated temperatures using the assumed rate of cooling. The major milestones shown are the point at which transportation began, the stripping time, and the loading time.

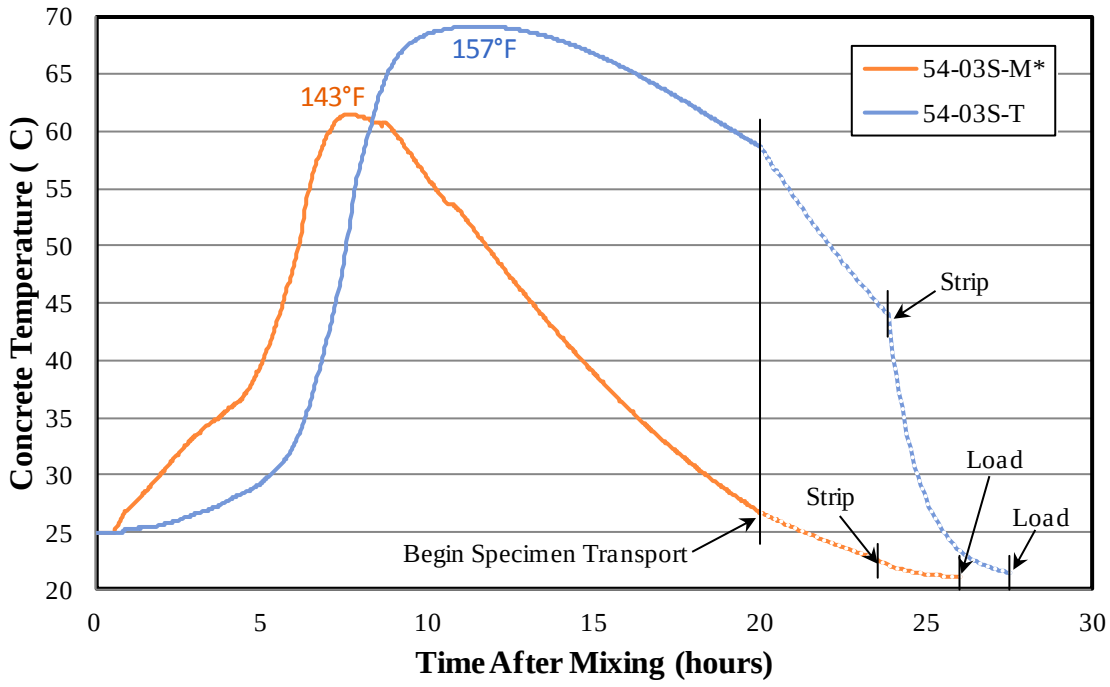

Figure B-1: Measured and Calculated Temperature Profile of Batch 54-03S

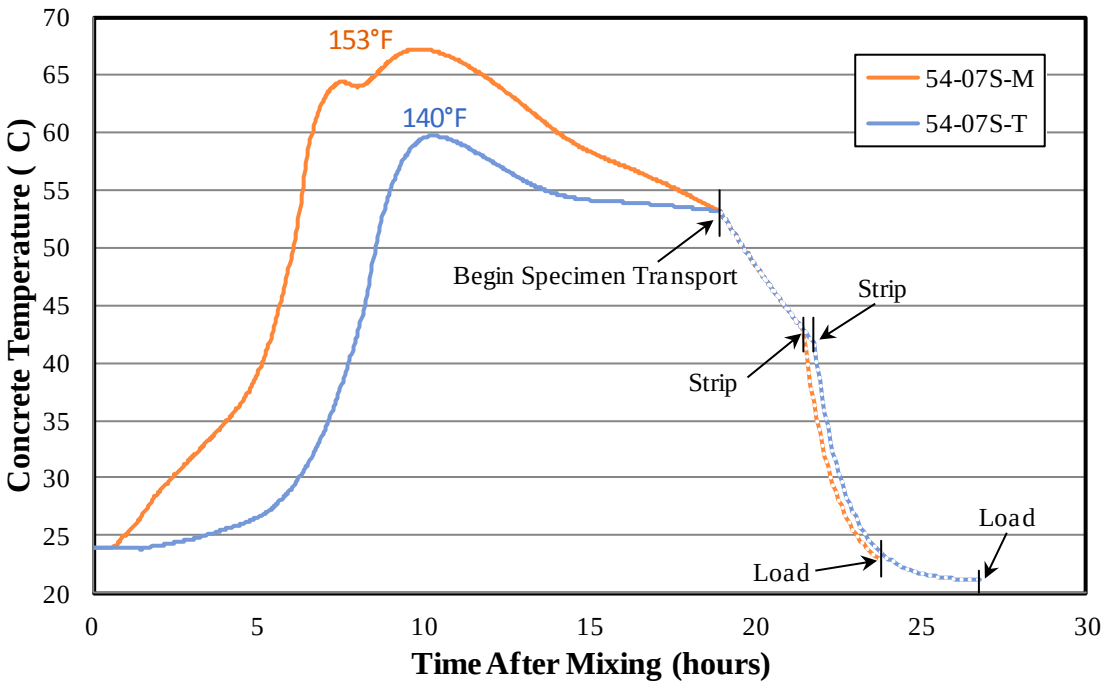

Figure B-2: Measured and Calculated Temperature Profile of Batch 54-07S

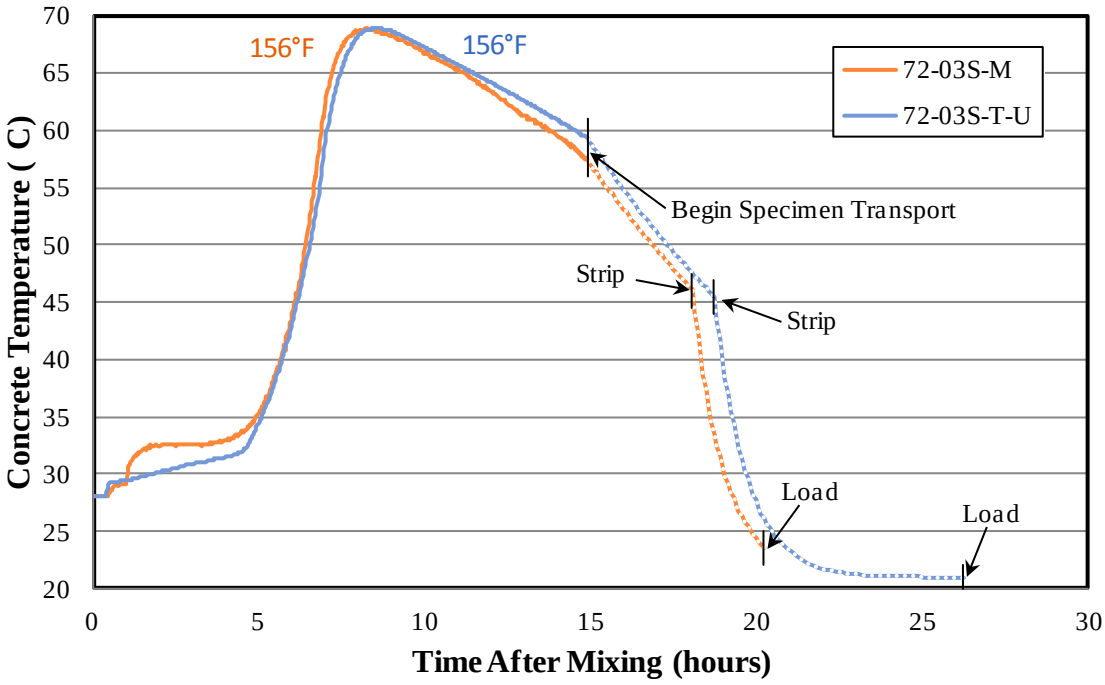

Figure B-3: Measured and Calculated Temperature Profile of Batch 72-03S

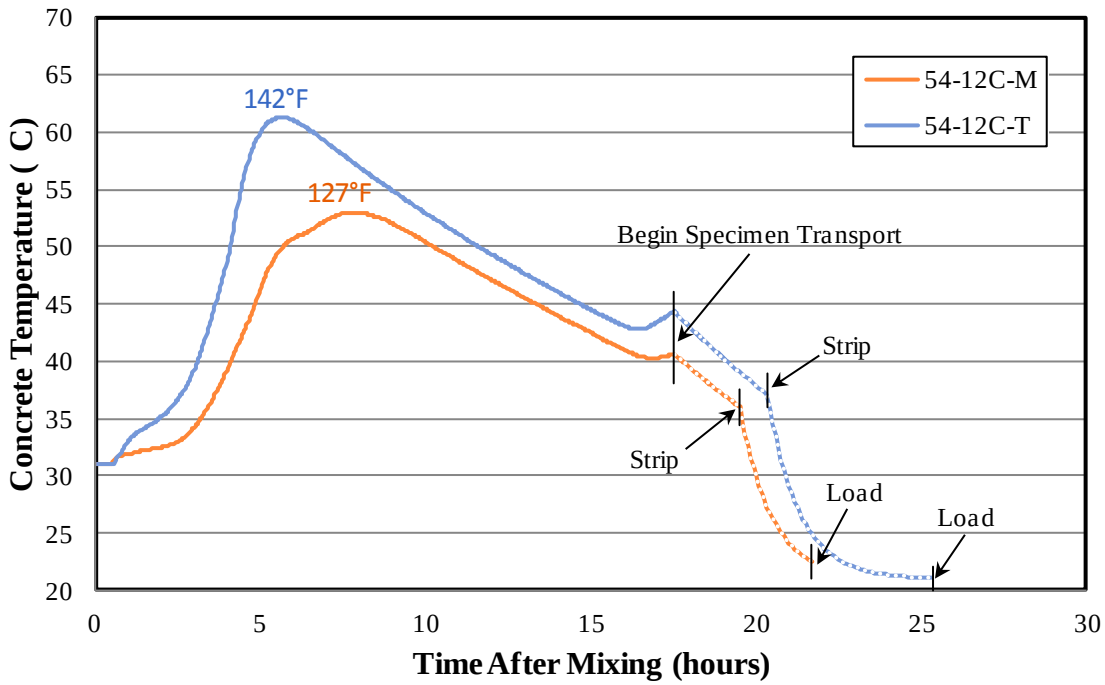

Figure B-4: Measured and Calculated Temperature Profile of Batch 54-12C

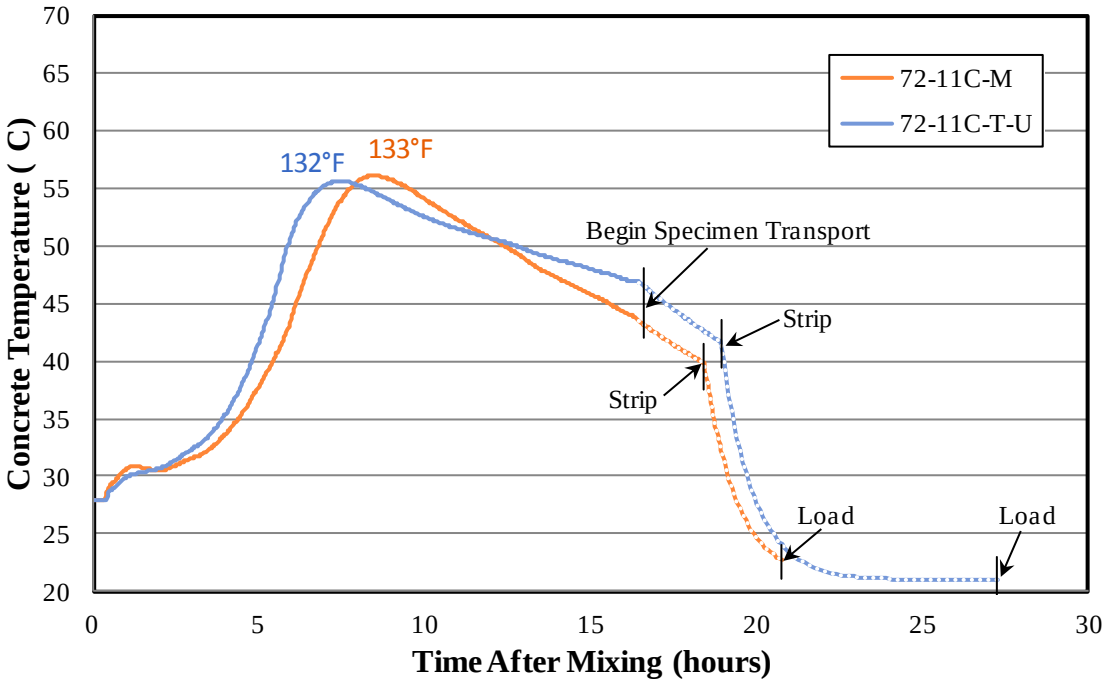

Figure B-5: Measured and Calculated Temperature Profile of Batch 72-11C

B.2. CONCRETE MATURITY

Figure B-6 through Figure B-15 graphs the maturity of concrete over time for each set of specimens. Each graph shows the chronological age of the concrete as well as the temperature-adjusted age to account for the elevated curing cycles. The "Temperature-Adjusted Age" represents the maturity predicted by MC 90, MC 90-99, MC 2010, and Eurocode. The "Temperature-Adjusted Age (KAV)" represents the maturity modified by Brian Kavanaugh in MC 90-KAV. The major milestones shown are the point at which transportation began, the stripping time, and the loading time.

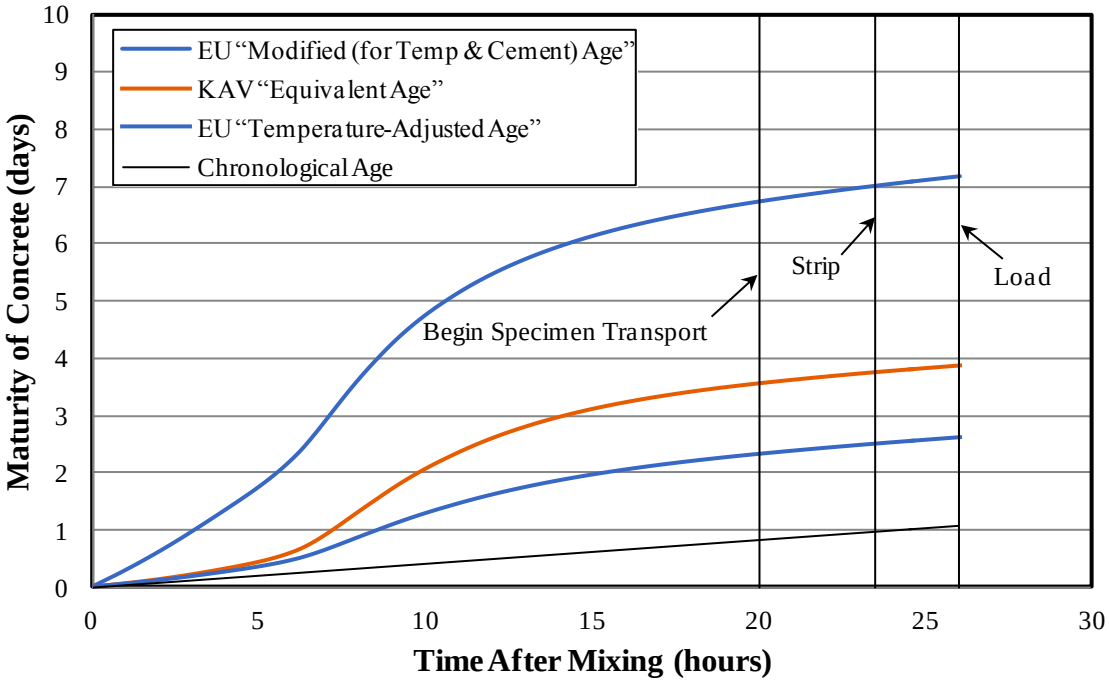

Figure B-6: Maturity of Specimens 54-03S-M*

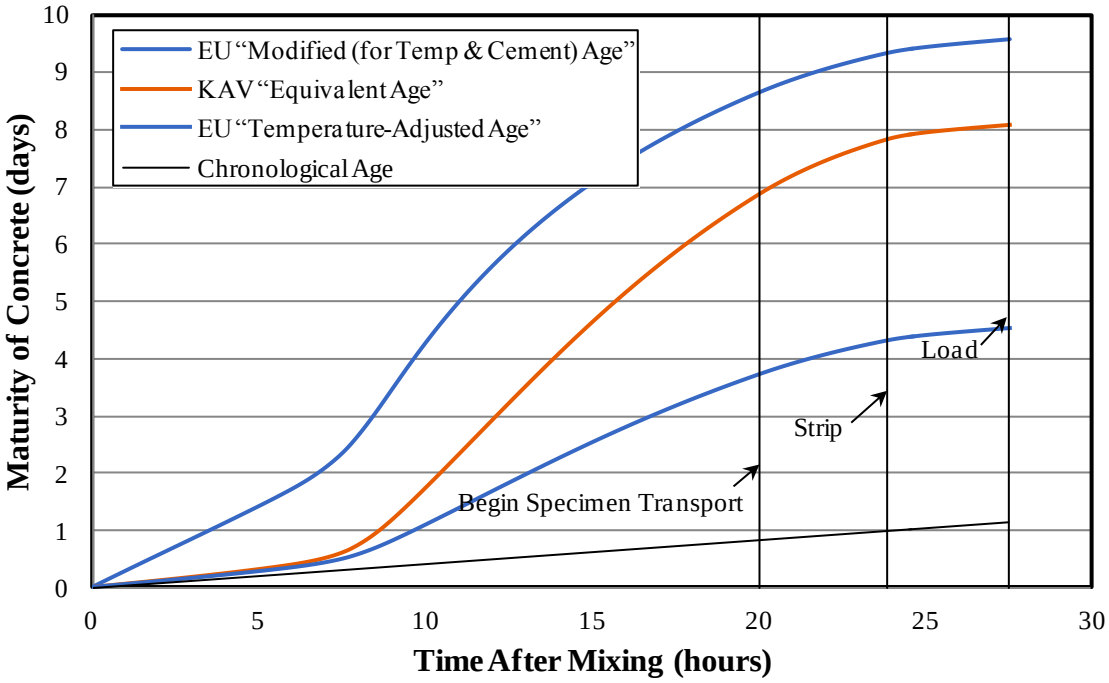

Figure B-7: Maturity of Specimens 54-03S-T

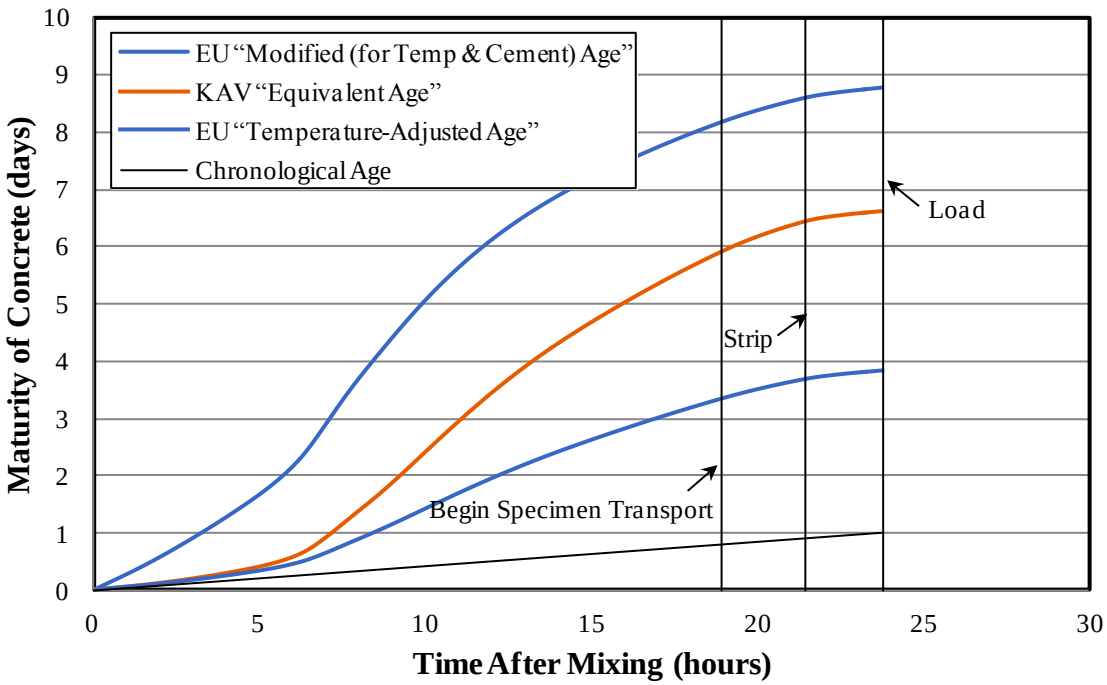

Figure B-8: Maturity of Specimens 54-07S-M

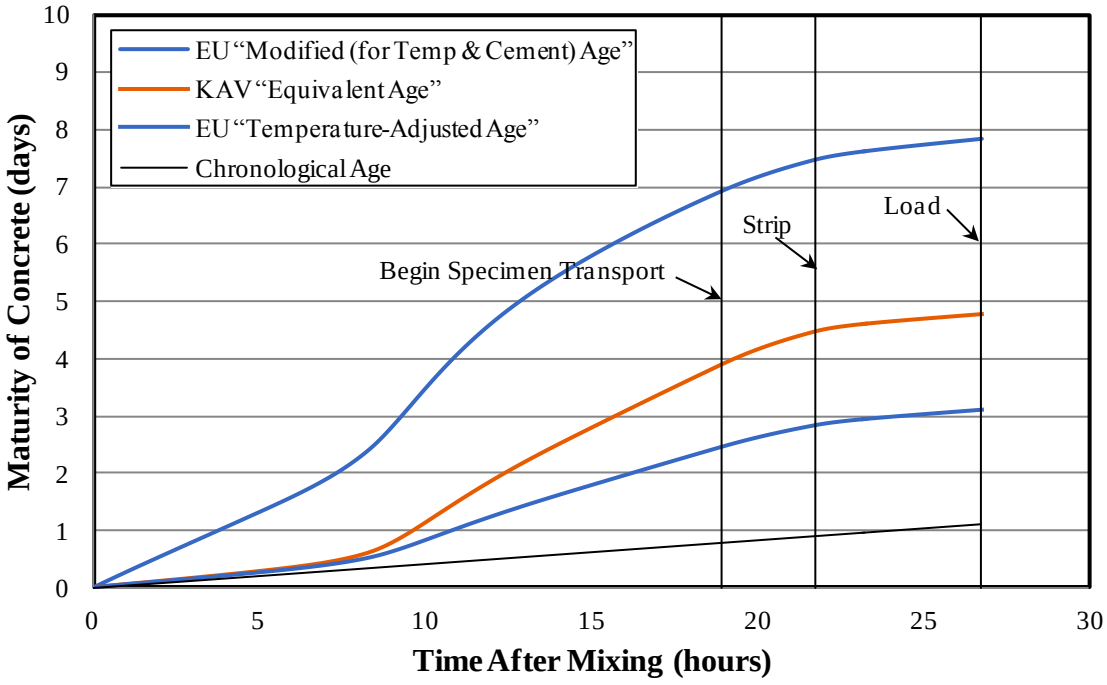

Figure B-9: Maturity of Specimens 54-07S-T

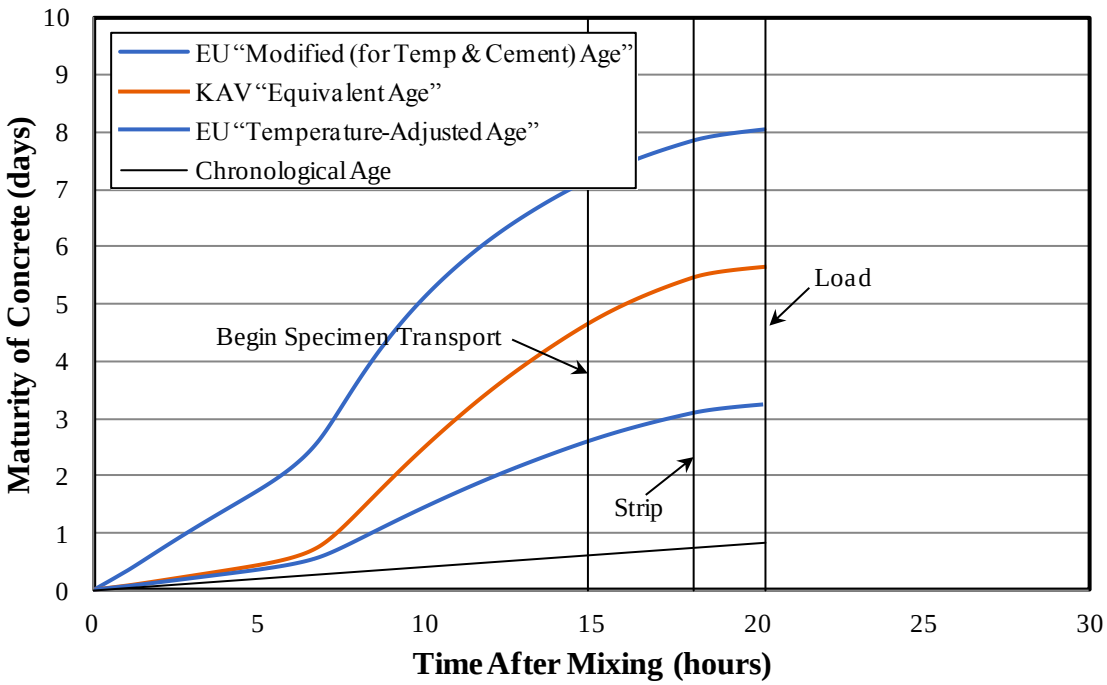

Figure B-10: Maturity of Specimens 72-03S-M

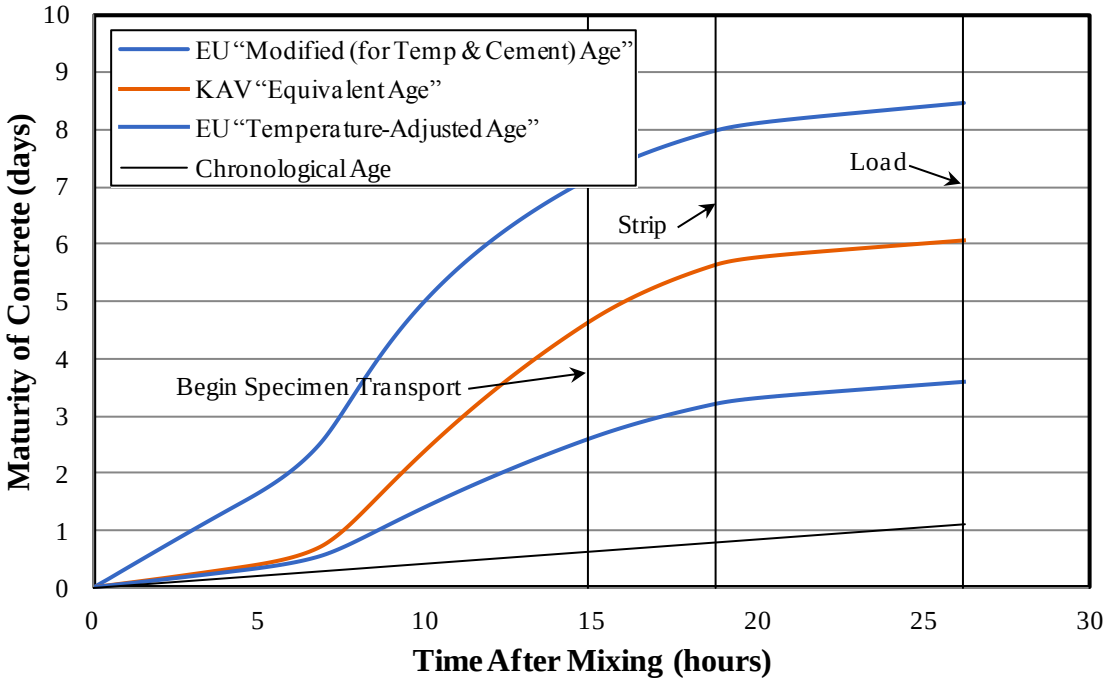

Figure B-11: Maturity of Specimens 72-03S-T-U

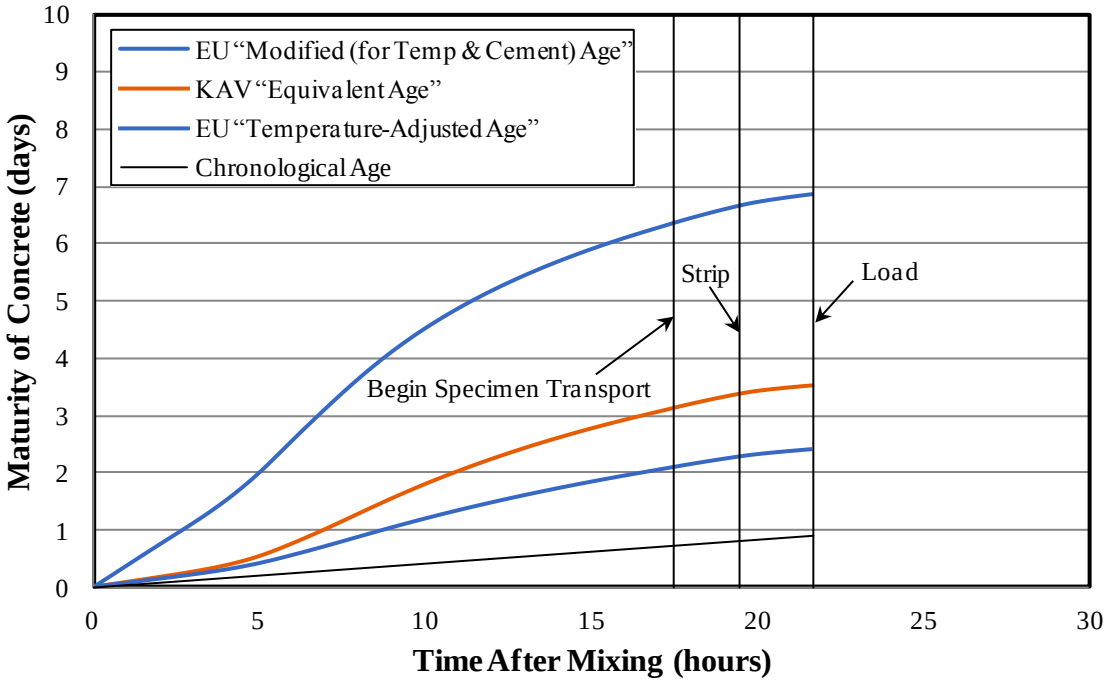

Figure B-12: Maturity of Specimens 54-12C-M

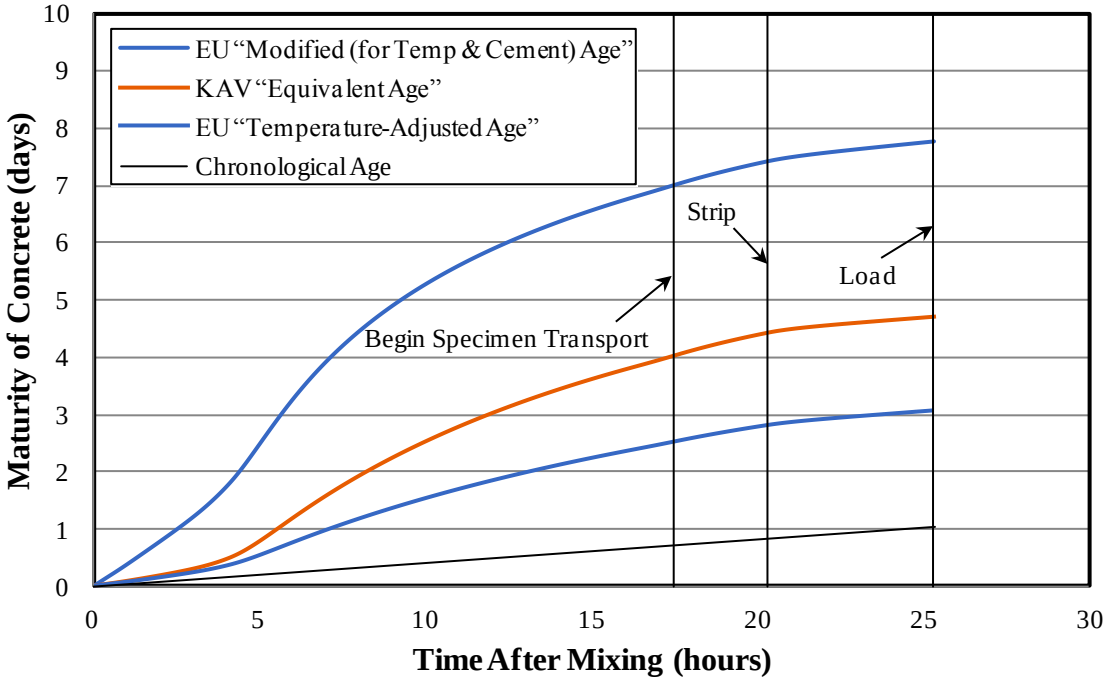

Figure B-13: Maturity of Specimens 54-12C-T

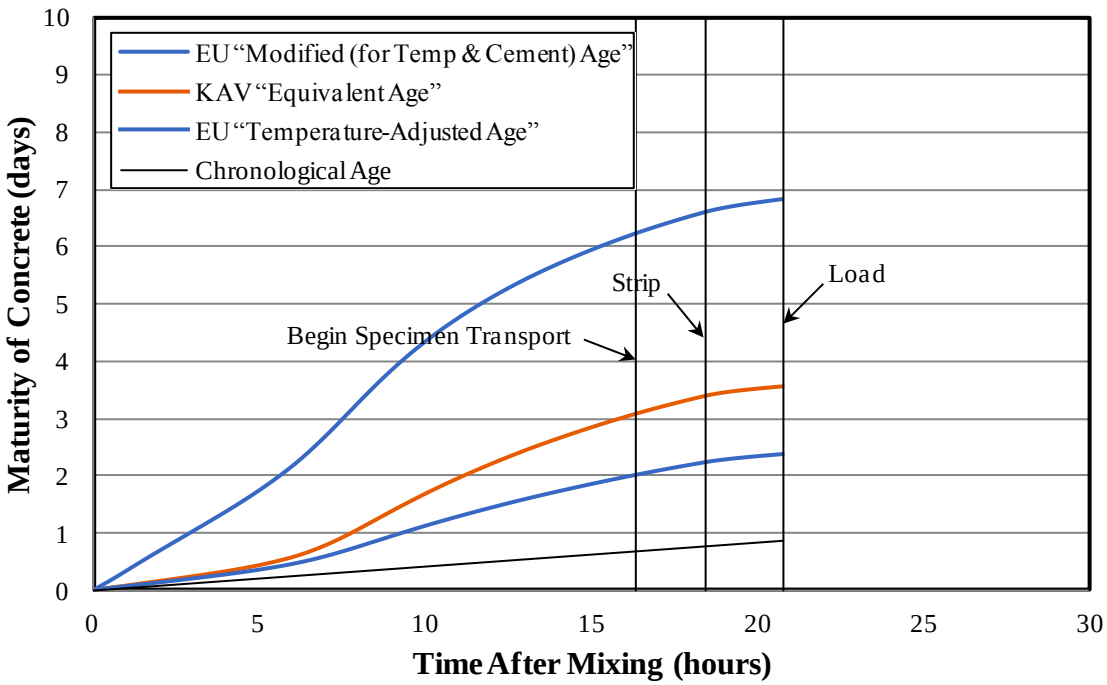

Figure B-14: Maturity of Specimens 72-11C-M

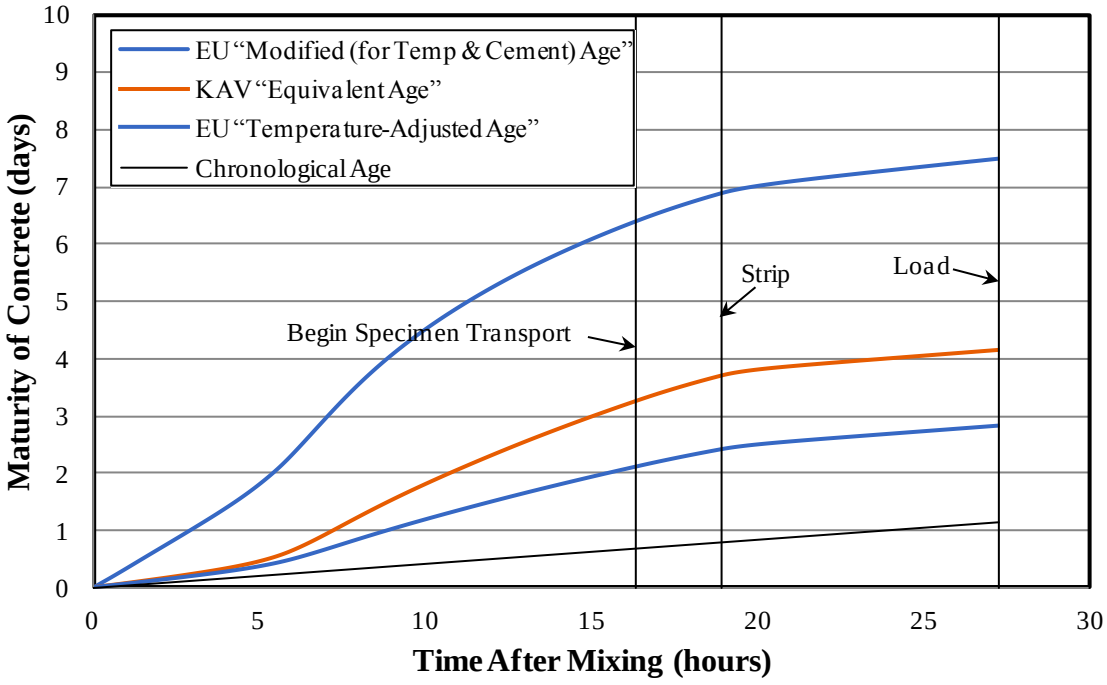

Figure B-15: Maturity of Specimens 72-11C-T-U

APPENDIX C
PREDICTED AND MEASURED STRAINS VERSUS TIME

C.1. LOAD-DEPENDENT STRAIN VERSUS TIME

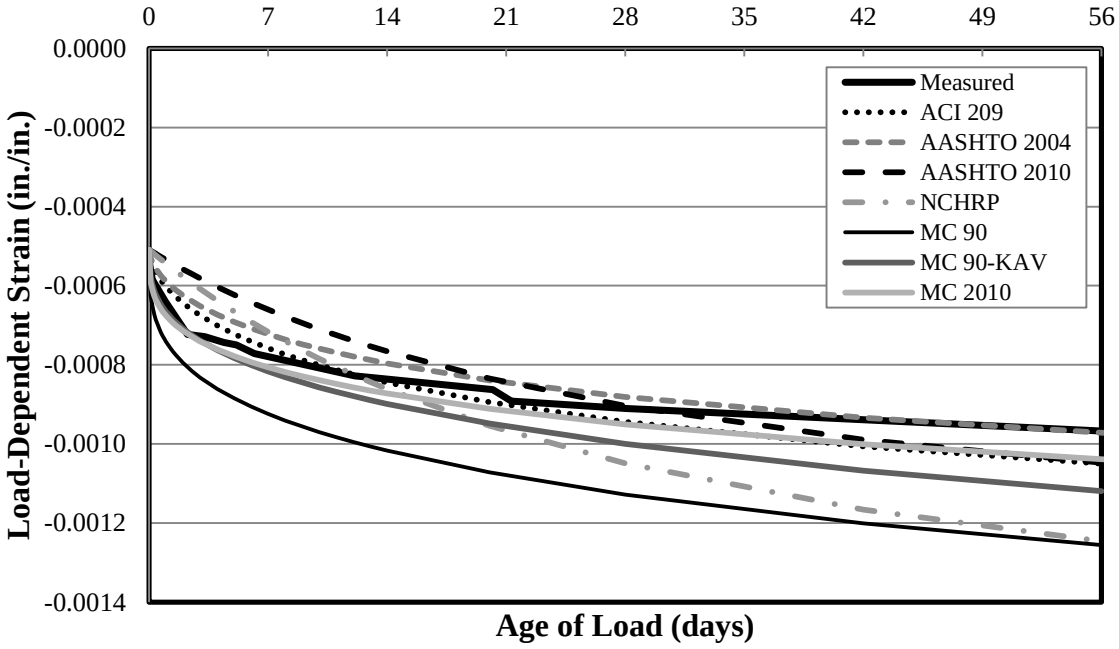

Figure C-1Figure C-1 through Figure C-20 contains all load-dependent strain data collected during this study for each of the ten sets of specimen. Each figure plots the measured load-dependent strain for a specific specimen as well as predicted strain for that specimen against the age of load and is presented at 56 days and 1 year. The prediction methods used for load-dependent strain are: ACI 209, AASHTO 2004, AASHTO 2010, NCHRP 628, MC 90, MC 90-KAV, and MC 2010. MC 90-99 and Eurocode are effectively equal to MC 2010 and are not shown. Also, for conventionally vibrated concrete mixtures, the strain due to load predicted by NCHRP 628 is equal to that predicted by AASHTO 2010.

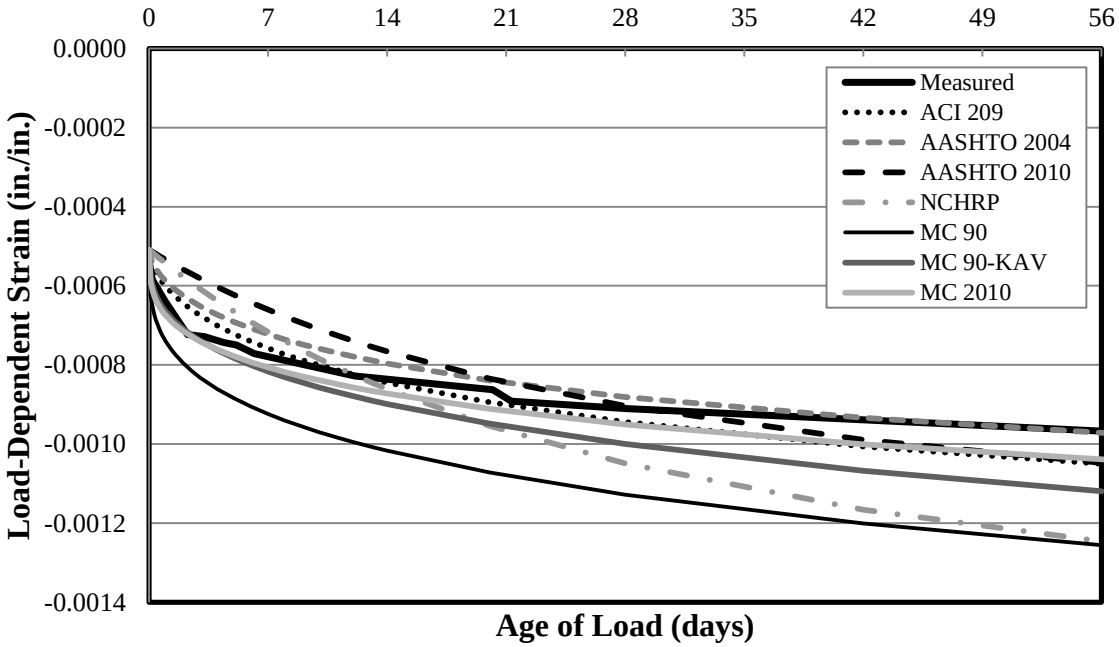

Figure C-1: Load-Induced Strain for Specimen 54-03S-M* up to 56 Days

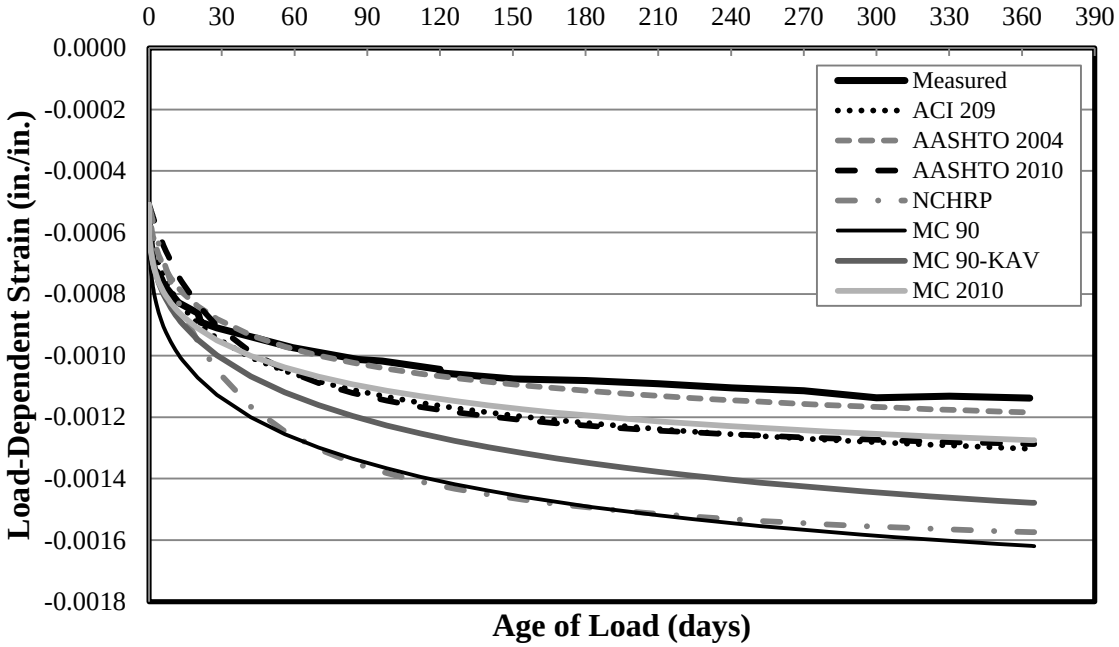

Figure C-2: Load-Induced Strain for Specimen 54-03S-M* up to 1 Year

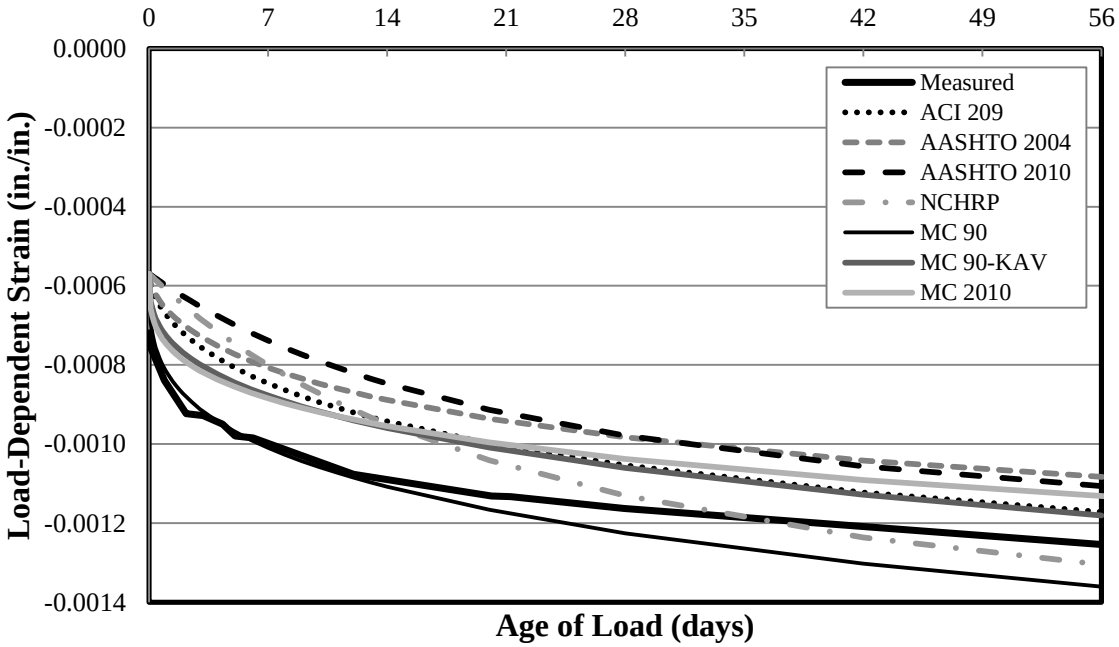

Figure C-3: Load-Induced Strain for Specimen 54-03S-T up to 56 Days

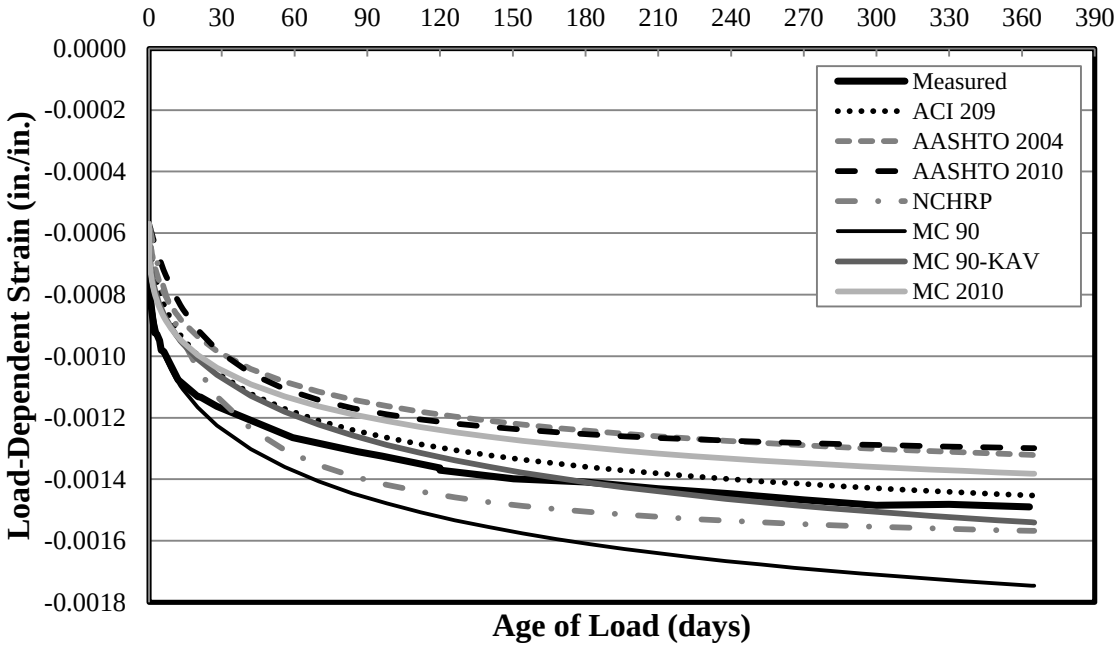

Figure C-4: Load-Induced Strain for Specimen 54-03S-T up to 1 Year

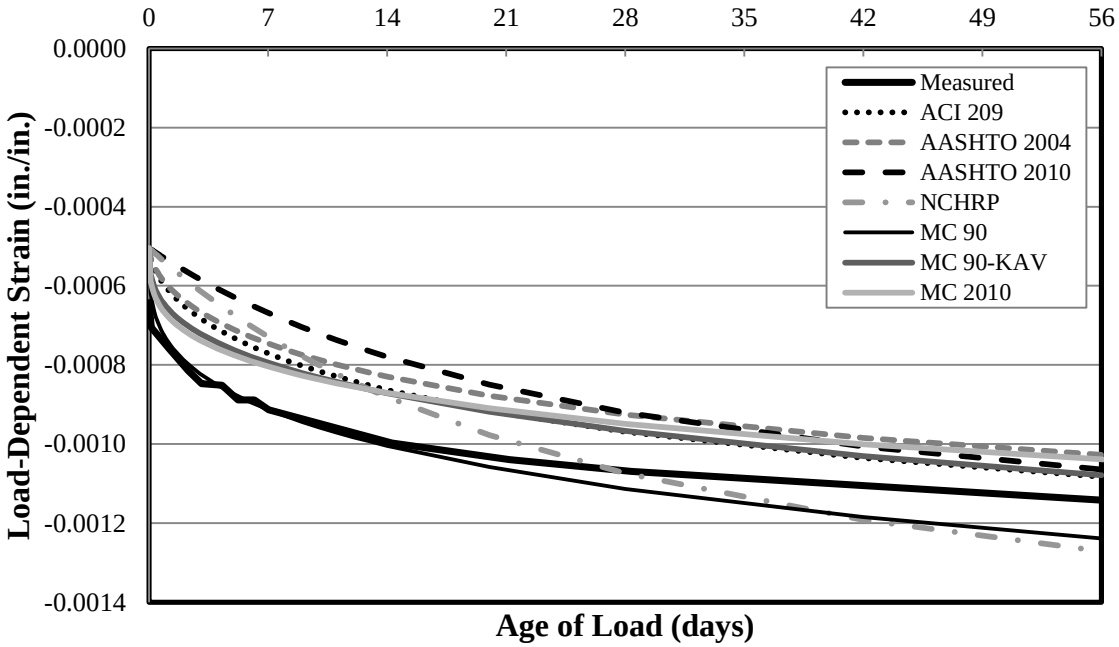

Figure C-5: Load-Induced Strain for Specimen 54-07S-M up to 56 Days

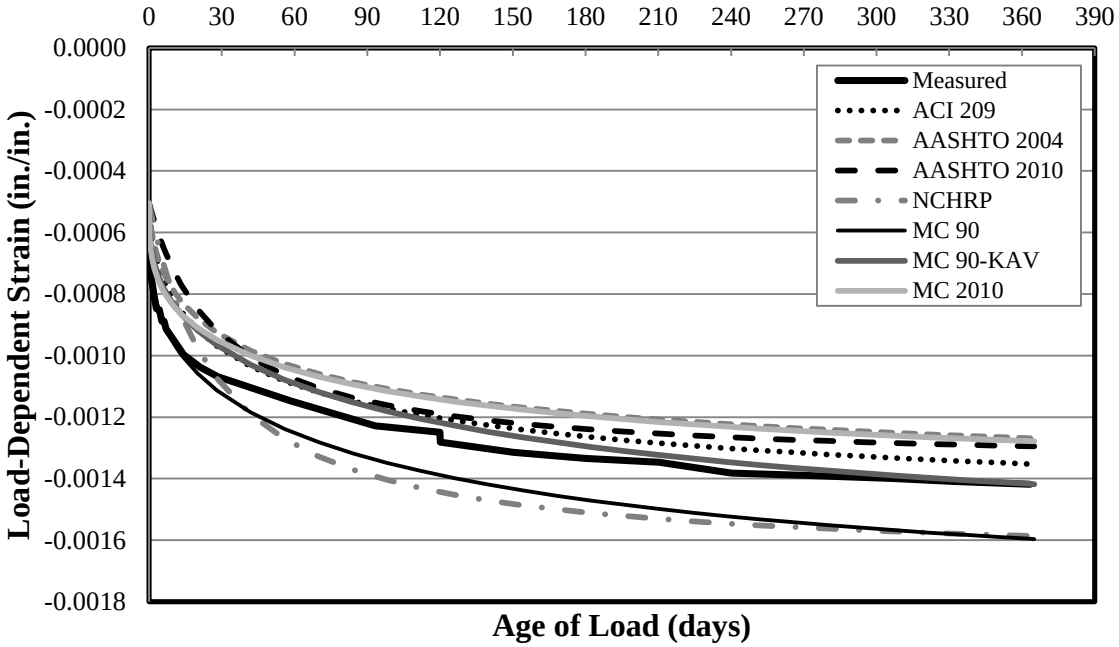

Figure C-6: Load-Induced Strain for Specimen 54-07S-M up to 1 Year

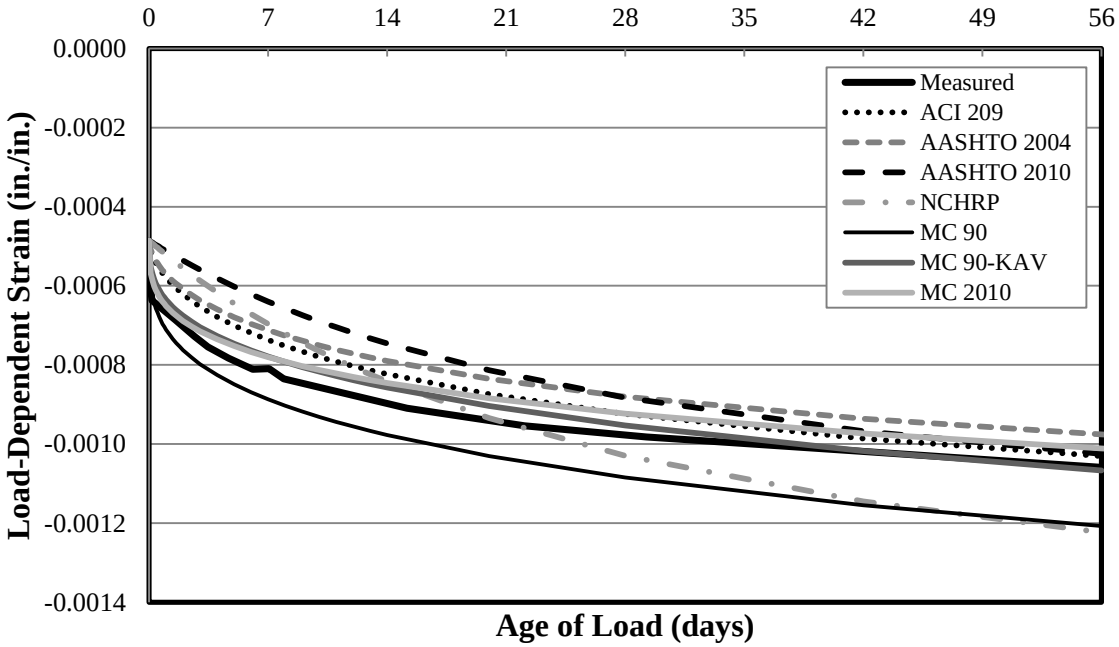

Figure C-7: Load-Induced Strain for Specimen 54-07S-T up to 56 Days

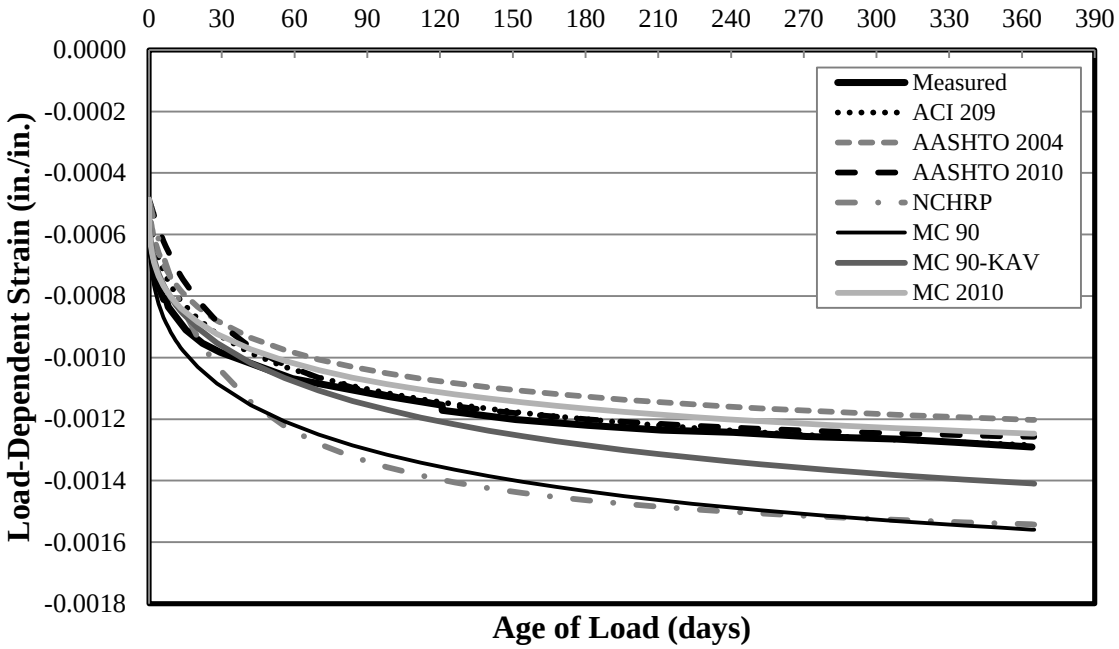

Figure C-8: Load-Induced Strain for Specimen 54-07S-T up to 1 Year

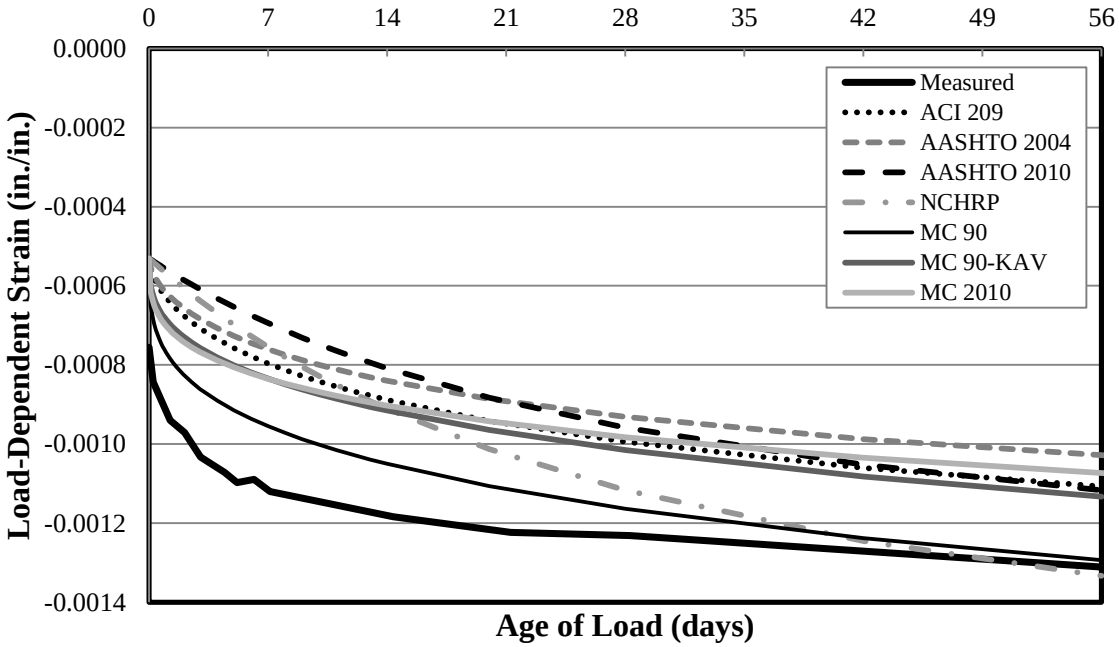

Figure C-9: Load-Induced Strain for Specimen 72-03S-M up to 56 Days

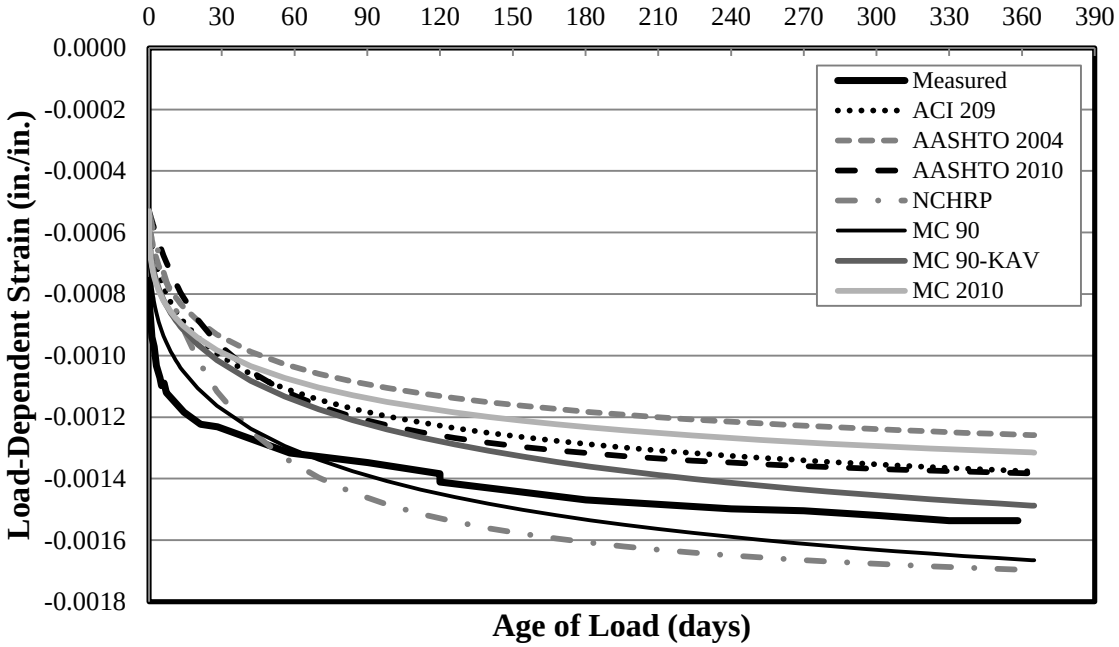

Figure C-10: Load-Induced Strain for Specimen 72-03S-M up to 1 Year

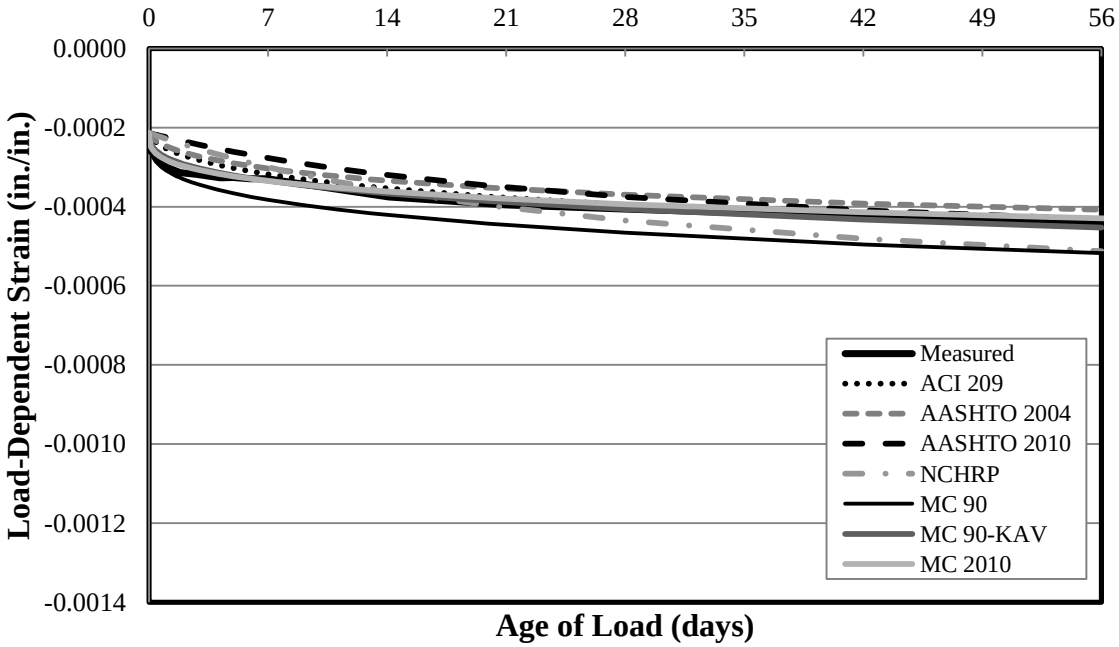

Figure C-11: Load-Induced Strain for Specimen 72-03S-T-U up to 56 Days

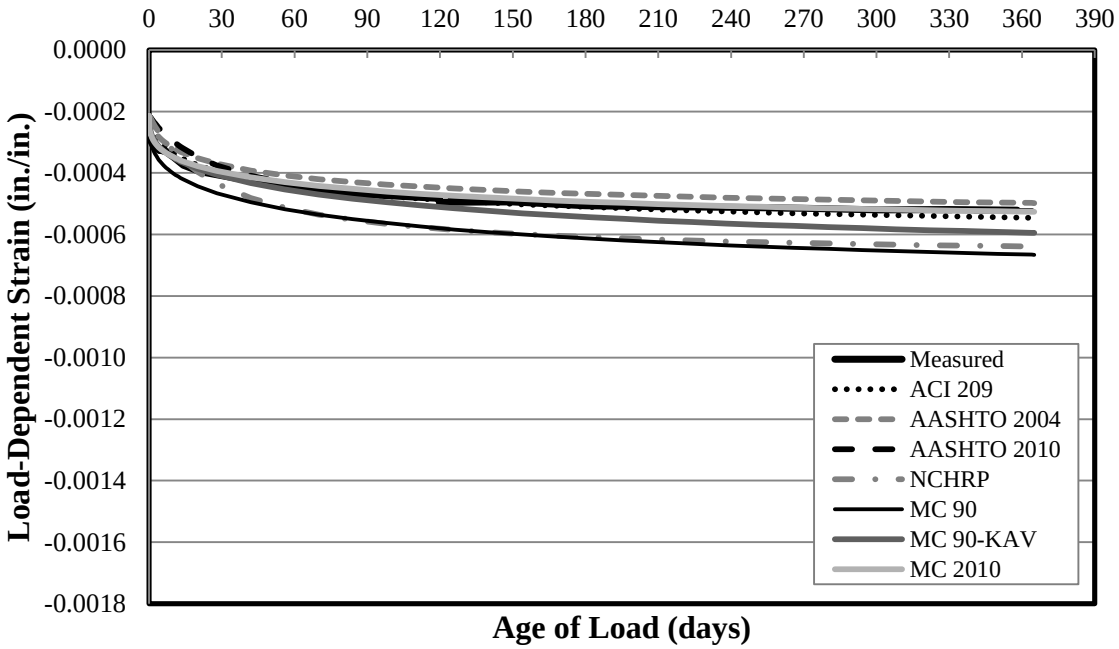

Figure C-12: Load-Induced Strain for Specimen 72-03S-T-U up to 1 Year

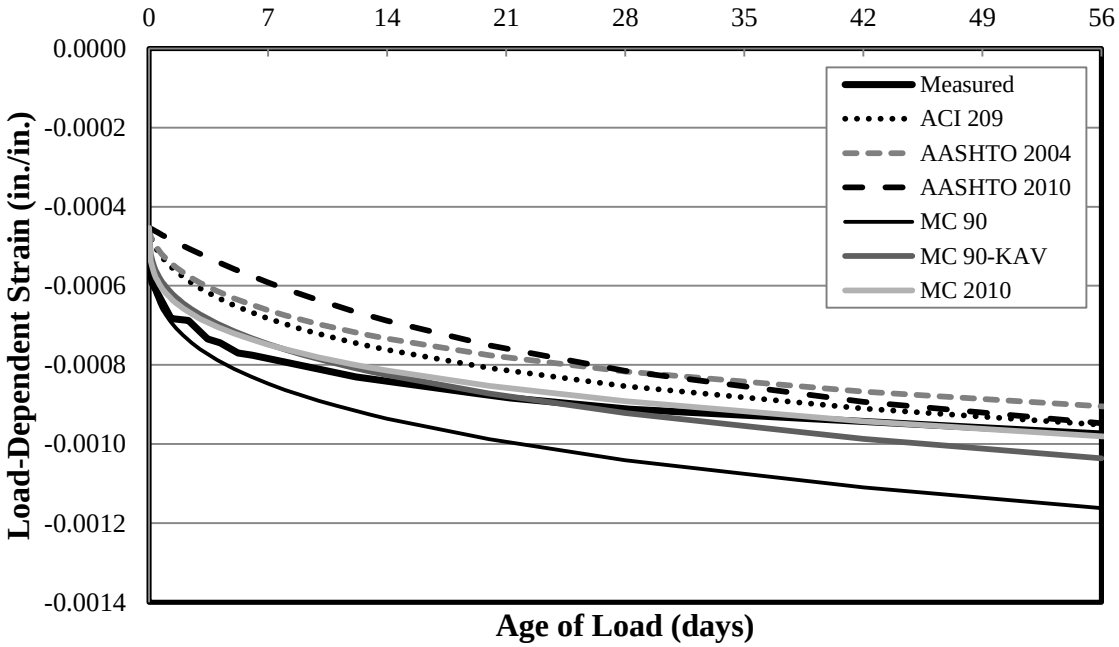

Figure C-13: Load-Induced Strain for Specimen 54-12C-M up to 56 Days

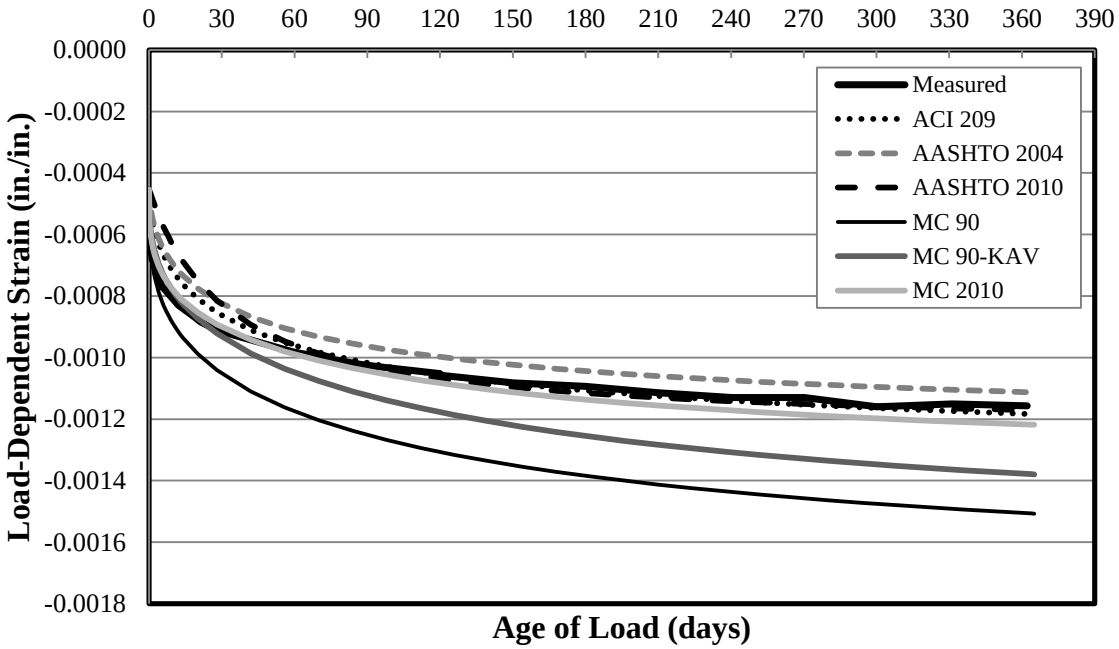

Figure C-14: Load-Induced Strain for Specimen 54-12C-M up to 1 Year

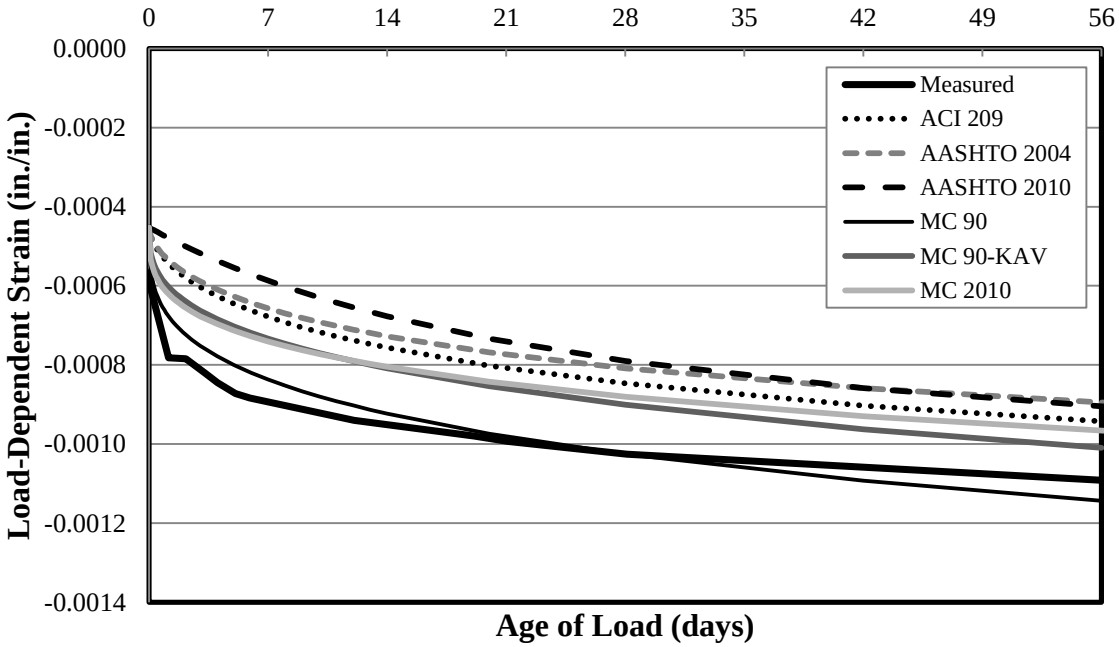

Figure C-15: Load-Induced Strain for Specimen 54-12C-T up to 56 Days

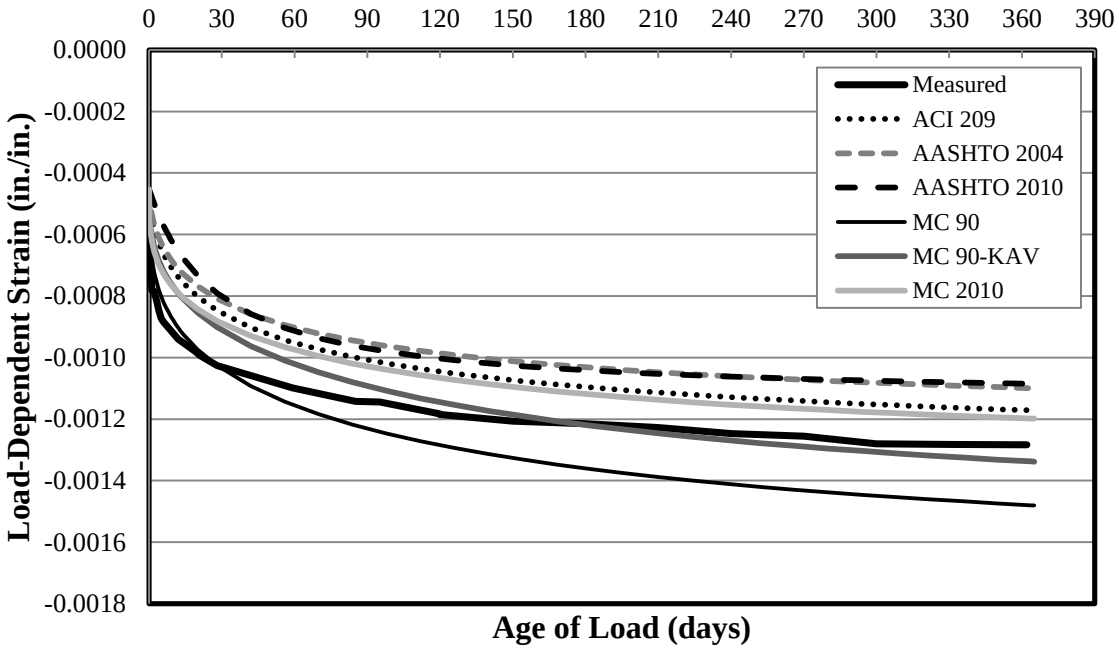

Figure C-16: Load-Induced Strain for Specimen 54-12C-T up to 1 Year

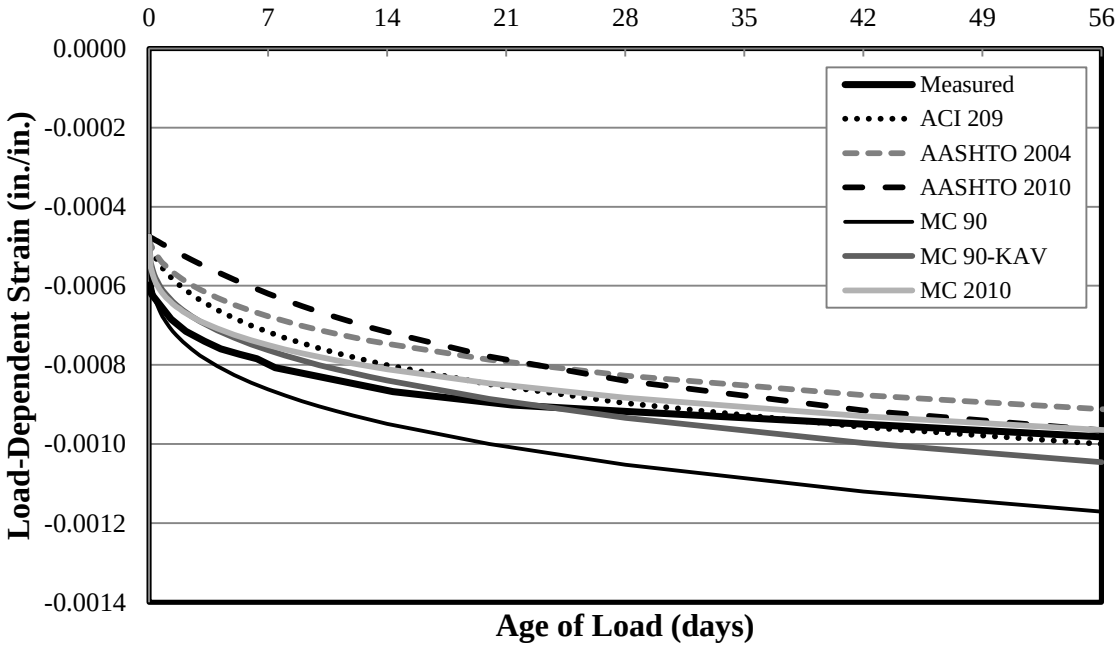

Figure C-17: Load-Induced Strain for Specimen 72-11C-M up to 56 Days

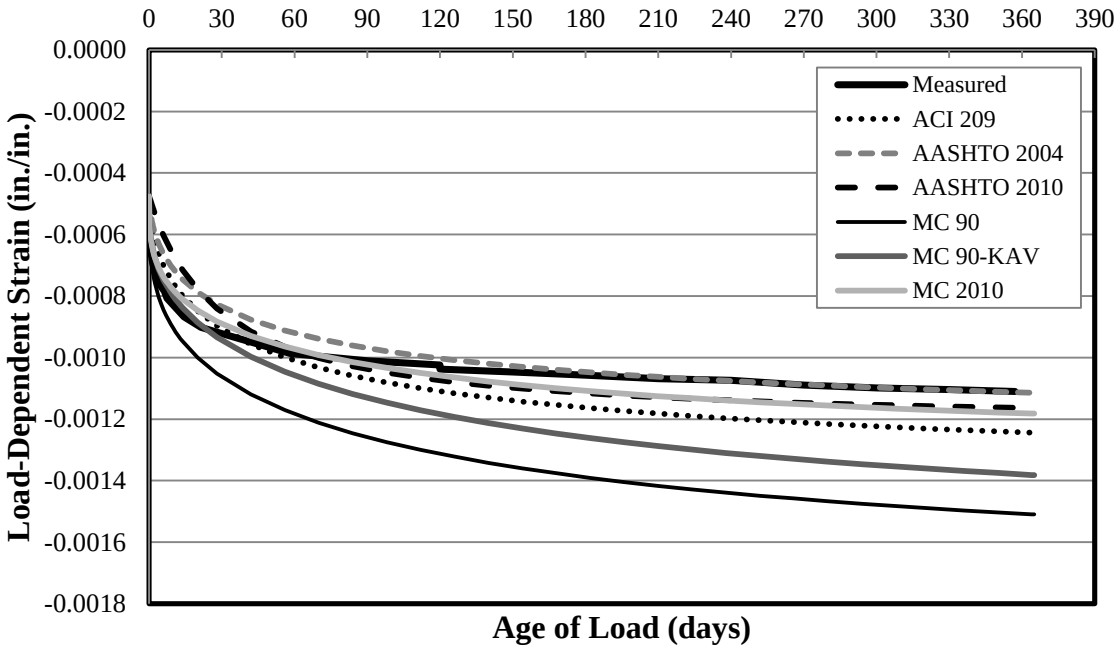

Figure C-18: Load-Induced Strain for Specimen 72-11C-M up to 1 Year

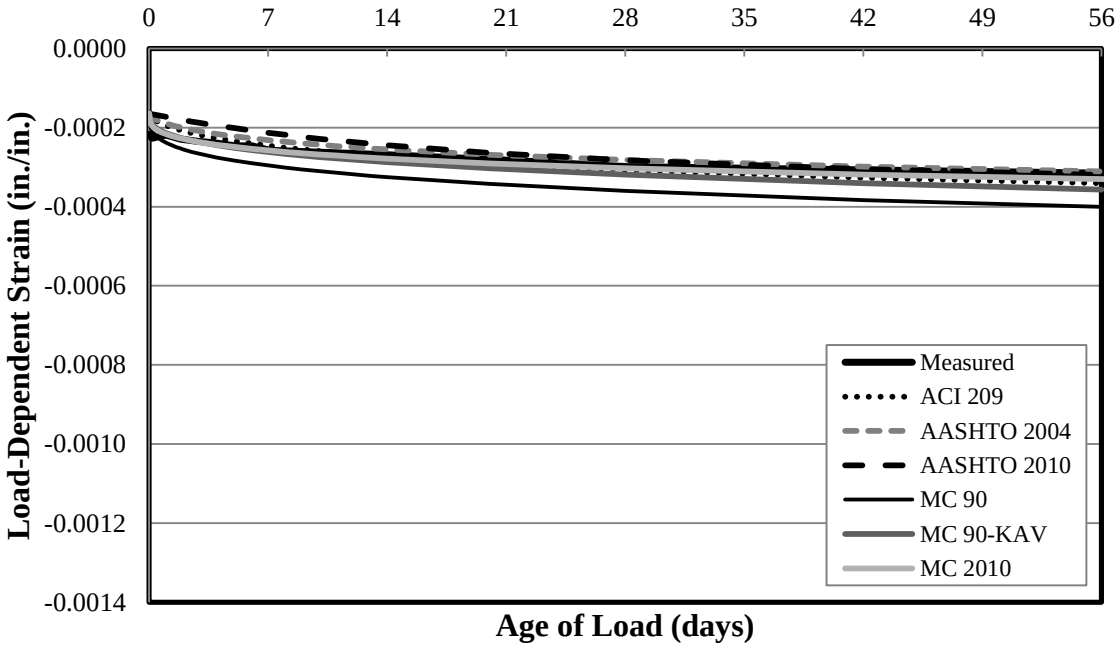

Figure C-19: Load-Induced Strain for Specimen 72-11C-T-U up to 56 Days

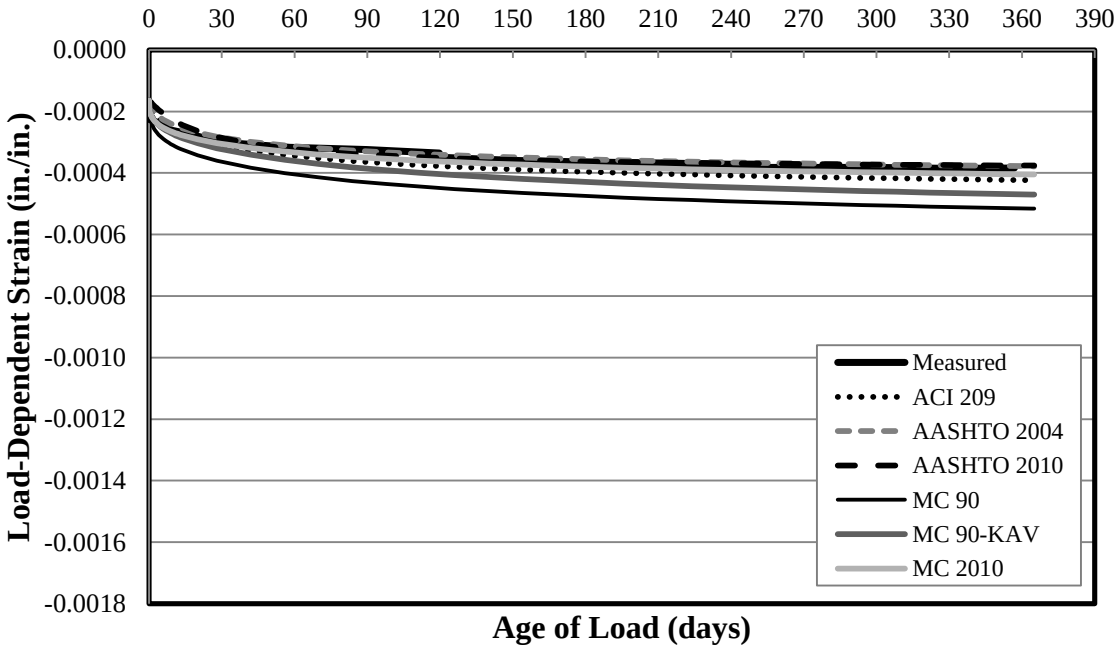

Figure C-20: Load-Induced Strain for Specimen 72-11C-T-U up to 1 Year

C.2. SHRINKAGE STRAIN VERSUS TIME

Figure C-21

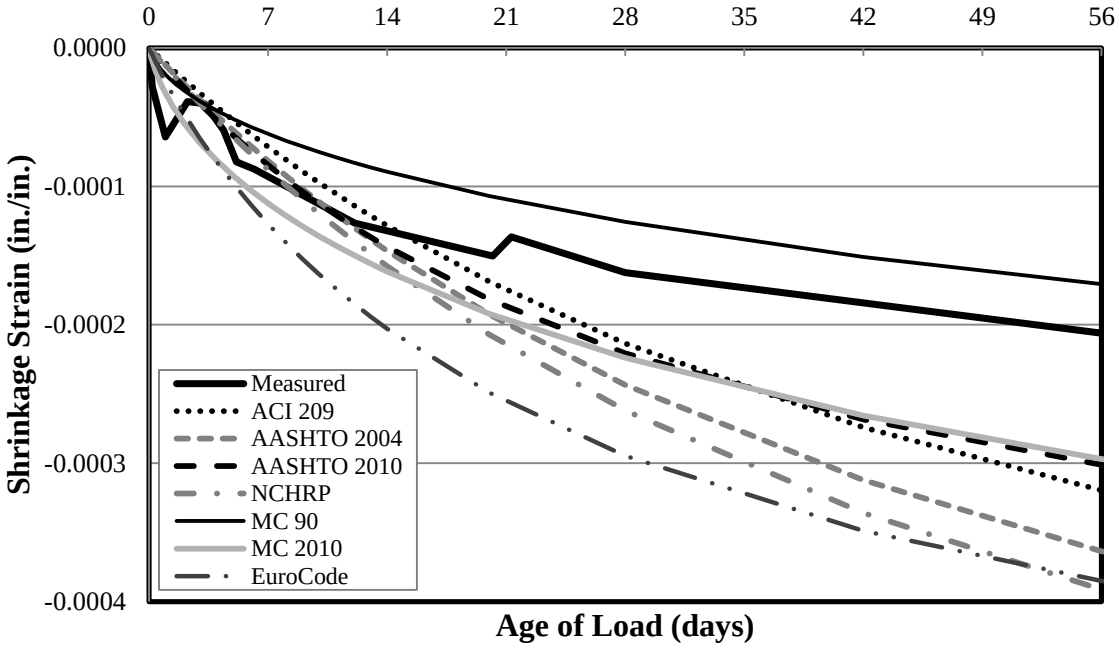

Figure C-21 through Figure C-40**Error! Reference source not found.** contains all shrinkage strain data collected during this study for each of the ten sets of specimen. Each figure plots the measured shrinkage strain for a specific specimen as well as predicted strain for that specimen against the age of load and is presented at 56 days and 1 year. The prediction methods used for shrinkage strain are: ACI 209, AASHTO 2004, AASHTO 2010, NCHRP 628, MC 90, MC 2010, and Eurocode. MC 90-99 is effectively equal to MC 2010 and MC-KAV is equal to MC-90, and these methods are not shown. Also, for conventionally vibrated concrete mixtures, the shrinkage strain predicted by NCHRP 628 is equal to that predicted by AASHTO 2004.

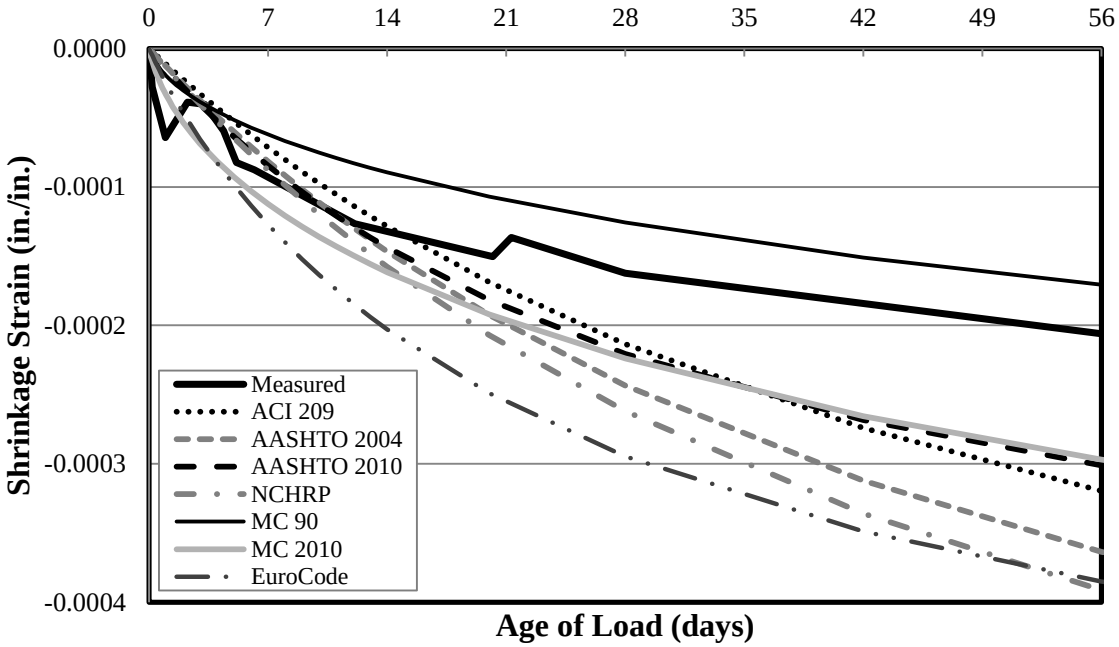

Figure C-21: Shrinkage Strain for Specimen 54-03S-M* up to 56 Days

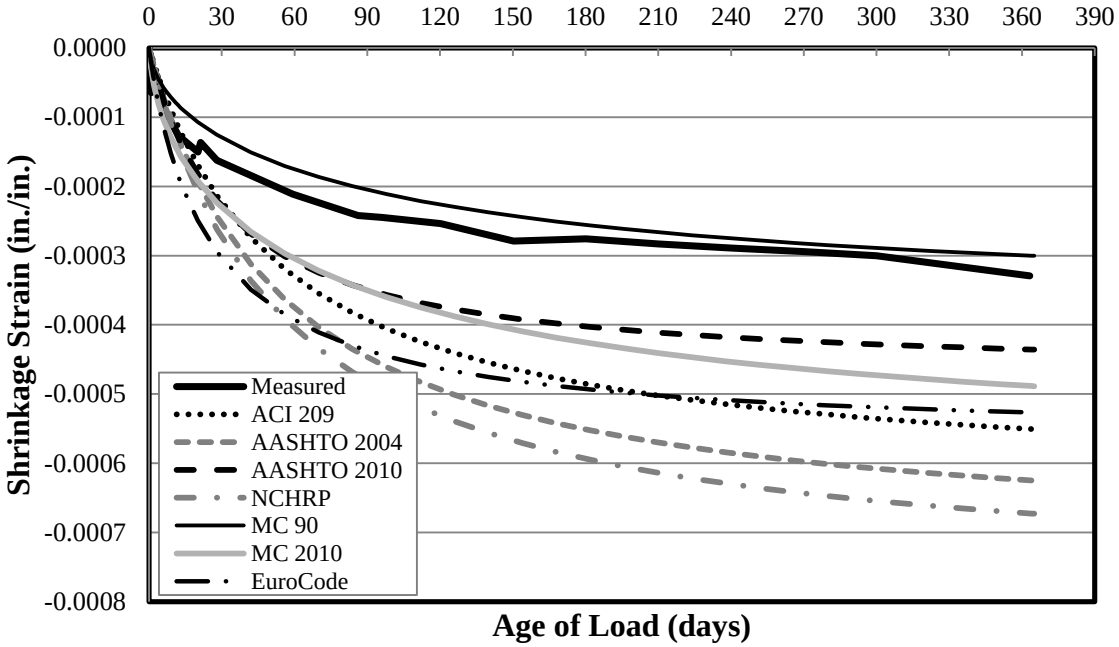

Figure C-22: Shrinkage Strain for Specimen 54-03S-M* up to 1 Year

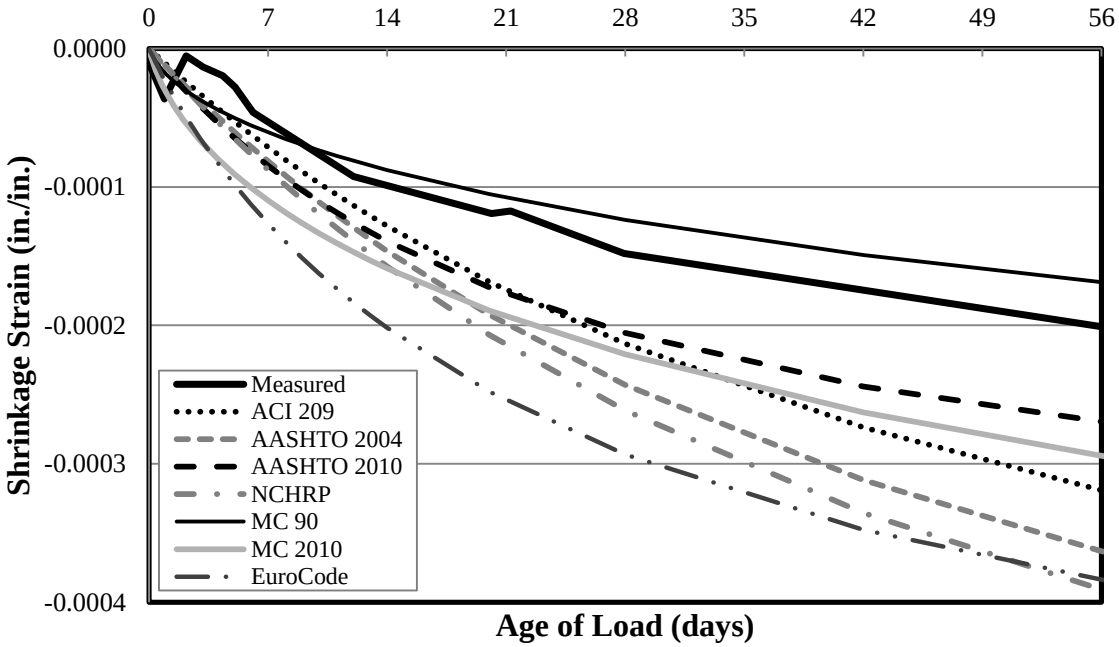

Figure C-23: Shrinkage Strain for Specimen 54-03S-T up to 56 Days

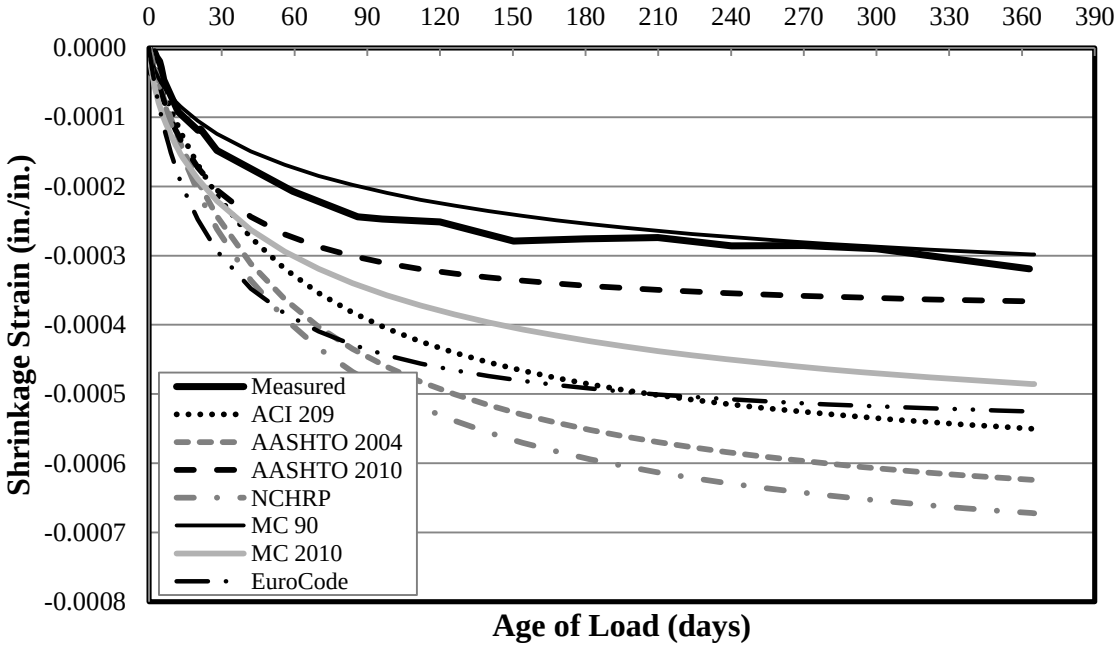

Figure C-24: Shrinkage Strain for Specimen 54-03S-T up to 1 Year

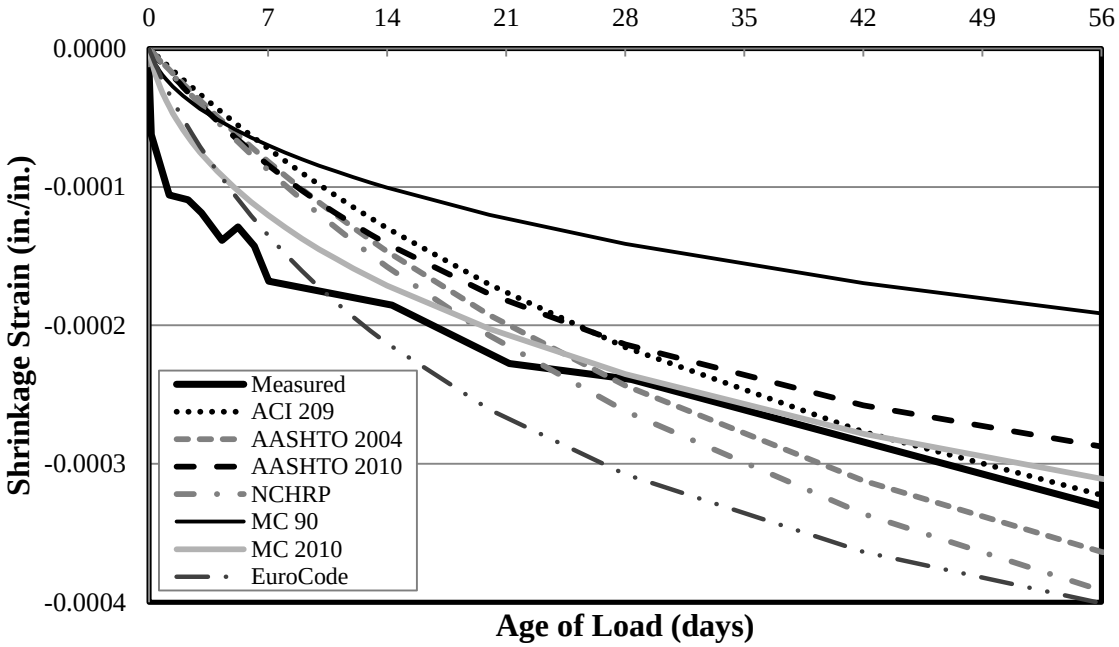

Figure C-25: Shrinkage Strain for Specimen 54-07S-M up to 56 Days

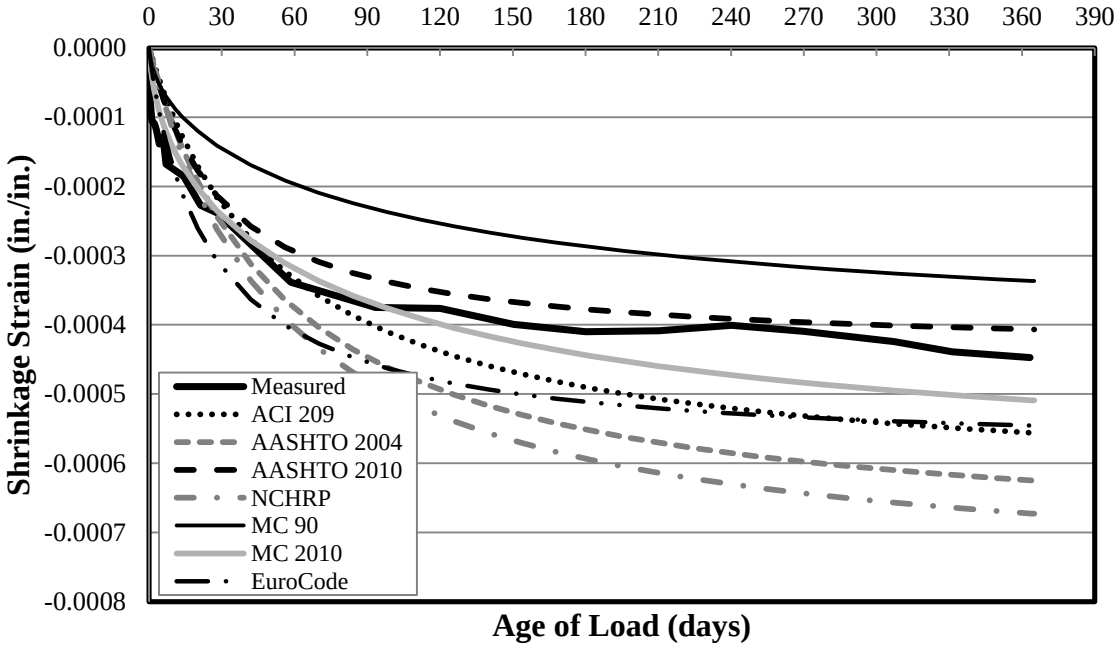

Figure C-26: Shrinkage Strain for Specimen 54-07S-M up to 1 Year

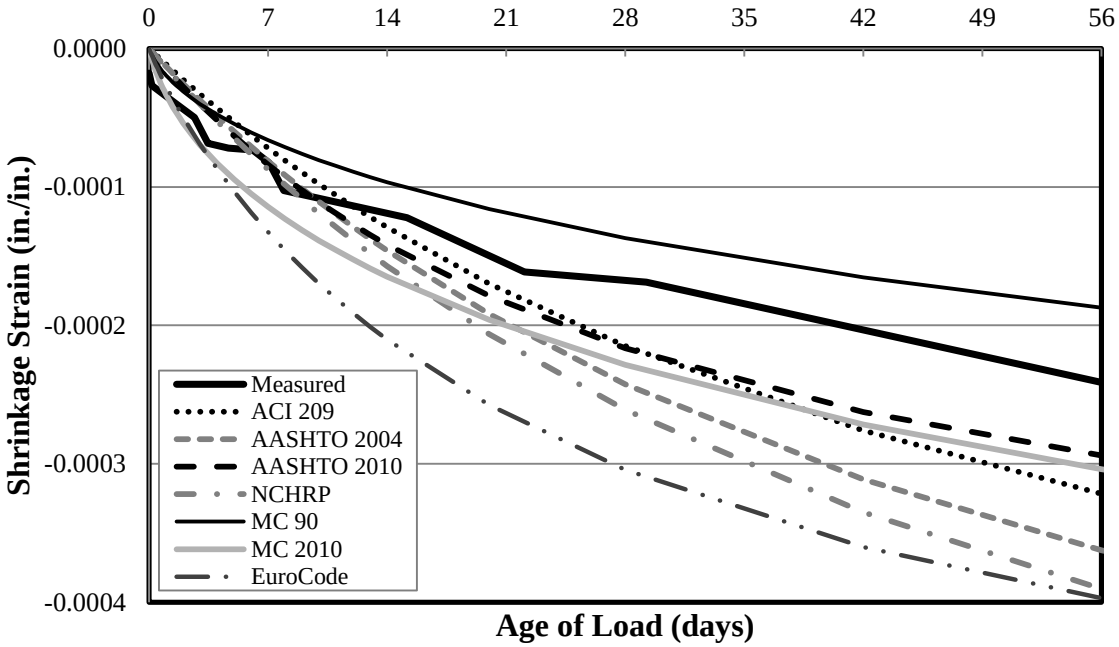

Figure C-27: Shrinkage Strain for Specimen 54-07S-T up to 56 Days

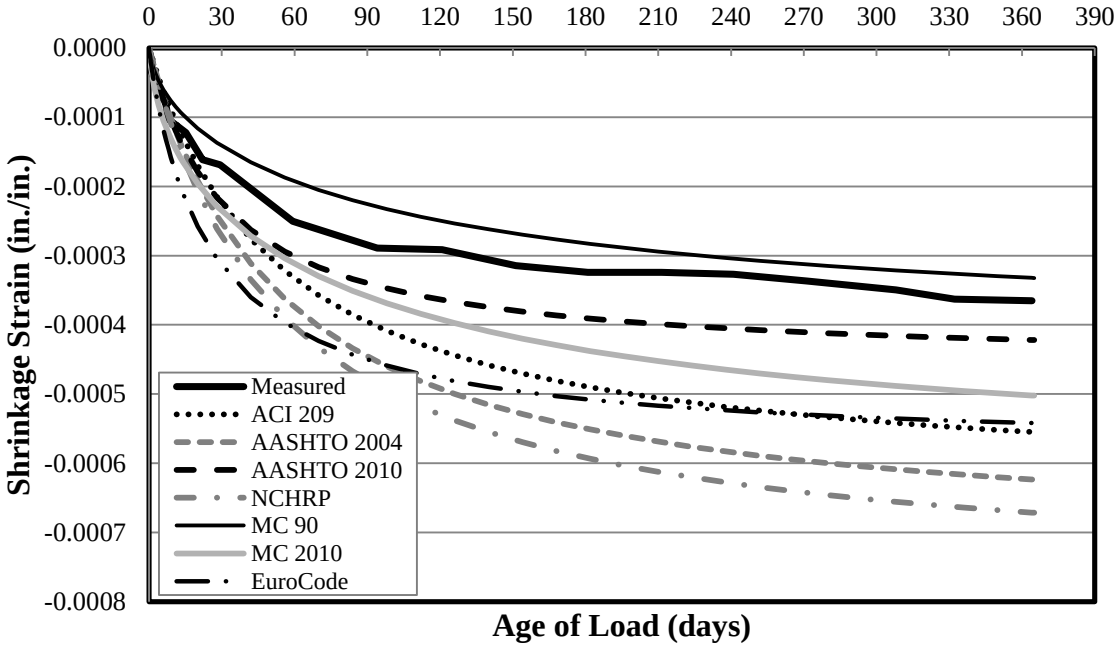

Figure C-28: Shrinkage Strain for Specimen 54-07S-T up to 1 Year

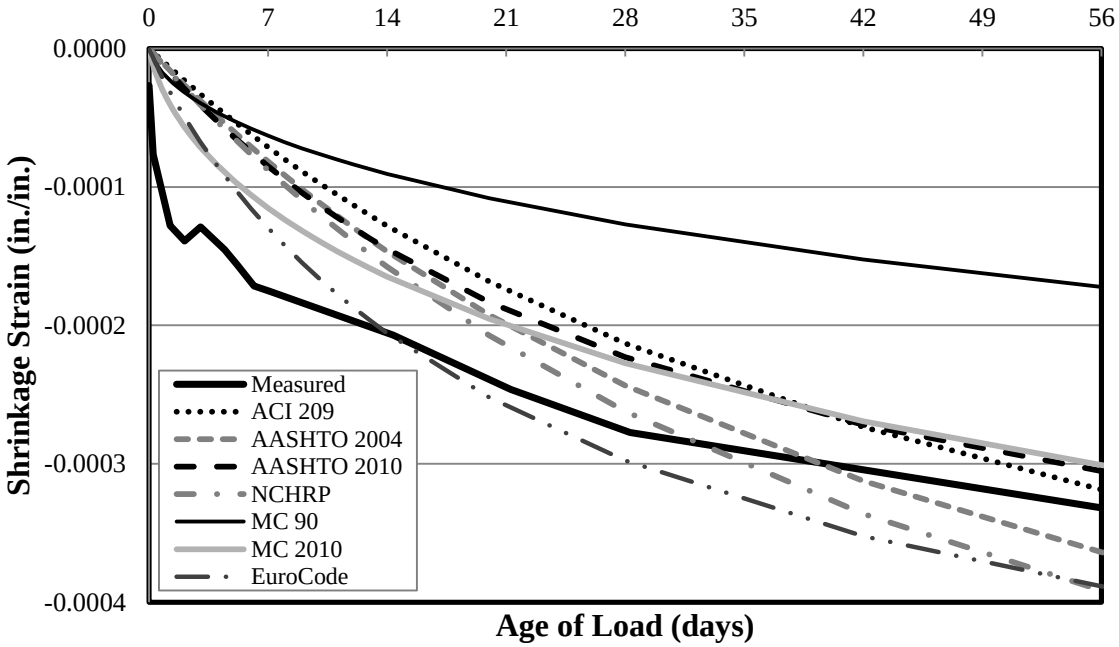

Figure C-29: Shrinkage Strain for Specimen 72-03S-M up to 56 Days

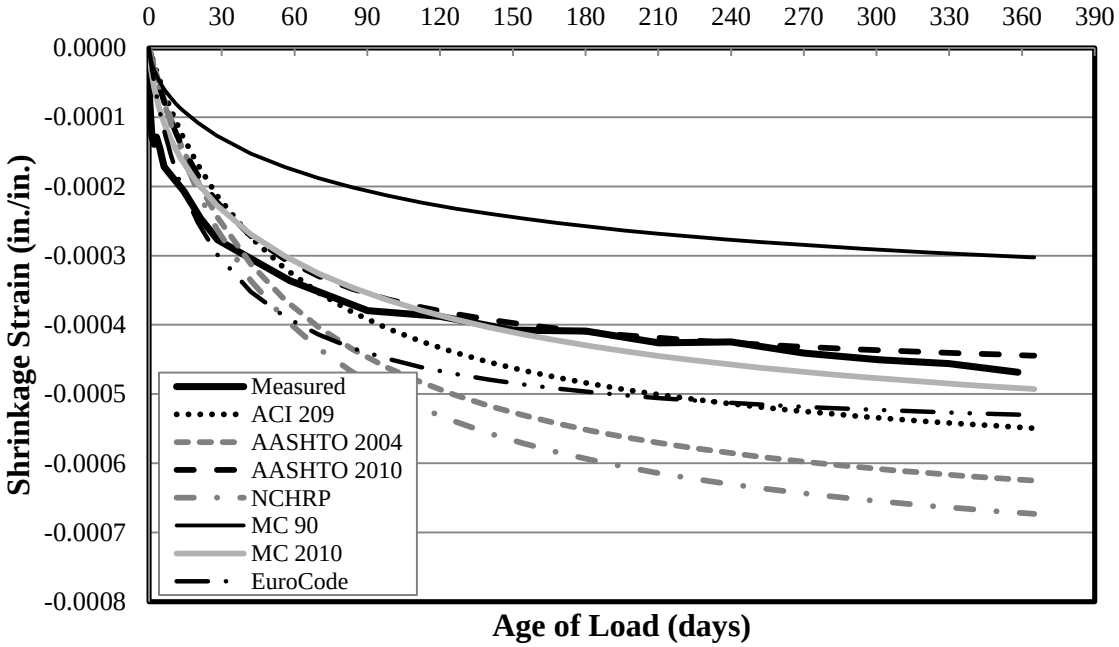

Figure C-30: Shrinkage Strain for Specimen 72-03S-M up to 1 Year

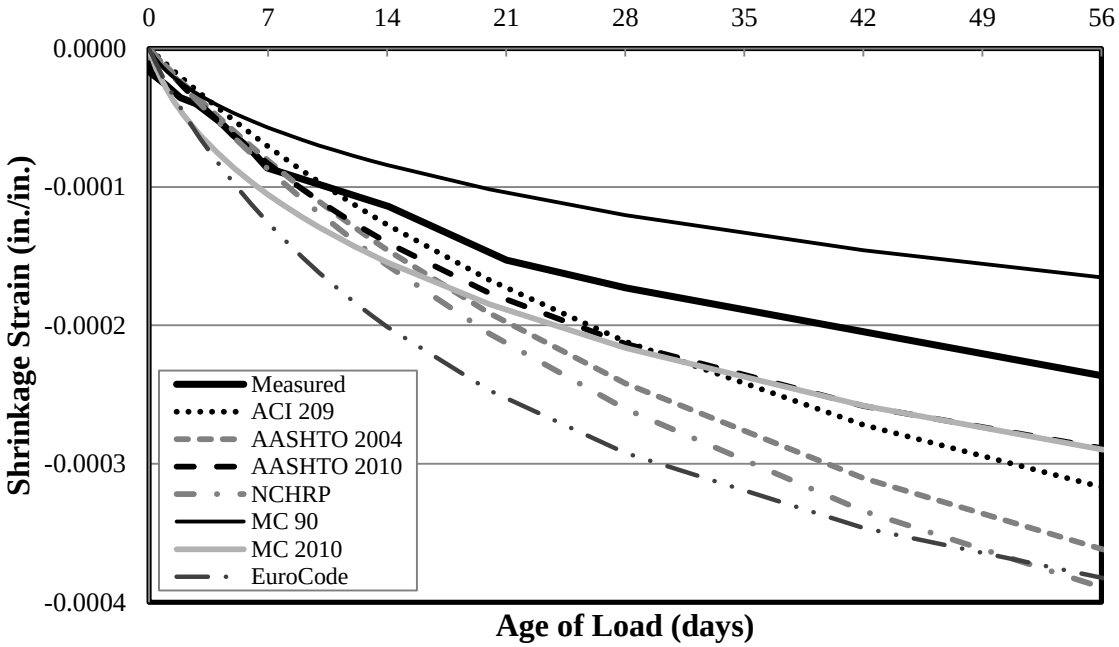

Figure C-31: Shrinkage Strain for Specimen 72-03S-T-U up to 56 Days

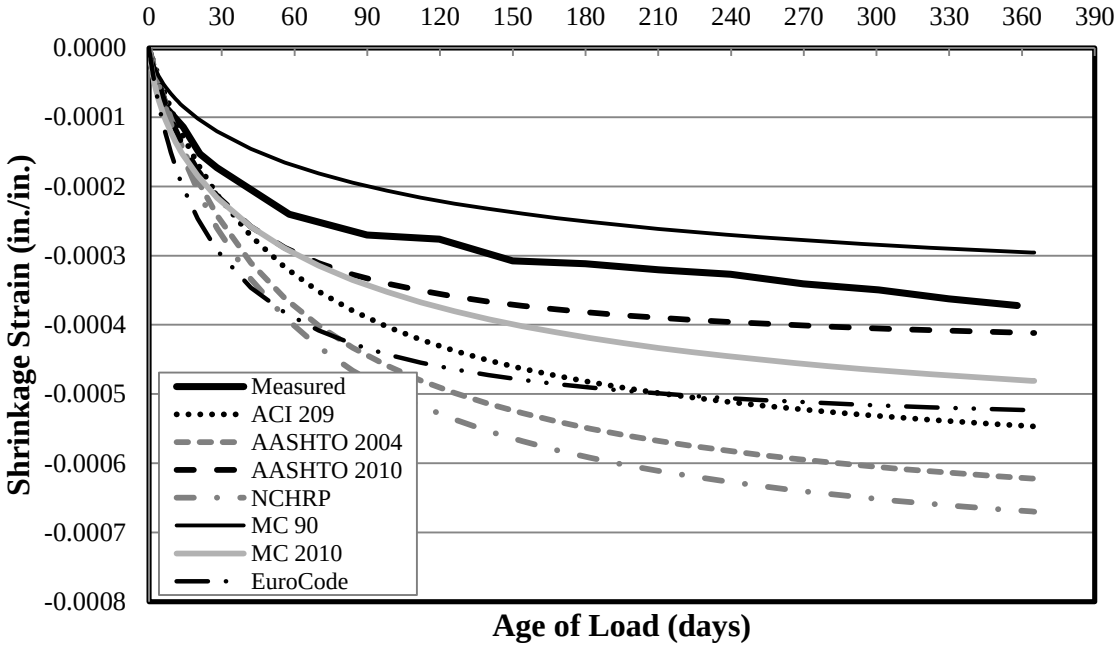

Figure C-32: Shrinkage Strain for Specimen 72-03S-T-U up to 1 Year

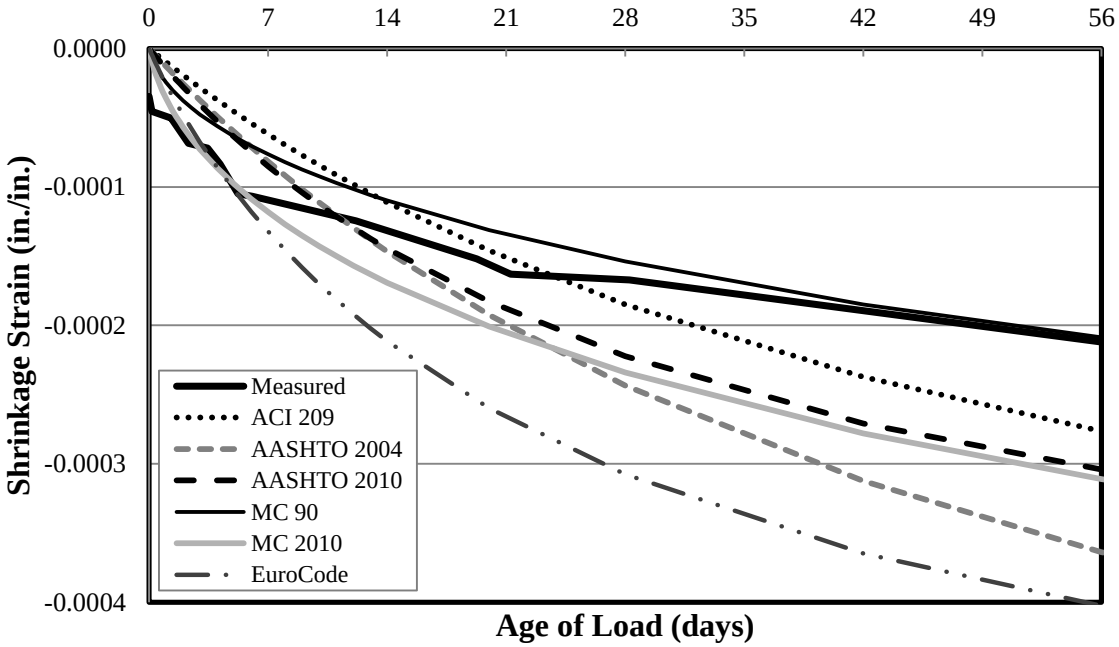

Figure C-33: Shrinkage Strain for Specimen 54-12C-M up to 56 Days

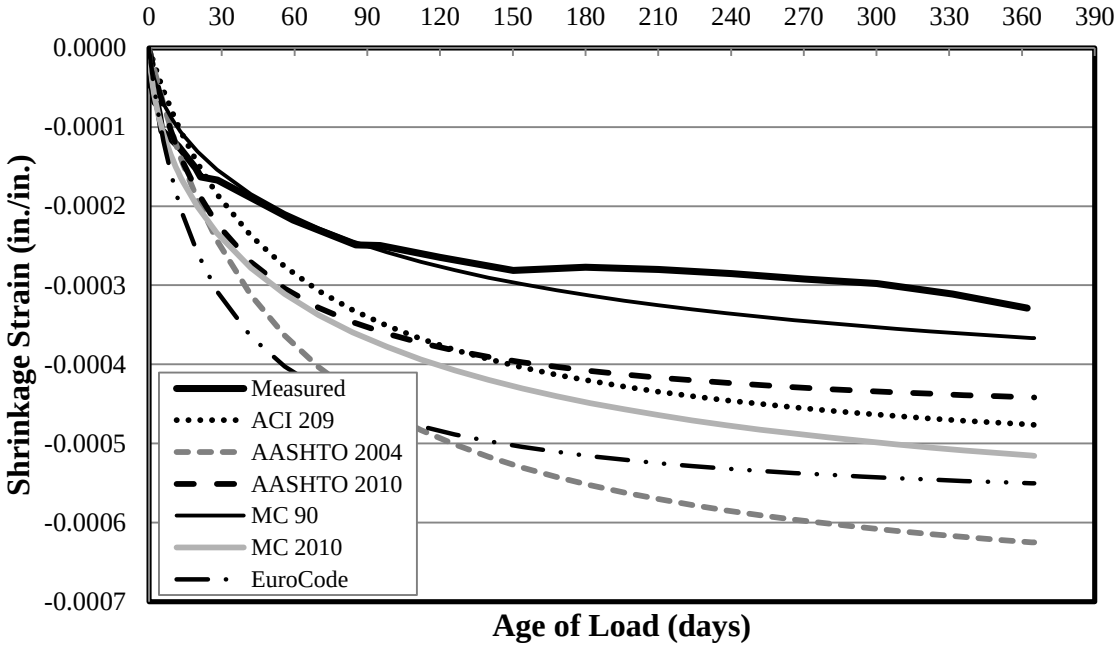

Figure C-34: Shrinkage Strain for Specimen 54-12C-M up to 1 Year

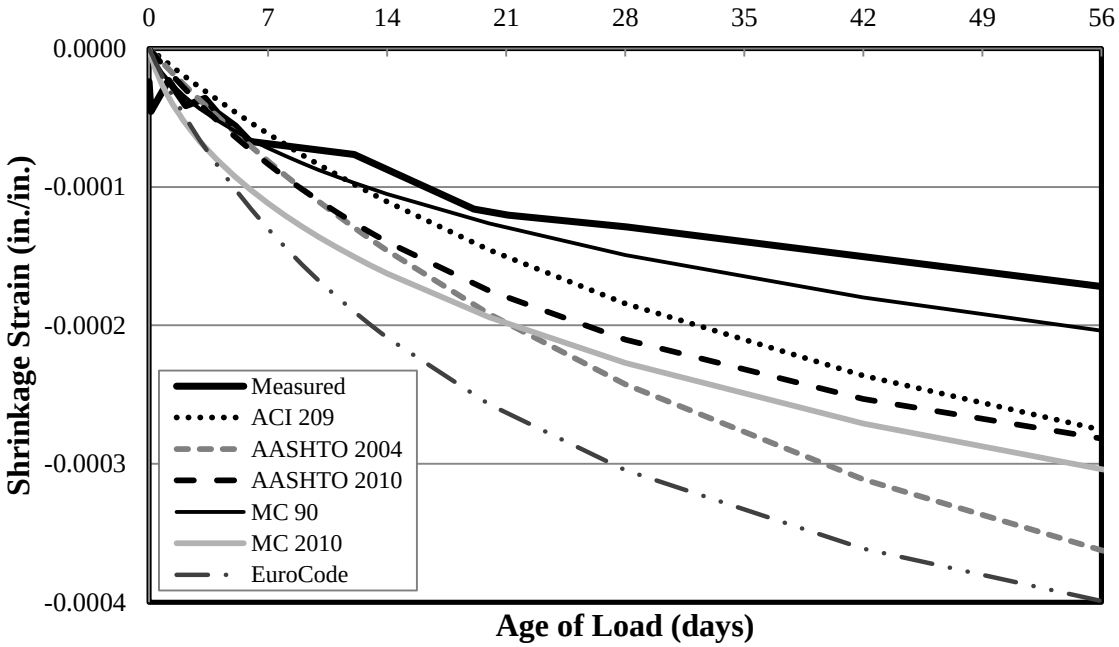

Figure C-35: Shrinkage Strain for Specimen 54-12C-T up to 56 Days

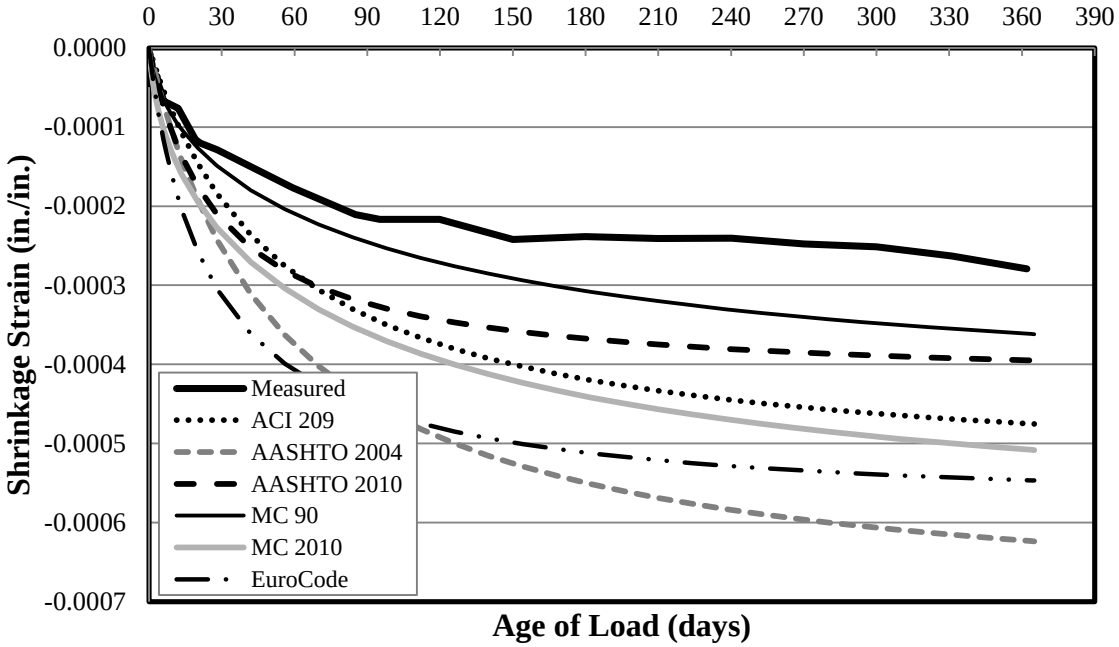

Figure C-36: Shrinkage Strain for Specimen 54-12C-T up to 1 Year

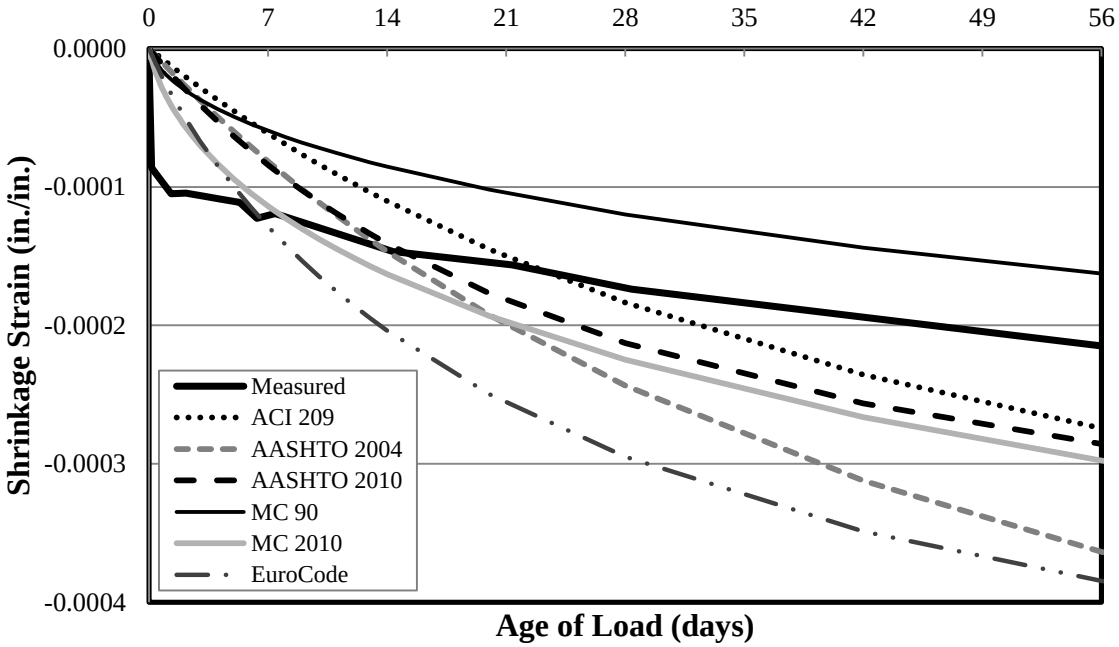

Figure C-37: Shrinkage Strain for Specimen 72-11C-M up to 56 Days

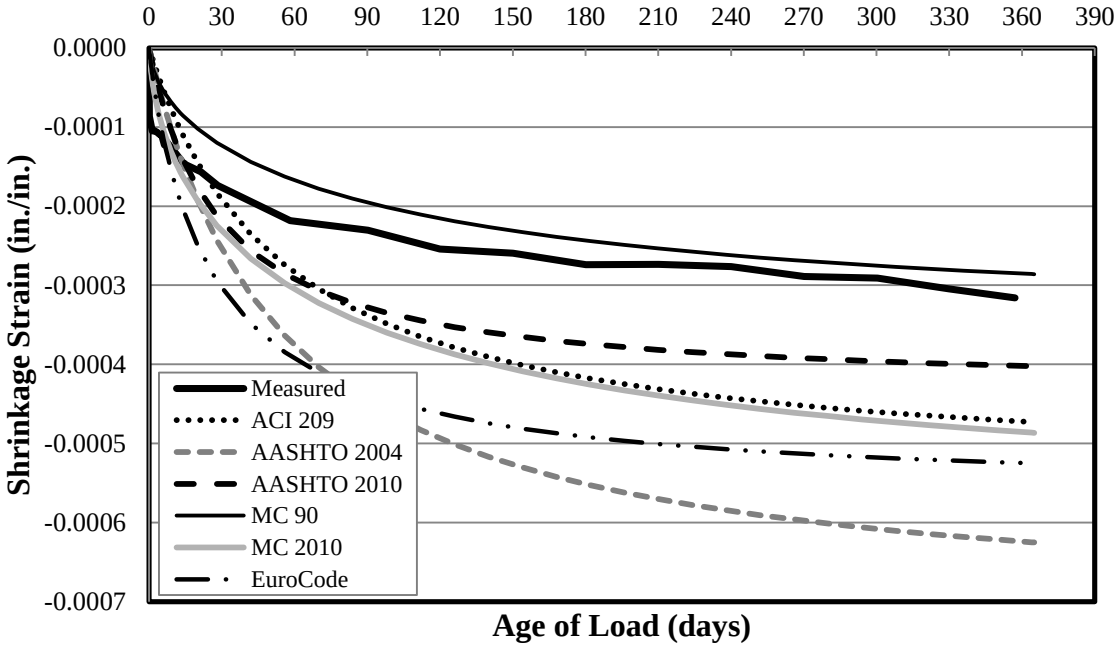

Figure C-38: Shrinkage Strain for Specimen 72-11C-M up to 1 Year

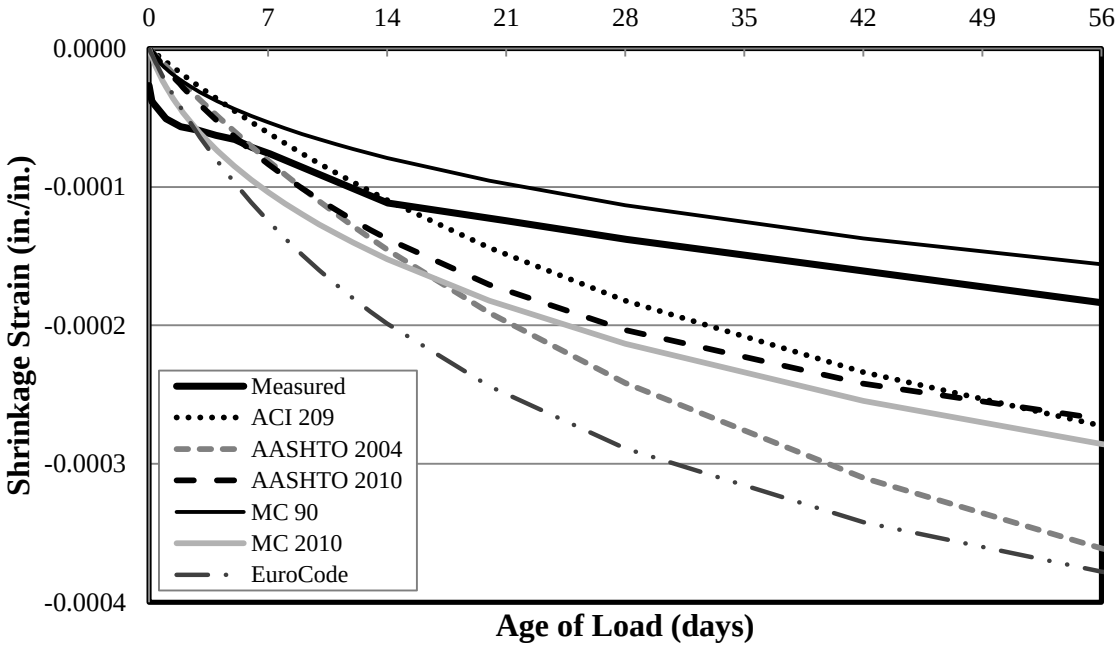

Figure C-39: Shrinkage Strain for Specimen 72-11C-T-U up to 56 Days

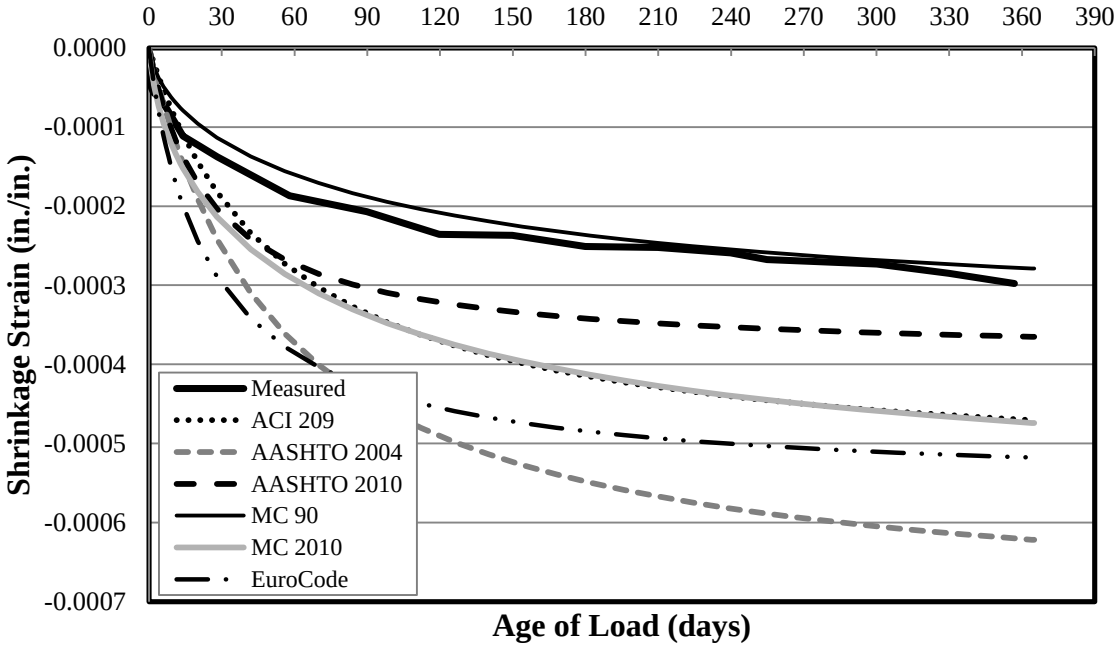

Figure C-40: Shrinkage Strain for Specimen 72-11C-T-U up to 1 Year

C.3. CREEP STRAIN VERSUS TIME

Figure C-41 through Figure C-60 contains all creep strain data collected during this study for each of the ten sets of specimen. Each figure plots the measured creep strain for a specific specimen as well as predicted strain for that specimen against the age of load and is presented at 56 days and 1 year. The prediction methods used for creep strain are: ACI 209, AASHTO 2004, AASHTO 2010, NCHRP 628, MC 90, MC 90-KAV, and MC 2010. MC 90-99 and Eurocode are effectively equal to MC 2010 and are not shown. Also, for conventionally vibrated concrete mixtures, the creep strain predicted by NCHRP 628 is equal to that predicted by AASHTO 2010.

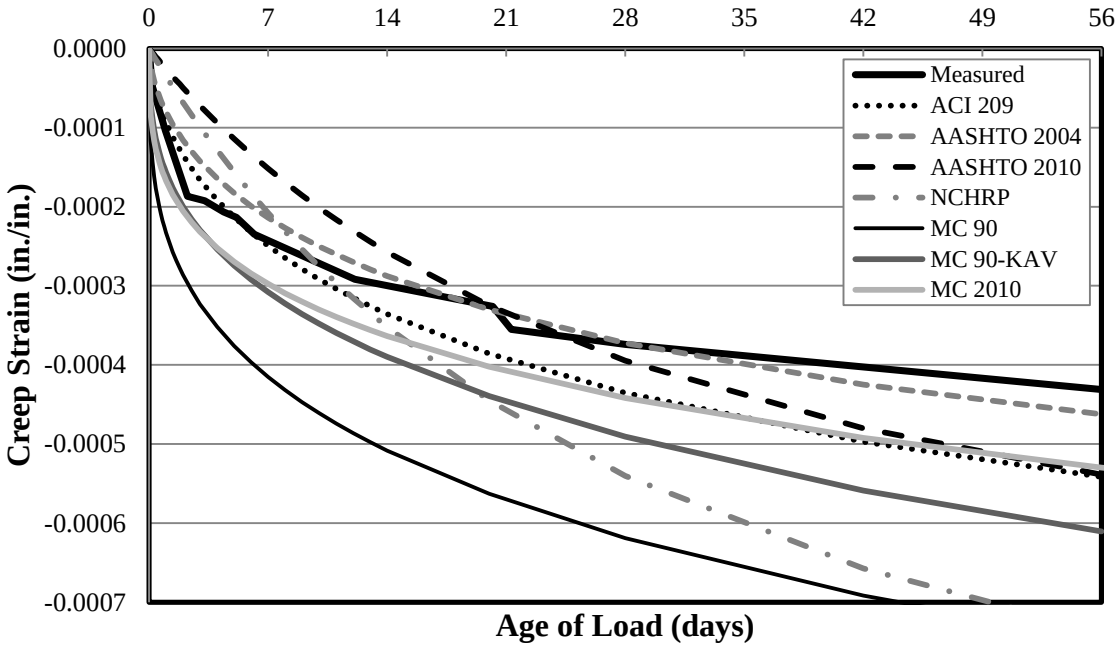

Figure C-41: Creep Strain for Specimen 54-03S-M* up to 56 Days

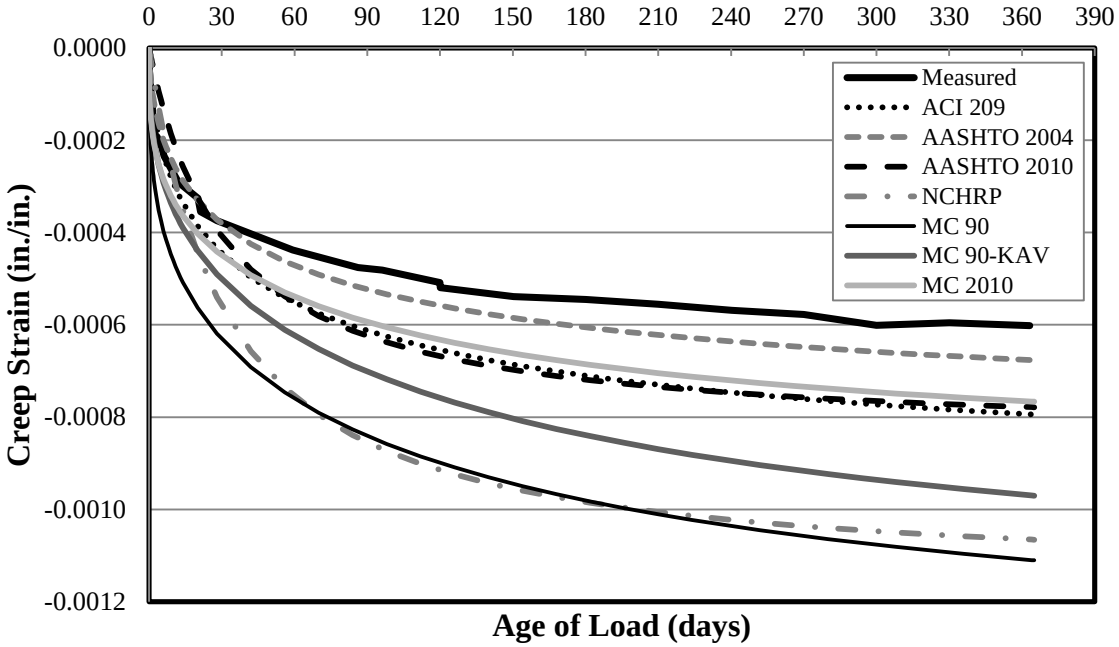

Figure C-42: Creep Strain for Specimen 54-03S-M* up to 1 Year

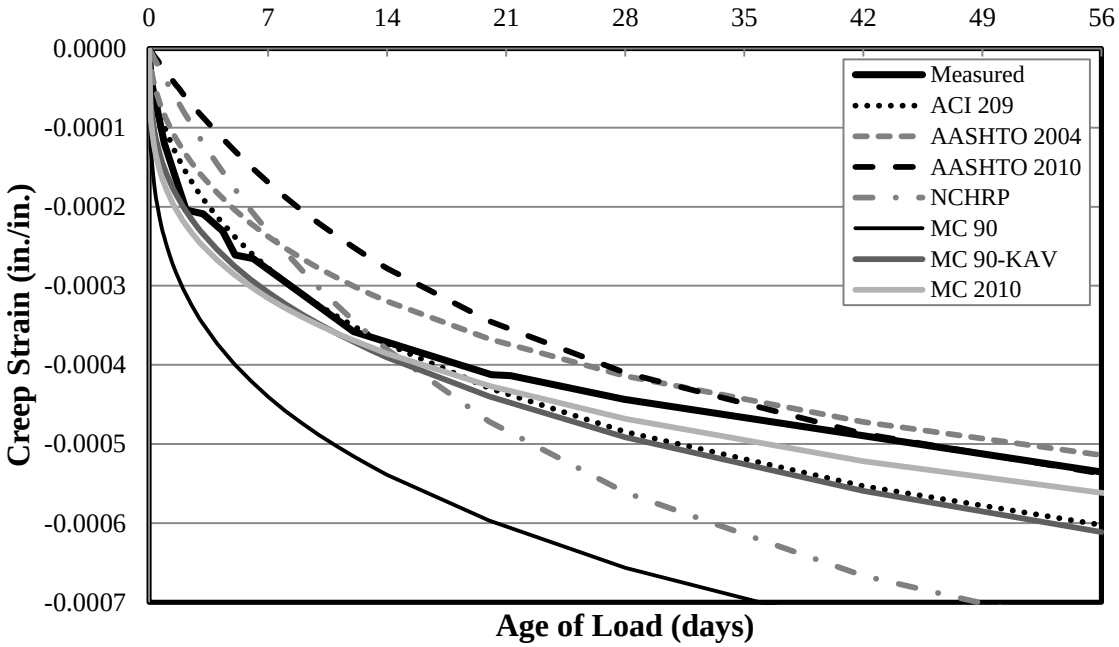

Figure C-43: Creep Strain for Specimen 54-03S-T up to 56 Days

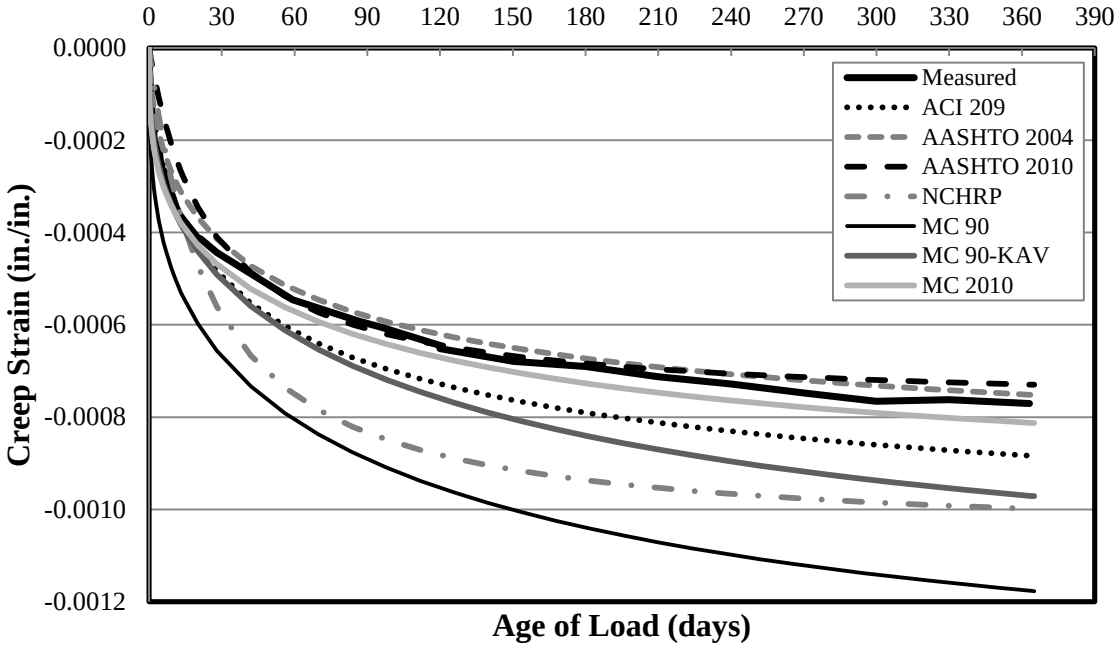

Figure C-44: Creep Strain for Specimen 54-03S-T up to 1 Year

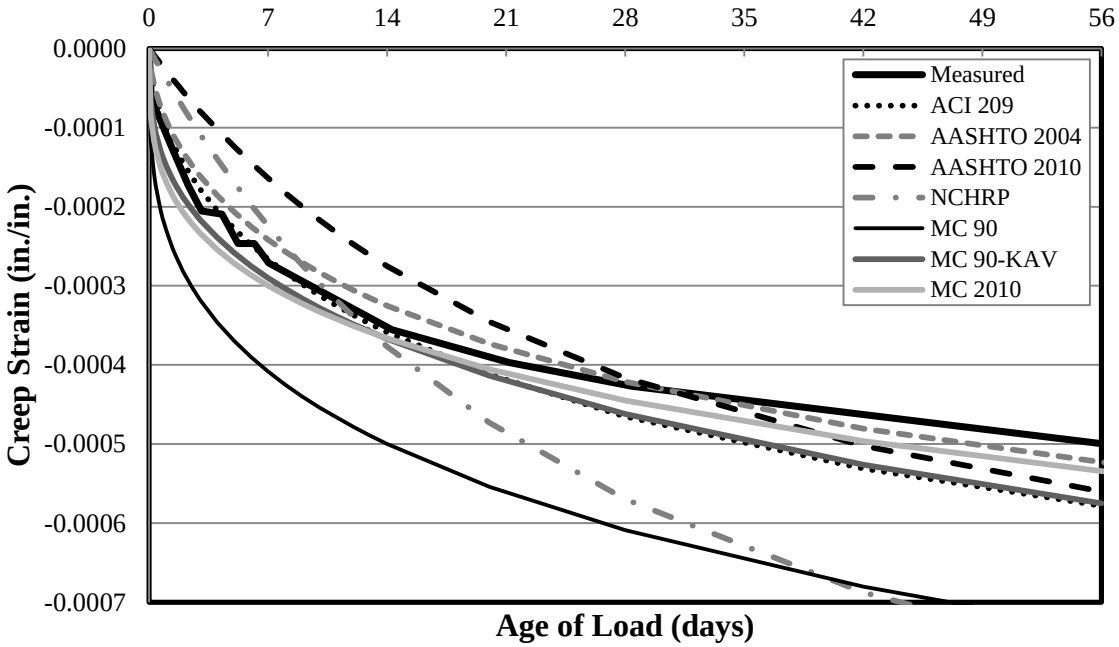

Figure C-45: Creep Strain for Specimen 54-07S-M up to 56 Days

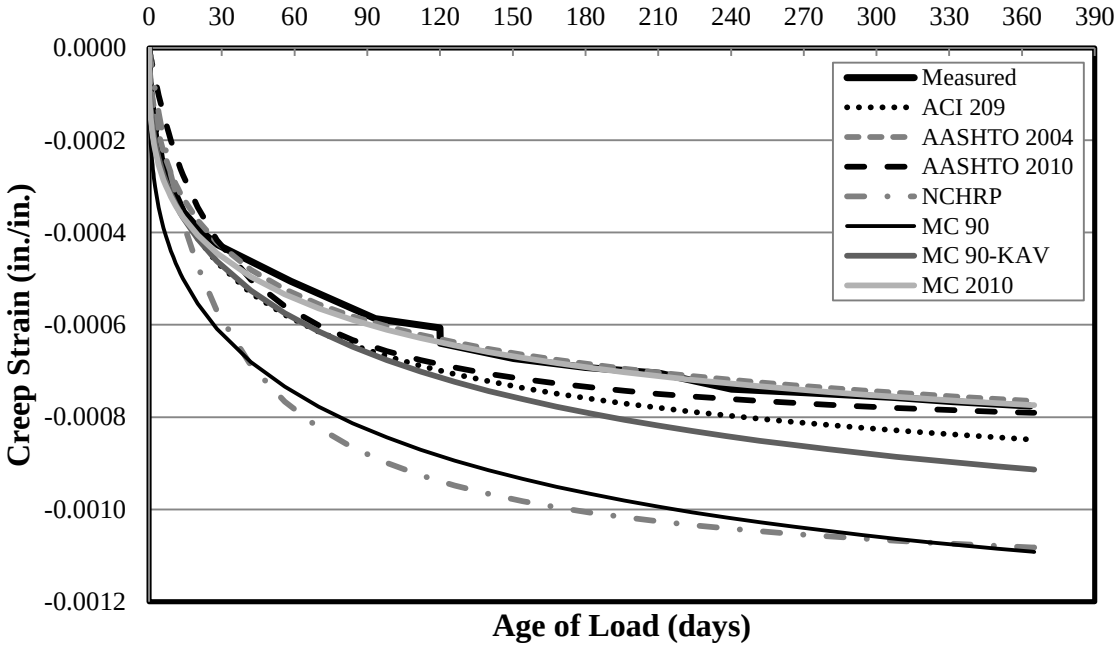

Figure C-46: Creep Strain for Specimen 54-07S-M up to 1 Year

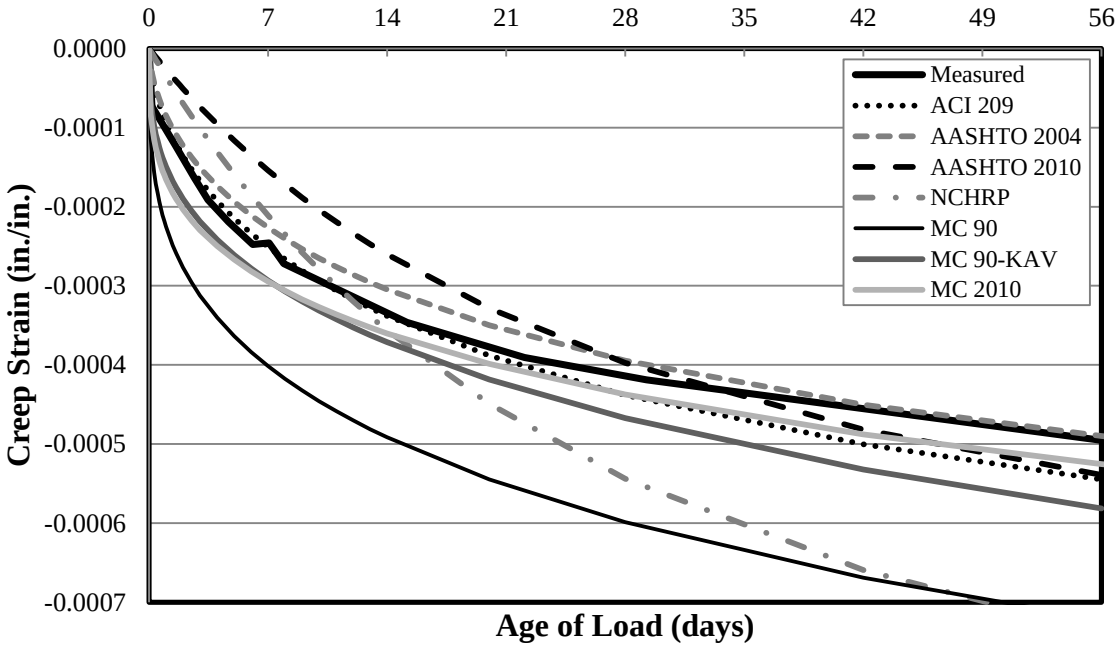

Figure C-47: Creep Strain for Specimen 54-07S-T up to 56 Days

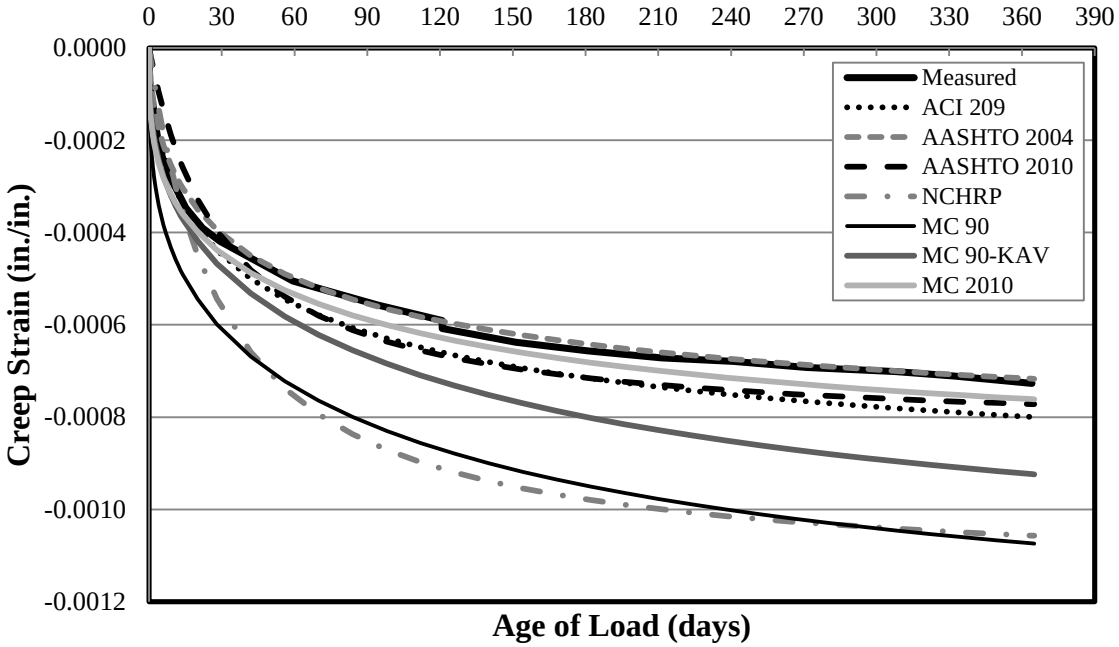

Figure C-48: Creep Strain for Specimen 54-07S-T up to 1 Year

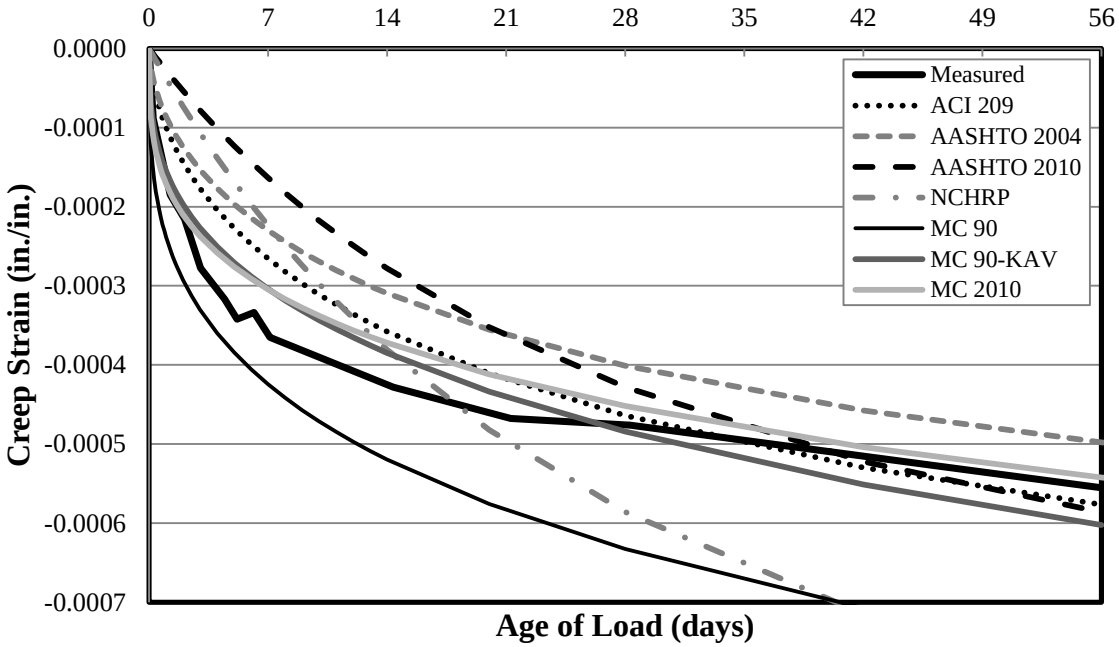

Figure C-49: Creep Strain for Specimen 72-03S-M up to 56 Days

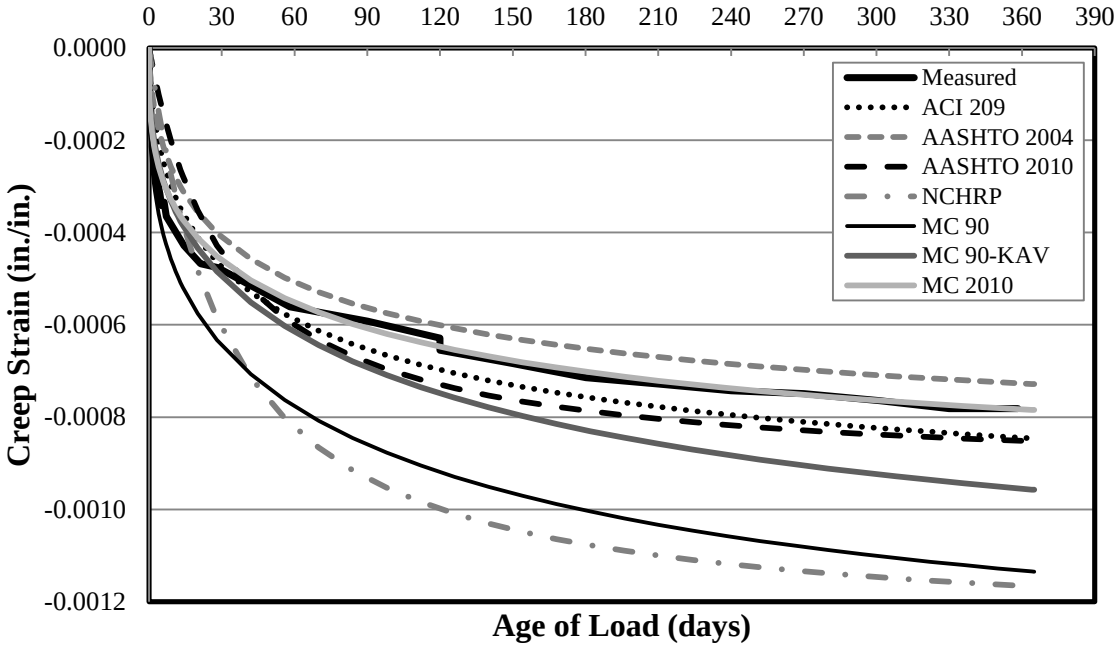

Figure C-50: Creep Strain for Specimen 72-03S-M up to 1 Year

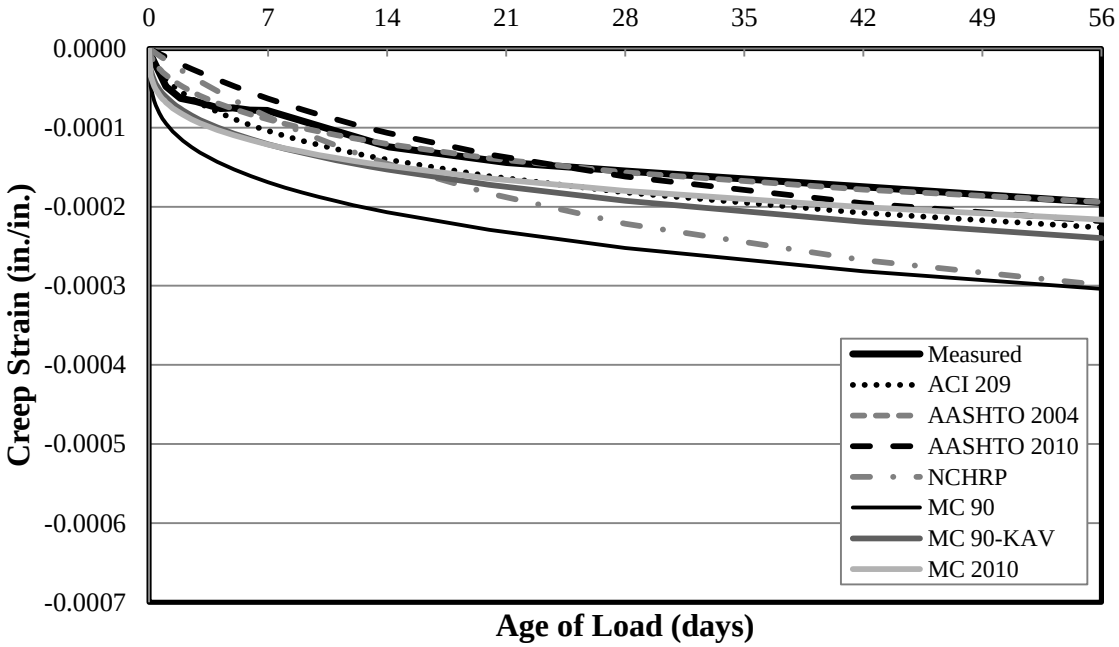

Figure C-51: Creep Strain for Specimen 72-03S-T-U up to 56 Days

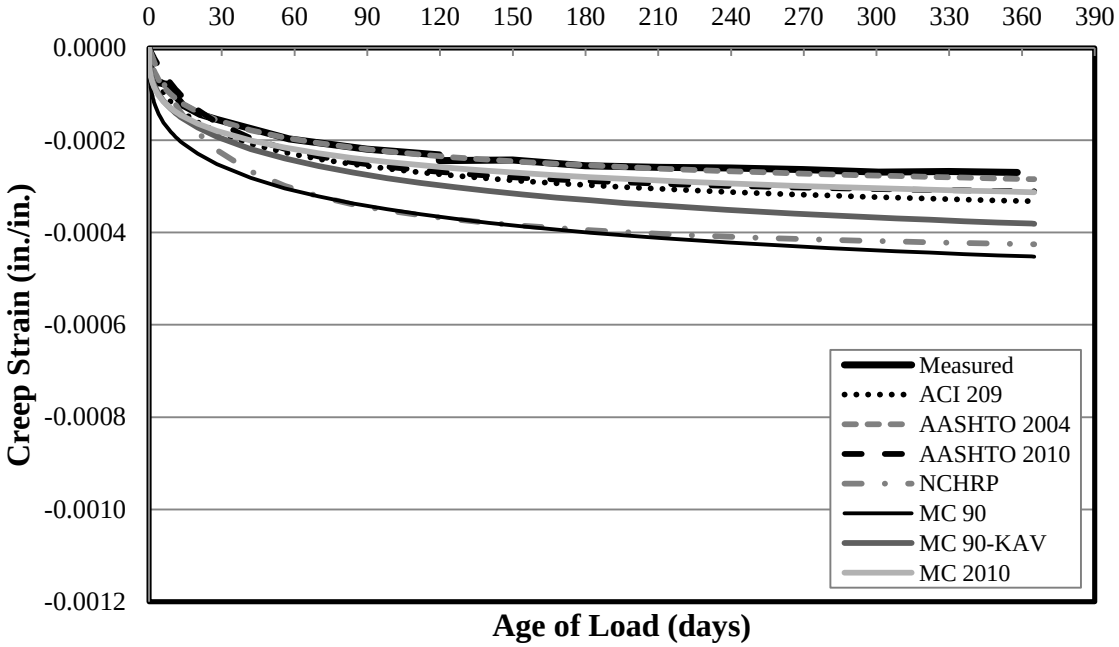

Figure C-52: Creep Strain for Specimen 72-03S-T-U up to 1 Year

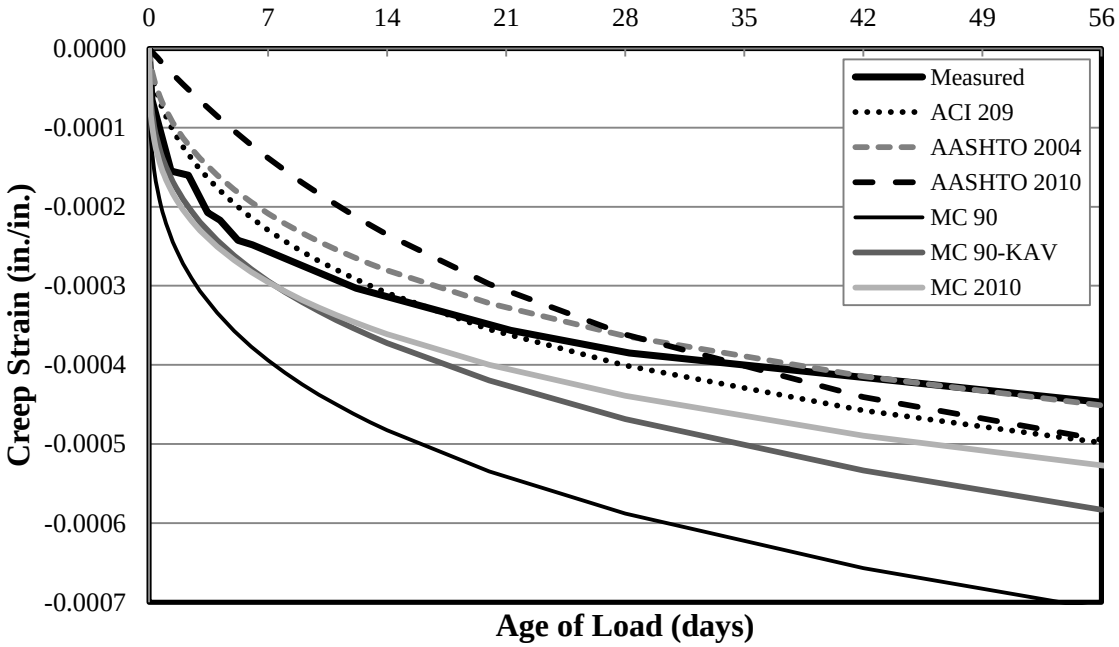

Figure C-53: Creep Strain for Specimen 54-12C-M up to 56 Days

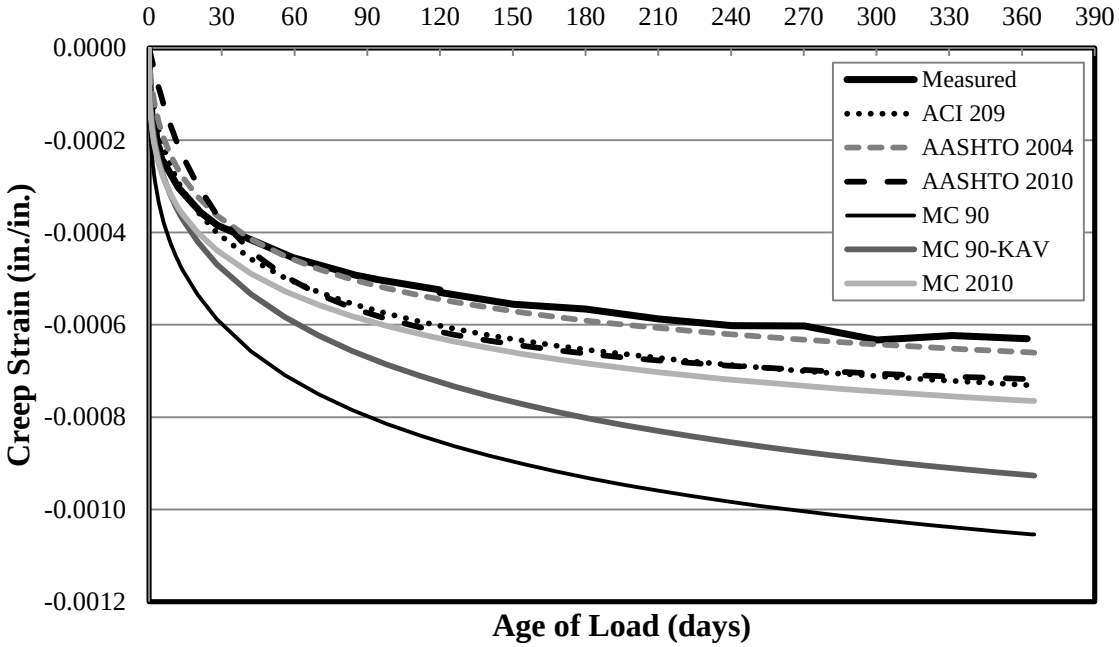

Figure C-54: Creep Strain for Specimen 54-12C-M up to 1 Year

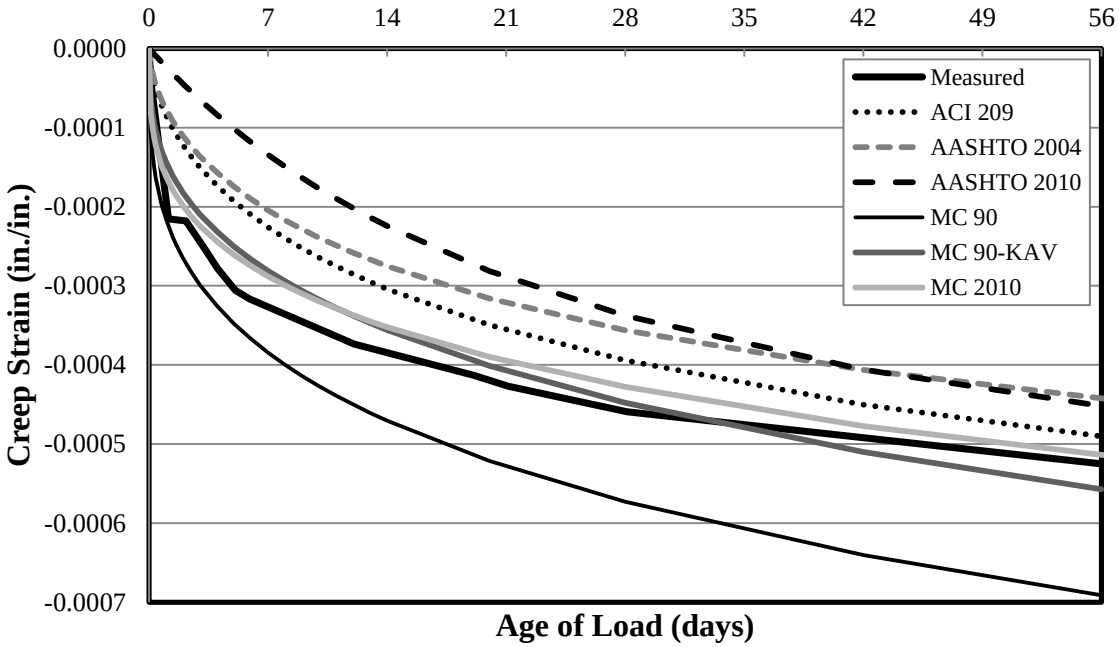

Figure C-55: Creep Strain for Specimen 54-12C-T up to 56 Days

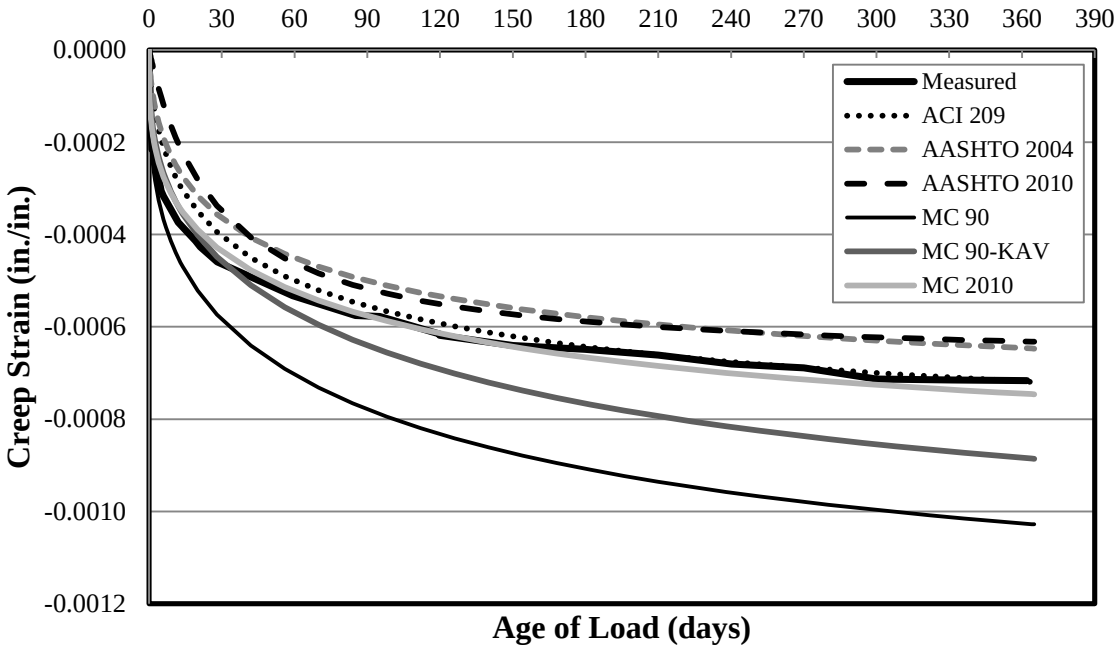

Figure C-56: Creep Strain for Specimen 54-12C-T up to 1 Year

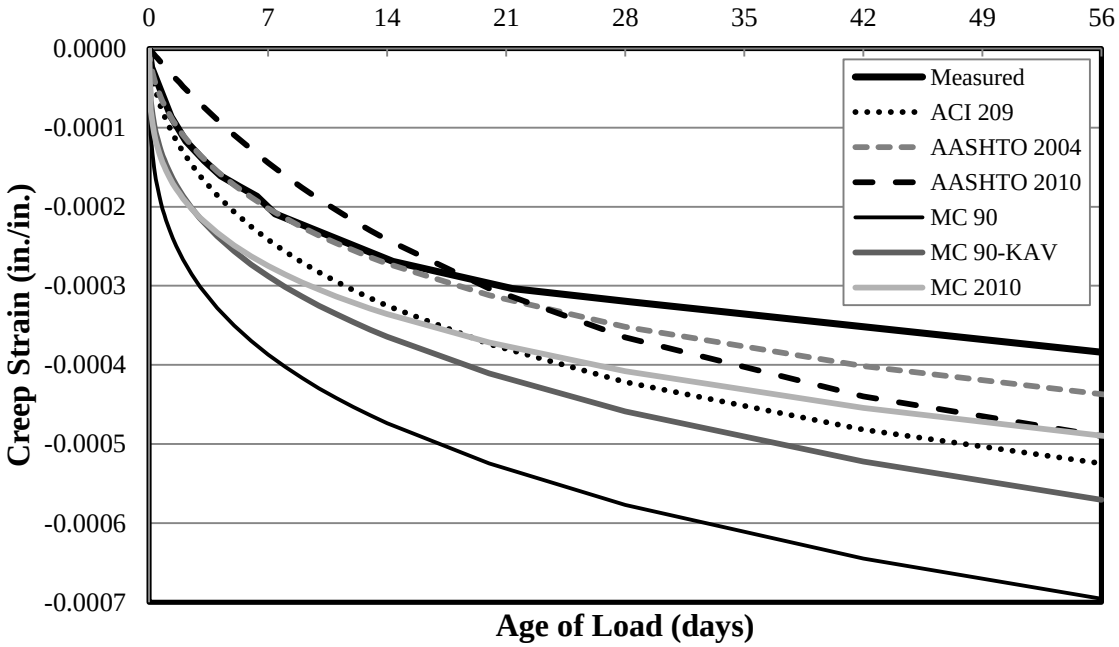

Figure C-57: Creep Strain for Specimen 72-11C-M up to 56 Days

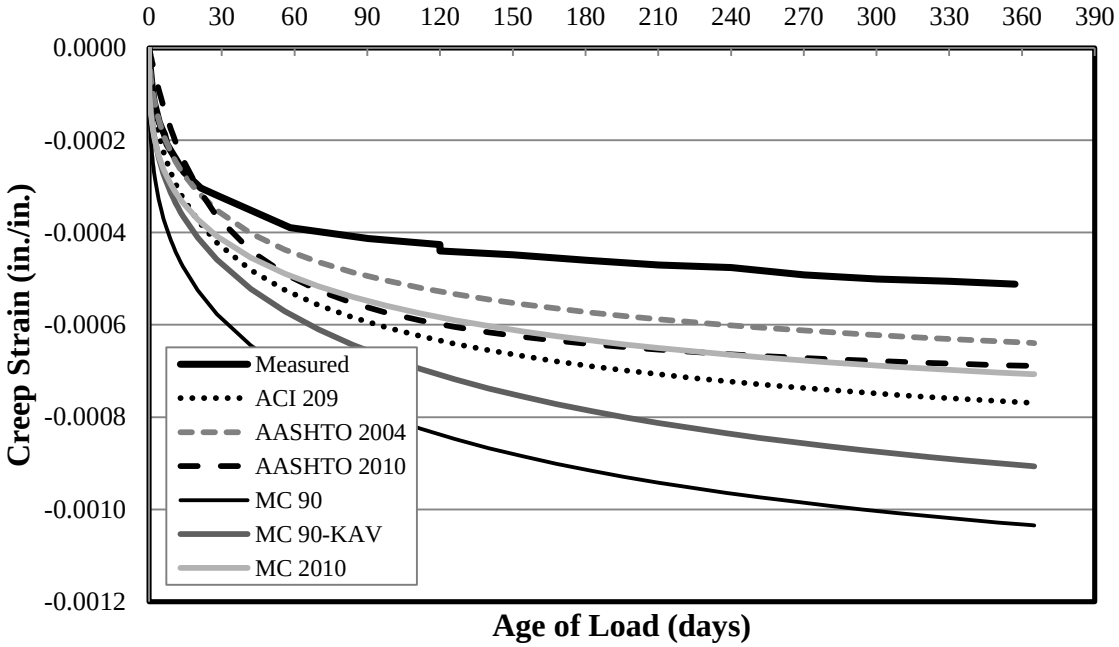

Figure C-58: Creep Strain for Specimen 72-11C-M up to 1 Year

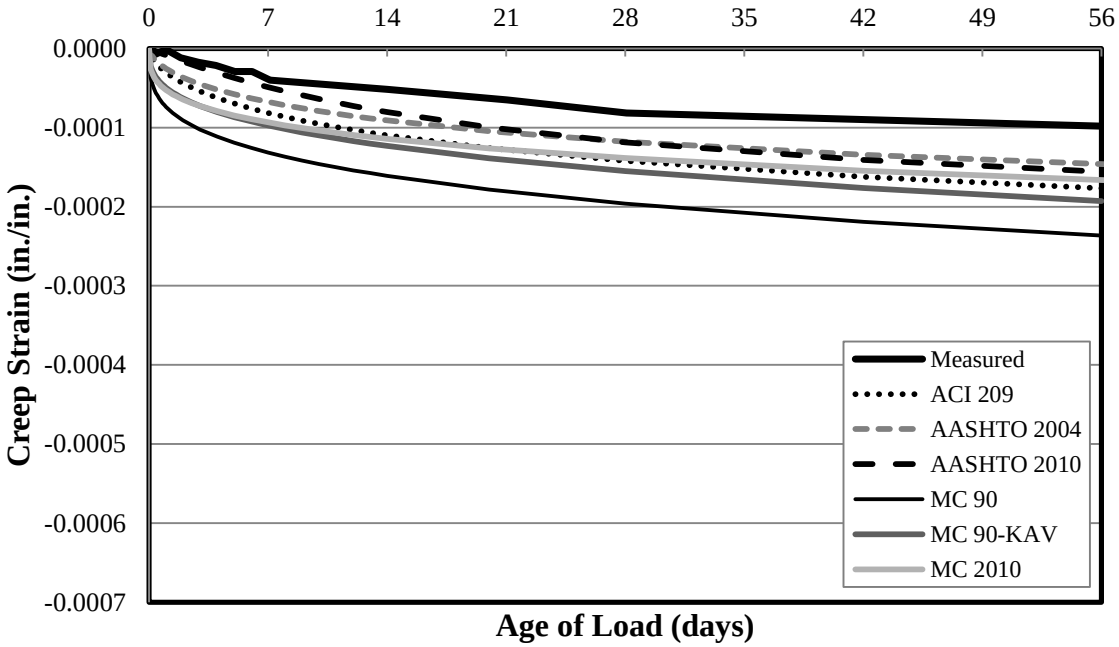

Figure C-59: Creep Strain for Specimen 72-11C-T-U up to 56 Days

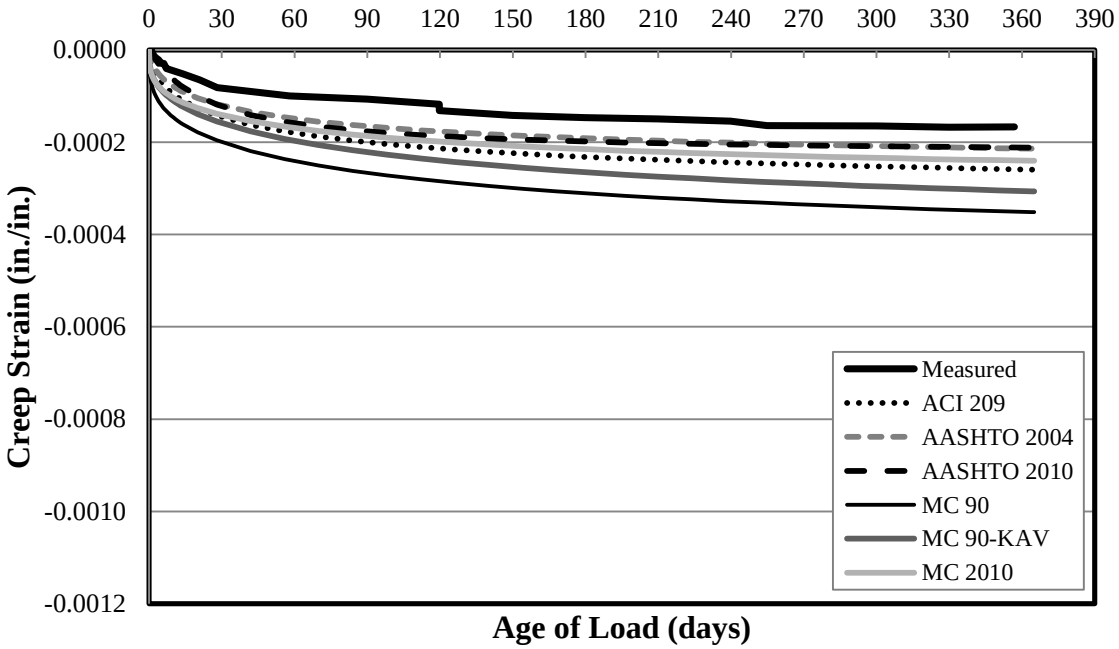

Figure C-60: Creep Strain for Specimen 72-11C-T-U up to 1 Year

C.4. CREEP COEFFICIENT VERSUS TIME

Figure C-61 through Figure C-80 contains all creep coefficient data collected during this study for each of the ten sets of specimen. Each figure plots the measured creep coefficients for a specific specimen as well as predicted coefficients for that specimen against the age of load and is presented at 56 days and 1 year. The prediction methods used for creep coefficients are: ACI 209, AASHTO 2004, AASHTO 2010, NCHRP 628, MC 90, MC 90-KAV, and MC 2010. MC 90-99 and Eurocode are effectively equal to MC 2010 and are not shown. Also, for conventionally vibrated concrete mixtures, the creep coefficient predicted by NCHRP 628 is equal to that predicted by AASHTO 2010.

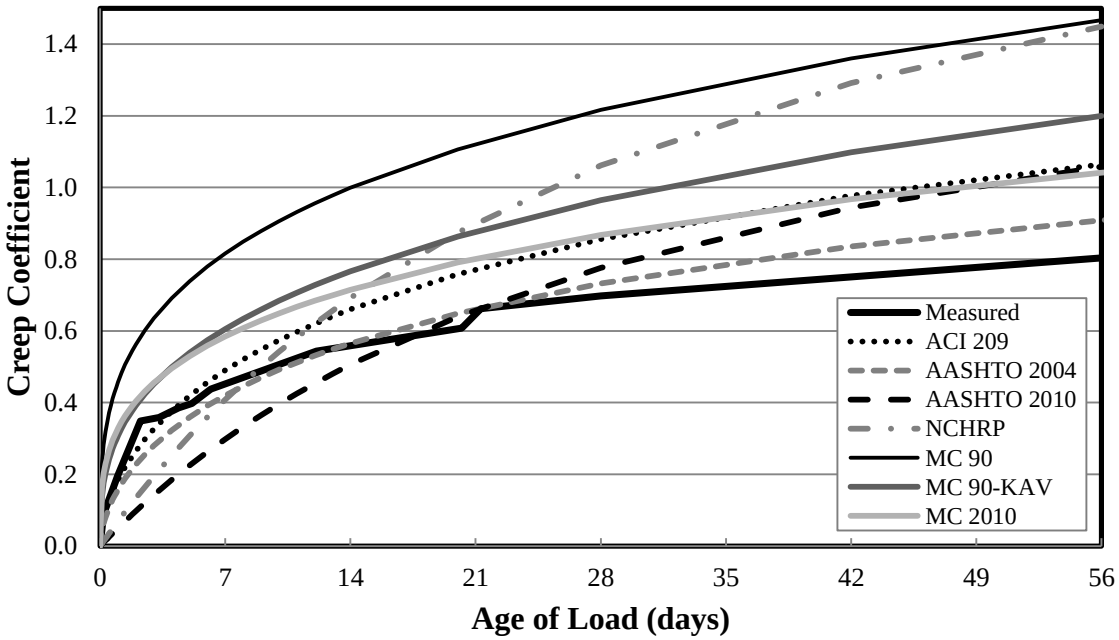

Figure C-61: Creep Coefficient for Specimen 54-03S-M* up to 56 Days

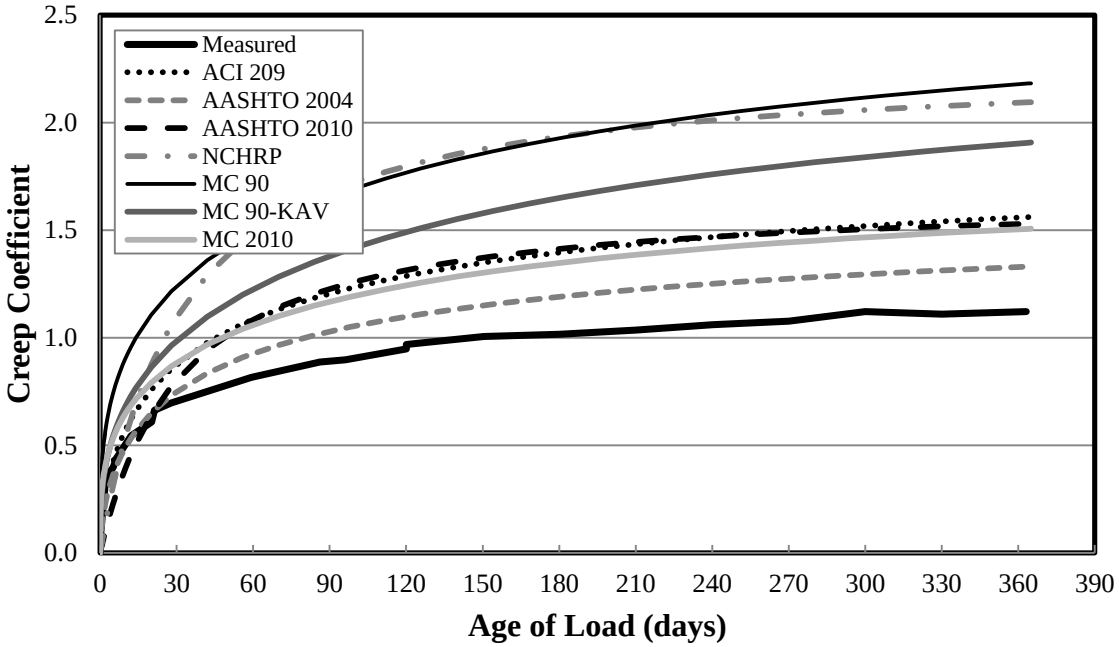

Figure C-62: Creep Coefficient for Specimen 54-03S-M* up to 1 Year

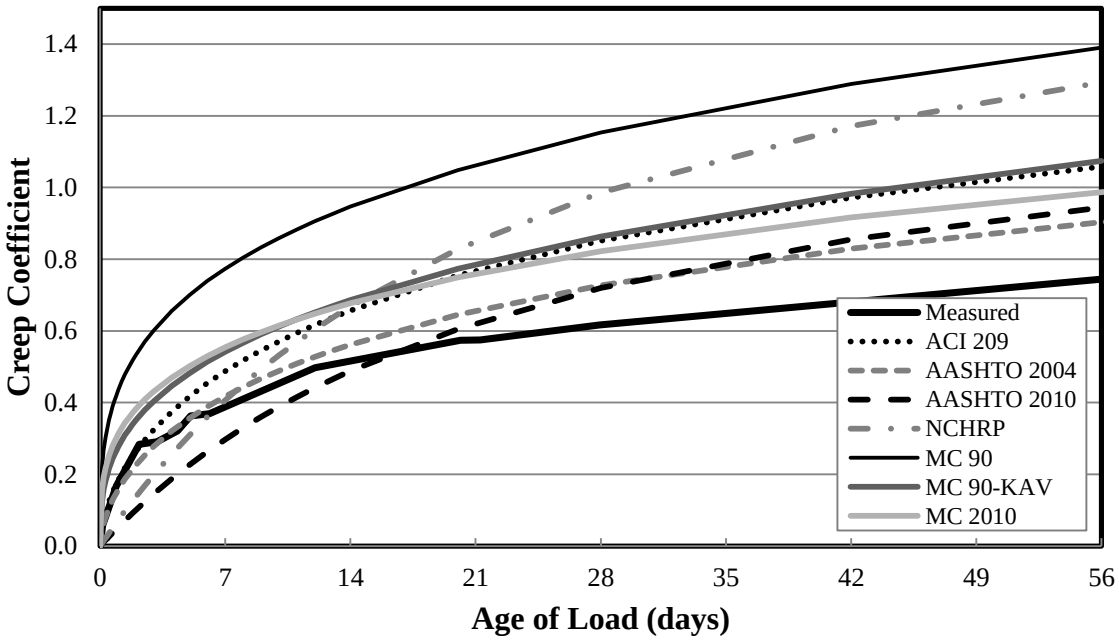

Figure C-63: Creep Coefficient for Specimen 54-03S-T up to 56 Days

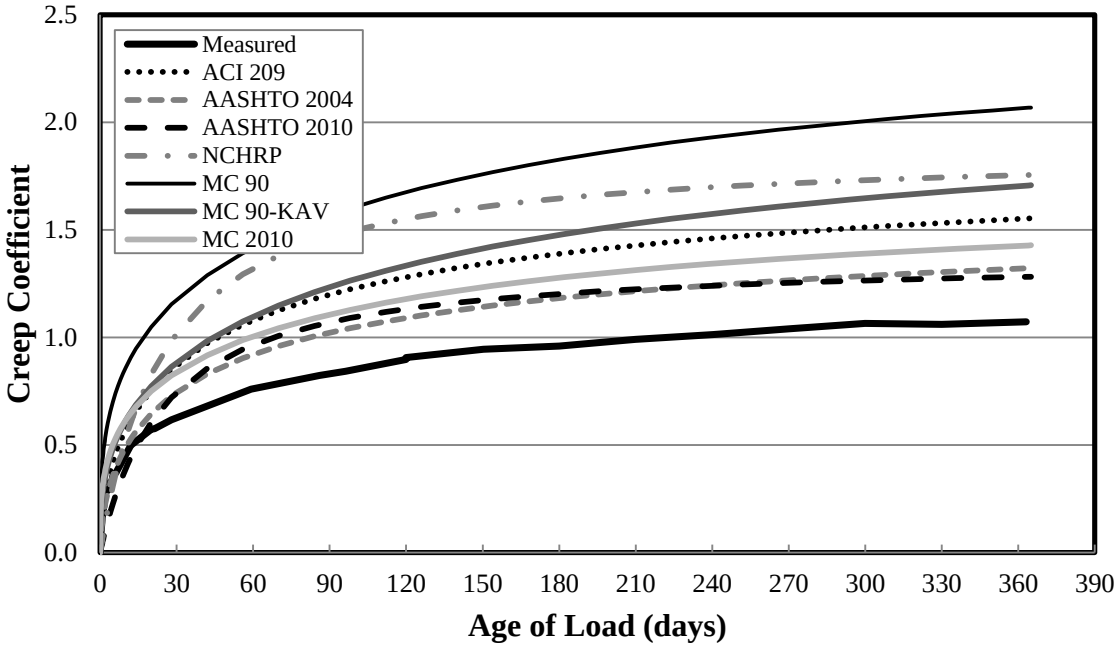

Figure C-64: Creep Coefficient for Specimen 54-03S-T up to 1 Year

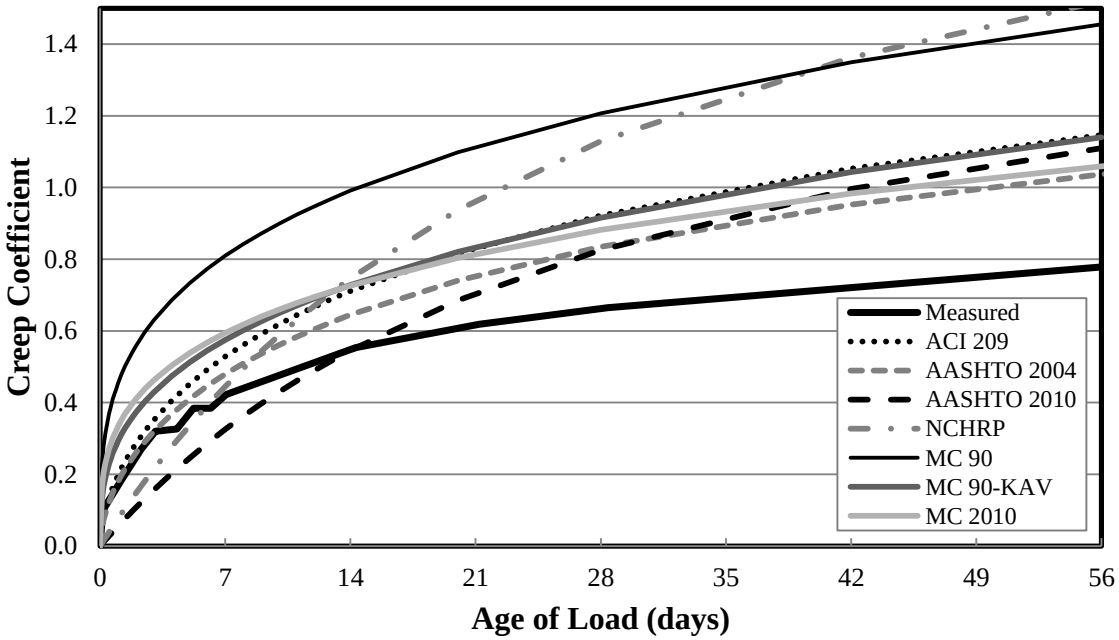

Figure C-65: Creep Coefficient for Specimen 54-07S-M up to 56 Days

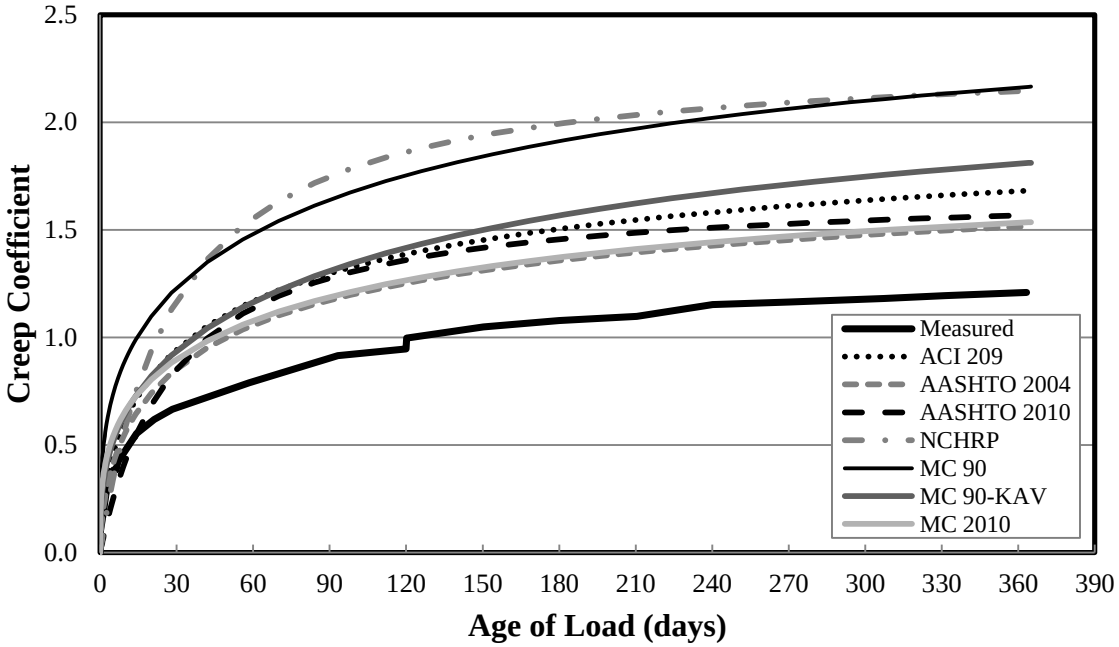

Figure C-66: Creep Coefficient for Specimen 54-07S-M up to 1 Year

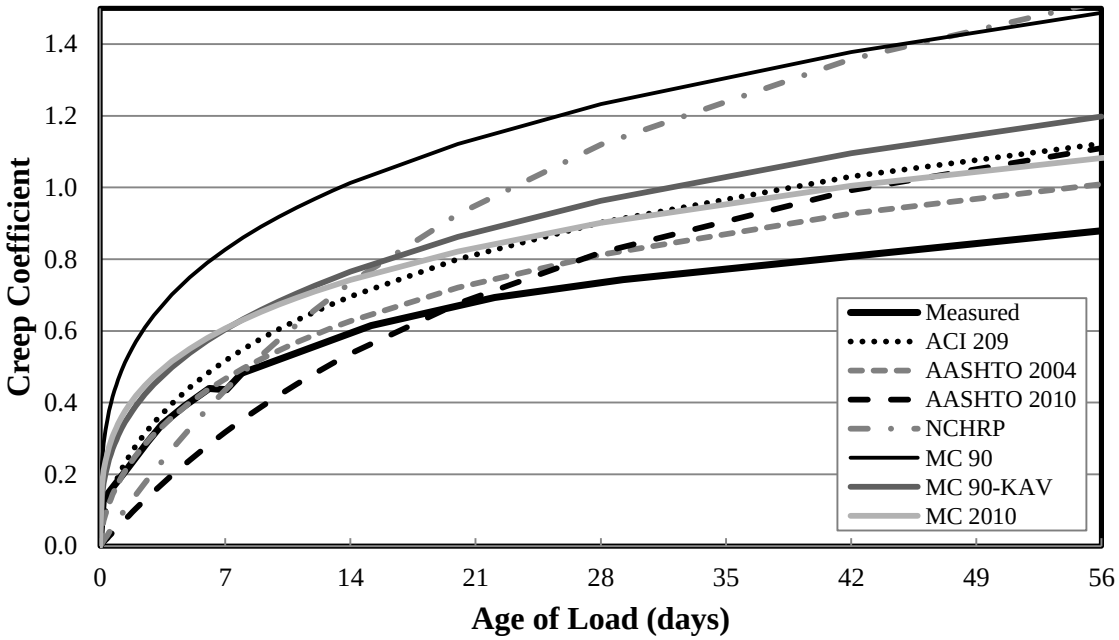

Figure C-67: Creep Coefficient for Specimen 54-07S-T up to 56 Days

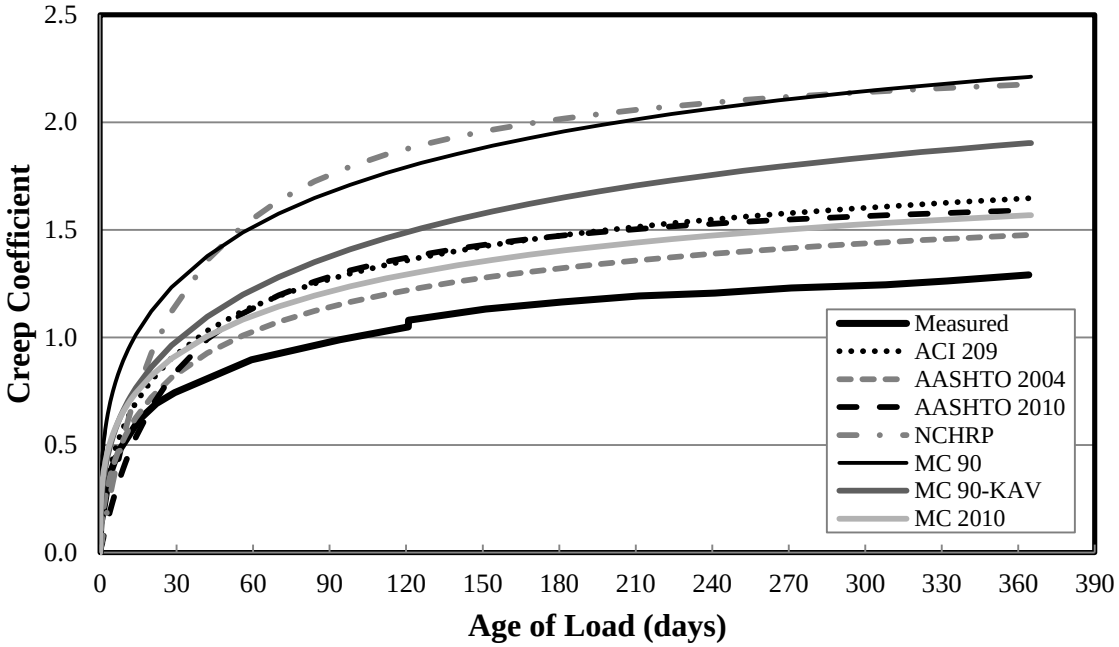

Figure C-68: Creep Coefficient for Specimen 54-07S-T up to 1 Year

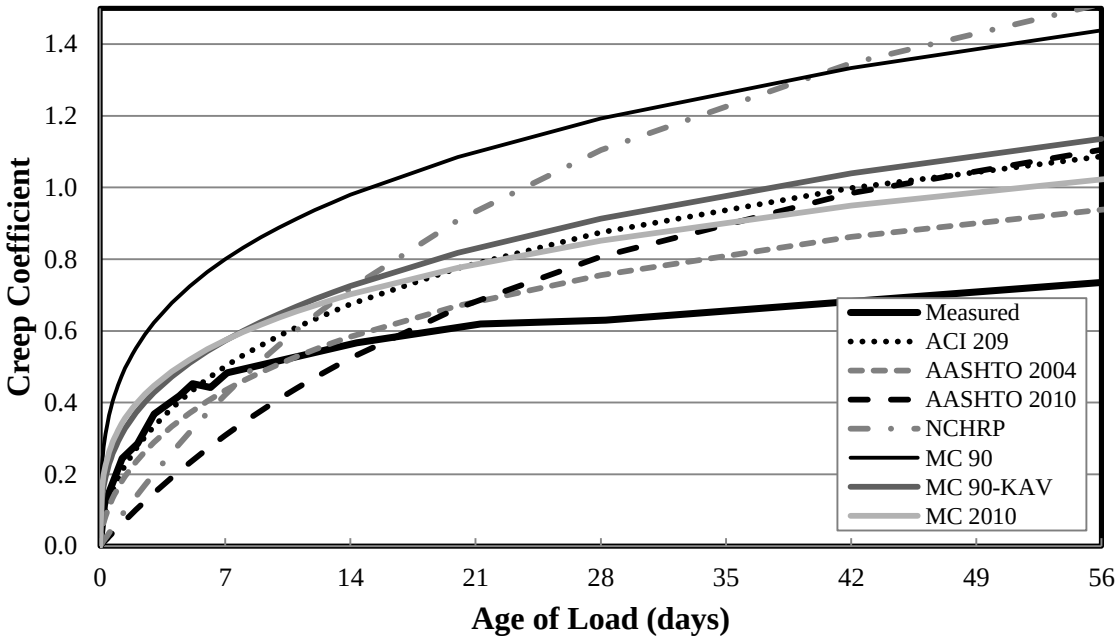

Figure C-69: Creep Coefficient for Specimen 72-03S-M up to 56 Days

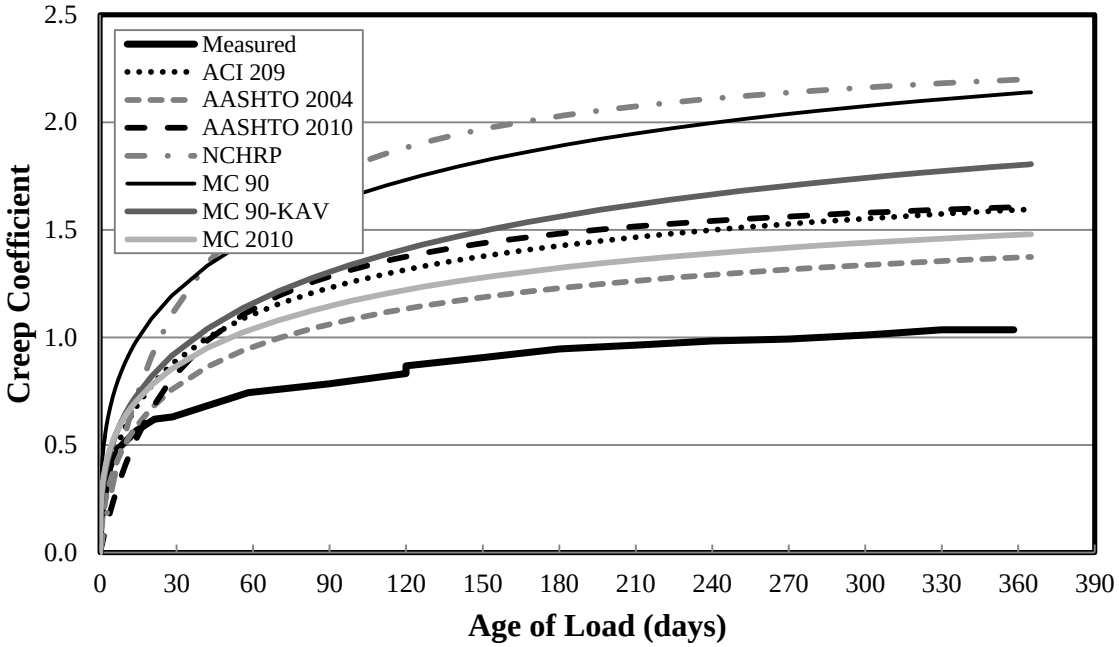

Figure C-70: Creep Coefficient for Specimen 72-03S-M up to 1 Year

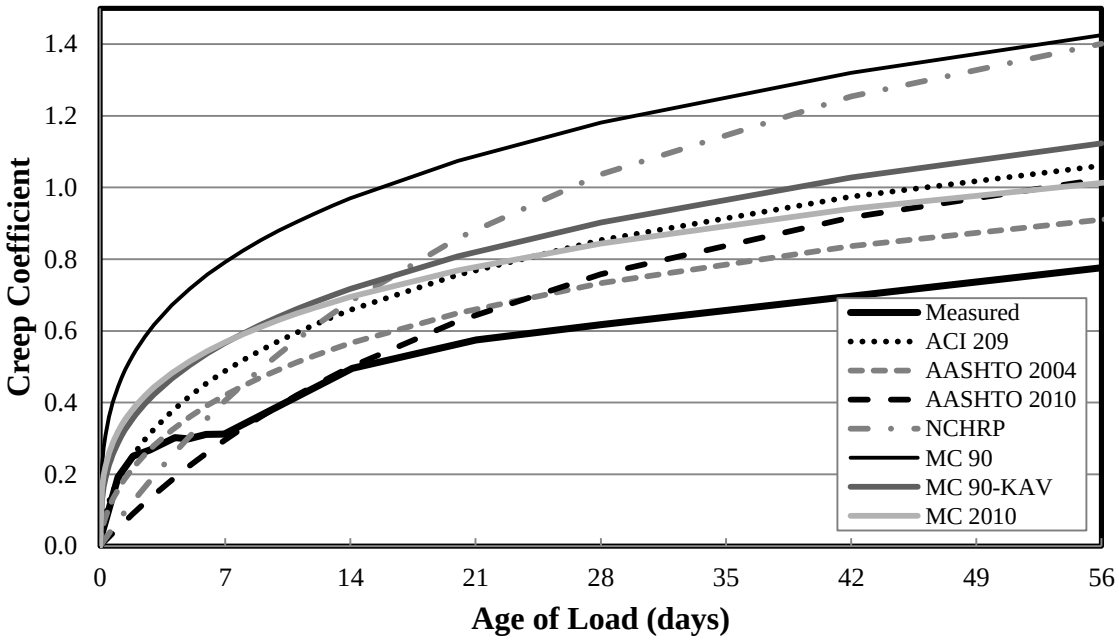

Figure C-71: Creep Coefficient for Specimen 72-03S-T-U up to 56 Days

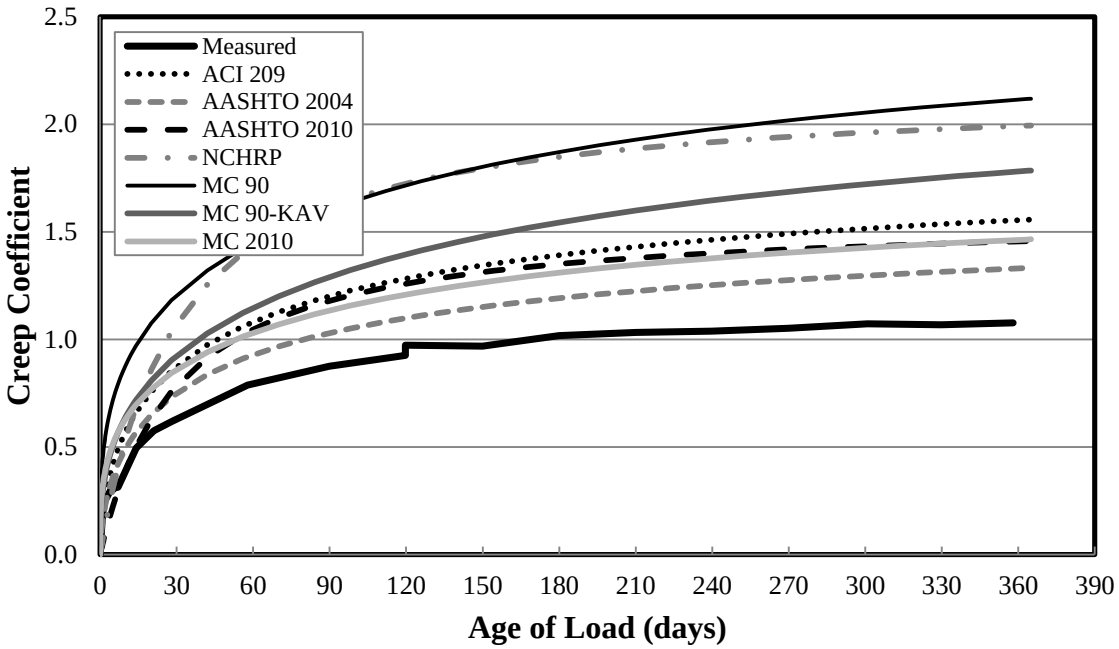

Figure C-72: Creep Coefficient for Specimen 72-03S-T-U up to 1 Year

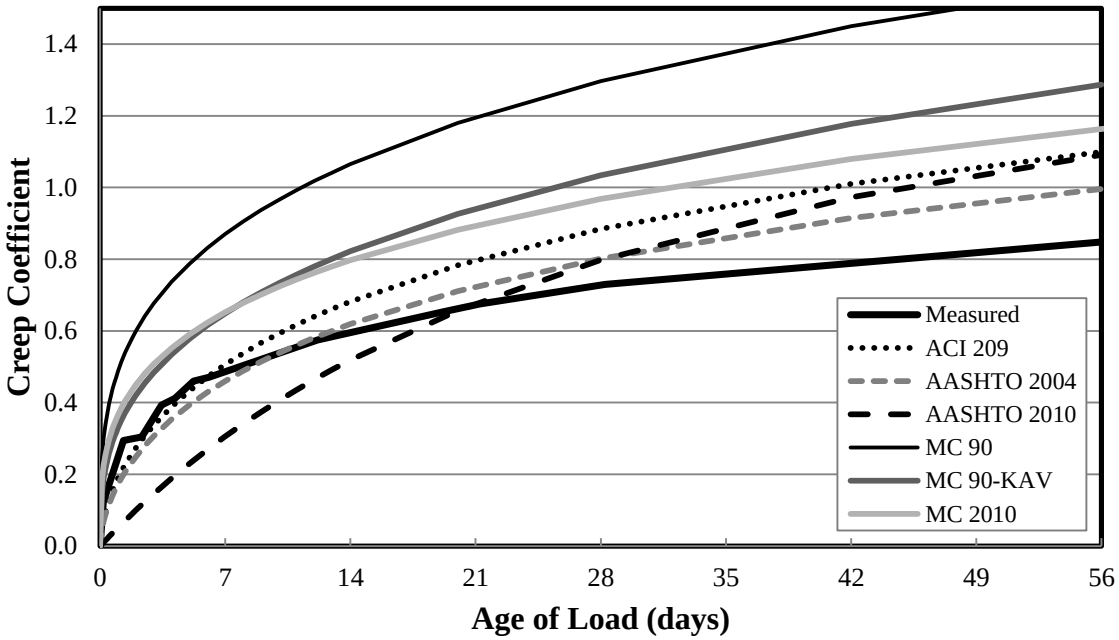

Figure C-73: Creep Coefficient for Specimen 54-12C-M up to 56 Days

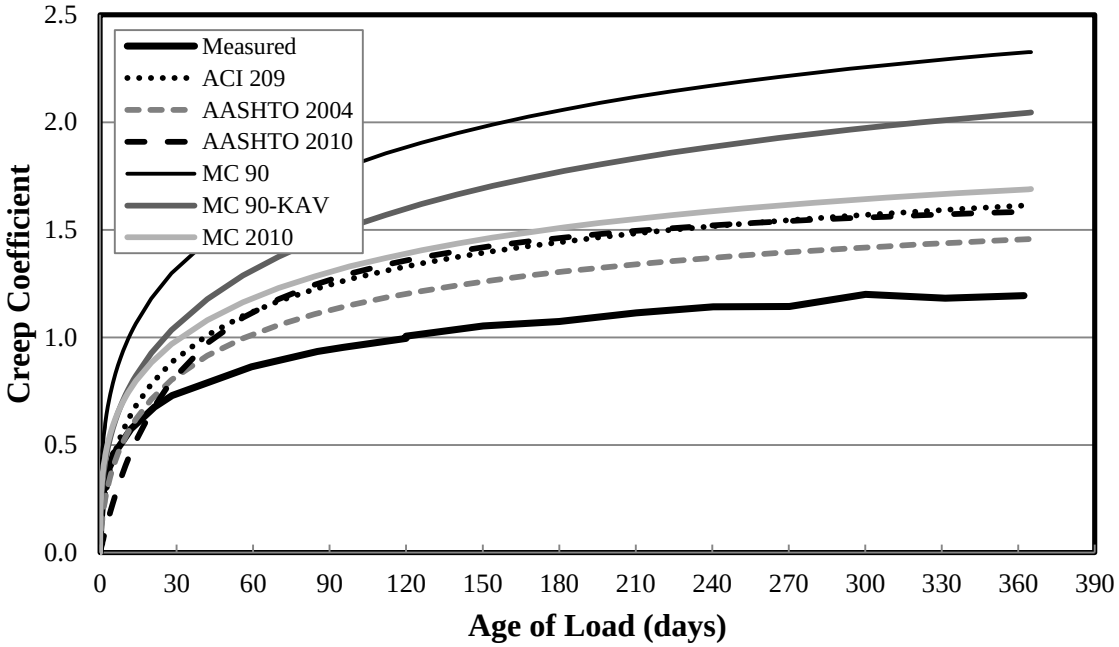

Figure C-74: Creep Coefficient for Specimen 54-12C-M up to 1 Year

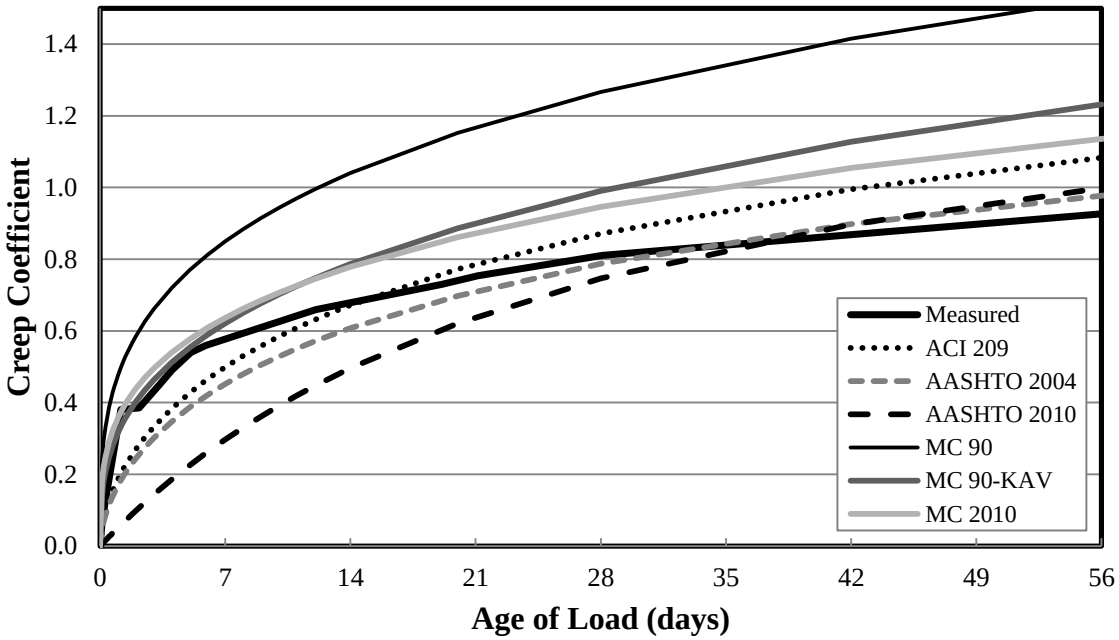

Figure C-75: Creep Coefficient for Specimen 54-12C-T up to 56 Days

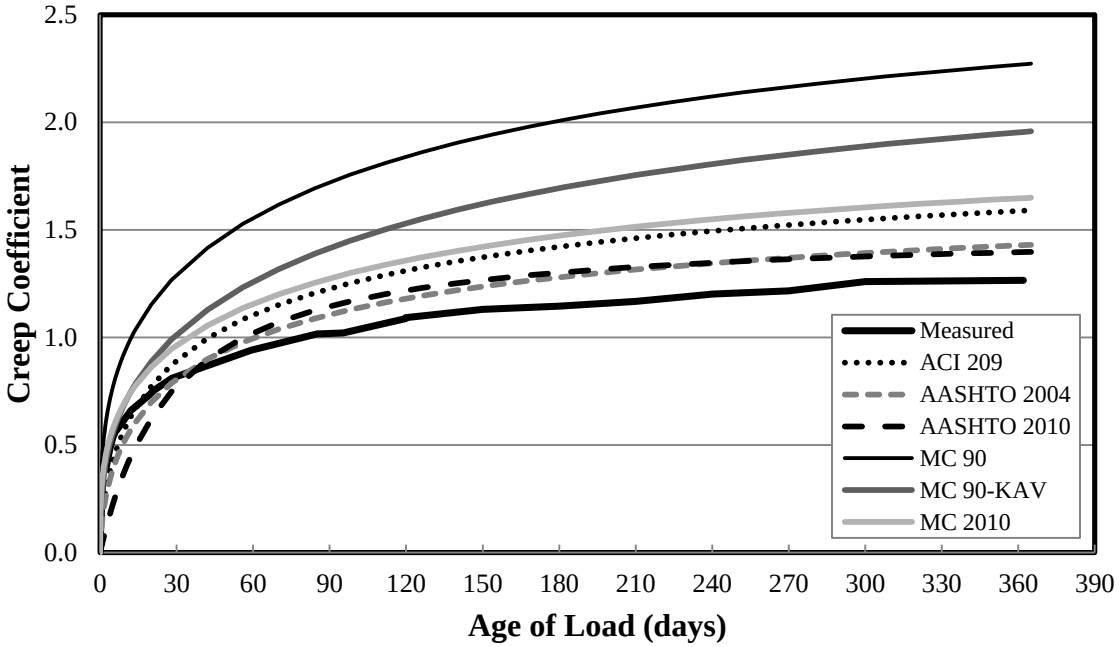

Figure C-76: Creep Coefficient for Specimen 54-12C-T up to 1 Year

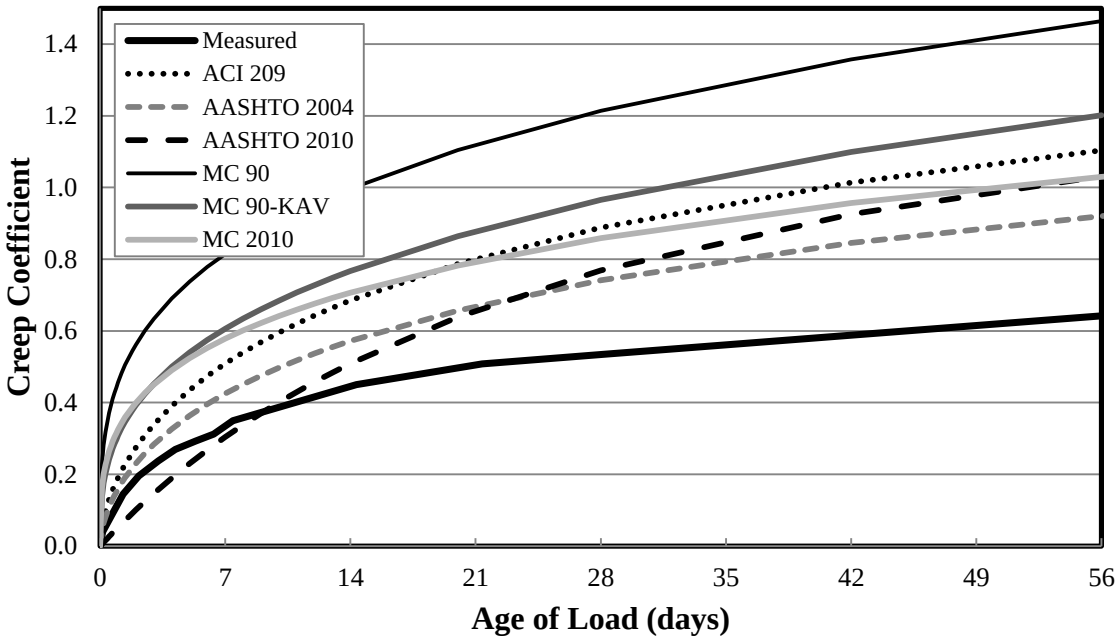

Figure C-77: Creep Coefficient for Specimen 72-11C-M up to 56 Days

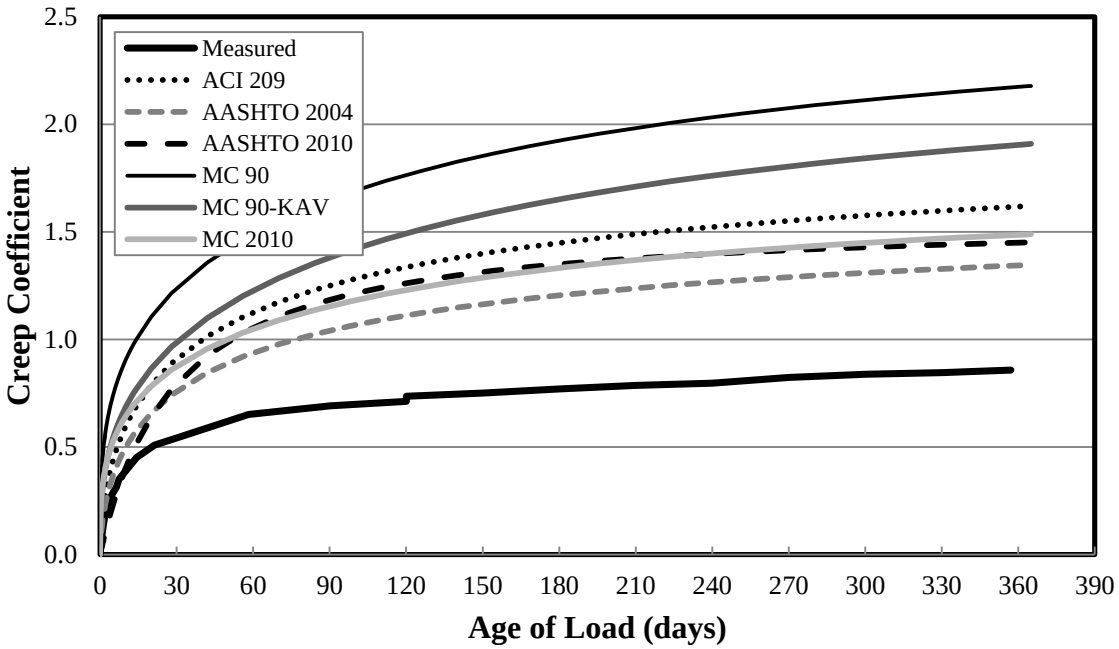

Figure C-78: Creep Coefficient for Specimen 72-11C-M up to 1 Year

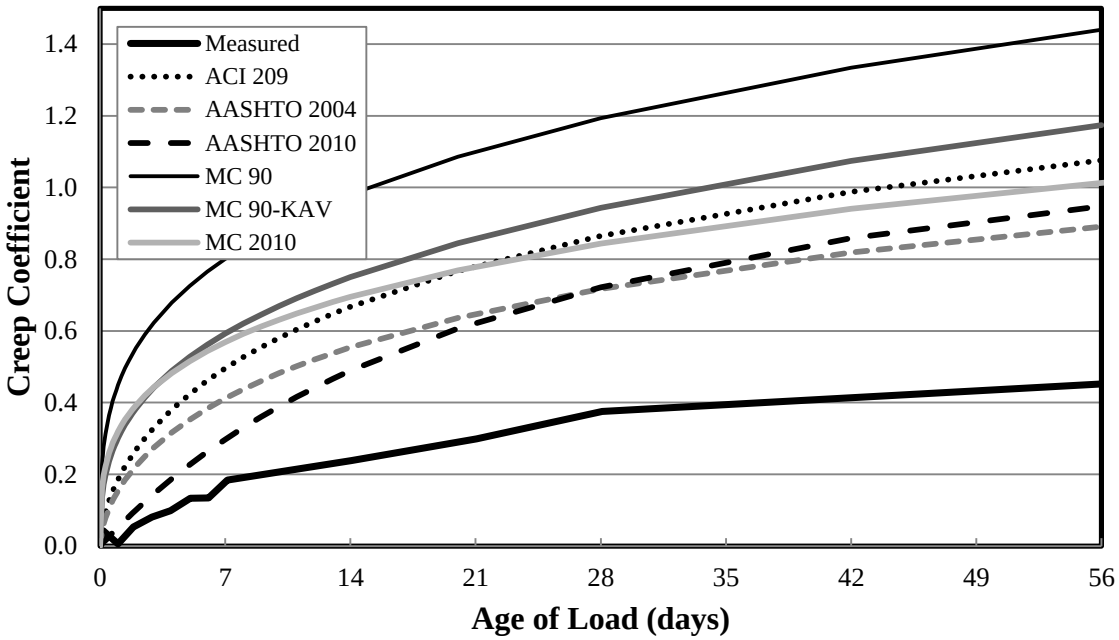

Figure C-79: Creep Coefficient for Specimen 72-11C-T-U up to 56 Days

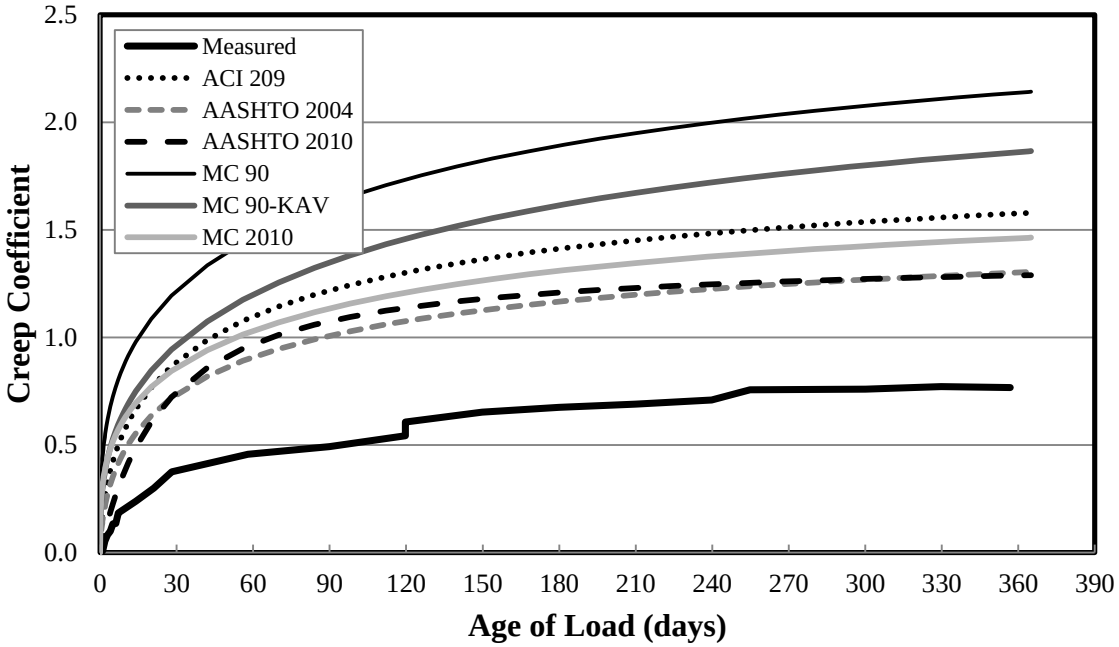

Figure C-80: Creep Coefficient for Specimen 72-11C-T-U up to 1 Year

APPENDIX D
MEASURED STRAINS VERSUS PREDICTED STRAINS

D.1. LOAD-INDUCED STRAINS

Figure D-1 through Figure D-7 graphs the measured load-induced strains versus the predicted load-induced strains for each of the prediction models evaluated in this research. The times plotted in this section are 1 day, 7 days, 56 days, and 365 days. The data is separated by SCC and CVC mixtures as well as by tarp-cured specimens and match-cured specimens. Predictions that fall within an error of ± 20% are considered to be in the acceptable range. The prediction methods used for load-dependent strain are: ACI 209, AASHTO 2004, AASHTO 2010, NCHRP 628, MC 90, MC 90-KAV, and MC 2010. Predictions made by MC 90-99 and Eurocode are effectively equal to those made by MC 2010 and are not shown. Also, for conventionally vibrated concrete mixtures, the strain due to load predicted by NCHRP 628 is equal to that predicted by AASHTO 2010.

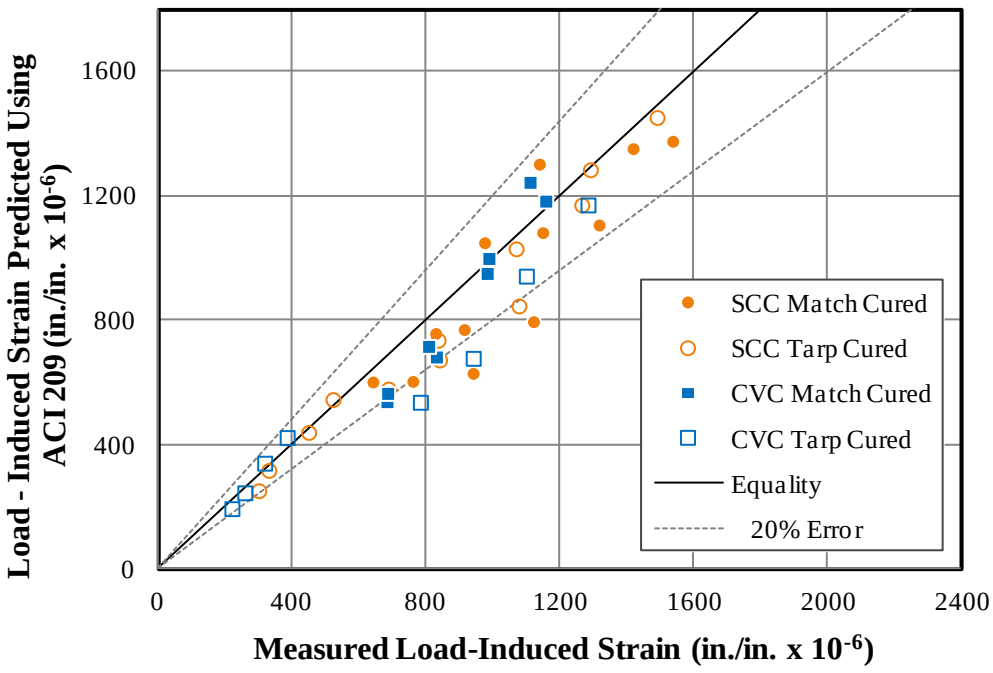

Figure D-1: Measured Versus Predicted Load-Induced Strains Using ACI 209

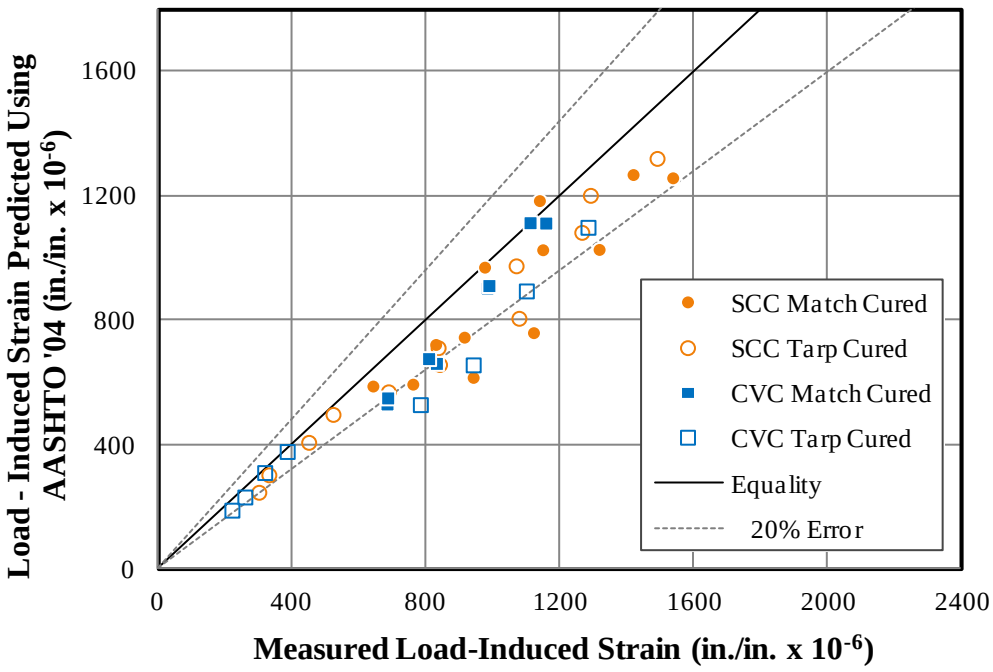

Figure D-2: Measured Versus Predicted Load-Induced Strains Using AASHTO 2004

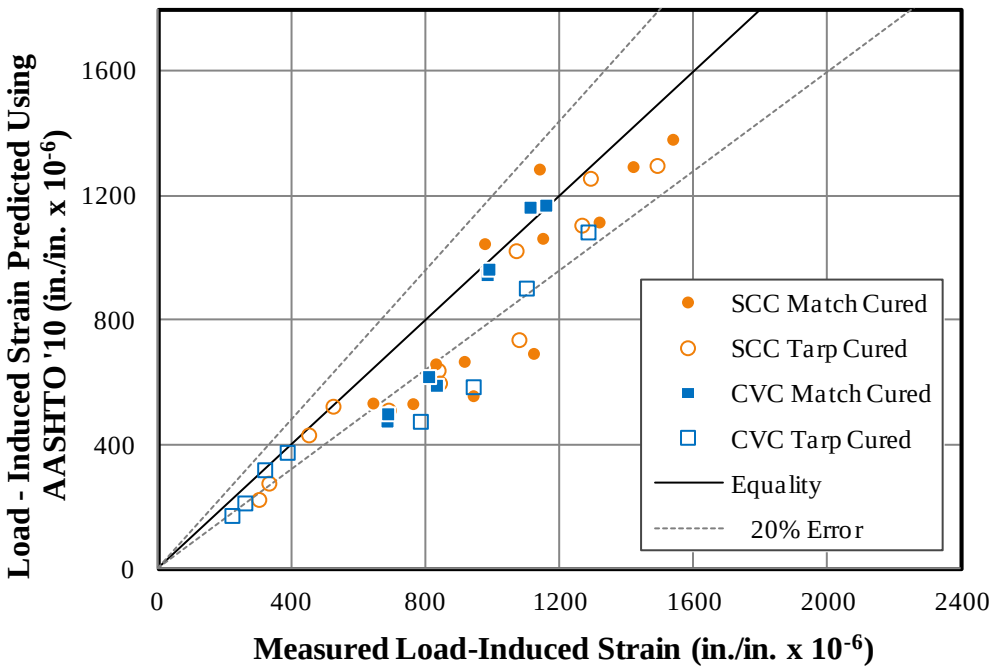

Figure D-3: Measured Versus Predicted Load-Induced Strains Using AASHTO 2010

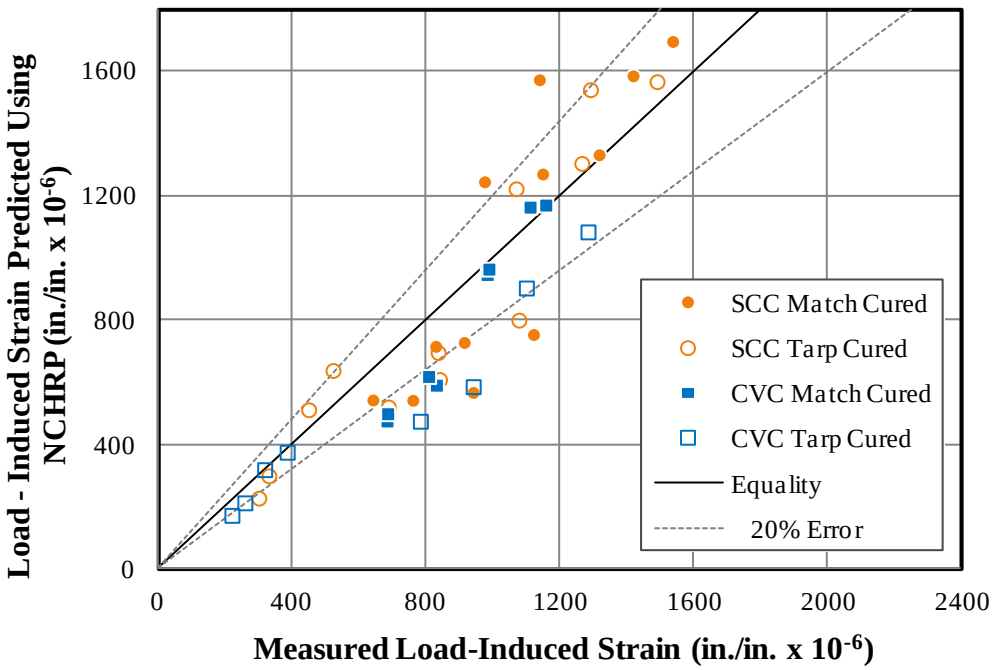

Figure D-4: Measured Versus Predicted Load-Induced Strains Using NCHRP 628

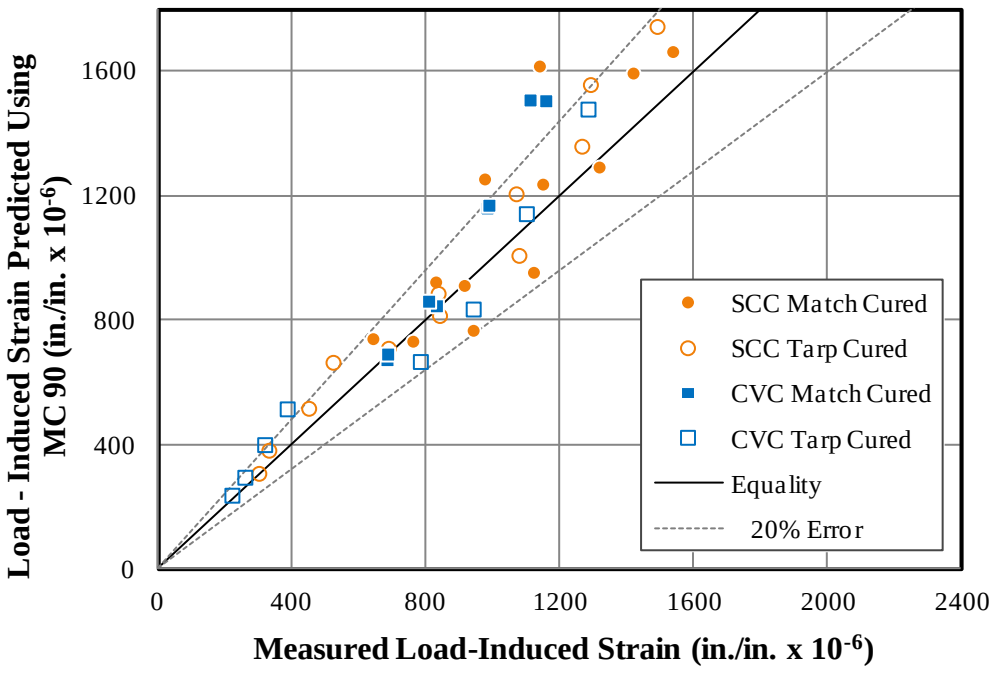

Figure D-5: Measured Versus Predicted Load-Induced Strains Using MC 90

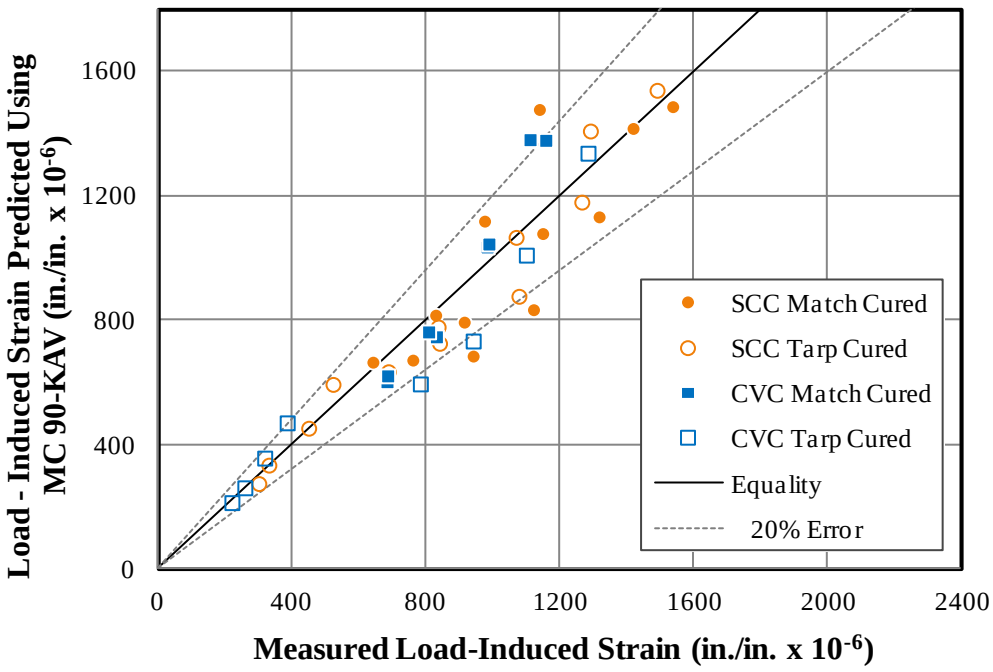

Figure D-6: Measured Versus Predicted Load-Induced Strains Using MC 90-KAV

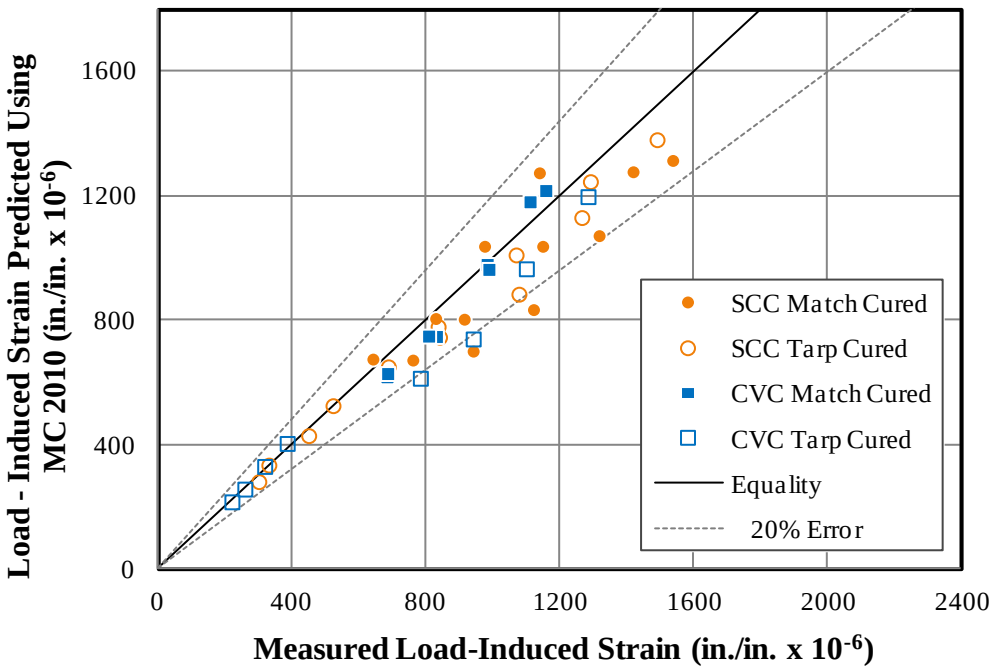

Figure D-7: Measured Versus Predicted Load-Induced Strains Using MC 2010

D.2. SHRINKAGE STRAINS

Figure D-8 through Figure D-14 graphs the measured load-induced strains versus the predicted shrinkage strains for each of the prediction models evaluated in this research. The times plotted in this section are 1 day, 7 days, 56 days, and 365 days. The data is separated by SCC and CVC mixtures as well as by tarp-cured specimens and match-cured specimens. Predictions that fall within an error of ± 20% are considered to be in the acceptable range. The prediction methods used for shrinkage strain are: ACI 209, AASHTO 2004, AASHTO 2010, NCHRP 628, MC 90, MC 2010, and Eurocode. MC 90-99 is effectively equal to MC 2010 and MC-KAV is equal to MC-90, and these methods are not shown. Also, for conventionally vibrated concrete mixtures, the shrinkage strain predicted by NCHRP 628 is equal to that predicted by AASHTO 2004.

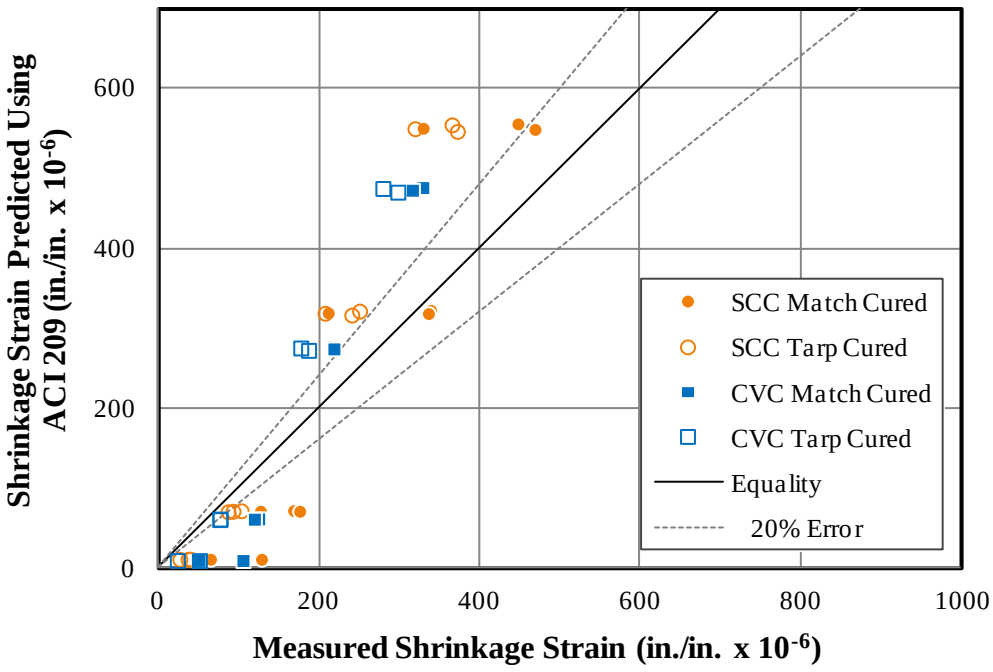

Figure D-8: Measured Versus Predicted Shrinkage Strains Using ACI 209

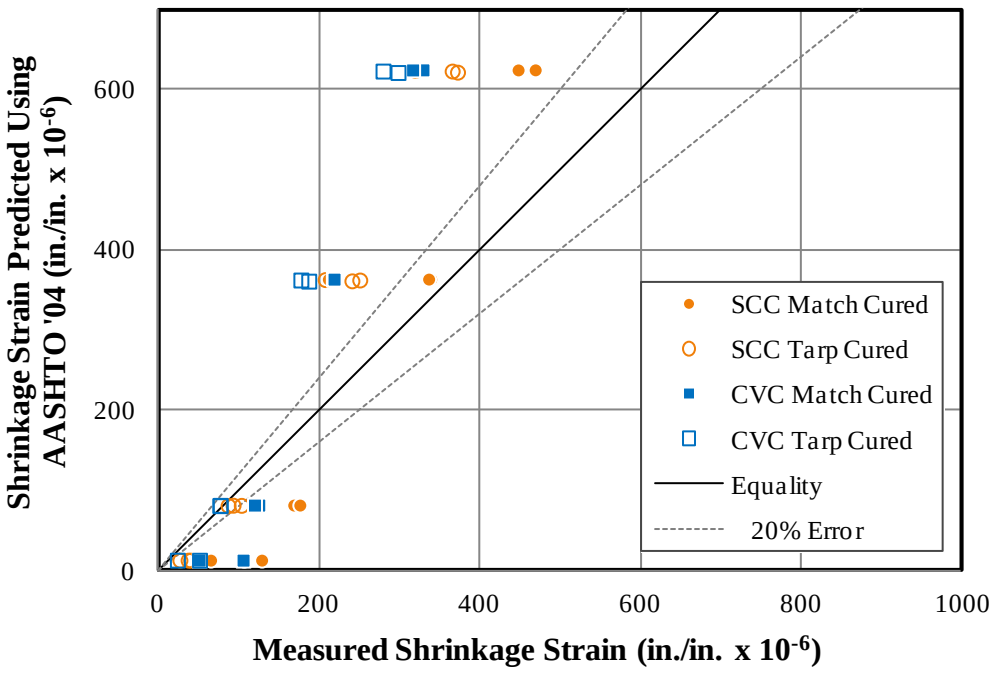

Figure D-9: Measured Versus Predicted Shrinkage Strains Using AASHTO 2004

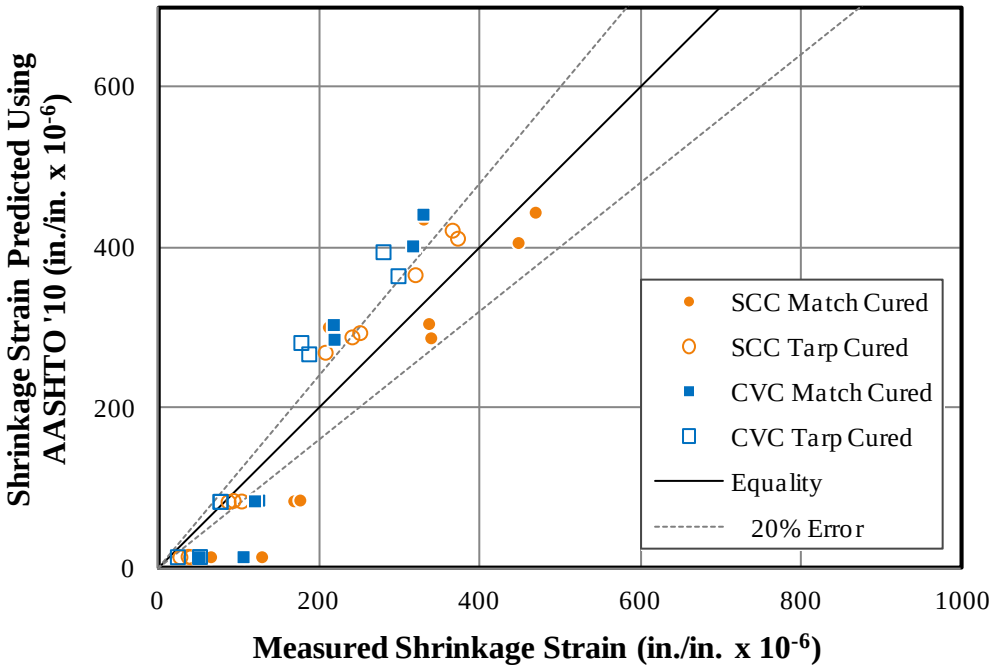

Figure D-10: Measured Versus Predicted Shrinkage Strains Using AASHTO 2010

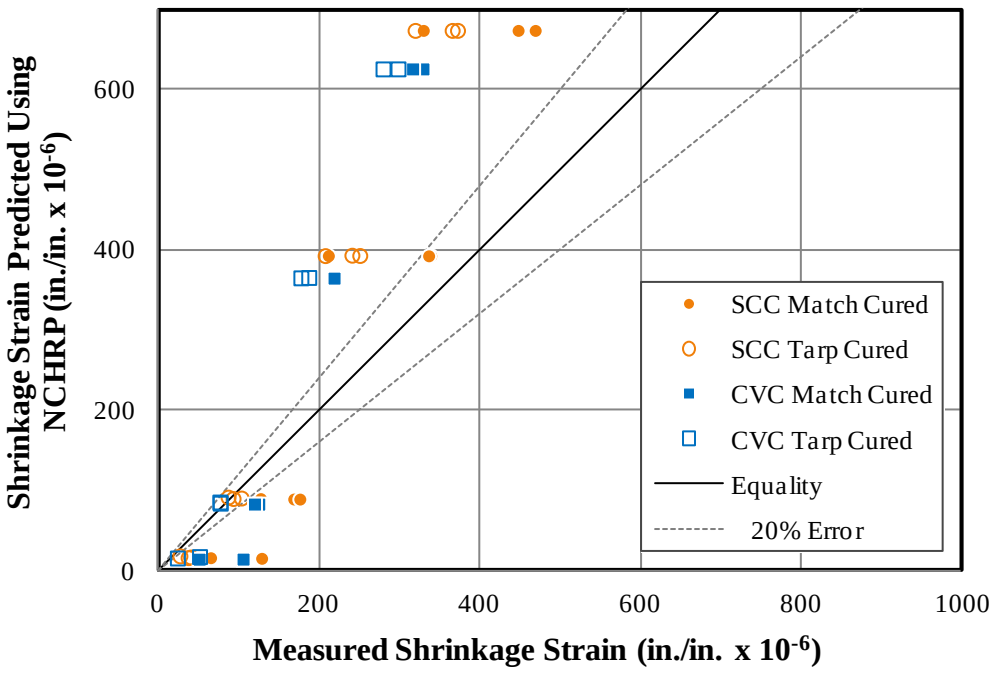

Figure D-11: Measured Versus Predicted Shrinkage Strains Using NCHRP 628

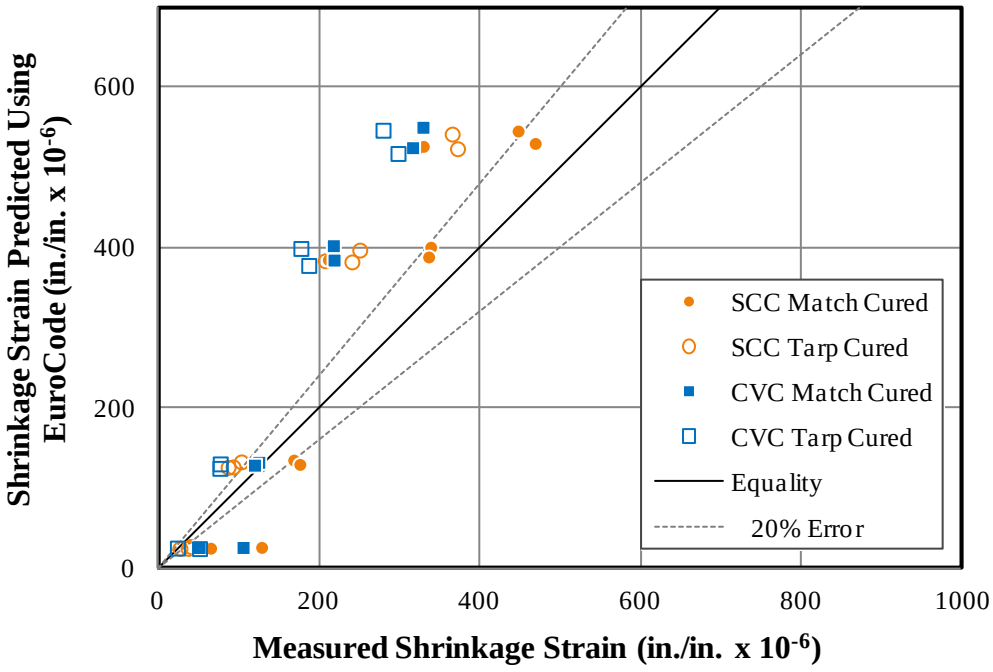

Figure D-12: Measured Versus Predicted Shrinkage Strains Using Eurocode

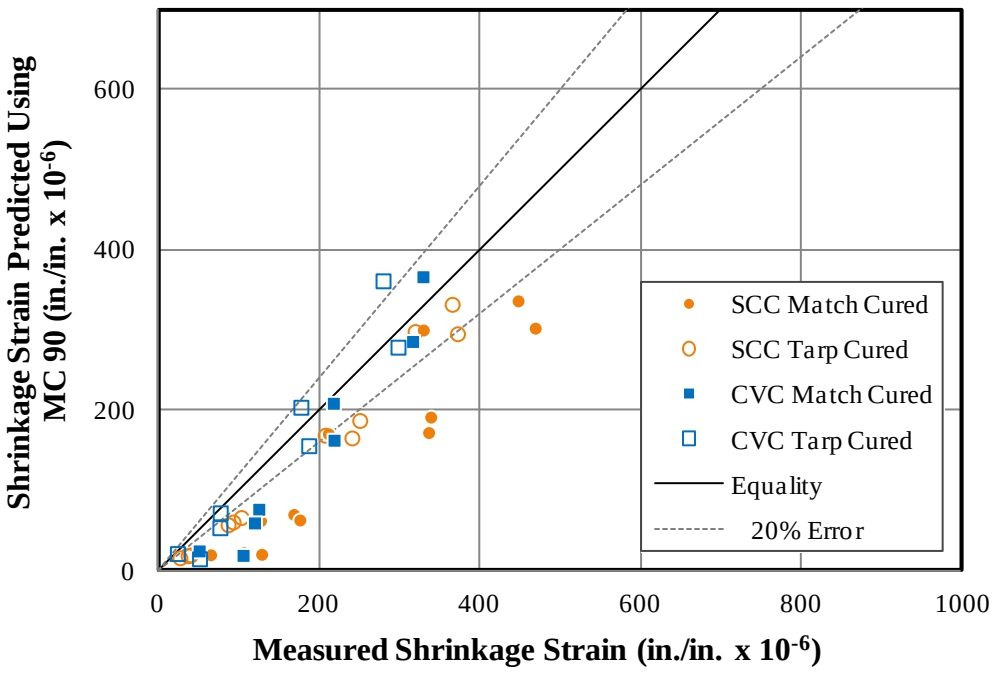

Figure D-13: Measured Versus Predicted Shrinkage Strains Using MC 90

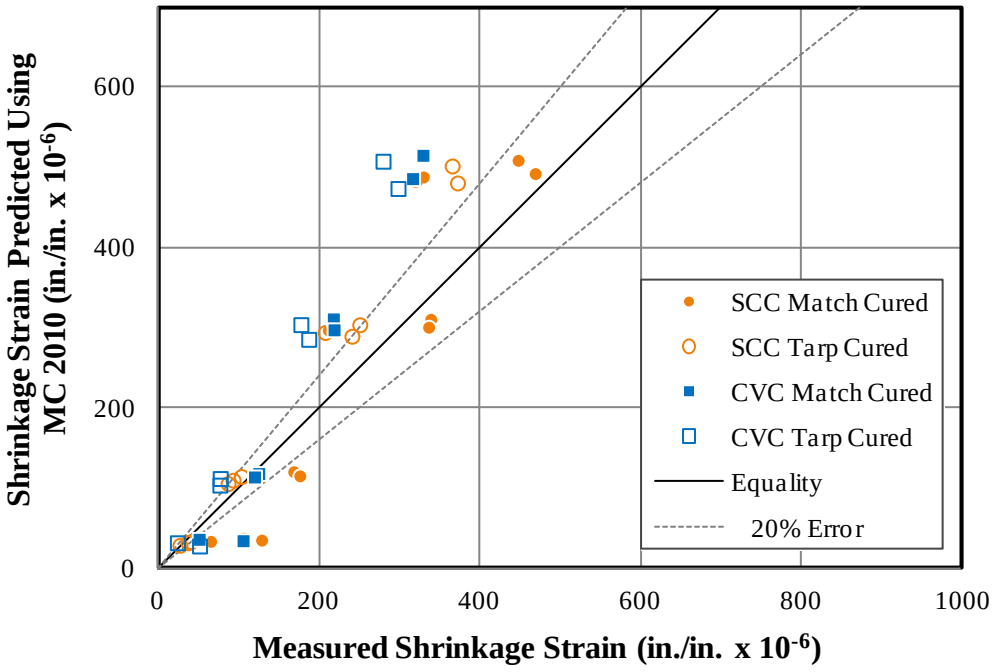

Figure D-14: Measured Versus Predicted Shrinkage Strains Using MC 2010

D.3. CREEP STRAINS

Figure D-15 through Figure D-21graphs the measured load-induced strains versus the predicted creep strains for each of the prediction models evaluated in this research. The times plotted in this section are 1 day, 7 days, 56 days, and 365 days. The data is separated by SCC and CVC mixtures as well as by tarp-cured specimens and match-cured specimens. Predictions that fall within an error of ± 20% are considered to be in the acceptable range. The prediction methods used for creep strain are: ACI 209, AASHTO 2004, AASHTO 2010, NCHRP 628, MC 90, MC 90-KAV, and MC 2010. MC 90-99 and Eurocode are effectively equal to MC 2010 and are not shown. Also, for conventionally vibrated concrete mixtures, the creep strain predicted by NCHRP 628 is equal to that predicted by AASHTO 2010.

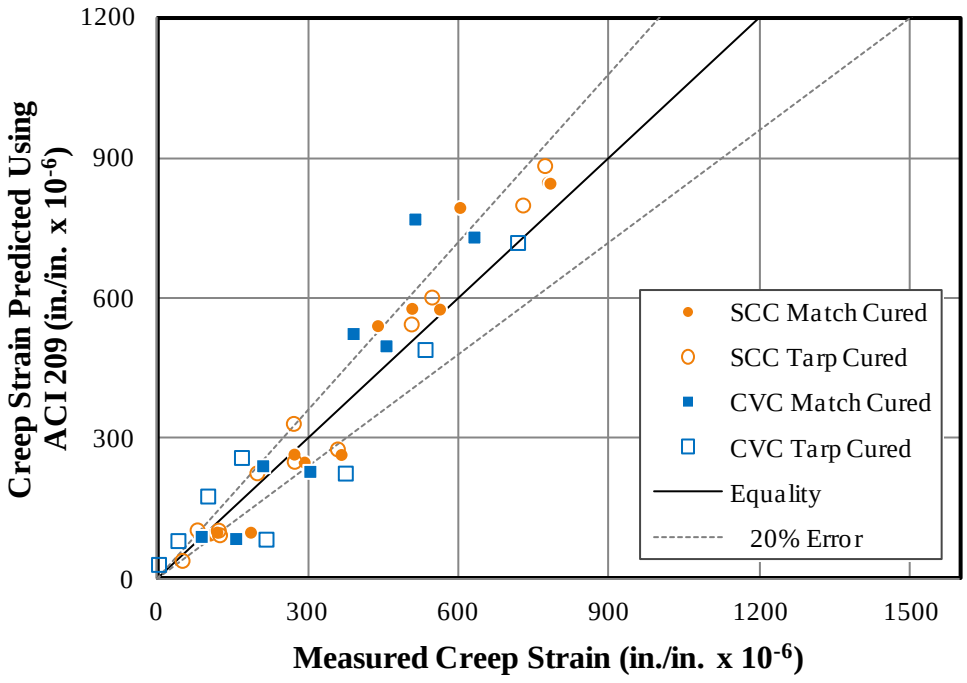

Figure D-15: Measured Versus Predicted Creep Strains Using ACI 209

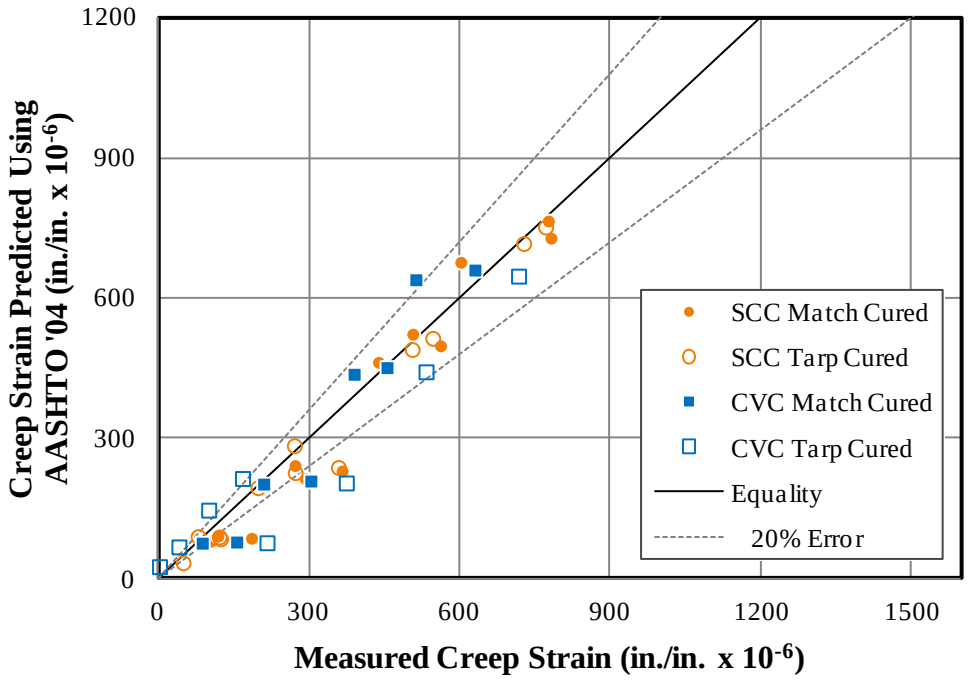

Figure D-16: Measured Versus Predicted Creep Strains Using AASHTO 2004

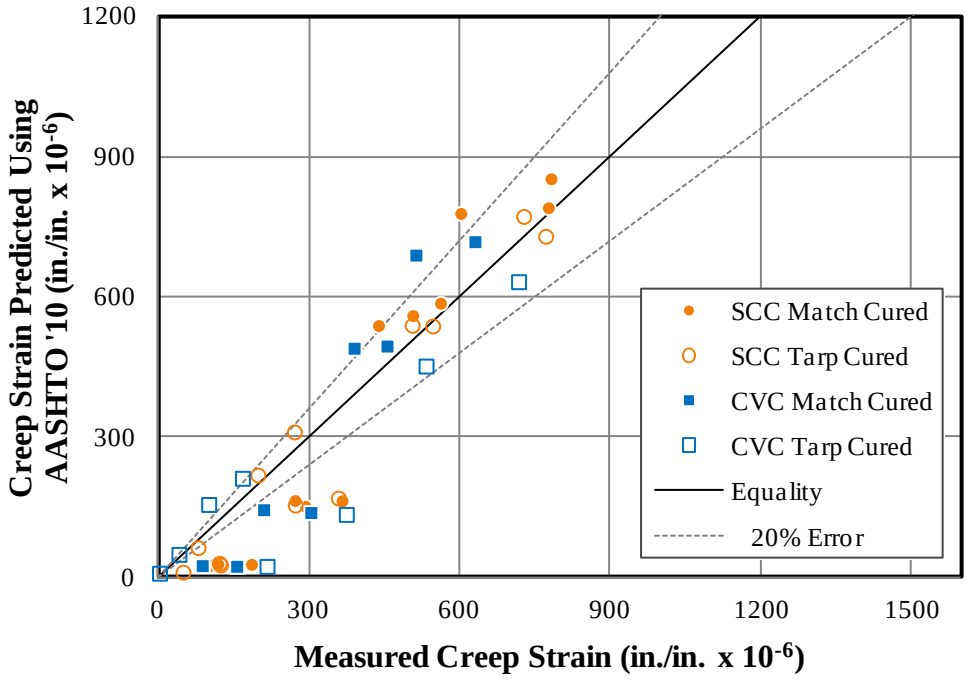

Figure D-17: Measured Versus Predicted Creep Strains Using AASHTO 2010

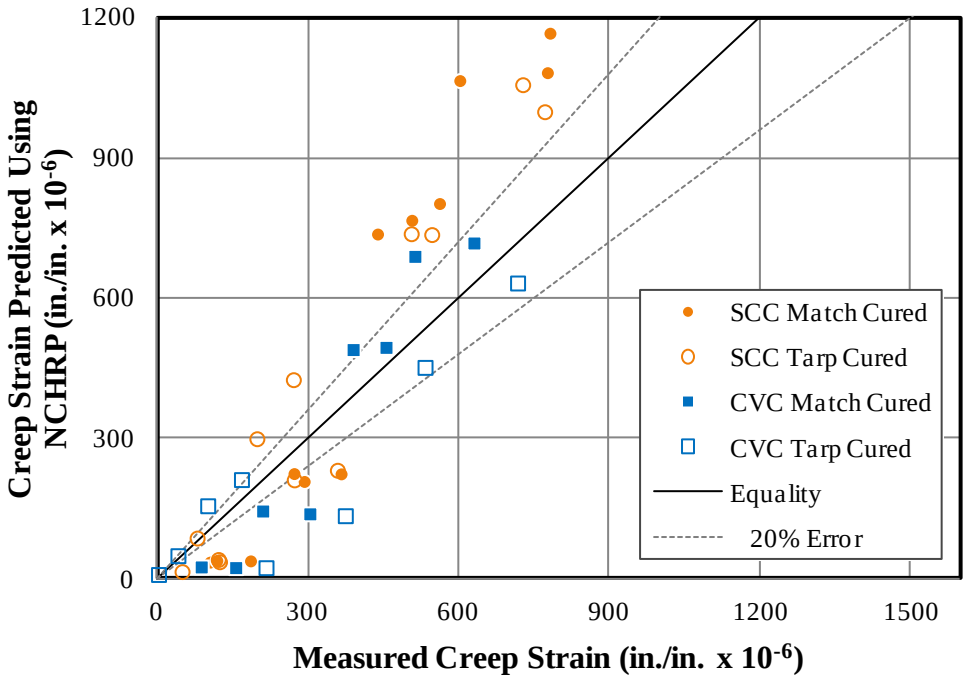

Figure D-18: Measured Versus Predicted Creep Strains Using NCHRP 628

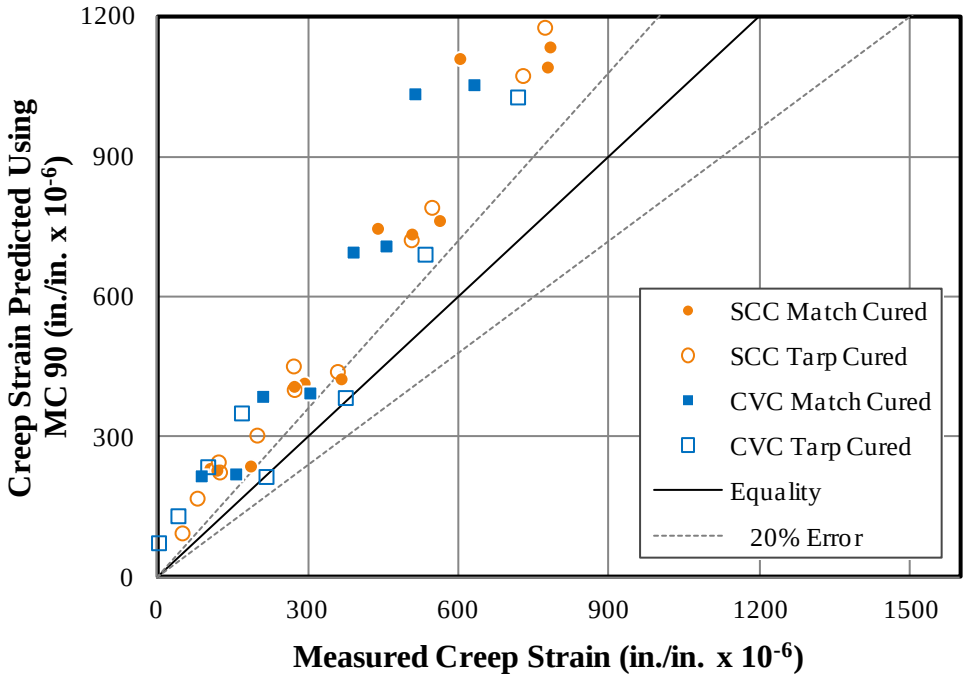

Figure D-19: Measured Versus Predicted Creep Strains Using MC 90

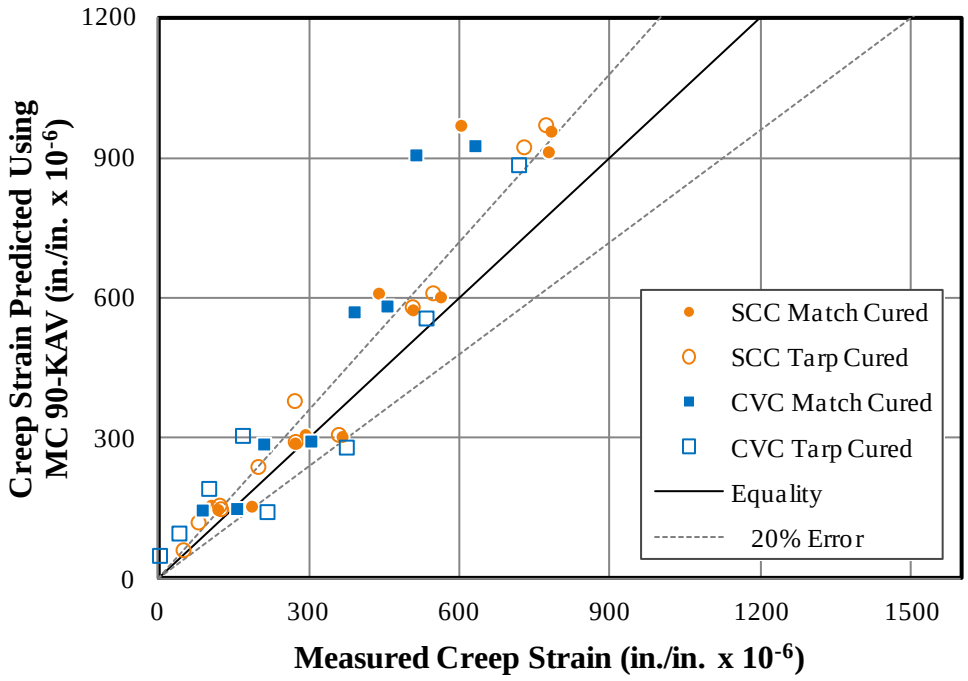

Figure D-20: Measured Versus Predicted Creep Strains Using MC 90-KAV

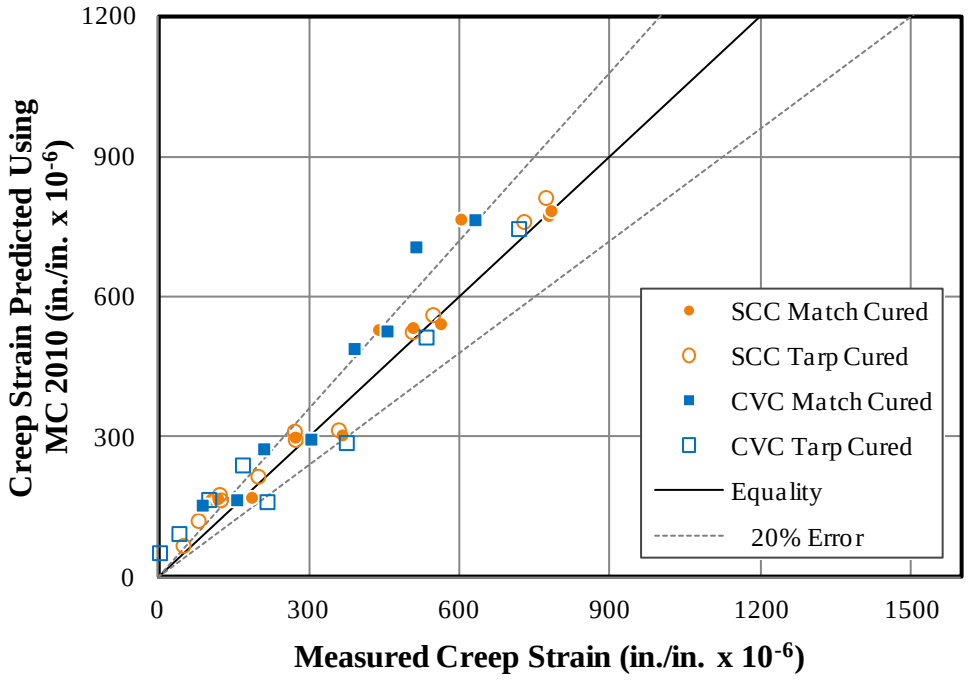

Figure D-21: Measured Versus Predicted Creep Strains Using MC 2010

D.4. CREEP COEFFICIENTS

Figure D-22 through Figure D-28 graphs the measured load-induced strains versus the predicted creep coefficients for each of the prediction models evaluated in this research. The times plotted in this section are 1 day, 7 days, 56 days, and 365 days. The data is separated by SCC and CVC mixtures as well as by tarp-cured specimens and match-cured specimens. Predictions that fall within an error of ± 20% are considered to be in the acceptable range. The prediction methods used for creep coefficients are: ACI 209, AASHTO 2004, AASHTO 2010, NCHRP 628, MC 90, MC 90-KAV, and MC 2010. MC 90-99 and Eurocode are effectively equal to MC 2010 and are not shown. Also, for conventionally vibrated concrete mixtures, the creep coefficient predicted by NCHRP 628 is equal to that predicted by AASHTO 2010.

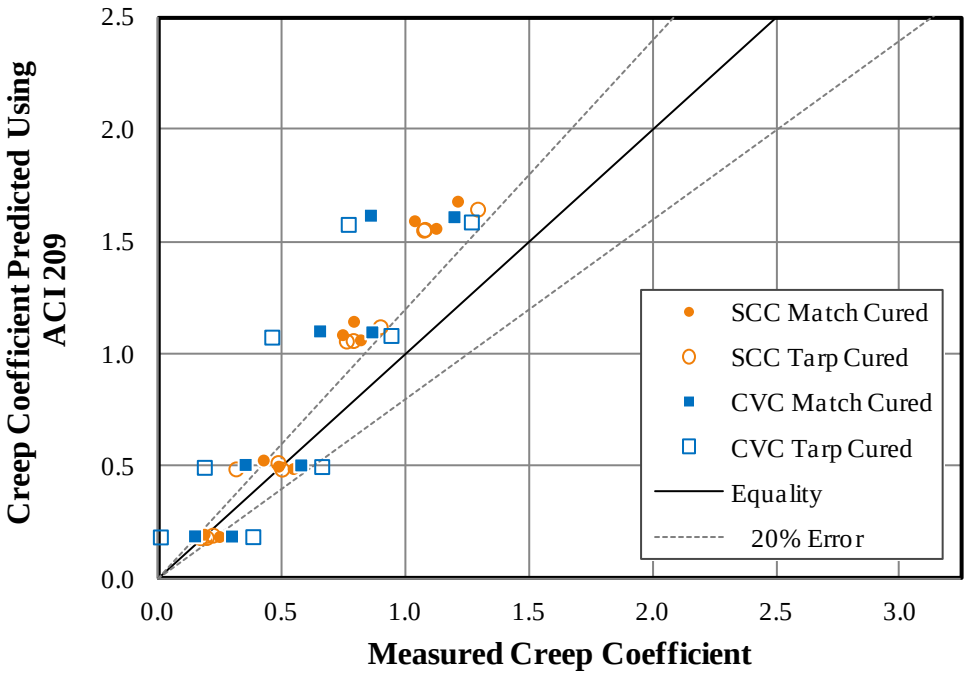

Figure D-22: Measured Versus Predicted Creep Coefficients Using ACI 209

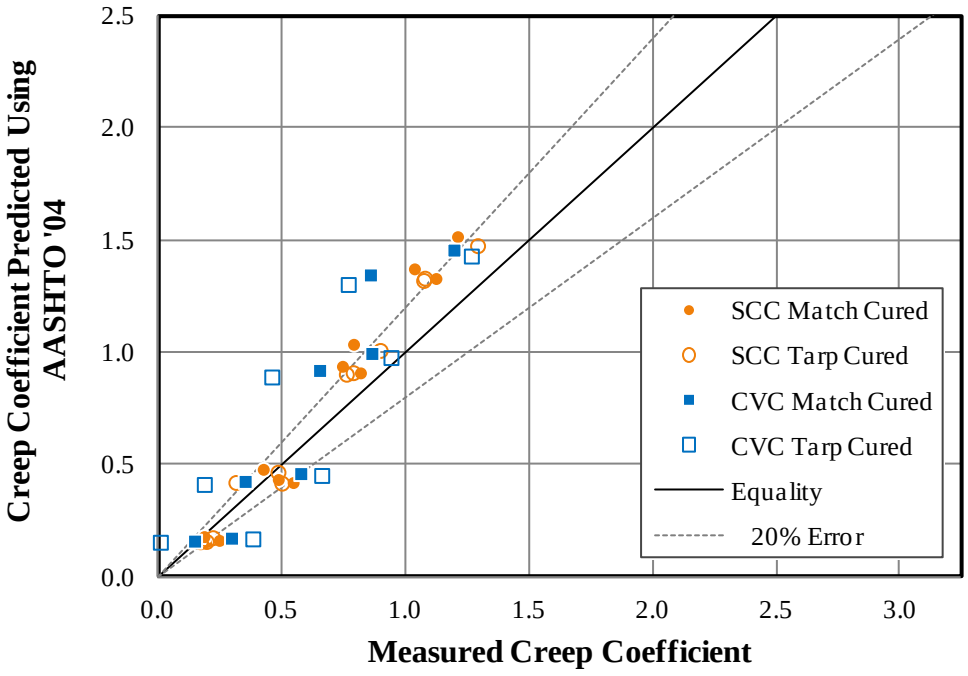

Figure D-23: Measured Versus Predicted Creep Coefficients Using AASHTO 2004

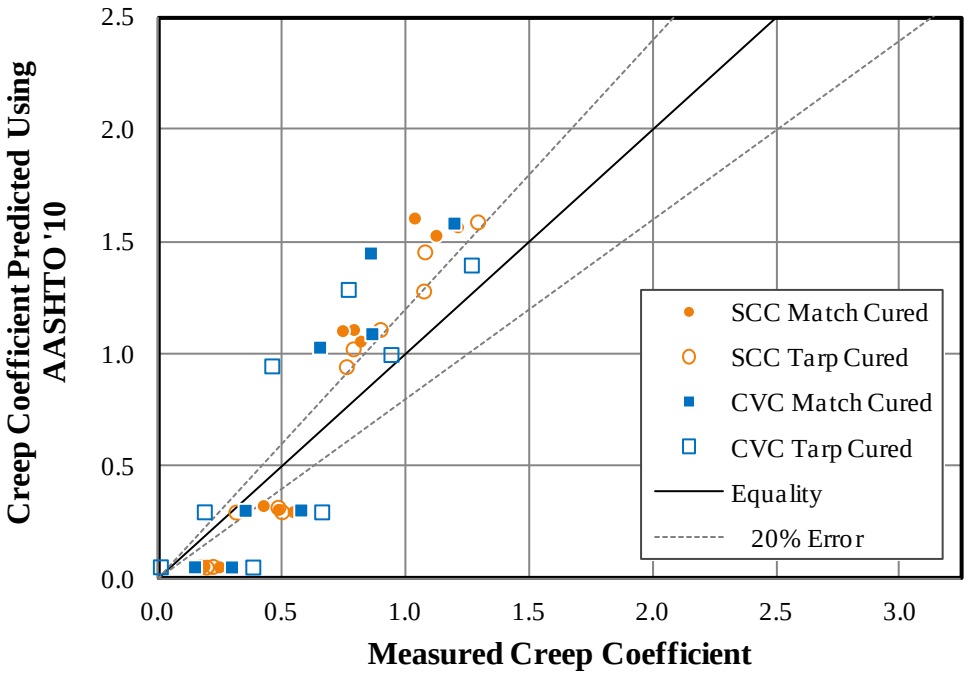

Figure D-24: Measured Versus Predicted Creep Coefficients Using AASHTO 2010

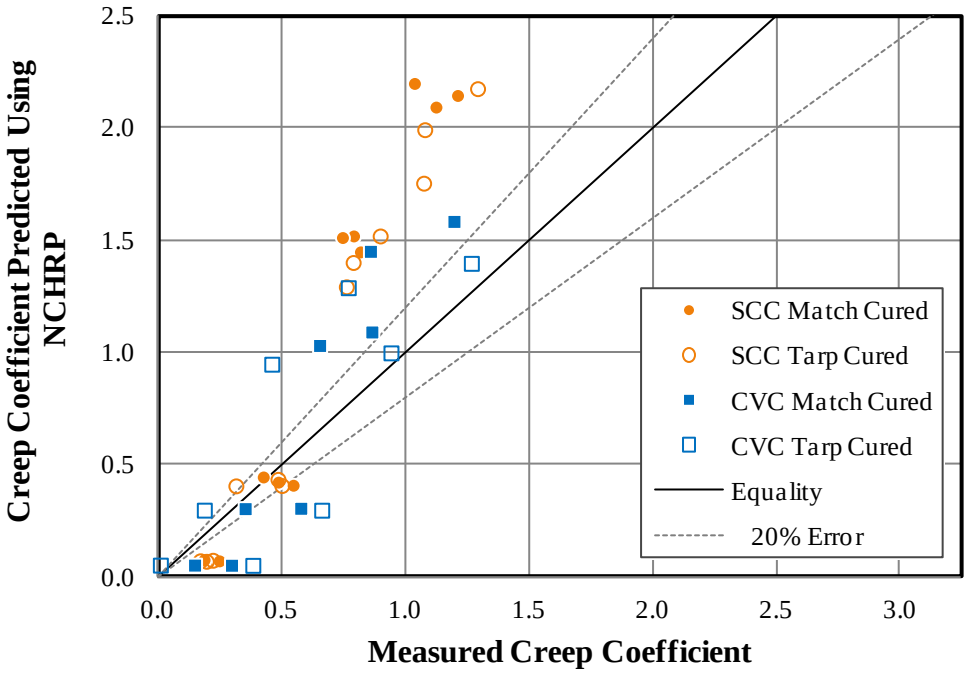

Figure D-25: Measured Versus Predicted Creep Coefficients Using NCHRP 628

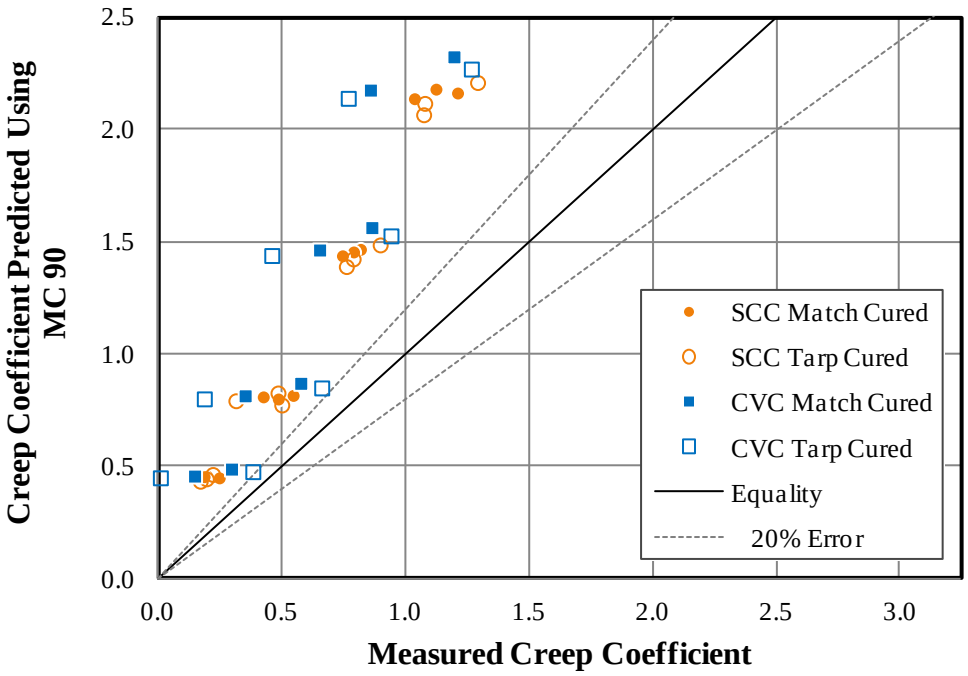

Figure D-26: Measured Versus Predicted Creep Coefficients Using MC 90

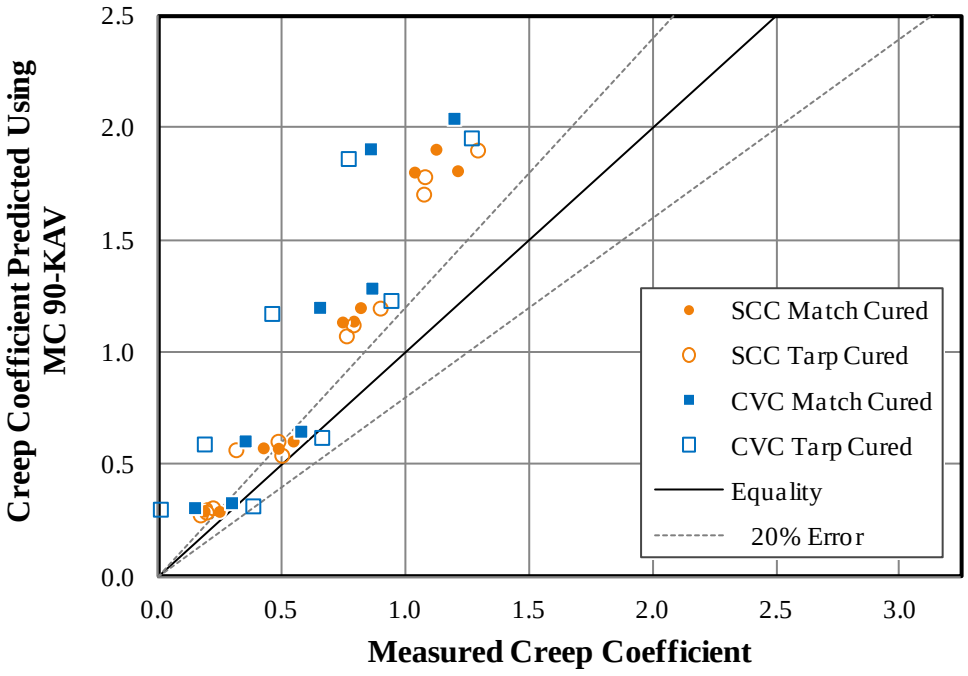

Figure D-27: Measured Versus Predicted Creep Coefficients Using MC 90-KAV

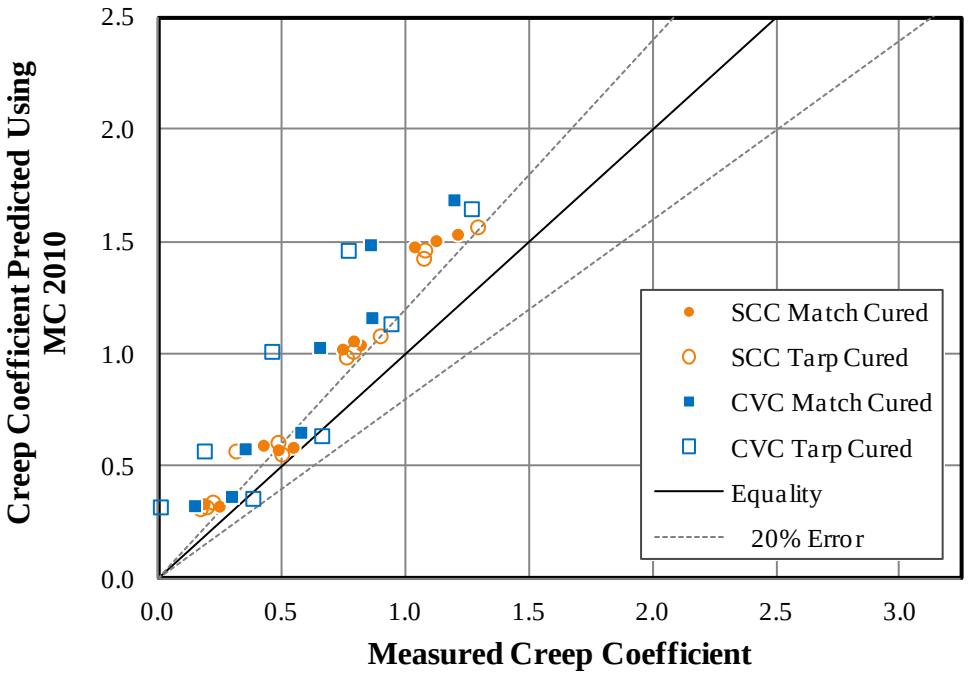

Figure D-28: Measured Versus Predicted Creep Coefficients Using MC 2010

APPENDIX E
ACCURACY OF PREDICTION METHODS

E.1. ACCURACY OF PREDICTED LOAD-INDUCED STRAINS

Figure E-1 through Figure E-6 graphs the predicted load-induced strains divided by the measured load-induced strains for each of the prediction models evaluated in this research. The times plotted for these figures are 56 days and 365 days. Figure E-7 to Figure E-8 show the unbiased estimate of the standard deviation for the percent error of the load-induced strain at 1 year. Each of these figures show the SCC mixtures and the CVC mixtures compared to all concretes combined for each prediction model. In addition, for the percent error, the tarp-cured and match-cured specimens are also compared to all mixtures combined. Note, however, that specimens that were under-loaded or improperly cured were not included in any of the averages. The prediction methods used for load-dependent strain are: ACI 209, AASHTO 2004, AASHTO 2010, NCHRP 628, MC 90, MC 90-KAV, and MC 2010. Predictions made by MC 90-99 and Eurocode are effectively equal to those made by MC 2010 and are not shown. Also, for conventionally vibrated concrete mixtures, the strain due to load predicted by NCHRP 628 is equal to that predicted by AASHTO 2010.

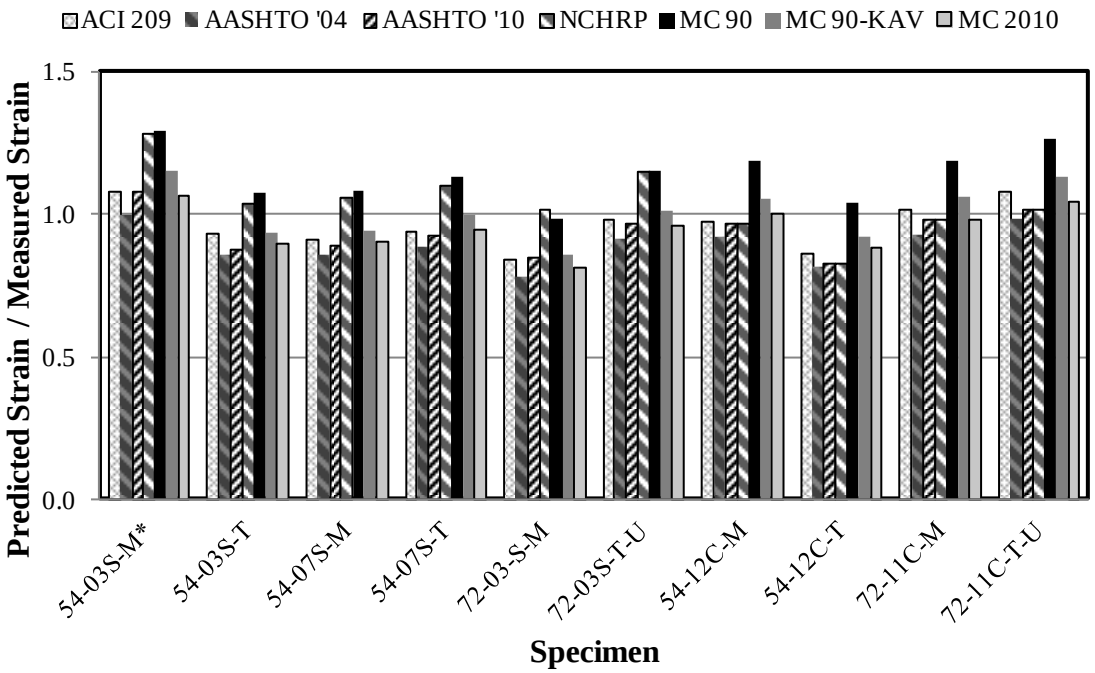

Figure E-1: Accuracy of Predicted Load-Induced Strains at 56 Days

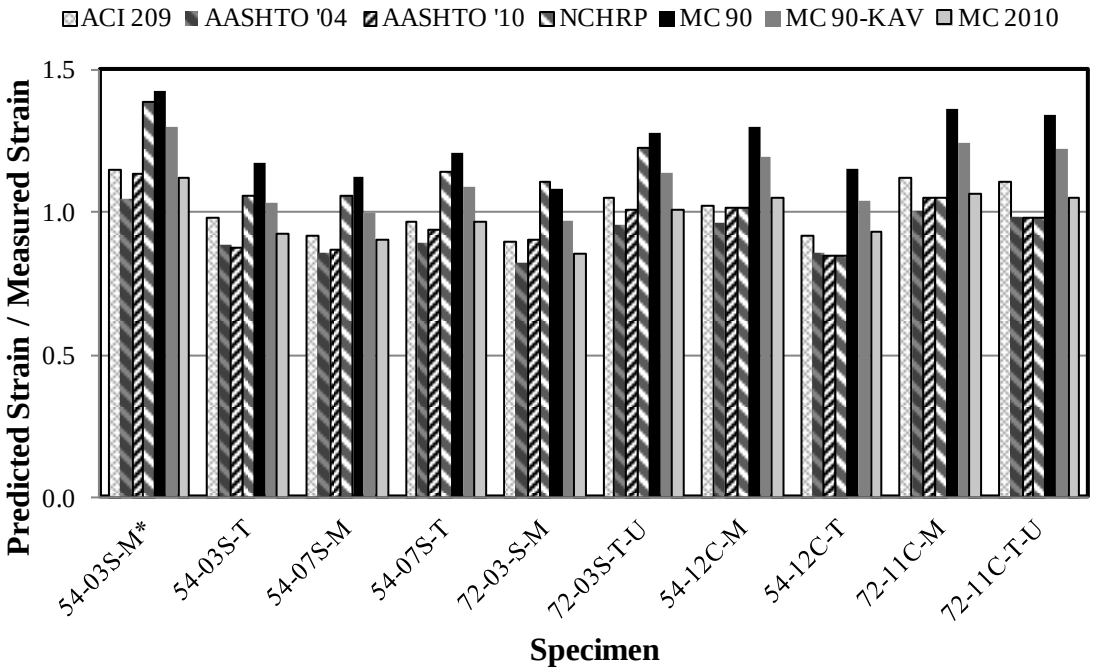

Figure E-2: Accuracy of Predicted Load-Induced Strains at 1 Year

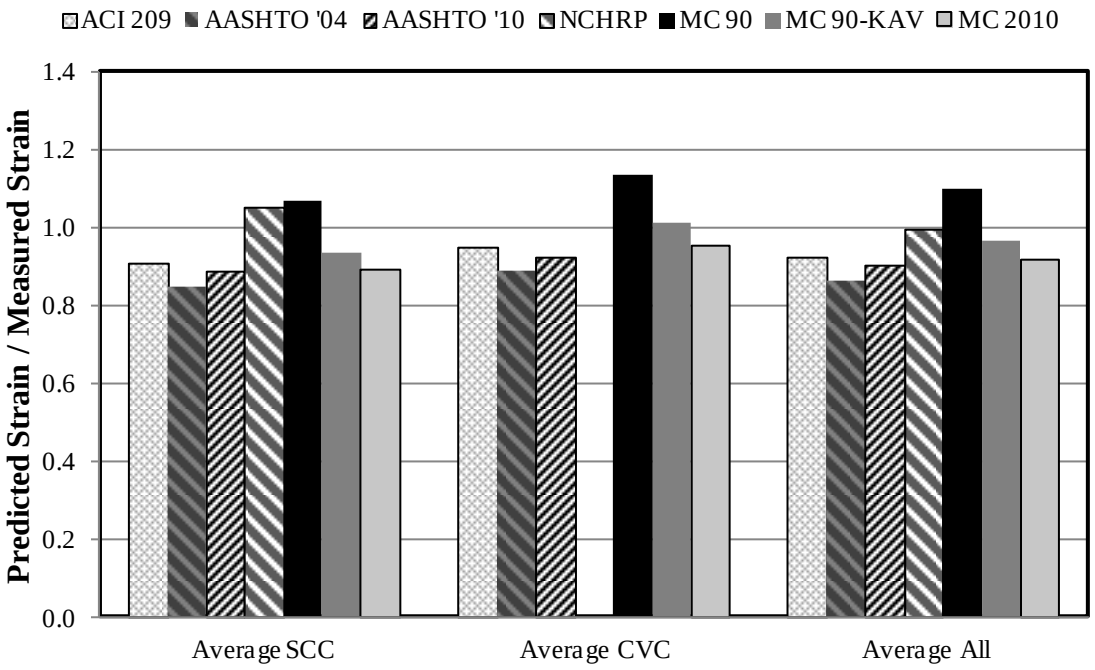

Figure E-3: Accuracy of Predicted Load-Induced Strains at 56 Days by Mixture Type

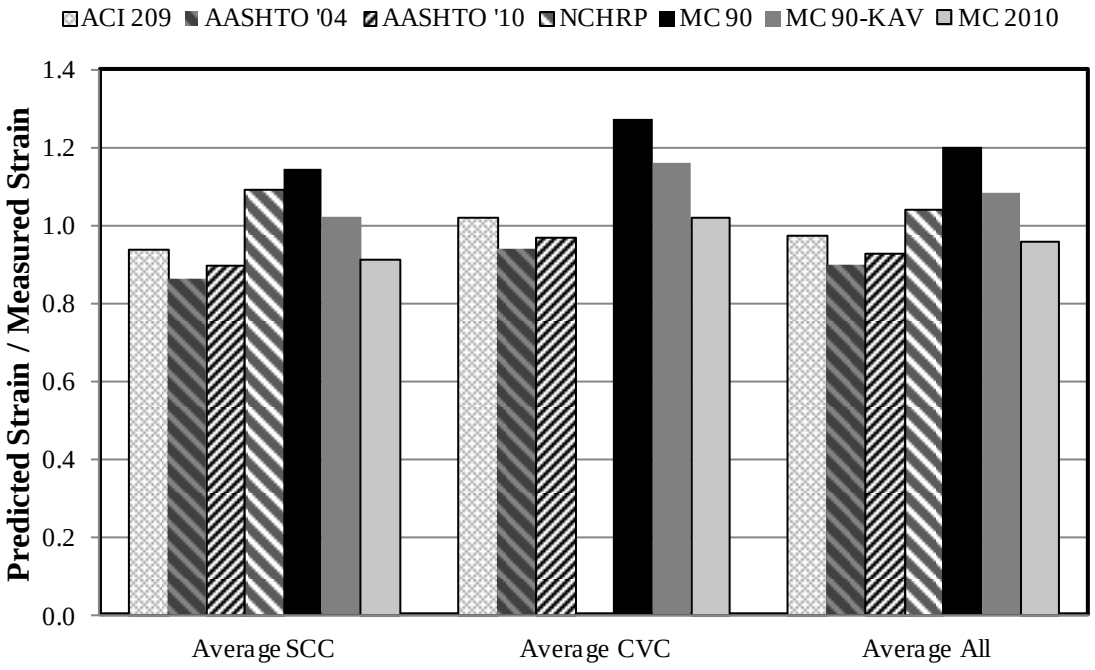

Figure E-4: Accuracy of Predicted Load-Induced Strains at 1 Year by Mixture Type

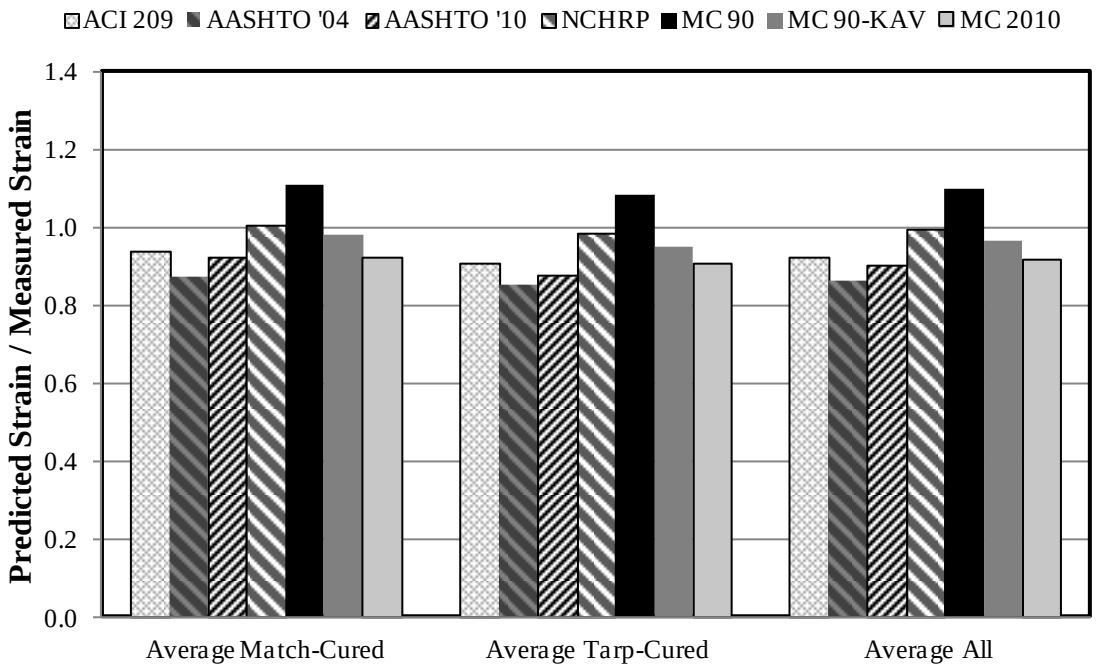

Figure E-5: Accuracy of Predicted Load-Induced Strains at 56 Days by Curing Method

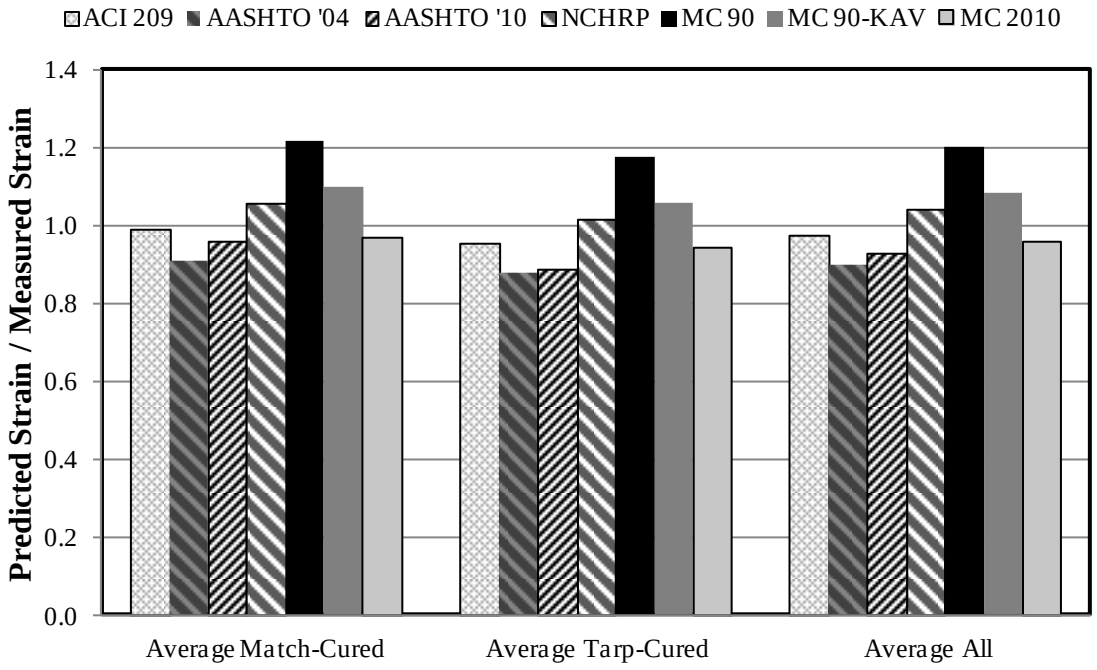

Figure E-6: Accuracy of Predicted Load-Induced Strains at 1 Year by Curing Method

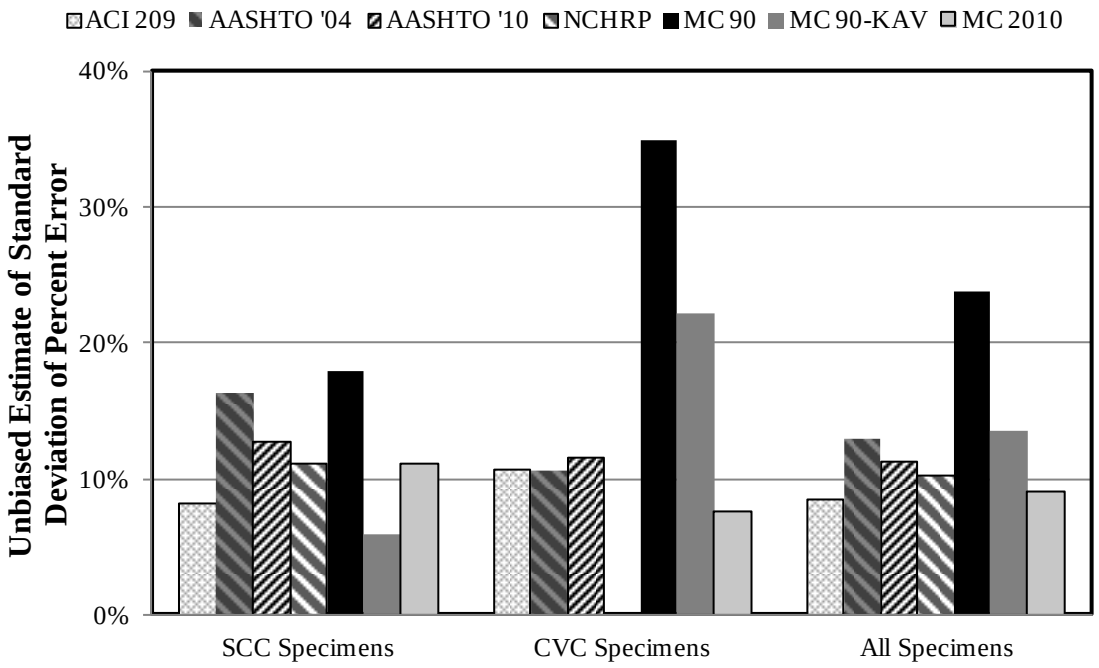

Figure E-7: Unbiased Estimate of Standard Deviation of Percent Error for Load-Induced Strains at 1 Year (by Mixture Type)

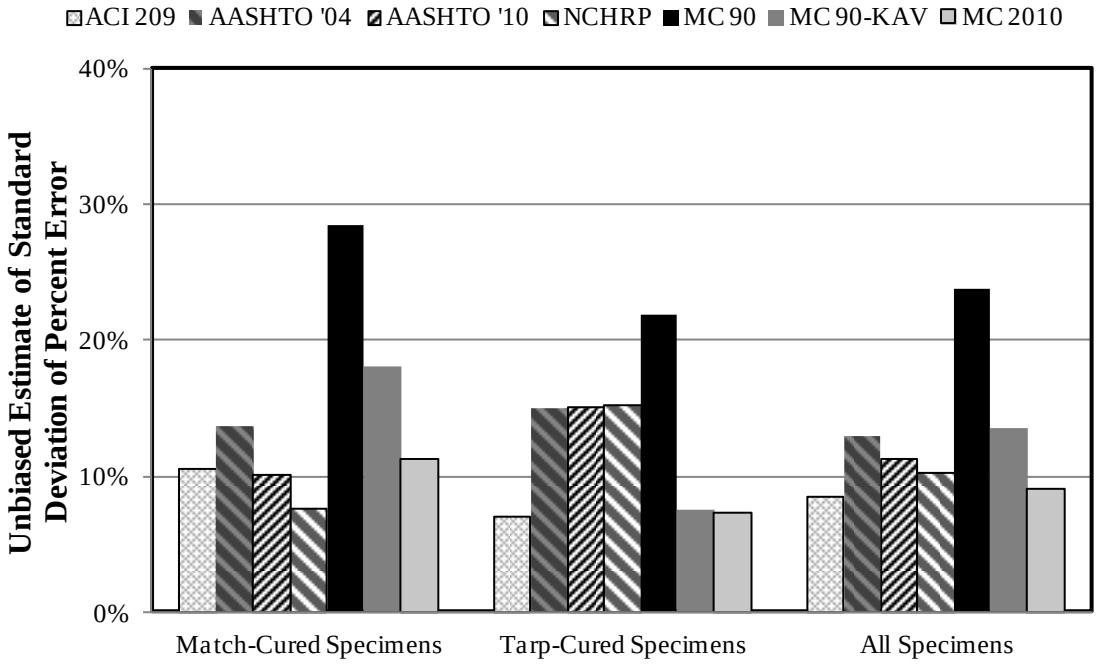

Figure E-8: Unbiased Estimate of Standard Deviation of Percent Error for Load-Induced Strains at 1 Year (by Curing Method)

E.2. ACCURACY OF PREDICTED SHRINKAGE STRAINS

Figure E-9 through Figure E-14 graphs the predicted shrinkage strains divided by the measured shrinkage strains for each of the prediction models evaluated in this research. The times plotted in this section are 56 days and 365 days. The times plotted for these figures are 56 days and 365 days. Figure E-15 to Figure E-16 show the unbiased estimate of the standard deviation for the percent error of the shrinkage strain at 1 year. Each of these figures show the SCC mixtures and the CVC mixtures compared to all concretes combined for each prediction model. In addition, for the percent error, the tarp-cured and match-cured specimens are also compared to all mixtures combined. Note, however, that specimens that were under-loaded or improperly cured were not included in the averages. The prediction methods used for shrinkage strain are: ACI 209, AASHTO 2004, AASHTO 2010, NCHRP 628, MC 90, MC 2010, and Eurocode. MC 90-99 is effectively equal to MC 2010 and MC-KAV is equal to MC-90, and these methods are not shown. Also, for conventionally vibrated concrete mixtures, the shrinkage strain predicted by NCHRP 628 is equal to that predicted by AASHTO 2004.

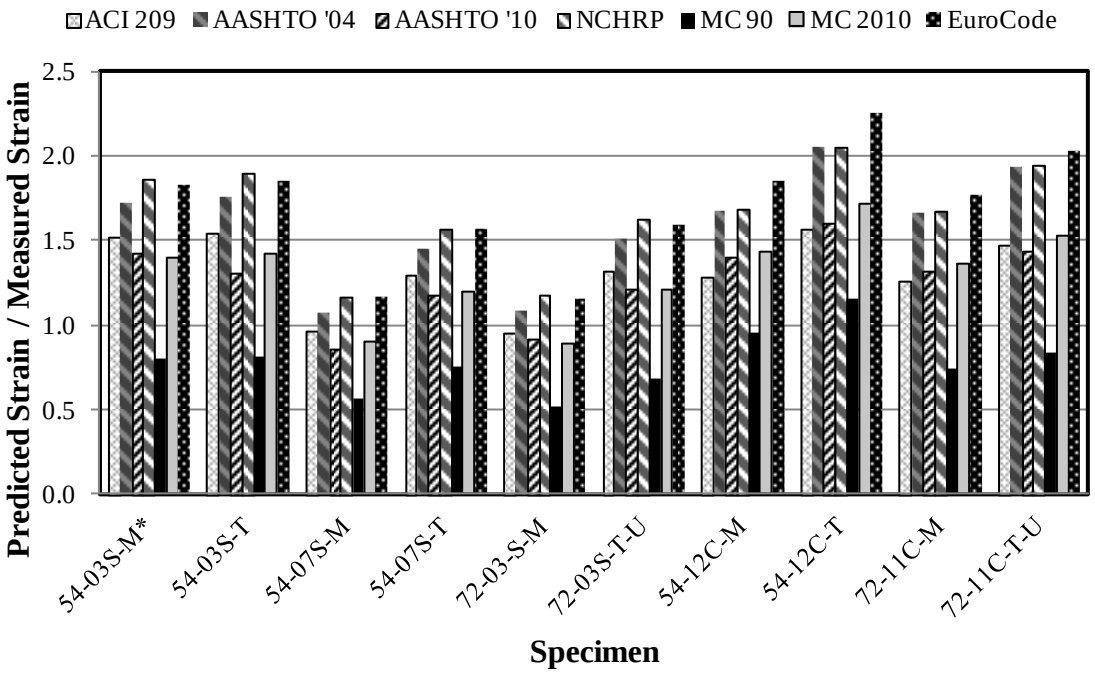

Figure E-9: Accuracy of Predicted Shrinkage Strains at 56 Days

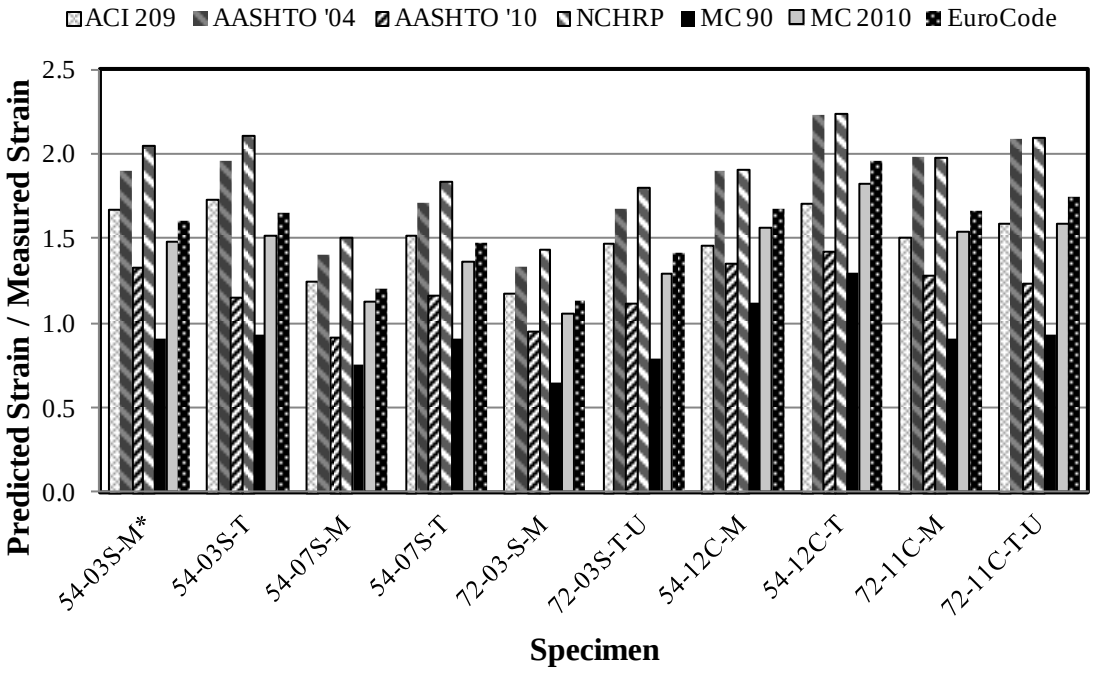

Figure E-10: Accuracy of Predicted Shrinkage Strains at 1 Year

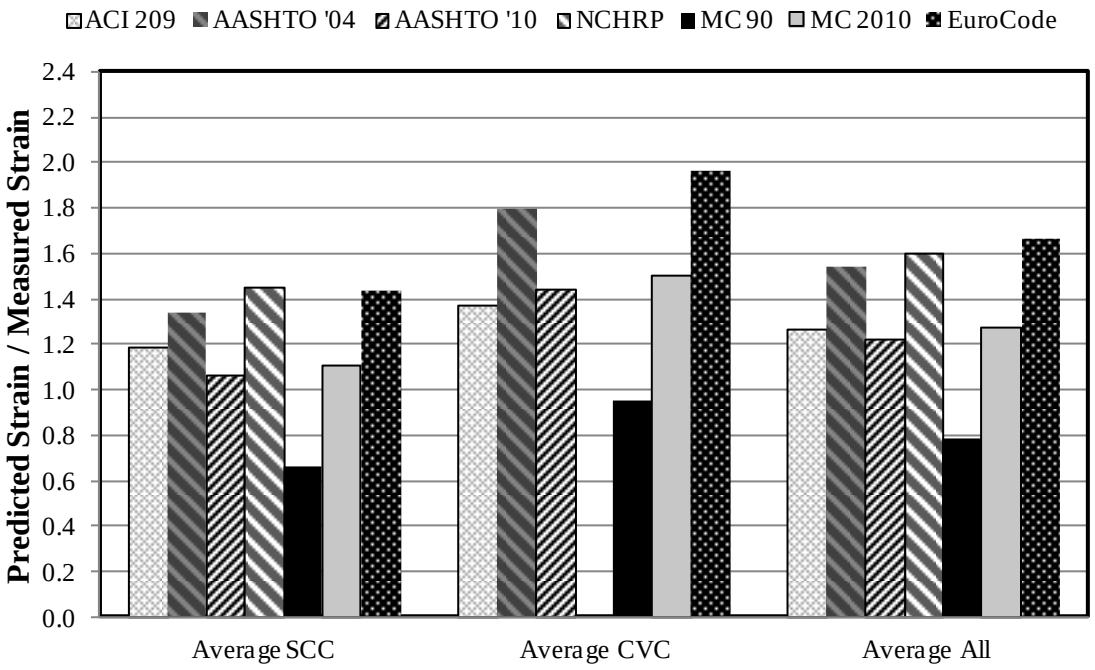

Figure E-11: Accuracy of Predicted Shrinkage Strains at 56 Days by Mixture Type

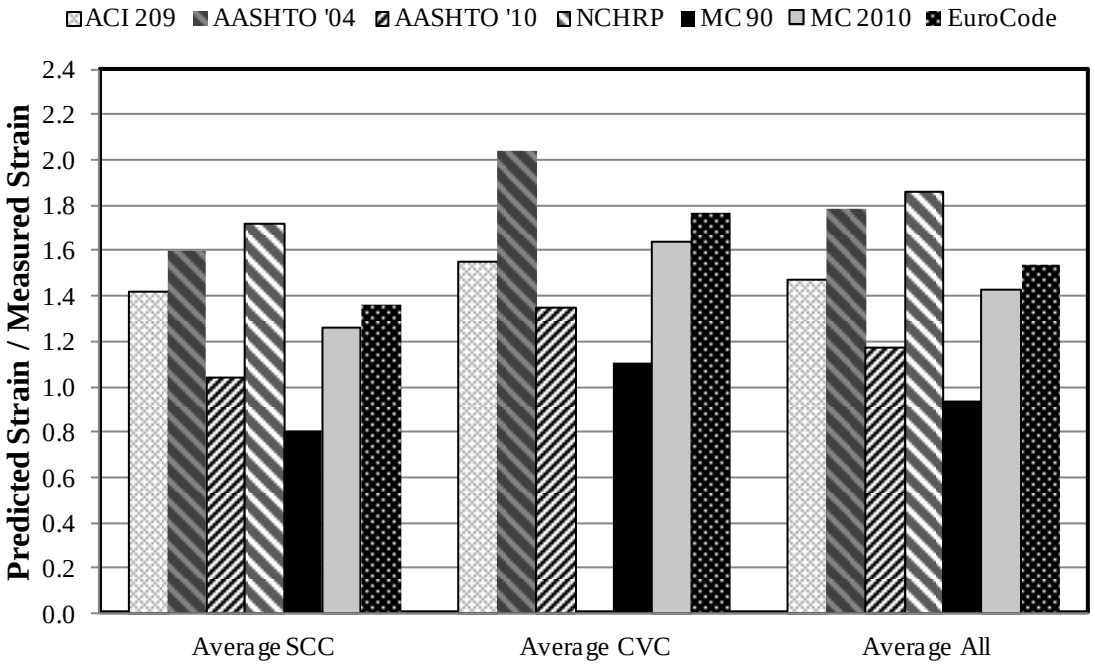

Figure E-12: Accuracy of Predicted Shrinkage Strains at 1 Year by Mixture Type

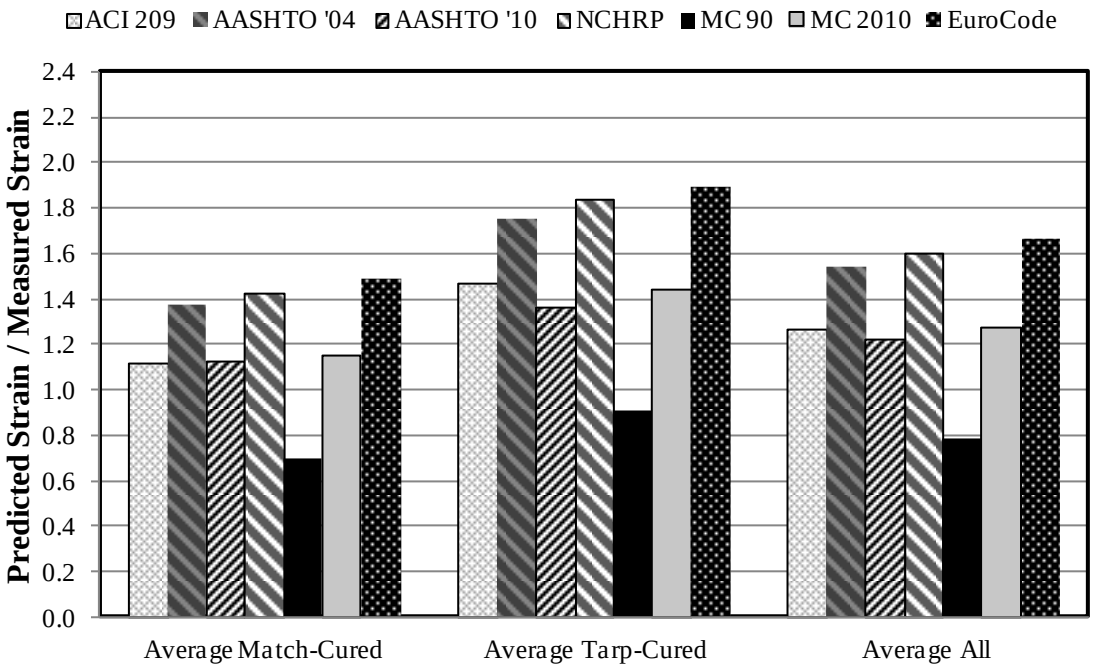

Figure E-13: Accuracy of Predicted Shrinkage Strains at 56 Days by Curing Method

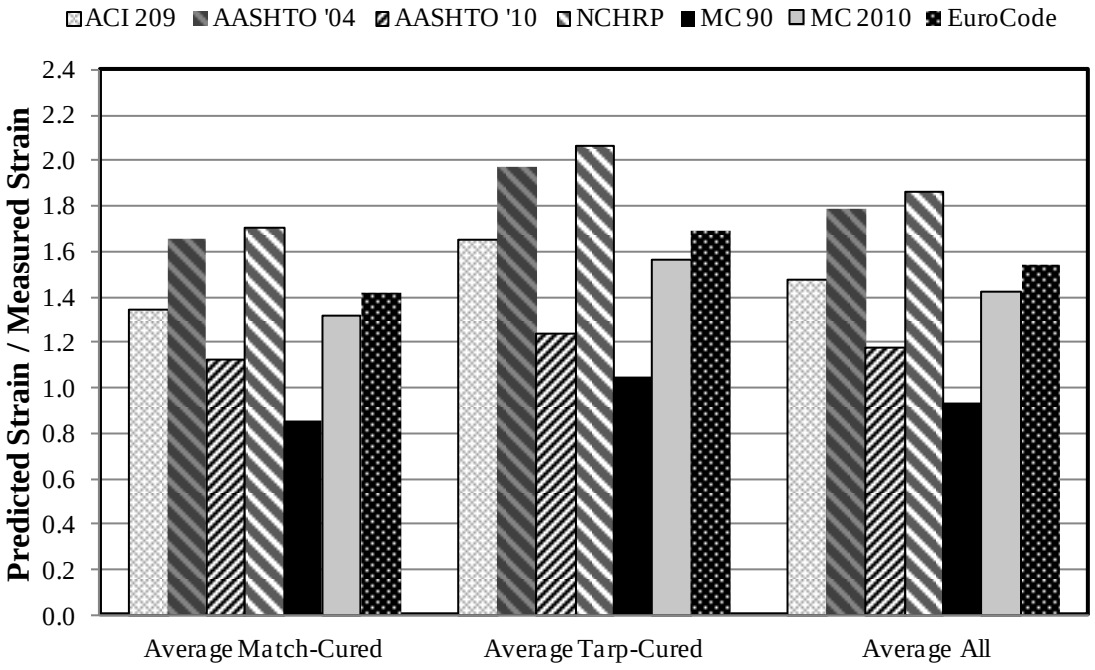

Figure E-14: Accuracy of Predicted Shrinkage Strains at 1 Year by Curing Method

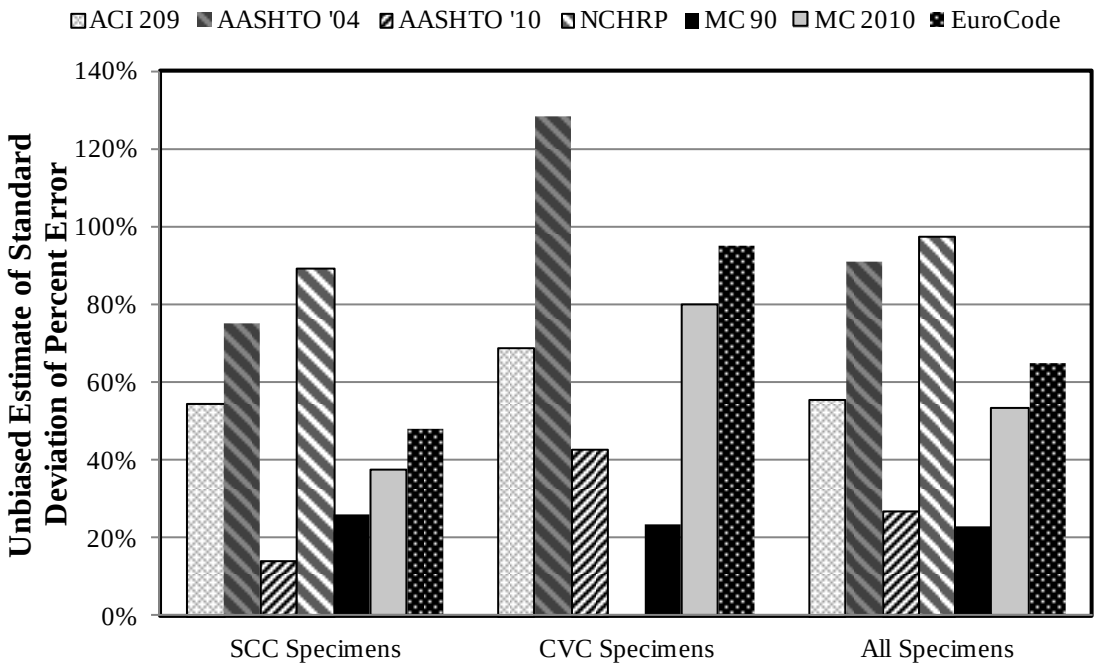

Figure E-15: Unbiased Estimate of Standard Deviation of Percent Error for Shrinkage Strains at 1 Year (by Mixture Type)

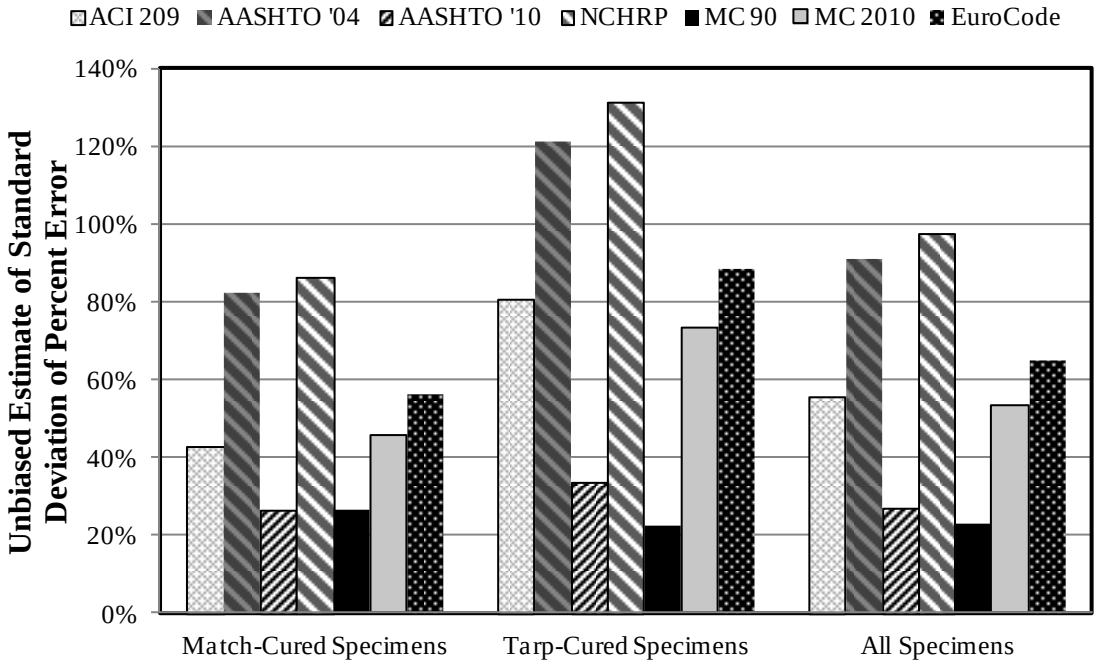

Figure E-16: Unbiased Estimate of Standard Deviation of Percent Error for Shrinkage Strains at 1 Year (by Curing Method)

E.3. ACCURACY OF PREDICTED CREEP STRAINS

Figure E-17 through Figure E-20 graphs the predicted creep strains divided by the measured creep strains for each of the prediction models evaluated in this research. T The times plotted for these figures are 56 days and 365 days. Figure E-21 to Figure E-22 show the unbiased estimate of the standard deviation for the percent error of the creep strain at 1 year. Each of these figures show the SCC mixtures and the CVC mixtures compared to all concretes combined for each prediction model. Note, however, that specimens that were under-loaded or improperly cured were not included in the averages. The prediction methods used for creep strain are: ACI 209, AASHTO 2004, AASHTO 2010, NCHRP 628, MC 90, MC 90-KAV, and MC 2010. MC 90-99 and Eurocode are effectively equal to MC 2010 and are not shown. Also, for conventionally vibrated concrete mixtures, the creep strain predicted by NCHRP 628 is equal to that predicted by AASHTO 2010.

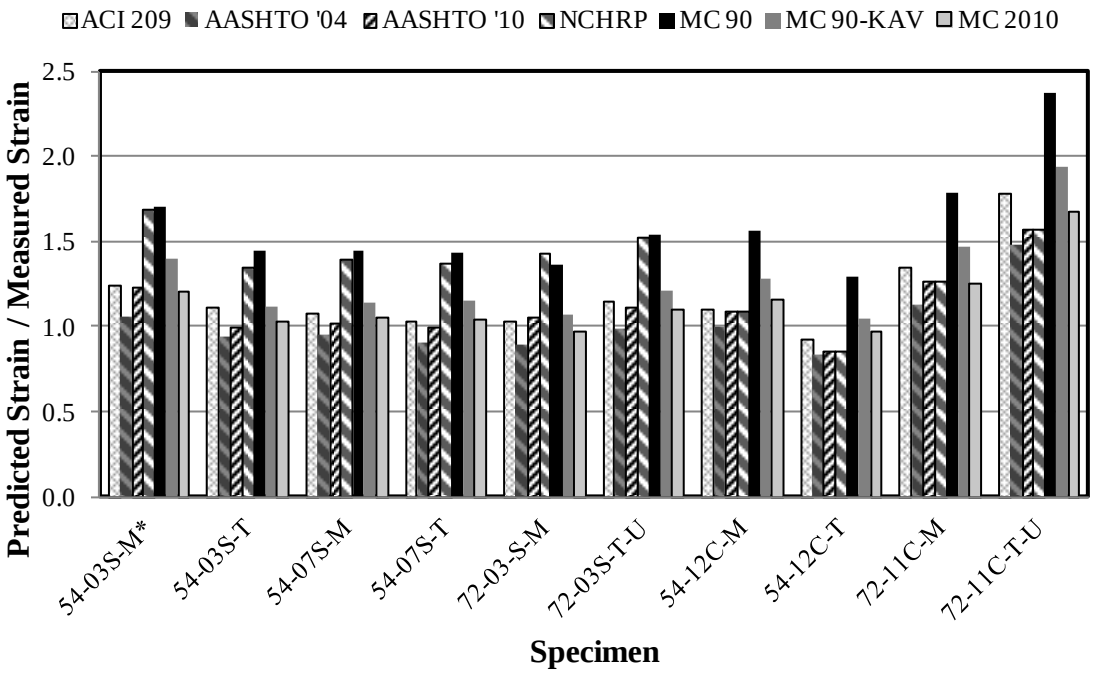

Figure E-17: Accuracy of Predicted Creep Strains at 56 Days

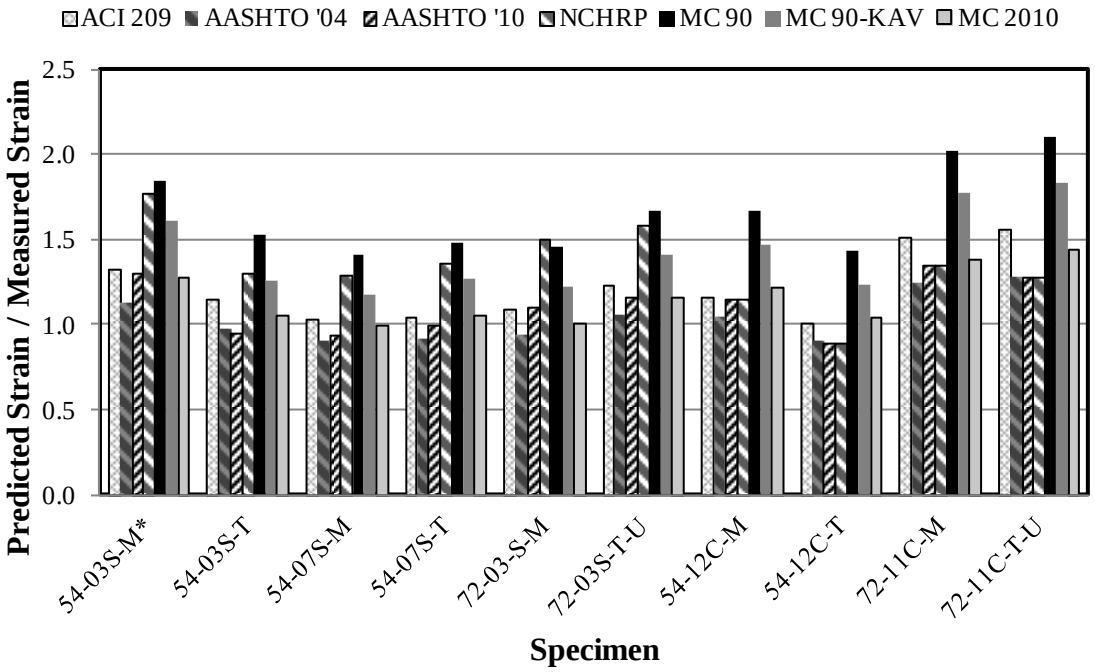

Figure E-18: Accuracy of Predicted Creep Strains at 1 Year

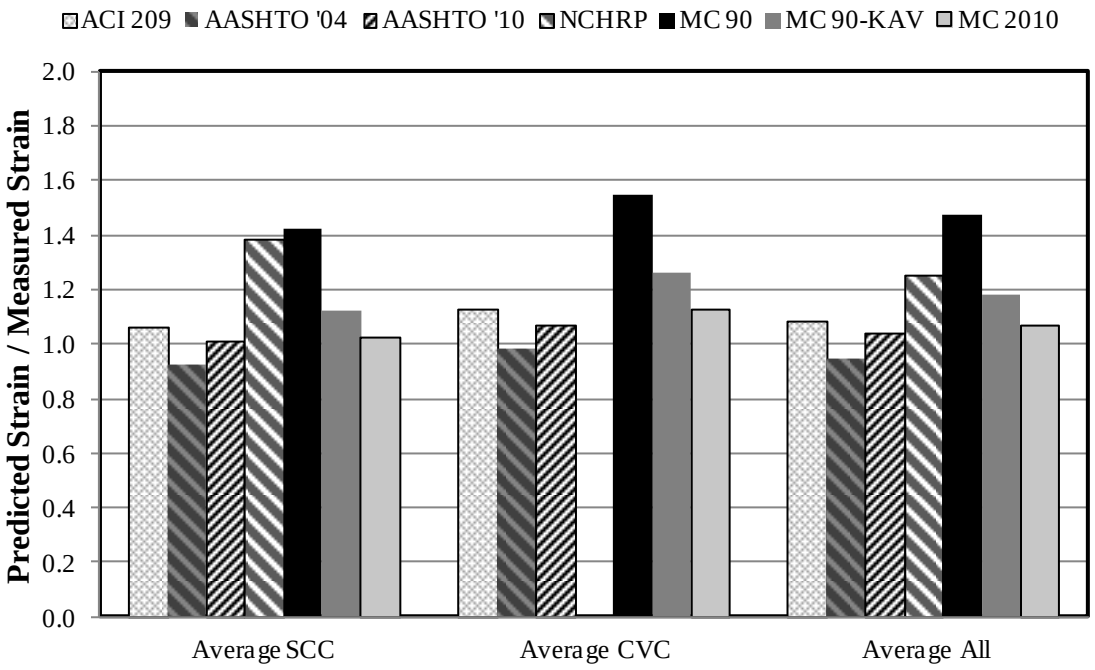

Figure E-19: Accuracy of Predicted Creep Strains at 56 Days by Mixture Type

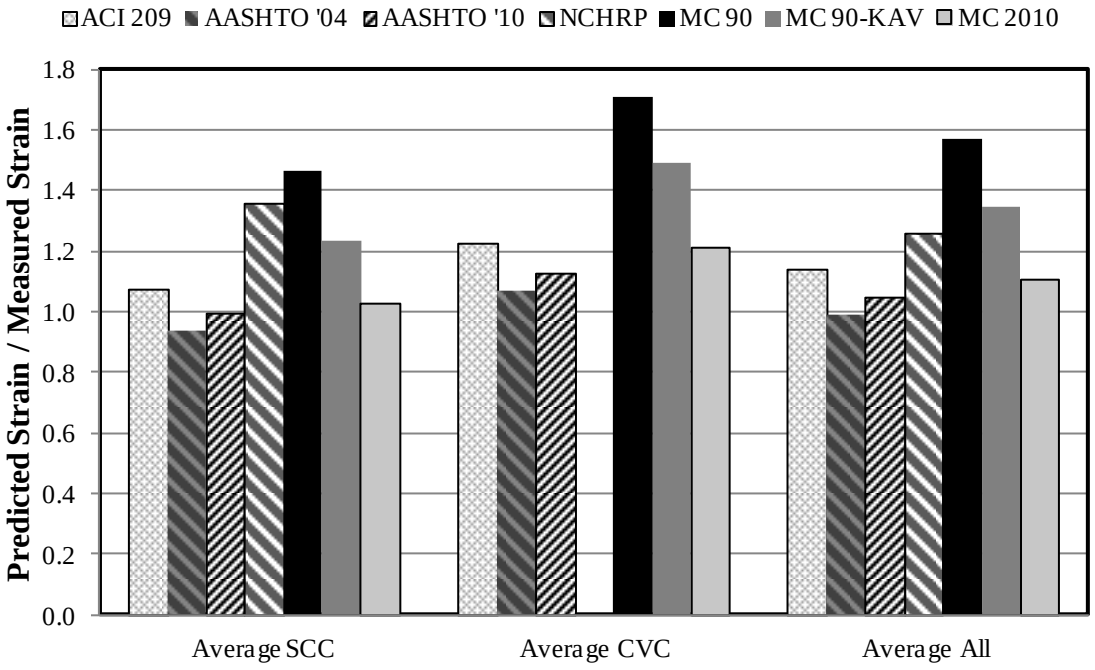

Figure E-20: Accuracy of Predicted Creep Strains at 1 Year by Mixture Type

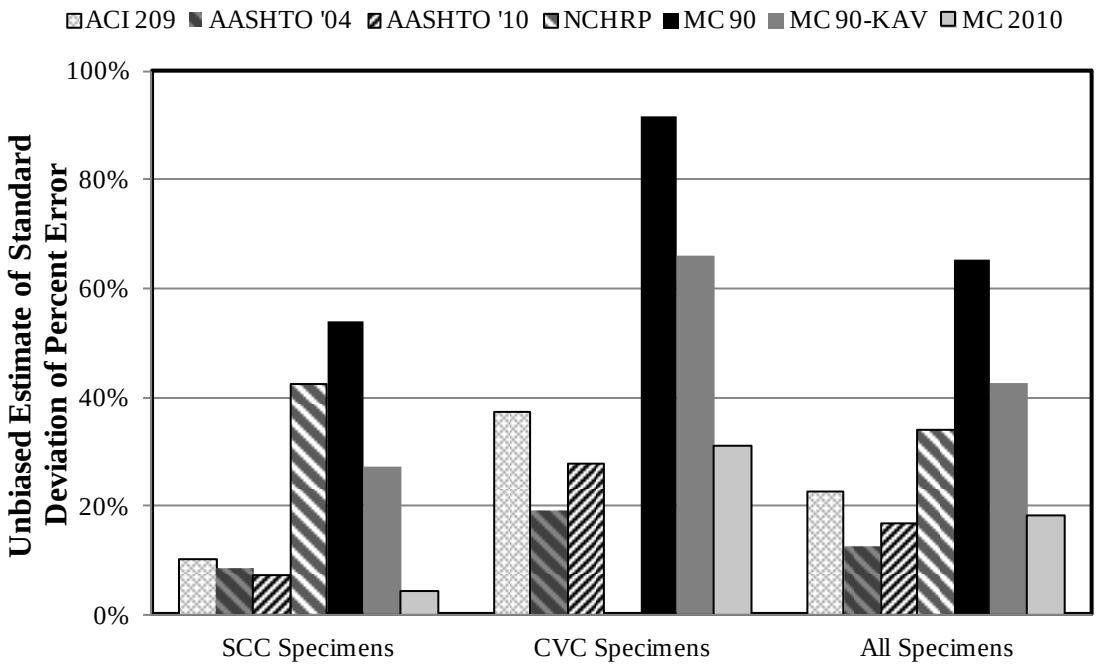

Figure E-21: Unbiased Estimate of Standard Deviation of Percent Error for Creep Strains at 1 Year (by Mixture Type)

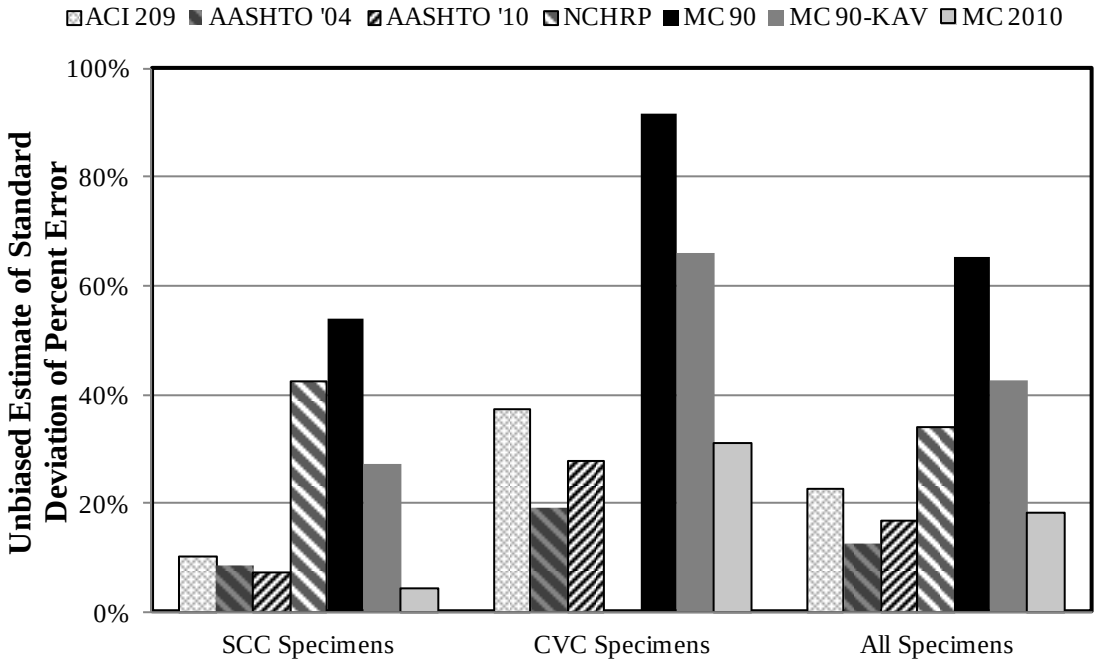

Figure E-22: Unbiased Estimate of Standard Deviation of Percent Error for Creep Strains at 1 Year (by Curing Method)

E.4. ACCURACY OF PREDICTED CREEP COEFFICIENTS

Figure E-23 through Figure E-26 graphs the predicted creep coefficients divided by the measured creep coefficients for each of the prediction models evaluated in this research. The times plotted for these figures are 56 days and 365 days. Figure E-27 to Figure E-28 show the unbiased estimate of the standard deviation for the percent error of the creep coefficient at 1 year. Each of these figures show the SCC mixtures and the CVC mixtures compared to all concretes combined for each prediction model. Note, however, that specimens that were under-loaded or improperly cured were not included in the averages. The prediction methods used for creep coefficients are: ACI 209, AASHTO 2004, AASHTO 2010, NCHRP 628, MC 90, MC 90-KAV, and MC 2010. MC 90-99 and Eurocode are effectively equal to MC 2010 and are not shown. Also, for conventionally vibrated concrete mixtures, the creep coefficient predicted by NCHRP 628 is equal to that predicted by AASHTO 2010.

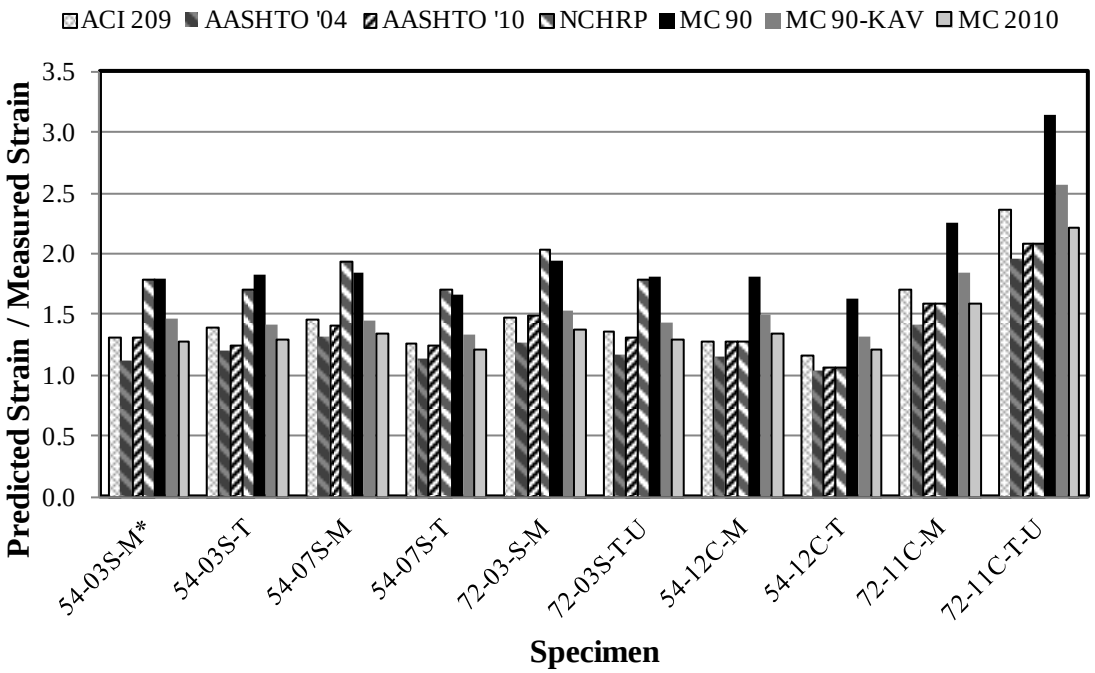

Figure E-23: Accuracy of Predicted Creep Coefficients at 56 Days

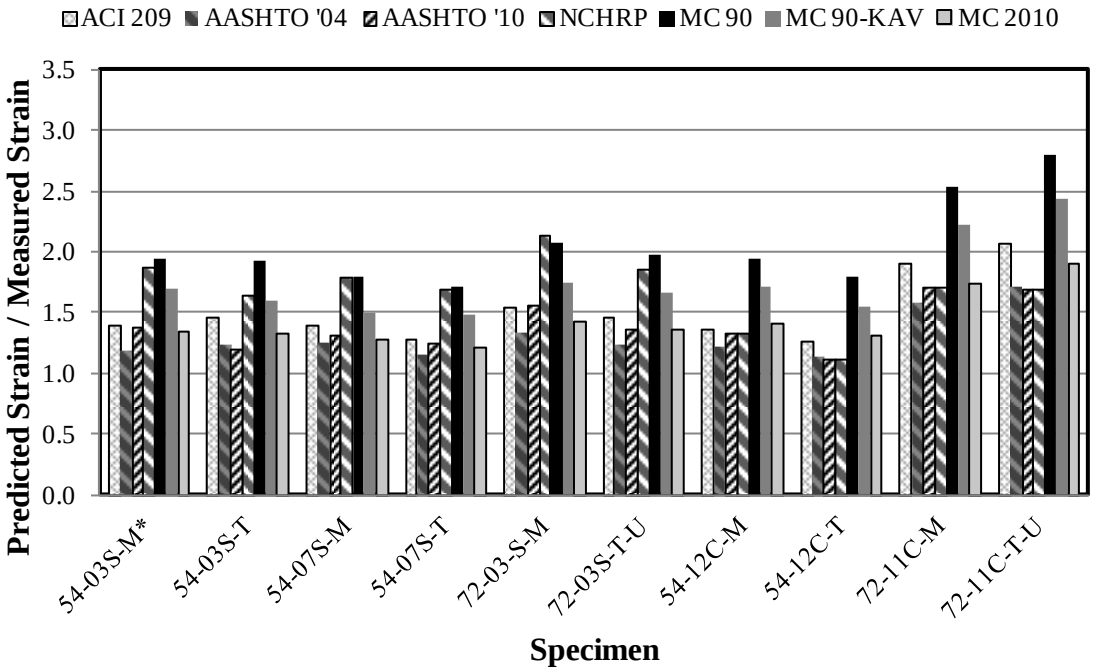

Figure E-24: Accuracy of Predicted Creep Coefficients at 1 Year

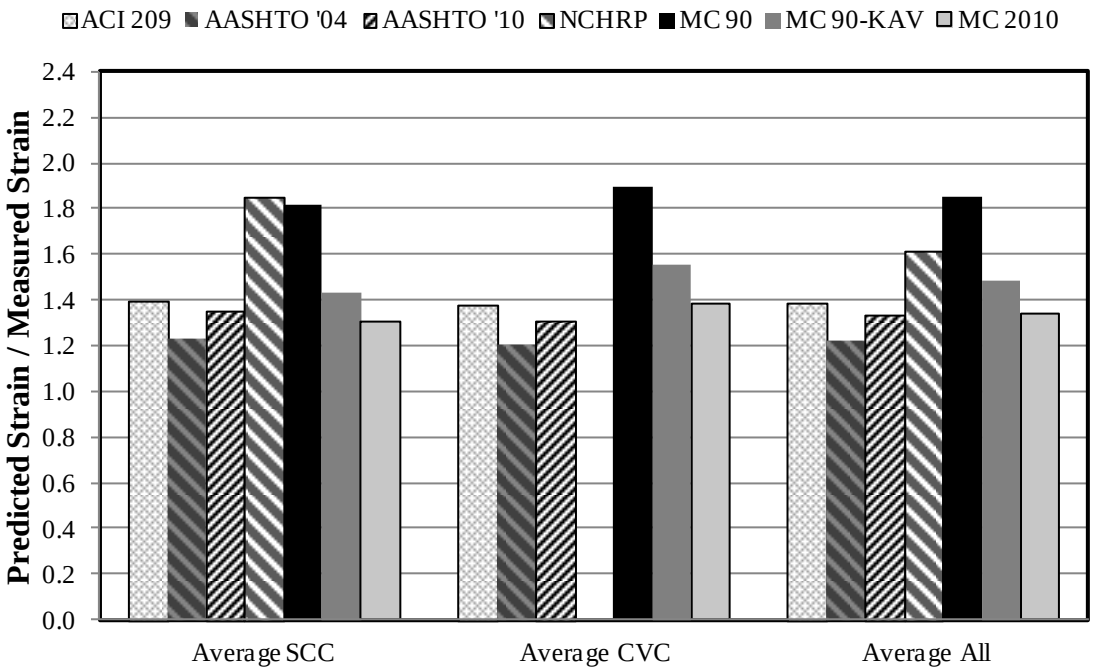

Figure E-25: Accuracy of Predicted Creep Coefficients at 56 Days by Mixture Type

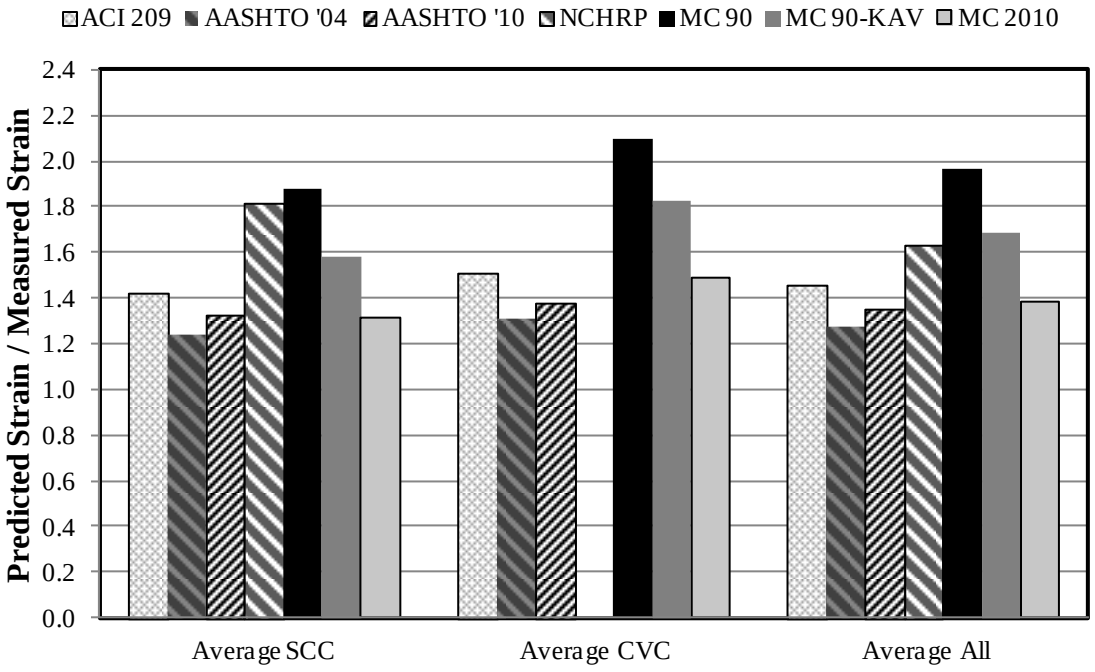

Figure E-26: Accuracy of Predicted Creep Coefficients at 1 Year by Mixture Type

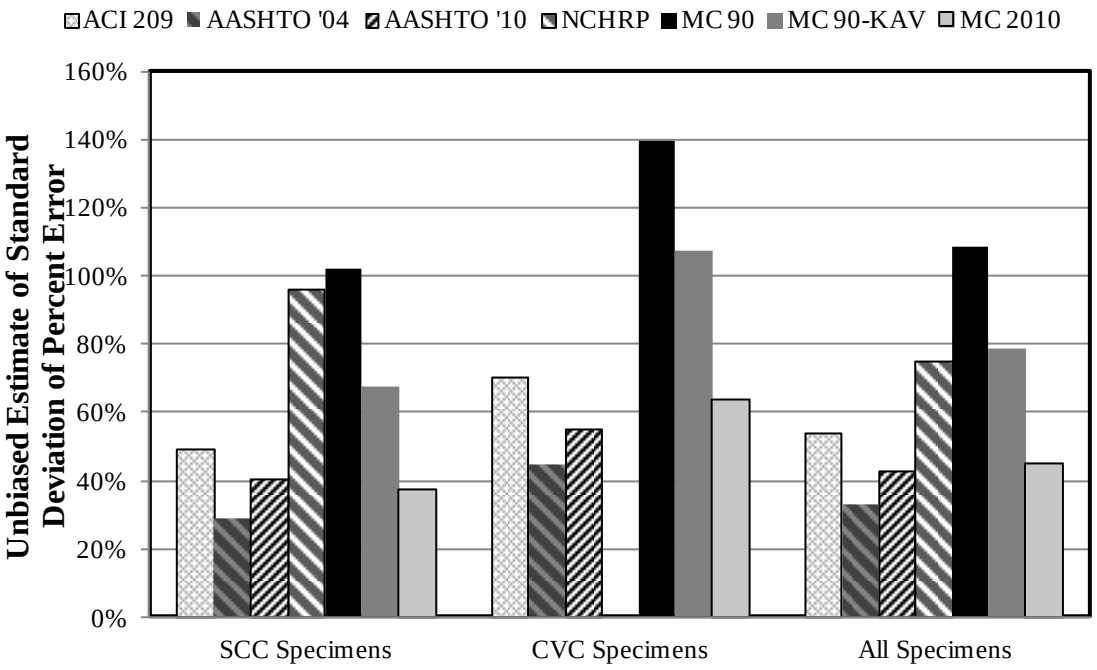

Figure E-27: Unbiased Estimate of Standard Deviation of Percent Error for Creep Coefficients at 1 Year (by Mixture Type)

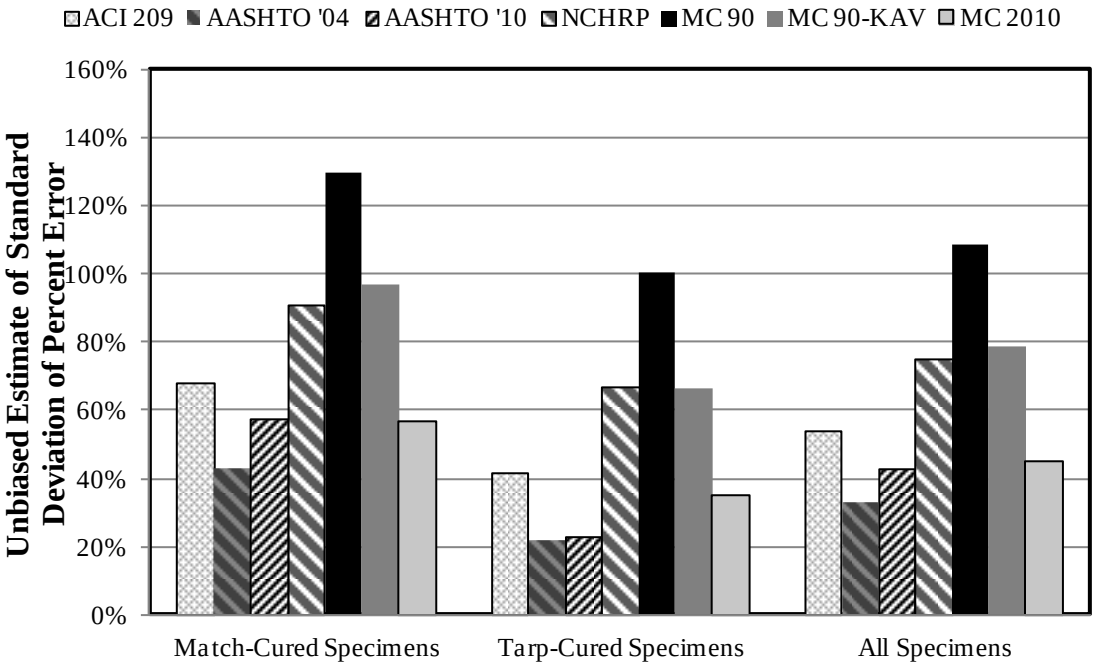

Figure E-28: Unbiased Estimate of Standard Deviation of Percent Error for Creep Coefficients at 1 Year (by Curing Method)